A LOW FREQUENCY PNEUMATIC SUSPENSION FOR AN AMBULANCE STRETCHER

R.J. HENDERSON

A Thesis Submitted for the Degree of
Doctor of Philosophy
at the Department of Mechanical Engineering
University of Canterbury
Christchurch
New Zealand

1997

With thanks to my mother

ABSTRACT

Ambulance suspensions often give a poor ride which may result in deterioration in the condition of ill or injured patients. To reduce patient vibration, purpose-built ambulances or ambulances with modified chassis can be used. A potentially lower cost and more effective alternative is to provide additional isolation for the stretcher only.

This thesis describes the design and performance of a pneumatic stretcher suspension which uses a novel linkage to provide isolation in bounce and pitch.

Results of linear and non-linear analyses are presented which characterise the behaviour of the suspension. The kinematics of the suspension linkage are shown to give rise to a vertical stiffness which reduces in compression.

Pneumatic cylinders connected to auxiliary tanks are used as springs. These give the suspension essentially load-independent natural frequencies of around 0.46 Hz in bounce and pitch. Damping is provided by fitting a flow restriction between the cylinders and tanks. By simulating the response of the stretcher to realistic random floor vibrations, it is concluded that a low level of damping is required and that an orifice restriction is preferable to a capillary restriction. These simulations are believed to be the first for which pneumatic damping is assessed by using a realistic random input. Additional simulation results demonstrate that improved isolation is possible by using an innovative semi-active pneumatic damper which is controlled according to the skyhook damping principle.

A mechanical shaker which uses adjustable stroke round cams is described. Suspension tests carried out using this shaker are detailed. Various combinations of patient mass, pneumatic damping level, and shaker stroke and frequency are used. Acceleration transmissibilities are presented which indicate both that good levels of vertical isolation are obtained (eg. greater than 90% isolation above 5.2 Hz), and that isolation performance is largely independent of patient mass. Coulomb damping is shown to have a detrimental effect on isolation - particularly for low acceleration or high frequency inputs.

The results of road tests are presented. These show that the suspension provides isolation above 1 Hz and reduces r.m.s. accelerations by 45-60%. The suspension is concluded to offer the potential to reduce patient vibration at reasonable cost, although improvements to the design are required in moving to a production model.

PUBLICATIONS

Raine, J.K. and **Henderson, R.J.** A vibration isolating ambulance stretcher suspension. *Proc. IPENZ Annual Conference*, Hamilton, February 1993, pp 221-232.

Henderson, R.J. and **Raine, J.K.** A two degree-of-freedom ambulance stretcher suspension. *Proc. IPENZ Annual Conference*, Dunedin, February 1996, pp 235-240.

Raine, J.K. and **Henderson, R.J.** A two degree-of-freedom ambulance stretcher suspension, Part 1: system overview. Accepted for review by the *Instn Mech. Engrs.*

Henderson, R.J. and **Raine, J.K.** A two degree-of-freedom ambulance stretcher suspension, Part 2: simulation of system performance with capillary and orifice pneumatic damping. Accepted for review by the *Instn Mech. Engrs.*

Henderson, R.J. and **Raine, J.K.** A two degree-of-freedom ambulance stretcher suspension, Part 3: laboratory and road test performance. Submitted to the *Instn Mech. Engrs.*

ACKNOWLEDGMENTS

I would like to sincerely thank Associate Professor J.K. Raine for his encouragement and guidance during the course this research project. I wish also to thank Mr K. Brown of the Mechanical Engineering Workshop for his careful and accurate construction of the suspension and shaker table described in this thesis.

I am grateful to other Department of Mechanical Engineering staff who have assisted in various ways. Of special mention are Mr A. Cree who provided guidance in setting-up a data acquisition system, and Mr G. Harris who provided various items of test equipment. I wish to thank also Mr J. Maley of the Department of Civil engineering who loaned an amplifier and accelerometers.

I wish to acknowledge the generosity of Hagley Kitchens Ltd., who loaned a van for initial suspension tests. The assistance provided by Mr R. Ball during this testing is also gratefully acknowledged.

I would like to thank Dr C.W. Stammers of the University of Bath and Professor J. Black (formerly of the University of Bath) for information on stretcher suspension systems.

I wish to thank also Mr G. Bailey who assisted in developing some photographs.

Finally, I would like to thank the Christchurch Ambulance Service who provided an ambulance and driver for suspension road trials.

CONTENTS

1 Introduction

1.1 Background 1
1.2 Thesis Outline 2
1.2.1 Overview of Objectives 2
1.2.2 Content 3
1.2.3 Original Work 4
1.2.4 Additional Comments 5

2 Patient Vibration in Ambulances

2.1 Ambulance Vibration 7
2.2 Human Sensitivity to Vibration 7
2.2.1 Seated and Standing Subjects 7
2.2.2 Motion Sickness 9
2.2.3 Supine Subjects 9
2.3 The Effects of Ambulance Vibration on Patients 11
2.4 Approaches to Reducing Patient Vibration 12
2.4.1 Reducing Ambulance Speed 12
2.4.2 Purpose-Built and Modified Ambulances 12
2.4.3 Stretcher Suspensions 13

3 Design Philosophy and Mechanical Embodiment

3.1 Introduction 19
3.2 Requirement Specification 19
3.3 Linkage 20
3.3.1 Linkage Kinematics 20
3.3.2 Mechanical Embodiment 23
3.4 Isolators 25
3.4.1 Overview 25
3.4.2 Suspension Natural Frequencies 26
3.4.3 Rubber Bellows 26
3.4.4 Pneumatic Cylinders and Tank 27
3.5 Height Levelling 29
3.5.1 Pneumatic Isolator Analysis 29
3.5.2 Height Levelling Systems 31

4 Suspension Analysis and Characterisation

4.1 Introduction 35
4.2 Linkage Geometry 35
4.3 Analysis 37
4.3.1 Linkage Kinematics 37
4.3.2 Cylinder Analysis 39
4.3.3 Dynamics 41
4.3.4 Method of Solution 44
4.3.5 Suspension Natural Frequencies 45
4.4 Suspension Forces and Restoring Rates 47
4.4.1 Suspension Forces 47
4.4.2 Suspension Restoring Rates 48
4.5 Simulation Examples 50
4.5.1 Coupling 50
4.5.2 Forced Vibration 53
4.5.3 Stability During Braking 56

5 Pneumatic Damping

5.1 Introduction 57
5.2 Capillary Damping 57
5.2.1 Flow Through a Capillary 57
5.2.2 Analysis of Capillary-Damped Isolators 59
5.2.3 Characteristics and Applications 62
5.3 Orifice Damping 64
5.3.1 Flow Through an Orifice 64
5.3.2 Analysis of Orifice-Damped Isolators 65
5.3.3 Characteristics and Applications 66
5.4 Stretcher Suspension Damping 67
5.5 Modelling 67
5.5.1 Stretcher Suspension 67
5.5.2 Pneumatic Isolator 69
5.5.3 Ambulance 71
5.5.4 Road Profile 73
5.5.5 Method of Solution 73
5.6 Simulation Results 73
5.6.1 Suspension Response to Sinusoidal Vibration 74
5.6.2 Suspension Response to Ambulance Floor Vibration 75
5.6.3 Restriction Type Evaluation and Selection 77
5.7 Suspension Performance 79
5.7.1 Bounce 79

5.7.2 Pitch 80
5.8 Summary 81

6 Semi-Active Pneumatic Damping
6.1 Introduction 83
6.2 Active Suspensions 83
6.2.1 Classification of Active Suspensions 84
6.2.2 Active and Advanced Pneumatic Suspensions 85
6.2.3 Semi-Active Pneumatic Damping 87
6.3 Adjustable Pneumatic Damper Control 88
6.3.1 Skyhook Damping 88
6.3.2 Control Strategy 89
6.3.3 Orifice Control Law 91
6.3.4 Modelling 94
6.4 Simulation Results 94
6.4.1 Continuously Variable Damping 94
6.4.2 Switchable Damping 96
6.4.3 Comparison of Systems 96
6.5 Prospects for Implementation 98
6.5.1 Hardware 98
6.5.2 Adaptation 99
6.5.3 Evaluation 100
6.6 Summary 101

7 Laboratory Tests
7.1 Introduction 103
7.2 Shaker Table 103
7.2.1 Actuation Method 103
7.2.2 Mechanical Embodiment 105
7.2.3 Performance 109
7.2.4 Experimental Validation 110
7.3 Acceleration Measurement and Processing 110
7.3.1 Accelerometers and Accelerometer Amplifiers 110
7.3.2 Signal conditioning in Hardware 112
7.3.3 Signal Sampling and Storage 112
7.3.4 Signal Post-Processing in Software 113
7.4 Bounce Tests 114
7.4.1 Tests Performed 114
7.4.2 Bounce Tests Results 116
7.5 Coulomb Damping 118

7.5.1 Introduction 118
7.5.2 Characteristics 119
7.5.3 Simulation Model 120
7.5.4 Simulation Results 122
7.6 Pitch Tests 124
7.6.1 Tests Performed 124
7.6.2 Pitch Test Results 124
7.6.3 Suggestions for Future Testing 126
7.7 Summary 127

8 Road Tests
8.1 Introduction 129
8.2 Quantitative Testing 129
8.2.1 Instrumentation 129
8.2.2 Road Description 131
8.2.3 Bounce Test Results 131
8.2.4 Pitch Test Results 137
8.2.5 Comparison of Patient Pitch and Bounce 139
8.3 Subjective Evaluation 140
8.3.1 Ride Quality 140
8.3.2 Additional Observations 141
8.4 Summary 143

9 Summary and Recommendations
9.1 Introduction 145
9.1.1 Summary of Project Aims 145
9.1.2 Summary of Research Activities 145
9.2 Results of Study 146
9.2.1 Theoretical 146
9.2.2 Design 148
9.2.3 Experimental 149
9.3 Recommendations for Further Work 150
9.3.1 Further Testing 150
9.3.2 Suspension Modifications 151

References 153

Appendices 165

E ***Matlab Simulation Files - Pneumatic Damping***
E1 Ambsim.m 195
E2 Ambeq.m 206

F ***Laboratory Test Results*** 213

G ***Manufacturing Drawings*** 217

A Suspension and Load Data

A1 Linkage Geometry 165
A2 Cylinder Location 166
A3 Load Data 167

B Suspension Analysis

B1 Kinematics 169
B1.1 Linkage Kinematics 169
B1.2 Cylinder Kinematics 173
B2 Dynamics 173
B2.1 Linkage Forces 173
B2.2 Force Moment Arms 176
B2.3 Coupling of Coordinates 176
B2.4 Cylinder Static Pressures 177
B2.5 Equations of Motion 179

C Natural Frequencies

C1 Introduction 181
C2 Kinematics 181
C2.1 Link Angles 181
C2.2 Common Trigonometric Expressions 182
C3 Cylinder Analysis 183
C3.1 Cylinder Kinematics 183
C3.2 Cylinder Forces 185
C4 Dynamics 185
C4.1 Link Forces 185
C4.2 Load Equations of Motion 186
C4.3 Coupling of Coordinates 186
C4.4 Natural Frequencies 187

D Pneumatic Damping Analysis - Additional Equations

D1 Rates of Change of Pressure 191
D1.1 Tank 191
D1.2 Cylinder 192
D2 Temperatures Masses and Volumes 193
D2.1 Tank and Cylinder Temperatures 193
D2.2 Tank and Cylinder Masses 193
D2.3 Cylinder Volume 194

NOTATION

a	vertical distance between pivots C (or D) and E at equilibrium (m)
A_c	pneumatic cylinder area (m^2)
A_{or}	orifice area (m^2)
$A_x..J_x$	horizontal suspension forces at pivots $A..J$ (N)
$A_x'..J_x'$	suspension forces at pivots $A..J$ in x' direction (N)
$A_y..J_y$	vertical suspension forces at pivots $A..J$ (N)
$A_y'..J_y'$	suspension forces at pivots $A..J$ in y' direction (N)
b	vertical distance between pivots A (or B) and C (or D) at equilibrium (m)
c	horizontal distance between pivots C (or D) and E at equilibrium (m)
c_b	stretcher suspension damping coefficient (Ns/m)
c_e	equivalent damping coefficient (Ns/m)
c_p	specific heat at constant pressure for air (J/kgK)
c_{pass}	passive damping coefficient (Ns/m)
c_s	ambulance suspension damper coefficient (Ns/m)
c_{sky}	skyhook damping coefficient (Ns/m)
c_t	ambulance tyre damping coefficient (Ns/m)
c_v	specific heat at constant volume for air (J/kgK)
C_d	orifice discharge coefficient
C_R	capillary restriction coefficient (m^5/Ns)
d_c	capillary tube diameter (m)
d_{or}	orifice diameter (m)
e	horizontal distance between pivots A (or B) and E at equilibrium (m)
e_e	offset of load (patient and stretcher) from suspension centre (m)
f	vertical distance between pivots A (or B) and E at equilibrium (m)
f_y	suspension natural frequency in bounce (Hz)
f_θ	suspension natural frequency in pitch (Hz)
$\mathbf{f}$	vector of load forces (N) and accelerations (m/s^2)
$\mathbb{F}$	matrix of suspension load data (kg, kgm^2) and distances (m)
F	cylinder force (N)
F_c	Coulomb damping force (N)
F_d	demand damping force (N)
F_{ij}	element (i,j) of matrix $\mathbb{F}$ (m)
F_{sky}	skyhook damping force (N)

g	acceleration due to gravity (m/s^2)
h	vertical distance between load centre-of-mass and pivot A (or B) (m)
h_c	specific enthalpy of cylinder air (J/kg)
h_t	specific enthalpy of tank air (J/kg)
I_{pat}	patient inertia at offset ε_{pat} from patient centre-of-mass (kgm^2)
I_r	inertia of camshaft, cam and counterbalance assembly (kgm^2)
I_{str}	stretcher inertia at offset ε_{str} from stretcher centre-of-mass (kgm^2)
$\mathbb{J}^{-1}$	inverse Jacobian for suspension linkage
k, k_1, k_2	spring stiffnesses (N/m)
k_s	ambulance suspension stiffness (N/m)
k_t	ambulance tyre stiffness (N/m)
l	cylinder pivot separation (m)
l_1, l_2	cylinder pivot positions (m)
L_c	capillary tube length (m)
L_1	lower arm length (m)
L_2	pitch arm length (m)
L_3	stabilising arm length (m)
$\dot{m}$	air mass flow rate (kg/s)
m_c	cylinder air mass (kg)
m_{cb}	shaker table counterbalance mass (kg)
m_l	shaker table load (kg)
m_{pat}	patient mass (kg)
m_s	1/4 ambulance sprung mass (kg)
m_{str}	stretcher mass (kg)
m_t	surge tank (auxiliary reservoir) air mass (kg)
m_u	1/4 ambulance suspension unsprung mass (kg)
M	suspended load mass (kg)
N	tank/cylinder volume ratio
p	pressure (Pa)
p_{at}	atmospheric pressure (Pa)
p_c	cylinder absolute pressure (Pa)
p_t	tank absolute pressure (Pa)
$\dot{Q}$	rate of damping heat loss (J/s)
r	cylinder force moment arm (m)
r_c	shaker table cam radius (m)
r_{cb}	counterbalance mass stroke (m)
r_s	shaker table stroke (m)

R	gas constant for air (J/kgK)
R_y	linearised ratio of δ: y
$S(\upsilon)$	road displacement power spectral density (m^2/(cycle/m))
t	time (s)
$T(\omega)$	transmissibility
T_c	cylinder air temperature (K)
$T_{\lim}$	limiting value of acceleration transmissibility
T_t	surge tank (auxiliary reservoir) air temperature (K)
$\dot{\mathbf{u}}$	vector of suspension load and ambulance floor rates (m/s or rad/s)
u_c	specific internal energy of cylinder air (J/kg)
u_t	specific internal energy of tank air (J/kg)
$\dot{\mathbf{v}}$	vector of link angle rates (rad/s)
V_c	cylinder volume (m^3)
V_t	surge tank (auxiliary reservoir) volume (m^3)
$\mathbf{w}$	vector of cylinder moments (Nm) and load accelerations (m/s^2)
w	road spectral slope index
${}^1w_7$	first component of element 7 of vector $\mathbf{w}$ (m/s^2)
${}^2w_7$	second component of element 7 of vector $\mathbf{w}$ (m/s^2)
x	horizontal displacement of load centre-of-mass (m)
x_A	horizontal distance between pivot A and load centre-of-mass (m)
x_B	horizontal distance between pivot B and load centre-of-mass (m)
x_s	horizontal displacement of ambulance floor (m)
y	stretcher or load vertical displacement (m)
y_A	vertical distance between pivot A and load centre-of-mass (m)
y_B	vertical distance between pivot B and load centre-of-mass (m)
y_g	road profile height (m)
y_s	ambulance floor, shaker table, or input vertical displacement (m)
y_{ts}	ambulance tyre static deflection (m)
y_u	ambulance unsprung mass displacement (m)
α	angle of suspension lower arm (rad)
β	angle of suspension pitch arm (rad)
δ	pneumatic cylinder extension (m)
Δ	small (usually linear) change in quantity
ε_{pat}	offset from patient centre-of-mass (m)
ε_{str}	offset from stretcher centre-of-mass (m)
γ	ratio of specific heats for air
κ	road roughness coefficient (m^2/(cycle/m)$^{(-w+1)}$)

μ	dynamic viscosity of air (kg/ms)
θ	stretcher rotation in pitch (rad)
θ_c	shaker table cam rotation (rad)
θ_s	ambulance floor, or shaker table rotation in pitch (rad)
ρ_c	cylinder air density (kg/m^3)
ρ_t	tank air density (kg/m^3)
υ	wave number (cycle/m)
ω_n	natural frequency (Hz)
ω_y	suspension natural frequency in bounce (rad/s)
ω_θ	suspension natural frequency in pitch (rad/s)
ξ	damping ratio
ξ_{sky}	skyhook damping ratio
ξ_y	suspension bounce damping ratio
ξ_θ	suspension pitch damping ratio
ψ	cylinder angle with suspension base frame (rad)

Additional Subscripts

0	static, equilibrium, or initial value
L	left-hand end of linkage
pat	patient
R	right-hand end of linkage
str	stretcher
x	horizontal
y	vertical or bounce
θ	rotational or pitch

CHAPTER 1

Introduction

1.1 BACKGROUND

The word ambulance is derived from the Latin word *ambulant*, which means walking. Horse-drawn military vehicles, which were equipped to dress wounds and accompanied soldiers into the field during the Napoleonic Wars, are considered as the forerunners of modern ambulances. Some were used as field hospitals, and others transported wounded soldiers to hospital [1]. Transport in these basic vehicles over the poor roads of the time must have been very uncomfortable. While modern ambulances generally travel over very much better surfaces, the road-induced vibration experienced by patients during the journey to hospital can still be unpleasant and/or harmful. The vibration of patients in ambulances has been the subject of a number of papers over the past 30 years, and the research effort in this area emphasises both that the problem is a very real one and that the quality of the ambulance suspension is an important influence on patient comfort.

Early suspensions for horse-drawn carriages, as the name suggests, literally did suspend the body of the carriage at the four corners by the use of very flexible laminated steel springs. In 1804, Obadiah Elliot revolutionised coach suspension design by mounting the coach body directly onto elliptical leaf springs attached to the axles [2]. Suspensions developed for the first automobiles used this same approach, and up until the 1960's, multi-leaf rear suspensions were the standard for mass produced cars. Modern suspension design for passenger vehicles has now polarised toward the use of coil springs [3]. In recent years, active suspensions have been proposed, and some have been tested. None have enjoyed widespread commercial production, and this is likely to remain the case for some time, given their increased cost and complexity over passive suspensions which are adequate for the majority of applications [4,5,6].

In a number of countries, including New Zealand, ambulance suspensions are based on those of commercial vehicles, and these often give a relatively poor ride. While purpose-built ambulances can offer improved isolation, they remain expensive due to the limited numbers required. A potentially lower cost alternative is to provide a secondary suspension for the stretcher and patient only.

The approach of using a stretcher suspension to reduce patient vibration is not unique to this thesis, and the literature contains a number of designs for stretcher suspensions.

Some of these designs have entered production and are used in a number of countries. A variety of spring types have been employed including torsion bars, coil springs, and hydro-pneumatic springs. The suspension developed during this research project uses pneumatic springs. These are ideally suited to the application, and are a well-accepted choice for high performance isolation systems.

While there are no examples of stretcher suspensions that use purely pneumatic springs (as distinct from hydro-pneumatic springs), examples of the use of pneumatic springs in other applications are numerous. Typical items of equipment that are isolated using pneumatic springs include an electron microscope [7], a fatigue testing machine [8], vehicle seats [9], a swimming pool [10], and tables for sensitive experiments and manufacturing processes [11-14]. Pneumatic springs are also used as shock/impact absorbers, although to a much lesser extent [15,16].

The use of pneumatic springs for road vehicles has long been of interest, and was first considered in the early part of this century. Patents were granted from 1906. Experience during the early 1950's in America, particularly on long distance coaches, established the use of pneumatic isolators as a good suspension method [17]. Following on from this, American automobile manufacturers fitted pneumatic suspensions to passenger vehicles in the late 1950's [18-25]. Their widespread use was, however, short lived. More recently, pneumatic suspensions have been used by Ford on the Lincoln Continental [26], by Land Rover on the Range Rover [27,28], by Toyota on the Soarer [29,30], and by Mitsubishi on the Galant [31]. Pneumatic suspensions are also used for improving the ride of passenger train carriages [32-35].

A key advantage of pneumatic suspensions over fixed stiffness mechanical suspensions is that they can readily be adapted to suit the mass of the load. This makes them particularly suitable for trucks, where laden/unladen sprung mass ratios can be high [36-38].

1.2 THESIS OUTLINE

1.2.1 Overview of Objectives

The original intention of this research project was simply to design, build, and test a pneumatic stretcher suspension which would provide an improved alternative to the suspensions currently in use. Key areas targeted for improvement were in terms of :

- Reducing weight.
- Reducing cost.
- Reducing encroachment onto valuable ambulance floorspace.

- Improving isolation levels (particularly at low frequencies).

These items are addressed in further detail in Chapters 2 and 3.

As the project progressed, effort became focused on evaluating various methods of pneumatic damping, and it became apparent that (1) there was scope for original research in this area, and that (2) pneumatic damping was a topic of research in its own right. Consequently, the chapters of this thesis which deal with pneumatic damping were useful not only in choosing a damping method for the stretcher suspension, but also for evaluating the properties of some pneumatic damping methods in general. The methods of pneumatic damping considered were:

- Capillary damping.
- Orifice damping.
- Semi-active damping (switchable and continuously variable)

Broadly then, the objectives of this thesis can be summarised as follows:

- To design, simulate/model, build, and test a pneumatic stretcher suspension aimed at providing an improved alternative to the suspensions currently in use.
- To review the literature on, and then compare by simulation, the performance of orifice, capillary, and semi-active pneumatic damping methods.

1.2.2 Content

Chapter 2 of this thesis begins by describing the nature of ambulance floor vibrations and the sensitivity of the human body to vibration. Examples of patient deterioration resulting from ambulance transport are then given and the methods used to improve patient comfort are summarised.

Following on from this, Chapter 3 describes the suspension linkage developed during this project and presents an overview of the functions and mechanical embodiment of various suspension components.

Considerable work has been done in analysing the dynamics of the suspension. This is summarised in Chapter 4. The method of analysis is first given and then some simulation results are presented which characterise the behaviour of the suspension. Both free and forced vibration are considered. Analytical expressions for the natural frequencies of the suspension are also developed.

In Chapter 5, orifice and capillary damping restrictions are compared. The comparisons are made first by way of a literature review, and then by simulation.

Chapter 6 goes on to consider semi-active pneumatic damping. To begin with some literature dealing with active and advanced suspensions is reviewed. Following this, simulation results are presented which illustrate that improvements to suspension performance are possible by using an adjustable pneumatic damper (rather than a passive pneumatic damper).

Chapter 7 first describes the results of laboratory tests and then makes comparisons with theoretical predictions. Differences between the experimental and theoretical results are explained by considering the detrimental effects of Coulomb damping.

In Chapter 8, road test results are described and the performance of the suspension is compared with existing designs. Subjective evaluations of ride quality are also made.

Finally, in Chapter 9, the key research findings are summarised, an overview of the features and performance of the stretcher suspension is given, and suggestions are made for improvements to the design would could be included in a production model.

1.2.3 Original Work

As far as the author is aware, the following areas of research are innovative and/or original:

- The linkage used for the suspension and the natural frequency expressions which were derived for it appear to be original.
- The literature review of pneumatic damping methods for suspensions and isolation systems appears to be the most comprehensive to date.
- The modelling and simulation of pneumatic damping methods uses a random input. In studying pneumatic damping methods, other researchers appear to have used (1) sinusoidal inputs, or (2) no input at all (free-vibration). This can be an unsatisfactory approach for certain types of damping.
- The performance of the suspension when fitted with semi-active pneumatic dampers has been modelled. This appears to be the first time that consideration has been given to using a compressible damping fluid in an adjustable damper.
- While the shaker table designed for this project is rather basic, and is capable of providing only simple sinusoidal inputs, its layout appears to be unique.

1.2.4 Additional Comments

For the most part, the theoretical and simulation work described in this thesis is intended to be either (1) useful in designing the suspension (eg. natural frequency equations), or (2) of interest from a more general point of view (eg. pneumatic damping). The experimental work is intended mainly to confirm key suspension parameters and provide initial indications of suspension performance. Aspects of suspension behaviour which cannot be either altered at the design stage or tuned during experiments are not considered in detail. Coupling, for example, receives only limited attention for these reasons.

Much of the research effort for this thesis has involved simulation work, and while the initial process of setting up and checking a simulation model was time consuming, generating a large number of results was relatively easy (once the model was working). In the interests of conciseness however, only key results are included here.

CHAPTER 2

Patient Vibration in Ambulances

2.1 AMBULANCE VIBRATION

Many ambulances are based on commercial vehicle chassis. In New Zealand, the Bedford CF chassis has been widely used [39] but is being replaced by the likes of the Fiat Ducato [40] and the Leyland Daf [41]. In the United Kingdom, similar vehicles are used [42,43].

Chassis of such commercial vehicles can give a poor ride compared to that of a typical car. Measurements presented by Snook [44] showed that on a medium quality road travelled at 64 km/h, the vertical r.m.s. acceleration in an ambulance was 0.06g, while that for a quality European automobile was 0.03g. In Figure 2.1, which is reproduced from [44], the vertical vibration in an ambulance, a research ambulance, and a private car are compared. The ride of the standard ambulance is shown to be poor compared with that of the car. This is partly a function of the natural frequency of ambulance suspensions, which are generally higher than those of a car, and typically between 1.2 and 2 Hz [45].

According to Leyshon and Stammers [46], who cite Oliver and Holt [47] among others, the dominant floor vibrations in ambulances are generally in the vertical sense and peak around 1.5-2 Hz. At higher frequencies, the acceleration levels reduce until resonances are met beyond 10 Hz.

2.2 HUMAN SENSITIVITY TO VIBRATION

2.2.1 Seated and Standing Subjects

Human response to vibration has been the subject of numerous documented studies [48]. The first studies appeared from 1918 and considered the effects of locally applied hand-arm vibration from power tools. Since World War II, the literature has covered whole-body vibration in passenger cars, earth-moving equipment, aircraft, and ships.

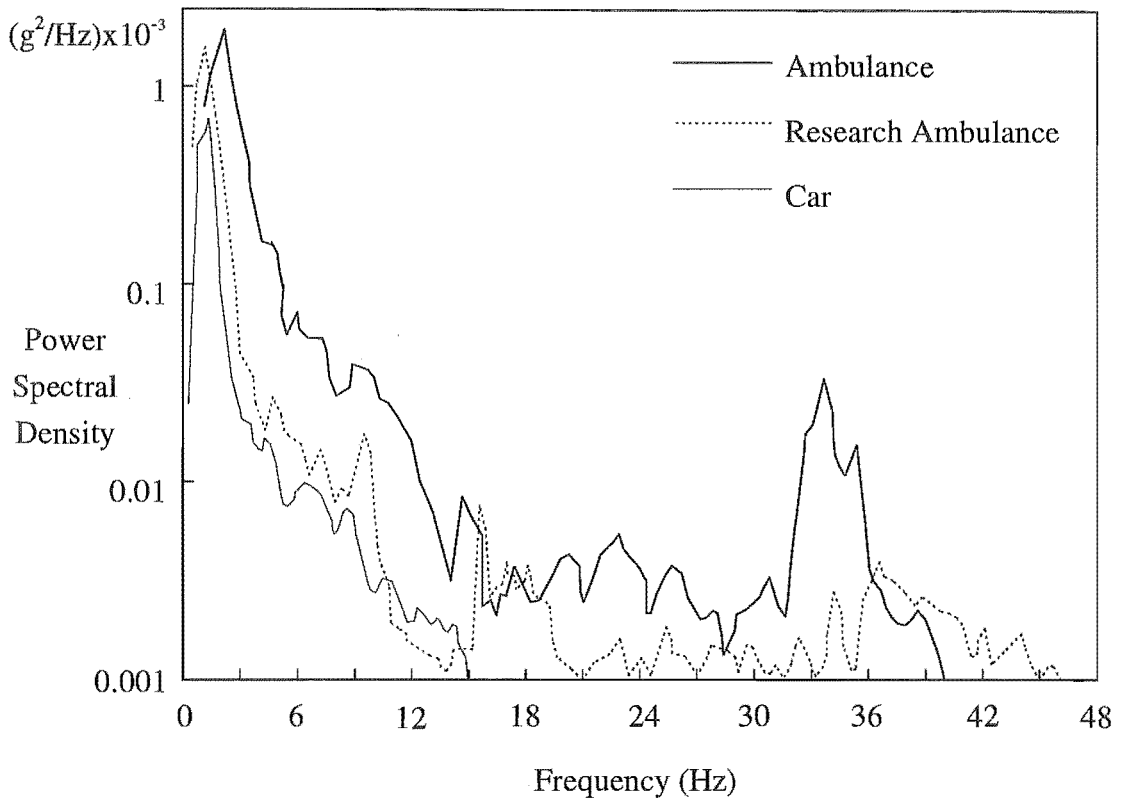

Figure 2.1 The Vertical Acceleration Power Spectral Density in an Ambulance, Research Ambulance, and Private Car (Reproduced from Snook [44])

Von Gierke and Goldman [49] review this literature, and discuss rather comprehensively mechanical modelling and resonances of the human body; the methods of testing and measurement of human response to vibration; and the physiological and mechanical effects of shock and vibration.

The bulk of research investigating human response to vibration has dealt with standing or seated subjects and has lead to the definition of vibration limits for the frequency range 1-90 Hz [50]. These limits set out the acceleration (as a function of vibration frequency and exposure duration) which causes reduced comfort, fatigue-decreased proficiency, or, should not be tolerated further (exposure limit). The utility of this approach is widely accepted, although there are differences between the reported frequency effects of vertical vibration [51]. The exact response of an individual to a particular vibration will depend on a host of factors in addition to the level of acceleration, its frequency, and the duration of exposure to it [48,52,53].

In some instances, pitch and roll may be more disturbing than other motions - particularly in tractors travelling over rough terrain or in aircraft during turbulence. Little or no information on the effects of such angular (or rotational) vibration is yet available [50].

2.2.2 Motion Sickness

Low frequency vibration, in the range 0.1-1 Hz, can cause motion sickness (kinetosis) [48,49,51]. This sickness has a different character to the effects of higher frequency vibrations, and the appearance of symptoms depends on complicated individual factors which are not simply related to vibration intensity, frequency, or duration of exposure [50]. Draft ISO limits, discussed by von Gierke and Goldman [49], indicate that peak sensitivity to vibration in this low frequency range occurs between 0.1 and 0.3 Hz.

Aside from the considerations of comfort, nausea induced by low frequency ambulance vibration could affect the survival of some patients (due to the effort expended by vomiting [44]).

2.2.3 Supine Subjects

The sensitivity of supine subjects (which is the posture for stretcher-borne patients) to vibration has received much less attention than seated or standing subjects.

Motivated in part by the comfort of passengers on rail-cars and ships, Miwa and Yonekawa [54] studied the response of supine subjects to vertical and horizontal vibration ranging from 0.5-300 Hz. Their paper first refers to the early work of Reiher and Meister [55], which was published in 1931, and then presents constant comfort curves for the vertical and horizontal directions by comparing sensitivity with the seated case (for which constant comfort curves exist [50]). They found that, for horizontal inputs, the direction of input (along or across the supine subject) made no difference to sensitivity across the full range of frequencies. Peak sensitivity occurred at low frequencies (0.5-3 Hz), and reduced with increasing frequency. Peak sensitivity to vertical vibration occurred at around 6 Hz.

As part of a study seeking to (1) reduce levels of patient vibration in ambulances, and (2) improve the comfort of bunks on buses used for over-night journeys, Chen and Gao [56] have generated constant comfort curves for supine vertical vibration. They report that peak sensitivity is at 6.3 Hz.

Oliver and Gibson [57] present vibration limits which define the sensitivity of healthy stretcher-borne subjects to vibration in three translational and two rotational modes. According to Leyshon and Stammers [46], these limits show that the sensitivity of the supine subject to side-to-side vibration is greatest below 2 Hz, while peak sensitivity to front-to-back vibration is greatest in the range 4-6 Hz. Over the frequency range studied (1.5-6 Hz), there was little variation in sensitivity to pitch vibration with frequency.

In a later paper, Stammers [58] comments further on the vibration limits of Oliver and Gibson [57] and emphasises that the supine patient is more sensitive to vibration than a standing or seated subject (as given by [50]). Figure 2.2, which is reproduced from [46], exemplifies this and shows that, in the range 4-8 Hz, the level of front-to-back vibration that is tolerated for 2.5 hours by a seated subject is tolerated for only five minutes by a supine subject.

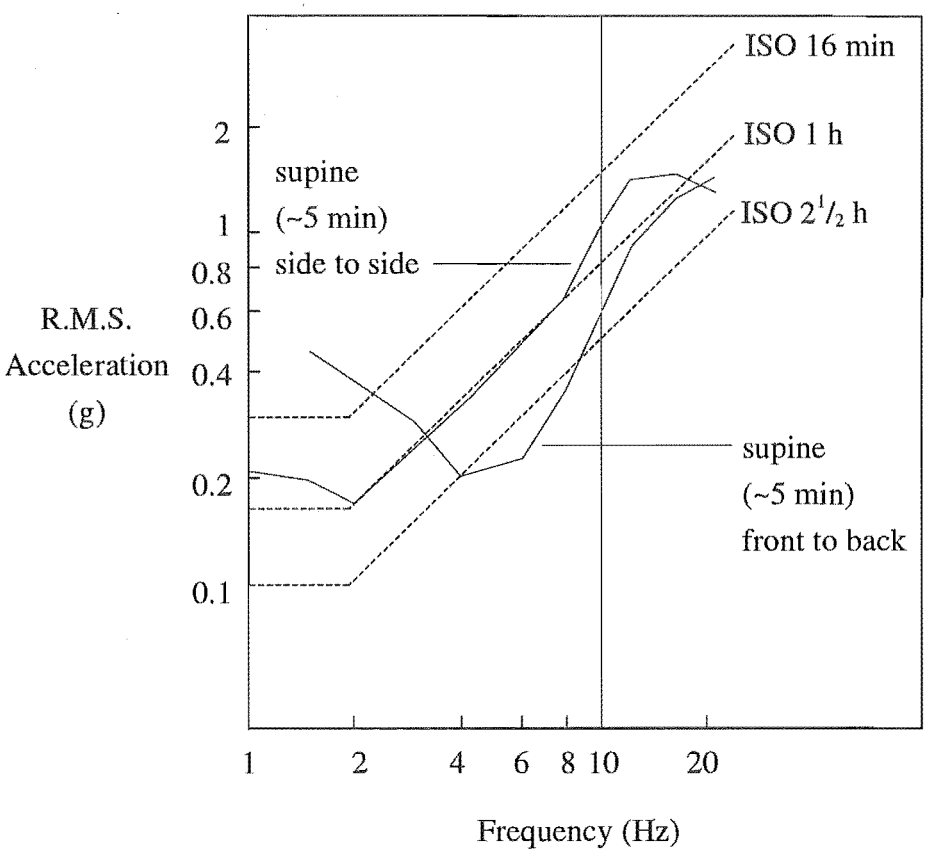

***Figure 2.2** Exposure Limits for Seated and Standing Persons (ISO 2631:1974) Compared with Supine Persons (Oliver and Gibson [57])*

The findings of [54],[56], and [57] are consistent in that peak sensitivity to vertical vibration for the supine subject occurs at around 6 Hz, and that peak sensitivity to horizontal vibration occurs at a lower frequency. These peak sensitivities coincide with resonances of sub-systems within the body, as discussed by von Gierke and Goldman [49].

2.3 THE EFFECTS OF AMBULANCE VIBRATION ON PATIENTS

Ambulance floor vibration has been shown to be detrimental to the condition of injured or seriously ill patients [59]. This is likely to be due in part to:

- The relatively high levels of ambulance floor vibration at frequencies where patient sensitivity is high (Sections 2.1, 2.2.3).
- The reduced tolerance of humans to vibration when in the supine position (Section 2.2.3).
- The reduced tolerance of the ill or injured to vibration.

A number of accounts of vibration-induced patient deterioration have been published by various authors. Some of these are mentioned below.

Cullen et al [60] give an account of a road accident victim dying after being transferred between hospitals by ambulance. This is in spite of the journey being over good roads at limited speeds (32-48 km/h). The poor quality of the ambulance ride is noted, and is regarded as being an important secondary factor in his death.

Snook [44] describes a number of cases of patient deterioration associated with ambulance travel, and cites one instance where the visible vertical jogging of a patient's badly fractured leg was severe enough to warrant stopping the ambulance. Snook also reviews the research of Pichard [61], who described a series of 430 ambulance journeys in which 6 % resulted in movement-related cardiovascular disturbances (ie. rise or fall in blood pressure).

The effect of ambulance transport on critically ill patients transferred to an intensive therapy unit from local hospitals has been studied by Waddell et al [62]. Cardiovascular response was noted in 19 of 46 patients. This was thought to result from the discomfort and pain experienced during the journey; the lack of facilities in the ambulance; and the motion of the ambulance (which reduced the ability of the attendants to provide treatment). A second group of patients was transferred where special care was taken that (1) the journey was slow and gentle, and (2) continuing medical attention was available. In this group, the detrimental effects of the journey were both less frequent and less severe.

In another paper, Waddell [63] studied the effects of moving critically ill patients within hospital. He first briefly reviewed the literature, and then described his own five month investigation - the results of which emphasise the sensitivity of critically ill patients to movement of any kind, whether it be in an ambulance or within hospital. In particular,

the vulnerability of patients with major chest injuries is noted, along with the problem of renewed bleeding resulting from fracture movement.

Wheble [64] notes the low tolerance to vibration of patients suffering severe pain. As an example, he refers to cancer sufferers with secondary deposits on the spine who need repeated radiotherapy treatments. For these patients, the vibration associated with the ambulance journey to and from hospital is often distressing, with some patients refusing to attend treatment.

2.4 APPROACHES TO REDUCING PATIENT VIBRATION

2.4.1 Reducing Ambulance Speed

Although reducing ambulance speed is a common approach to reducing ambulance floor vibration [46,58], it is not an ideal solution. This is because of the increased time between the patient becoming ill (or injured) and hospital treatment. Minimising this time has been shown to be important to patient survival, particularly where injuries involving severe blood loss are concerned and prompt surgical treatment at a hospital is required [65].

2.4.2 Purpose-Built and Modified Ambulances

Purpose-built ambulances (and ambulances based on substantially modified commercial vehicle chassis) have been proposed and are used in some countries.

London [67] describes an early example of a special purpose ambulance which was designed by Bothwell [66]. This featured front wheel drive with independent suspension but never went into production. Cullen et al [60] refer to the merits of the ambulances based on the Citroën Safari which were used on Spanish and French roads.

Snook [44] tested a prototype research ambulance developed by Dennis Bros and measured a reduced level of vibration compared to commercially available ambulances (Figure 2.1). This ambulance was expensive and did not go into production [45].

At reduced cost, modular bodied ambulances (which use a removable spring unit secured to a commercial vehicle chassis) have been developed by Porsche in Germany [45], and by the Dodge Motor Company in the United States of America [68]. The latter used a hydro-pneumatic system.

Wheble [64] refers to the Citroën ambulance which uses the well known hydro-pneumatic suspension, and to the work of some ambulance authorities in the United Kingdom who have considered modifications to the Ford Transit and the Bedford van. More recent developments are described by [43], who mentions the pneumatic suspension conversions manufactured by CRD Sparshatt which are available for the likes of the Renault Master, Fiat Ducato, and the Volkswagen Transporter.

While such special purpose ambulances and ambulances with modified suspensions offer improvements in ride (compared to using a substantially standard commercial vehicle chassis), a high proportion of ambulance work (96 % in the United Kingdom [64]) involves transportation of people to hospital for non-urgent appointments (where a good ride is not of prime importance). Consequently, it is hard to justify the cost associated with reducing ambulance floor vibration for the needs of the 4 % who are critically ill or injured.

From the point of view of reducing both travel time and vibration, the helicopter can be regarded as an ideal ambulance [58,64,65]. It is not, however, a realistic alternative to the road ambulance for the majority of journeys, given its high cost [58] and requirement for suitable landing and take-off areas.

2.4.3 Stretcher Suspensions

a) Review

As an alternative to focusing on reducing ambulance floor vibration, additional suspension can be provided for the stretcher only. This approach offers no improvement in the ride for the ambulance attendants, but does give the opportunity to provide good isolation for the patient at a lower cost than if the ambulance suspension was improved. In theory, better isolation is possible by using a stretcher suspension as the designer is freed from the constraints imposed by vehicle handling considerations. These dictate the use of spring and damper rates that are too high for best isolation, but must be used to control vehicle attitude during manoeuvring.

For good levels of isolation, a stretcher suspension should:

- Have a low natural frequency - preferably 1.0 Hz or less to provide isolation at 1.5 Hz where ambulance floor vibrations are significant.
- Be capable of adapting to suit the mass of the patient which could range from 30-130 kg [45]. In practice, this requires that (1) the stiffness of the springs should increase with load to give a constant natural frequency, and that (2) the ride height should be independent of load. In the absence of any load

adaptation, low stiffness suspensions (which are more sensitive to load change than stiff suspensions) function poorly and can be unusable for extremes of load.

An obvious and simple approach to providing additional suspension for the patient is to use a polyurethane foam mattress which stiffens under load. To provide a suitably low natural frequency (say 0.8 Hz), a foam thickness of at least 700 mm would be required, and this would be impractical [45].

Several designs for stretcher suspensions have appeared in the literature. The discussion to a paper by London [67] shows a torsion bar stretcher suspension designed by Dr J.R. Singham of BMC, which included a pendulum and lever system to pivot the suspension about its longitudinal axis when cornering. No mention was made of the ability of the suspension to adapt to patient mass. Reportedly, 10% of those using the suspension in a trial experienced motion sickness. This was thought to be partly a result of the disconcerting visible movement of the ambulance walls relative to the suspended patient.

Blok [69] describes a four degree-of-freedom system developed at the University of Delft for which specifications are given in Table 2.1. Suspension was provided by two independent mechanical systems which used a spring acting through a lever and movable pivot. By adjusting the pivot position with an electric motor, a load-independent ride height was achieved. Roll and transverse suspension were combined in a compound pendulum system which aligned itself with the resultant acceleration associated with vehicle cornering or road camber.

***Table 2.1** Specifications of the Dutch 'Floating Stretcher' Prototype [69]*

Degree-of-Freedom	*Natural Freq. (Hz)*	*Load Adaptation*	*Stroke (top-top)*
Vertical	0.6	load-independent	400 mm
Pitch	0.7	practically load-independent	30°
Horizontal	1.5	load dependent	60 mm
Roll/Transverse	0.6	load-independent	12°, 120 mm

Snook and Pacifico [59] report on the performance of the so-called Dutch 'floating stretcher' developed by Blok. This stretcher offered a reduction of 42 % in vertical r.m.s. acceleration, and best isolation was realised in the 3-10 Hz range. Subjective ride tests with 100 patients, of whom 91 could grade the ride, led to 47 classifying the ride as

very good, 33 good, 7 average, and 4 fair. Generally, the suspension evoked a positive response on the smoothness of the ride. Unlike the system described by London [67], only 4 of the patients admitted to any feeling of nausea, and then only when specifically asked. Importantly, the attendants ability to provide treatment for the patient was not adversely affected by the floating action of the stretcher. This suspension was heavy and expensive, costing £5,000 (1976).

Dalyell [70] described a patented system, designed by Black [71] at the University of Bath, which used British Leyland Hydragas units as springs and provided isolation in pitch and bounce. At the same University, Stammers and Leyshon have developed a system also providing pitch and bounce isolation. The basic principle of operation is similar in some respects to that of Blok [59,69], in that variable lever arms and mechanical coil springs are used, but the design is simpler and more compact [45,68]. The system has a vertical natural frequency of 0.9 Hz and a vertical stroke of about 100 mm up or down, although in operation normal relative travel is less than 50 mm up or down. Road and shaker tests, which are described by Leyshon and Stammers [46], indicate that good levels of isolation are obtained (see Chapter 8 for details). This suspension is now sold commercially in the United Kingdom and is used by a number of ambulance services. By 1991 approximately 100 had been sold [58].

Stretcher suspensions are also used in France and Germany, and are described by Stammers and Leyshon [45,68]. The French system, which is marketed by Petit, uses a hydro-pneumatic approach developed by BINZ and has a natural frequency in the range 0.5-0.7 Hz. The German system of Miessen appears to be similar to that of the Dutch system of Blok [59,69]. A natural frequency of 1 Hz is claimed for a wide range of patient masses.

b) University of Canterbury Suspensions

At the Department of Mechanical Engineering (University of Canterbury), three undergraduate students have worked on pneumatic stretcher suspensions. The first work was done by Sutton [72] in 1986 who first reviewed the problem of patient vibration and then designed, built, and tested (in the laboratory) a pneumatic stretcher suspension. Following on from this work, additional final year projects were completed by Wylie [73] in 1989, and Pettigrew [74] in 1991. All three students used suspensions based on the scissor linkage. This linkage gives a single degree-of-freedom in bounce. Springing was provided by rubber air bags. Although differing slightly in detail, the suspensions of all three students were conceptually similar (Figure 2.3).

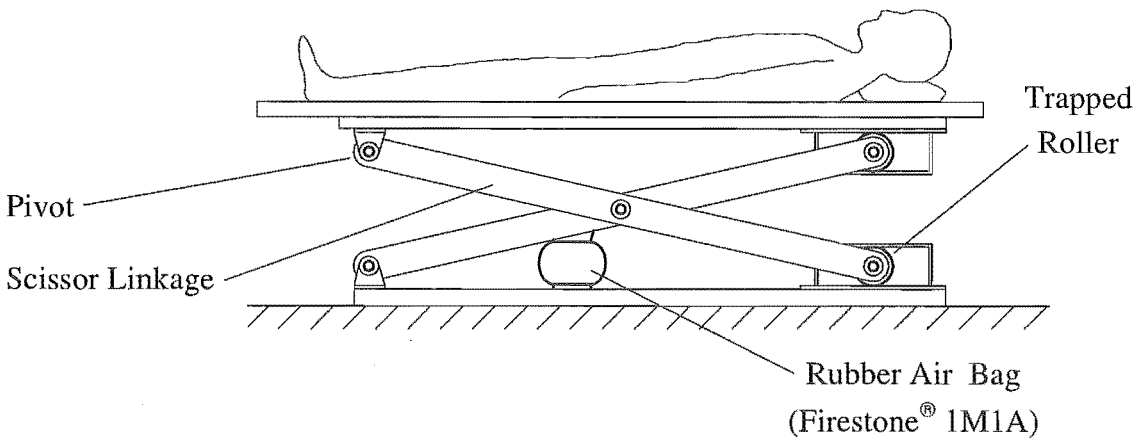

***Figure 2.3** Schematic Showing Key Features of Previous University of Canterbury Stretcher Suspensions*

Only the suspension designed by Pettigrew [74] was tested in an ambulance. It was found that the stroke was insufficient to cope with the worst bumps. In addition, measurements indicated that there was little isolation occurring below 3 Hz. This was due to the natural frequency of the suspension being too high at 2 Hz - well above its design value of around 1 Hz. As part of the preliminary work completed for this thesis, the cause of the poor agreement between the theoretical and measured natural frequencies was investigated. The following two problems were identified:

- An orifice was included in the pneumatic circuit to provide damping [74]. As explained in detail in Chapter 5, orifice size affects not only pneumatic damping level but also system natural frequency. This relationship was not considered by Pettigrew, and the small orifice size he employed had the effect of increasing natural frequency.
- Wylie's analysis of the stiffness of a pneumatic spring contained errors. This mistakenly lead him to believe that a sprung accumulator should be included in his pneumatic circuit. Pettigrew, in basing his work on Wylie's report, also unnecessarily included a sprung accumulator. This lead to differences between the predicted and actual natural frequencies. Additional detail on this can be found in the appropriate student reports [73,74]. The correct analysis for the stiffness of a pneumatic spring is presented in the following chapter.

In spite of these problems, subjective impressions from 'patients' riding on the suspension of Pettigrew were good [75].

c) Active Stretcher Suspensions

A more sophisticated alternative to the passive stretcher suspensions described thus far is to use an active suspension. Sharp [76] comments that this is a good application for

active suspension technology, while Craighead [77] has simulated the performance of a single degree-of-freedom active hydraulic stretcher suspension. His results show that superior isolation is possible compared to using a passive system. Naturally, such active suspensions would be expensive and unlikely to enjoy widespread use.

d) Critical Evaluation

While the suspensions currently in use are effective to various degrees, some of the mechanical systems tend to be rather heavy. The suspended part of Blok's system, for example, weighs 50 kg when unloaded [69]. The total weight of the suspension, which includes the base and electric motors, is somewhat greater than this which makes transfer of the unit between ambulances awkward.

Most designs of suspension do not accept a standard wheeled stretcher such as is used in New Zealand or the UK - the design of Leyshon and Stammers [46] being a notable exception. In addition, it is common practice for the suspension units to be located centrally on the ambulance floor. This is necessary because of their bulk, and limits the ambulance to transporting only one patient at time.

Some systems are thought to be unnecessarily complex. This introduces penalties not only in terms of size and weight, but also cost - the four degree-of-freedom system of Blok for example costs about 25% of that of an ambulance [68].

The suspension described in this thesis aims to provide an alternative to the systems currently in use but without drawbacks discussed above. This is addressed further in the following chapter.

CHAPTER 3

Design Philosophy and Mechanical Embodiment

3.1 INTRODUCTION

In this chapter, the suspension developed as part of this thesis is introduced. To begin with, the geometry of the linkage is described and details of its construction are given. The pneumatic springs and associated height levelling circuits are then discussed.

3.2 REQUIREMENT SPECIFICATION

The following was used as the requirement specification for the suspension:

- Isolate pitch and bounce.
- Have low natural frequencies.
- Have a long stroke.
- Have a load-independent ride height.
- Have a load-independent natural frequency.
- Have a load-independent damping ratio.
- Incorporate features to prevent pitch due to ambulance braking.
- Accommodate patient masses from 30-130 kg.
- Accept a standard wheeled stretcher.
- Allow roll on/off loading/unloading of the stretcher.
- Be compact and capable of fitting around the ambulance wheel arch.
- Have a low weight.
- Have a low cost.
- Be easy to use.

These items are in no particular order.

3.3 LINKAGE

3.3.1 Linkage Kinematics

a) Isolated Vibration Modes

Ideally, a stretcher suspension would provide isolation for the patient in all six degrees-of-freedom. Of these degrees-of-freedom, the dominant vibrations of the ambulance floor are in bounce, pitch, and roll. As far as the patient is concerned, pitch is more harmful than roll because the stretcher is aligned parallel to the ambulance roll axis. Lateral, longitudinal, and yaw ambulance floor accelerations tend to result from vehicle manoeuvring (rather than road induced vibration) and are steady (long period) rather than vibratory. Hence they are difficult to isolate.

In light of this, and in the interests of keeping costs low, it was decided to design a suspension which would provide isolation in two degrees-of-freedom only - bounce and pitch. Others designers working with two degree-of-freedom systems have also chosen to isolate bounce and pitch [45,71].

b) Suspension Pitch-Centre

Location of the pitch-centre in relation to the centre-of-mass of the load (ie. patient and stretcher) is an important consideration in choosing a suspension geometry that will provide pitch isolation. Initially, a linkage which had a pitch-centre at ambulance floor level was considered [75]. It was thought that this arrangement could reduce longitudinal patient vibration associated with floor pitch. (The patient is situated some distance above the ambulance floor, so that pitch of the floor results in longitudinal vibration of the patient.) However, as a low natural frequency was desired, this design tended to dive during ambulance braking and squat during acceleration. Other stretcher suspensions have used locking devices which prevent pitch during ambulance braking [45], but it was thought best to avoid this complication.

It was therefore decided to locate the pitch-centre at the centre-of-mass of the load. While this approach does reduce pitching due to longitudinal acceleration of the ambulance, there is no opportunity to provide isolation of longitudinal stretcher vibration associated with floor pitch.

There are a number of methods by which the pitch-centre can be situated at the load height in a stretcher suspension. The suspension designed by Leyshon and Stammers,

for example, uses a pivot located at the load centre-of-mass height. This pivot slides on a vertical shaft which is mounted to one side of the suspension [46].

In the interests of designing a suspension which would fit entirely beneath the stretcher, it was decided to use a linkage with kinematics which would locate the pitch-centre in the desired way. This linkage is shown in Figure 3.1. It is believed to be original. In the position shown, the suspension is at its equilibrium height (design height) and the angles of the pitch arms AC and BD are such that the instantaneous centre-of-pitch (which is situated at the imaginary intersection of the links AC and BD) is near the centre-of-mass of the load. Naturally, as the suspension moves (Figure 3.2), the position of the pitch-centre alters with respect to the load. In practice, this effect is small enough not to be important (refer to Chapter 4, Section 4.5.3).

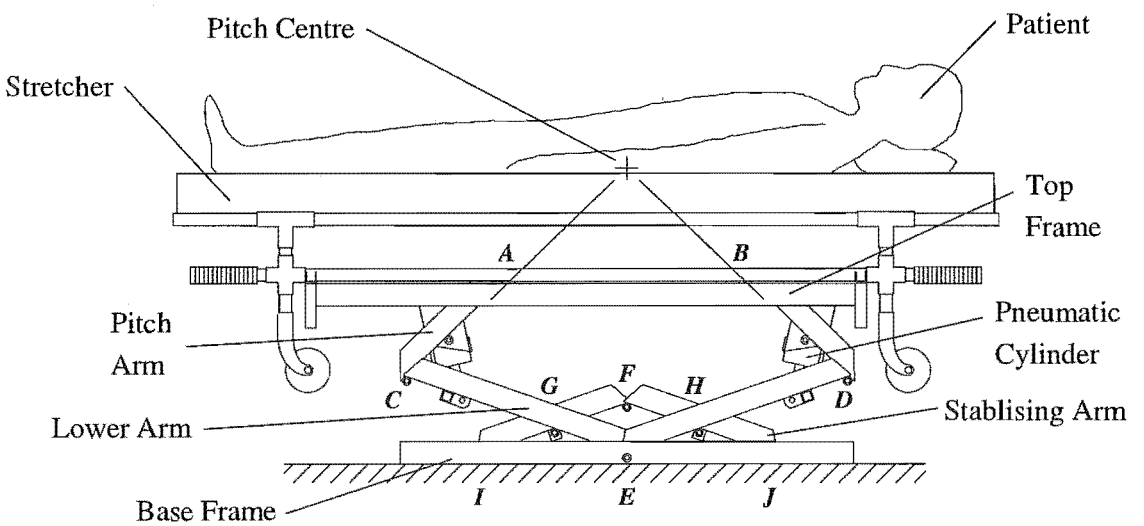

***Figure 3.1** The Suspension Linkage at Equilibrium*

c) Linkage Geometry

The lengths of the links of the suspension shown in Figure 3.1 are given in Appendix A1 and were chosen to provide the suspension with:

- Equal natural frequencies in bounce and pitch.
- A working space (stroke) in bounce and pitch sufficient to prevent frequent contact with the bump/rebound buffers. (While bump/rebound buffers were not fitted to the prototype suspension they would be included in a production version).

- A collapsed height of less than 250 mm to allow roll on/off loading/unloading of the stretcher.
- Long pitch links to reduce the change in pitch-centre with suspension movement.

d) Range of Movements

As shown in Figure 3.2, pitch of the stretcher is accommodated by the upper arms *AC* and *BD*. During vertical motion, both the pitch arms (*AC* and *BD*) and lower arms (*CE* and *DE*) move.

From the design ride height there is ±160 mm of useful suspension working space in bounce - this being typical of that for other stretcher suspensions [58,69]. The lowest 25 mm of vertical stroke is used for loading.

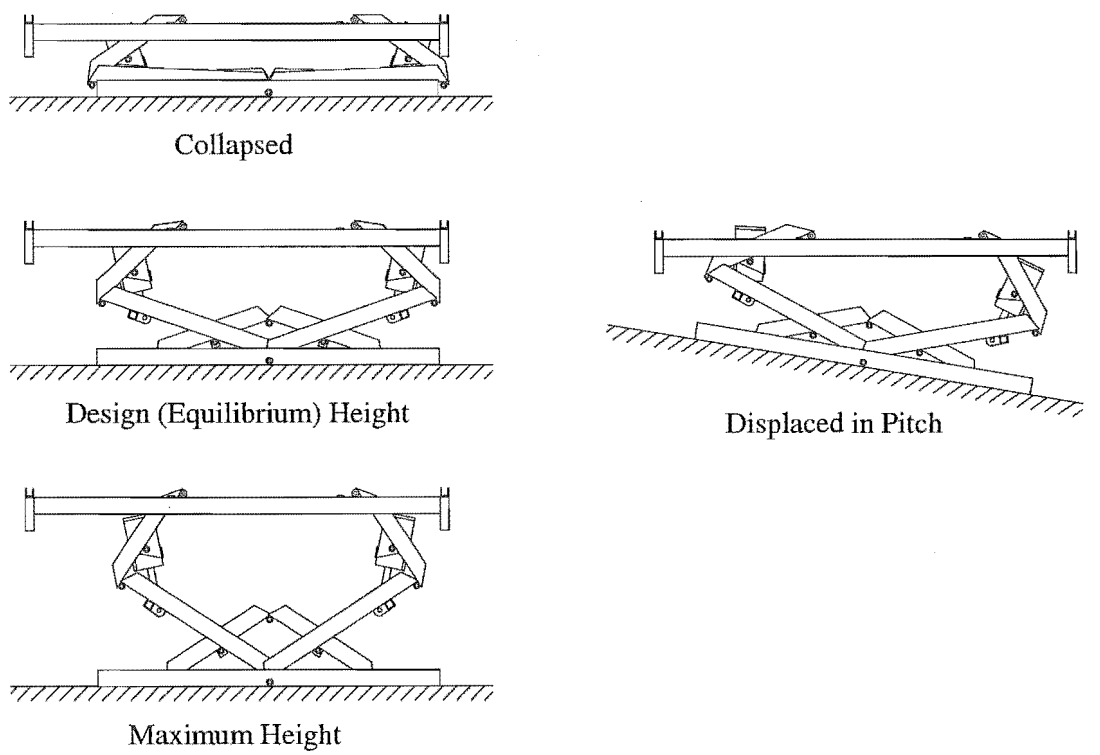

***Figure 3.2** Movement of the Suspension Linkage*

The working space in pitch is ±9.5° when the suspension is at its design height, but this reduces with vertical suspension movement. When the suspension is at the bottom or top of its vertical travel, no pitching of the top frame is possible.

3.3.2 Mechanical Embodiment

Figure 3.3 shows an isometric view of the suspension linkage. Figure 3.4 shows an earlier version of the linkage which was never built. Manufacturing drawings for the linkage of Figure 3.3 can be found in Appendix G.

a) Materials and Manufacture

To keep the weight of the suspension low, the linkage (including the top and base frames) is fabricated from structural aluminium alloy sections - mostly 6063 T6. The pivots consist of 10 mm diameter cold drawn stainless steel axles (AISI 304) running in grease lubricated, molybdenum disulphide impregnated nylon bushes.

Aluminium proved to be a difficult material to work with, given that it distorts readily when welded. Many of the links needed to be straightened in a press after fabrication, and there were difficulties in aligning the pivot bushes accurately - the housings of which were welded to the links. In a production version of the suspension, the bushes might be better bolted (or otherwise mechanically fixed) to the linkage. This would enable them to be more accurately aligned. Alternatively, the use of steel rather than aluminium for the links might be preferable.

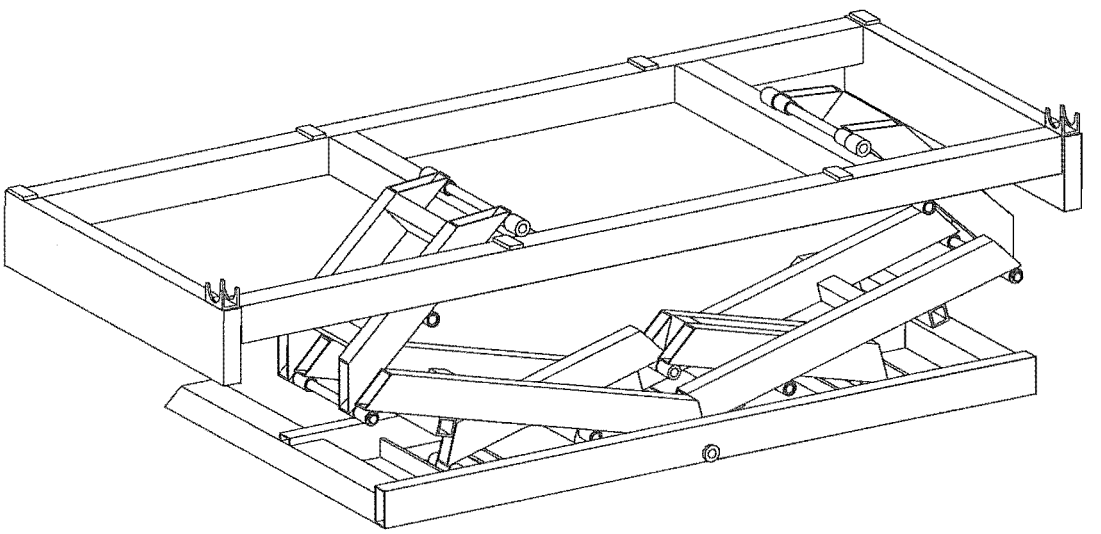

***Figure 3.3** The Stretcher Suspension Linkage*
(pneumatic springs not shown for clarity)

b) Top and Base Frames

As space in an ambulance is limited, the suspension is designed to fit around the ambulance rear wheel arch. This means that the stretcher and suspension take up no more room than is normal. (Generally in a New Zealand ambulance there are two stretchers - one located over either rear wheel arch.) For this reason, the suspension top and base frames are offset laterally from the linkage as shown by Figure 3.3. The top frame is also offset longitudinally on the linkage so that, for a patient of average mass and inertia, the springs are equally loaded. This means that pitch and bounce are uncoupled for a patient of average mass and inertia. (The centre-of-mass of the human body lies closer to the head than the feet, Appendix A3.)

The stretcher sits in lugs which are welded to the top frame. In a production version of the suspension, a clamp would probably be included to ensure that the stretcher could not accidentally become detached from the suspension unit.

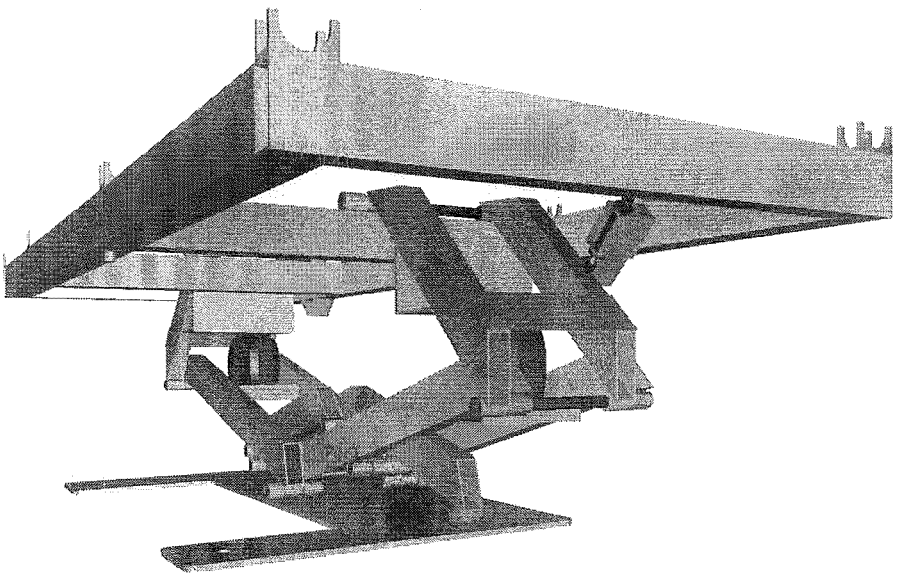

***Figure 3.4** An Earlier Version of the Stretcher Suspension Linkage (shown fitted with rubber air bags)*

c) Stabilising Mechanism

The function of the stabilising arms *FI* and *FJ* (as labelled in Figure 3.1) is to constrain the lower links *CE* and *DE* to be at the same angle - irrespective of the movement of the

suspension (Figure 3.2). By doing this, the linkage is stable to moments due to unsymmetrical loading, pitch of the ambulance floor and/or stretcher, and ambulance braking or acceleration.

The stabilising arms have nylon wheels at *I* and *J* (not shown in Figure 3.1) which roll on horizontal plates welded into the base frame. The links are pinned together at *F*, and to the rest of the linkage at *G* and *H*. As the kinematic mechanism formed by these links is over-constrained, the original intention was to incorporate a small amount of clearance into the rollers at *I* and *J*. However, the manufacturing tolerances were such that clearance at the rollers *I* and *J* was too great. To remedy this, a short rectangular bar was fixed above the roller at *I* so that it was constrained to move horizontally (ie. between the horizontal bar and base frame plate). The roller at *J* then became inoperative and did not contact the base frame plate.

3.4 ISOLATORS

In order for the stretcher suspension to be effective it must have springs which can (1) provide a low natural frequency, and (2) be capable of adapting to suit the mass of the patient. Pneumatic springs have these properties and are ideally suited to the stretcher suspension application.

3.4.1 Overview

Isolation systems which employ pneumatic springs consist of a load which is supported on a cylinder, or rubber bag, which is filled with air [78,79] (Figure 3.5). Most commonly, rubber bellows rather than cylinders are used [79,80] as they:

- Have the ability to stroke through an arc.
- Can accommodate side loads.
- Do not have moving seals which cause stiction.
- Require little or no maintenance
- Are virtually leak proof.

In addition, rubber bellows can be designed to have a specified force/deflection characteristic by arranging for the area to change with displacement in a particular way [81]. This is not possible with a cylinder where the area is constant.

By arranging for the air volume of the spring to be large by using an additional volume (variously referred to as an auxiliary reservoir or surge tank), very low spring stiffnesses and therefore system natural frequencies are possible. It is important that the connecting

pipe is of sufficient cross-sectional area to prevent restriction of flow between the two volumes [81].

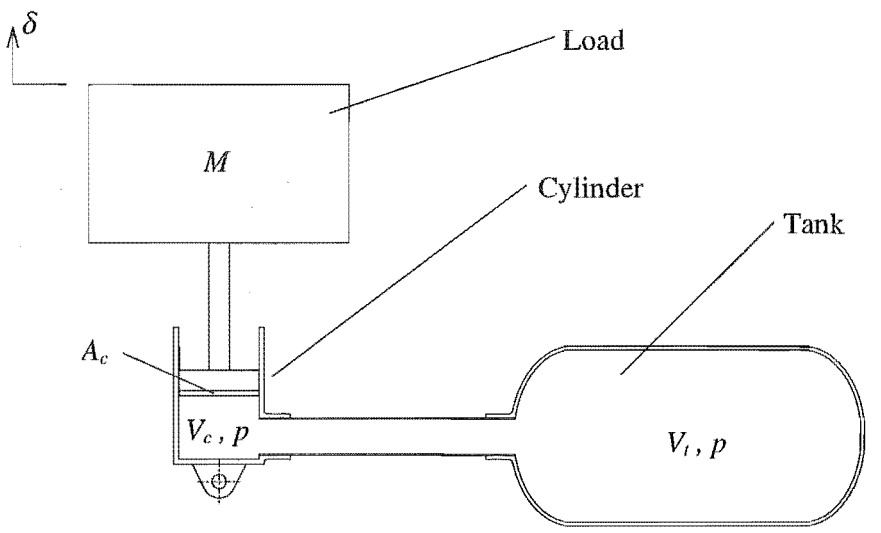

Figure 3.5 Schematic of Pneumatic Spring

3.4.2 Suspension Natural Frequencies

The pitch and bounce natural frequencies of the stretcher suspension are functions of the geometry of the linkage and the stiffness of the springs, as indicated by Equations 4.21 and 4.22 of Chapter 4. A nominal natural frequency in bounce and pitch of 0.46 Hz was chosen - this being at the lower end of the natural frequencies used by others [45,58,69]. It was not considered prudent to use a lower value (which would provide better isolation) as the suspension would be too unstable to external force (eg. from an ambulance attendant leaning on the stretcher). In addition, a lower natural frequency would result in greater relative deflections of the suspension during isolation. This would require the use of a longer suspension stroke, which would be difficult to achieve with the limitations on space.

3.4.3 Rubber Bellows

Rubber bellows have advantages over cylinders as discussed in Section 3.4.1a. However, if they were to be mounted directly to the linkage, as shown in Figure 3.4, then the direction of force they would provide would be difficult to analyse. (At times their end caps would be non-parallel and offset from each other.) The importance of this is discussed further in Section 4.4.1 of Chapter 4.

In an attempt to make analysis easier and more accurate, the end caps of the bellows were constrained to move in line and parallel to each other by using the sliding bracket shown in Figure 3.6. This arrangement was not successful as the bellows, which were stacked two-high to achieve the required stroke, tended to buckle. Hence, cylinders are used in the suspension as detailed in the following section.

3.4.4 Pneumatic Cylinders and Tank

Compact non-cushioned cylinders are used (Martonair M/90063/100). They are 63 mm in diameter, have a stroke of 100 mm, and employ extruded aluminium barrels. They are capable of providing a force in both directions (ie. double-acting), but are used as single-acting units in this application by venting one side to atmosphere. Given that only one side of the cylinder volume needs to be air-tight, the rod seals and one of the two piston seals are removed to reduce friction.

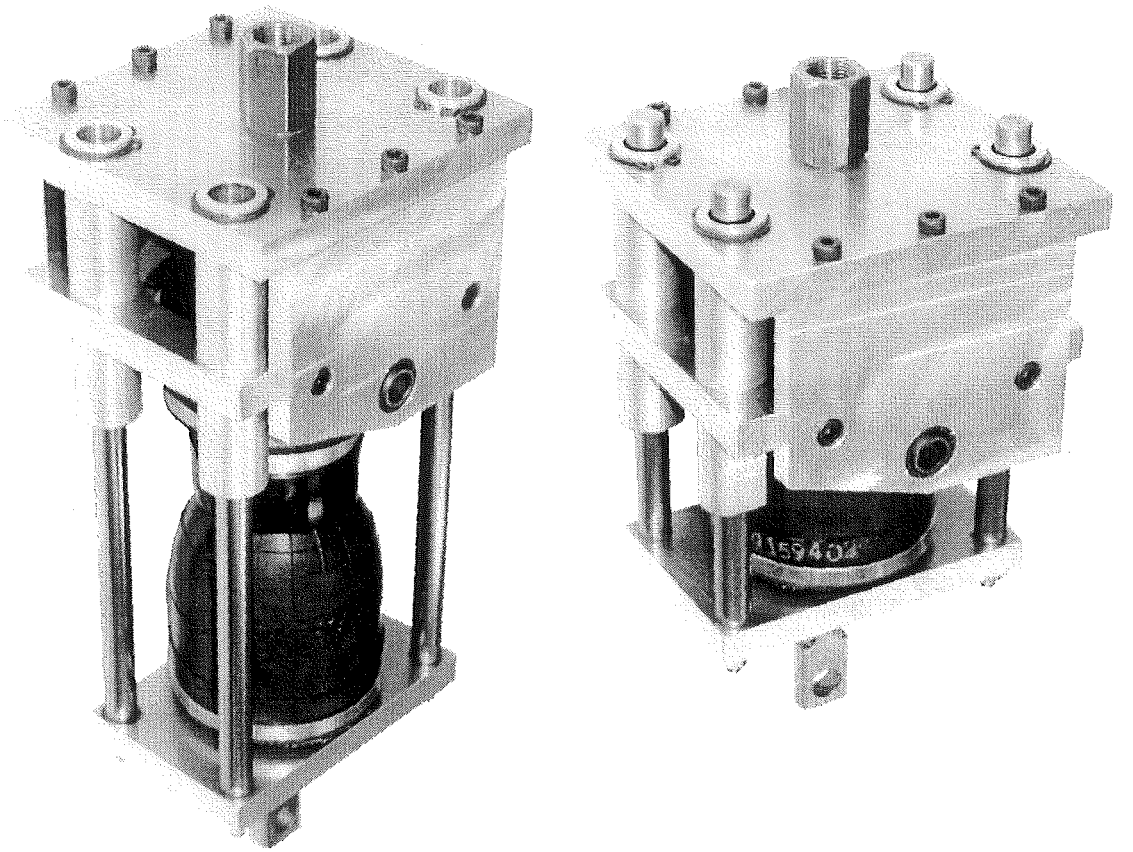

***Figure 3.6** Rubber Bellows Attachment Brackets, Shown Extended and Collapsed (manufacturing drawings in Appendix G)*

The cylinders are fixed into brackets fabricated from aluminium plate which, in turn, are pinned to the suspension pitch arms. Spherical rod ends are used to attach the cylinder rods to the lower arms. This arrangement results in a spring installation ratio of 3.42:1. (The spring installation ratio is the ratio of suspension vertical deflection to spring deflection [82].) As shown in Figure 3.2, the cylinders are located so that they inclined at an angle of 12.2° to the vertical direction when the suspension is at its design height. This is done so that the vertical restoring force of the suspension varies more linearly with displacement. The importance of this is discussed in Section 4.4.2 of Chapter 4.

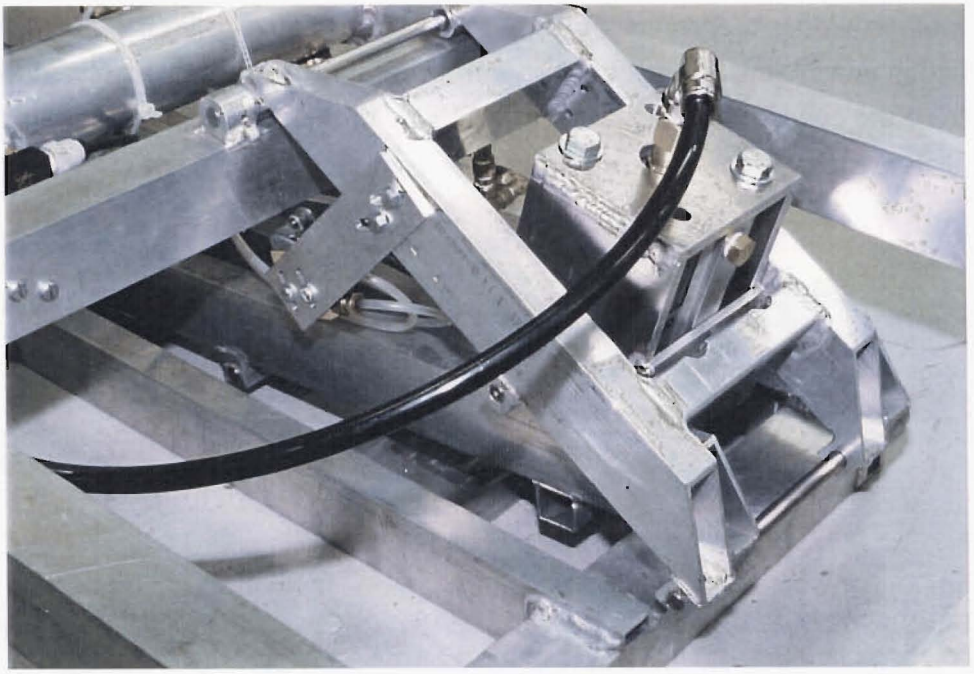

Figure 3.7 *Suspension Pitch Arm and Cylinder (linkage in collapsed position)*

Each cylinder is connected to a 1.123 litre tank using a length of 8.5 mm nylon tube (Figure 3.7). The end caps of the cylinders are fitted with larger than standard ports (G3/8 compared with original size of G1/4) to allow essentially unrestricted flow between the cylinders and tanks. Each tank consists of a length of 60.25 mm diameter tube welded into the top frame.

The cylinders are filled with air at between 2.4 and 8.3 bar (35 and 120 psig). The actual value of pressure depends both upon the weight of the patient and the positioning of the patient on the stretcher (Equations B38 and B39 of Appendix B).

3.5 HEIGHT LEVELLING

The essentially constant natural frequency characteristic of the suspension relies on maintaining a ride height which is independent of suspended load.

The reason for this is explained in the analysis which follows.

3.5.1 Pneumatic Isolator Analysis

a) Spring Stiffness

Using the notation of Figure 3.5, the stiffness k of a pneumatic spring can be derived as below [83]:

Assuming adiabatic compression, the pressure p and volume $(V_c + V_t)$ of the spring for a given displacement δ are related to the static pressure p_0 and initial volume $(V_{c0} + V_t)$ by

$$p(V_c + V_t)^\gamma = p_0(V_{c0} + V_t)^\gamma, \tag{3.1}$$

where the instantaneous volume of the cylinder is given by

$$V_c = V_{c0} + A_c\delta. \tag{3.2}$$

The stiffness of the spring is given by the rate of change of force with respect to spring displacement. ie.

$$k = -\frac{d}{d\delta}(pA_c), \tag{3.3}$$

which can be written as

$$k = \frac{\gamma p_0 A_c^{\,2}}{V_{c0} + V_t}\left(\frac{1}{1 + \dfrac{A_c\delta}{V_{c0} + V_t}}\right)^{\gamma+1}, \tag{3.4}$$

by using Equations 3.1 and 3.2. If the small non-linear term (in the brackets) is ignored, we can write the spring stiffness as

$$k = \frac{\gamma p_0 A_c^2}{V_{c0} + V_t}. \tag{3.5}$$

In practice, compression of air within the spring will be adiabatic only at higher frequencies. At lower frequencies, isothermal compression is more likely. The transition from adiabatic to isothermal behaviour typically occurs around 3 Hz, but depends upon the thermal insulation of the spring [79,81,83]. Irrespective of the exact thermodynamic nature of the air compression process, the resulting spring stiffness will tend to increase in compression [81].

b) Load Adaptation

As indicated by Equation 3.5, stiffness varies in direct proportion to absolute static pressure (p_0), but is inversely proportional to the isolator volume at equilibrium ($V_{c0} + V_t$). ie.

$$k \propto \frac{p_0}{V_{c0} + V_t}.$$

The load capable of being supported by the spring varies as a function of the spring static gauge pressure. ie.

$$Mg = (p_0 - p_{at})A_c,$$

or

$$M \propto (p_0 - p_{at}).$$

Since natural frequency is given by

$$\omega_n = \sqrt{\frac{k}{M}},$$

then we can write

$$\omega_n \propto \sqrt{\frac{p_0}{(V_{c0} + V_t)(p_0 - p_{at})}}.$$

If a height levelling device is used to adjust the mass of air in the spring so that the ride height is the same, no matter how heavy the load is, then the volume of the spring when at equilibrium ($V_{c0} + V_t$) will be constant and the equation above simplifies to

$$\omega_n \propto \sqrt{\frac{p_0}{(p_0 - p_{at})}}. \tag{3.6}$$

Or, in words, natural frequency varies little with load because both stiffness and load carrying capacity increase with spring pressure. However, as stiffness varies with absolute pressure p_0, but load carrying capacity with gauge pressure ($p_0 - p_{at}$), there is a small reduction in natural frequency with increasing load. For high mean values of static pressure this reduction is less marked.

3.5.2 Height Levelling Systems

a) General

A variety of height adjusting systems are used for pneumatic suspensions. The earlier pneumatic automobile suspensions [18-25] used mechanically-actuated height levelling valves. These controlled the mean suspension height by admitting or exhausting air to/from the springs depending on suspension deflection. To limit the consumption of air and prevent the height levelling function from interfering with isolation, a time delay of about 5 seconds was usually built into these valves [82]. A higher rate of levelling was often employed during loading.

More recently, electronically controlled height levelling systems have been developed for commercial vehicles [36], passenger vehicles [26,28], and the stretcher suspension designed by Pettigrew [74]. These systems employ solenoid actuated valves which are controlled by an ECU. The ECU typically receives information from suspension height sensors. Such systems have advantages over mechanically-actuated valves in that the ride height can be readily adjusted. This is beneficial for trucks whose height can be altered to suit that of loading bays [37], or for off-road vehicles whose ground clearance can be increased over rough terrain [27].

b) Stretcher Suspension System

In the stretcher suspension application, continuous height levelling action is not required. This is because the weight supported on the suspension will not change once loading has been completed. Consequently, a simple pneumatic height levelling circuit can be used as shown in Figure 3.8. Generally, the suspension will not be loaded

symmetrically and the two pneumatic springs will be at different pressures. This dictates the use of two height levelling devices - one for each of the cylinders.

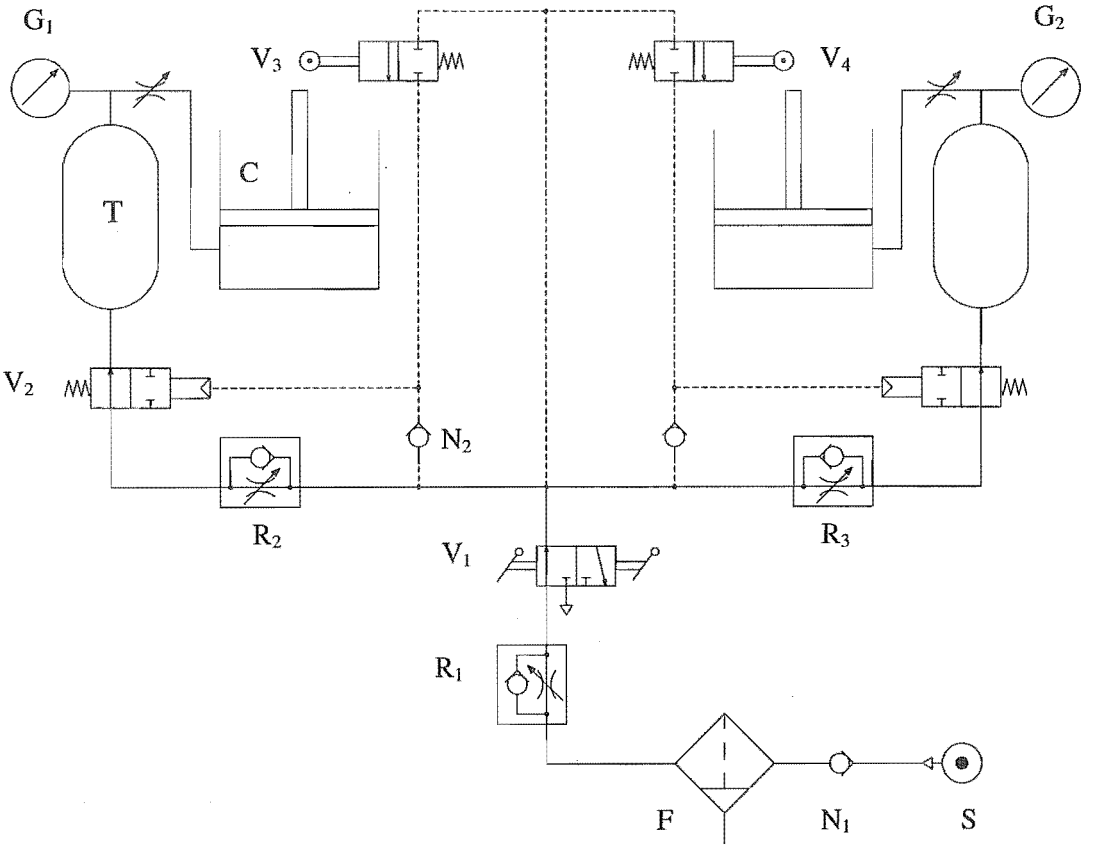

Figure 3.8 Height Levelling Circuit Diagram

A two-position valve V_1, actuated by a toggle (up/down) switch, is used to initiate raising/lowering of the suspension. When in the 'up' position, air is admitted through this valve and (considering the left-hand circuit) into the tank T (and hence the cylinder C) via a normally open pilot-actuated spring return 2-port/2-position valve V_2. When the suspension linkage on the left-hand side has risen to the required height and contacts the roller of valve V_3, air is admitted along the pilot line to close V_2 which prevents further air from being admitted to the cylinder. Actuation of the roller mechanism of V_3 during vibration will have no effect. At the completion of the journey, V_1 is switched to the 'down' position, the pilot line is exhausted via the non-return valve N_2, V_2 is opened, and air is exhausted from the system. Although raising or lowering is controlled by a single valve (V_1), the air flow to/from either cylinder is independent of the other.

A filter F is included in the supply line, along with a non-return valve N_1, which prevents the suspension from exhausting should the supply S become disconnected. An adjustable flow restriction valve R_1 is used to control the rate of suspension lift, while

R_2 and R_3 are used to control the rate of suspension lowering. The best rate of lift has yet to be finalised, but would probably be in the order of 5-10 seconds [58]. For experimental purposes, pressure gauges G_1 and G_2 are fitted to measure the tank pressures. These would not be required on a production version.

The pneumatic components of the circuit are attached to the underside of the suspension top frame. The height limit valves V_3 and V_4 are fixed to the pitch arms and actuated by contacting a cross-member of the suspension top frame, as shown by Figures 3.7 and 3.9.

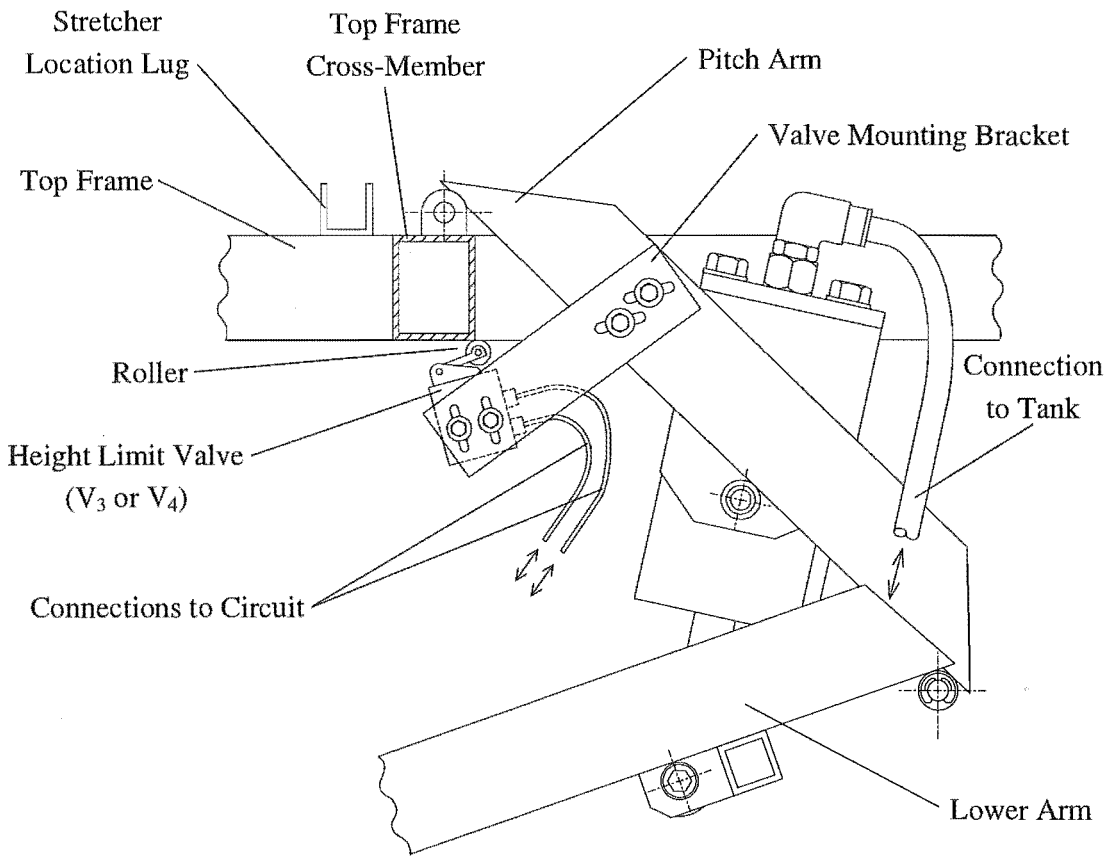

***Figure 3.9** Schematic Showing Contact of Limit Valve Roller With Top Frame*

c) Air Supply

For laboratory tests, the suspension used pressurised air from a mains supply. For road tests, a small 12 volt pump was used. In a production version, air could be supplied from a 6 litre diver's tank storing air at 200 bar. This would provide sufficient air for

approximately 72 journeys. Alternatively, a 12 volt compressor could be used. To reduce noise, this would be best situated in the ambulance engine compartment.

d) Testing and Evaluation

While the fundamental operation of the height leveling circuits was in accordance with expectation, some problems were encountered. These are listed below:

- When high rates of lift were used, the suspension would overshoot the required design height. This is a reflection of the difficulty of trying to accurately position a mass with a low stiffness spring in the presence of friction and linkage non-linearities (Chapter 4, Section 4.4.2). By using a lower rate of lift, overshoot was reduced.
- The ride height achieved proved to be very sensitive to the accuracy with which the height limit valves V_3 and V_4 could be positioned. This is because a large change in suspension ride height corresponds to only a small movement of the height trip valves relative to the top frame cross-member (Figure 3.9). Hence a small error in valve position causes a large error in the ride height.
- For cases where the load was not located symmetrically on the stretcher, the height levelling circuits failed to give a level suspension. This occurred because the light end of the stretcher rose more rapidly than the heavy end. (The cylinder at the light end requires less pressure and therefore less air.) The suspension cross-member at the light end was thus at an angle when contacted by the roller of the limit valve - this causing the valve to be actuated prematurely. This problem could be eliminated by using the base frame, rather than the top frame, to actuate the valve. The ride height at which valve actuation would occur would then be independent of stretcher angle.

CHAPTER 4

Suspension Analysis and Characterisation

4.1 INTRODUCTION

In the first part of this chapter, the key equations used to model the suspension kinematics and forces are presented. Where appropriate, reference is made to additional detail contained in Appendices B and C. Following this, the character of the suspension is investigated by presenting a number of simulation results. None of the simulations include consideration of damping, which is analysed in later chapters. While a number of the vibration examples are not realistic (from the point of view of what would be expected in an ambulance), they do serve to provide an understanding of the suspension.

4.2 LINKAGE GEOMETRY

The geometry of the linkage, as shown in Figure 4.1a, is defined by the link lengths e, h, L_1, L_2 and L_3. Also shown in Figure 4.1a are labels for the linkage pivots (A-J), and the additional distances a, b, c and f which can be defined in terms of the link lengths. The offset of the load centre-of-mass from the suspension pitch-centre is assigned the variable e_e. Its value depends both upon the mass of the patient and the positioning of the patient on the stretcher.

In Figure 4.1b, the locations of the cylinders and the angles of the links and cylinders are defined. The subscript '0' is used to indicate that the values apply for the case where the linkage is at its design height.

Numerical values and algebraic expressions for the link lengths, distances, and angles shown in Figures 4.1a and 4.1b can be found in Appendix A.

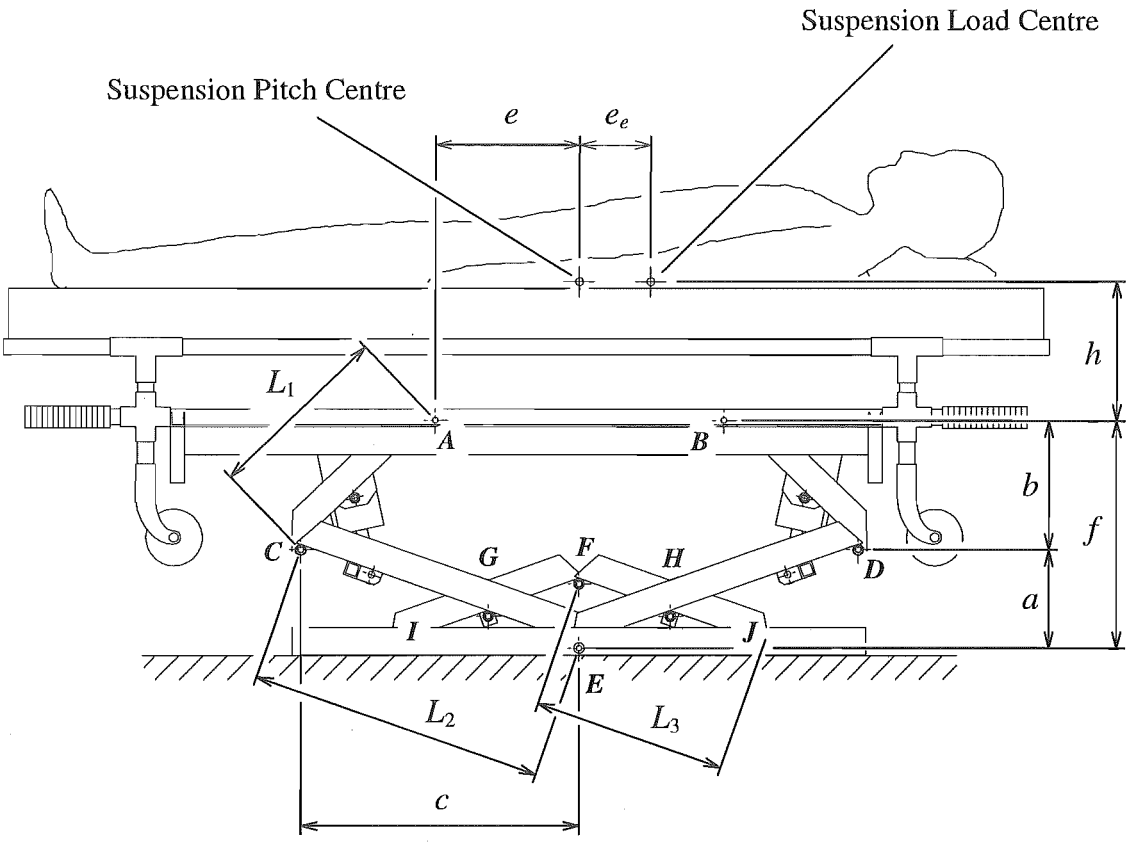

Figure 4.1a *Linkage Geometry (shown at design height)*

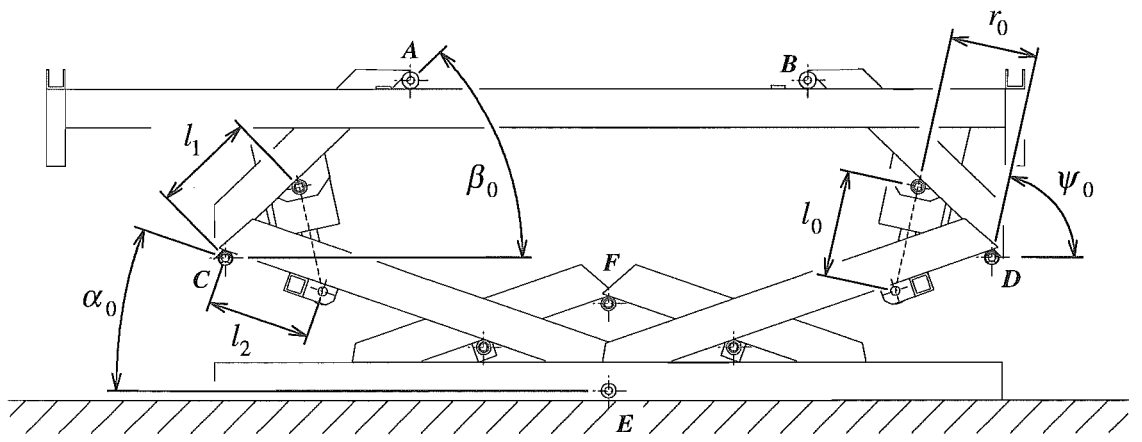

Figure 4.1b *Cylinder Locations and Link Angles (shown at design height)*

4.3 ANALYSIS

4.3.1 Linkage Kinematics

a) Link Angles

As the suspension linkage has two degrees-of-freedom (y and θ), its position can be uniquely defined by two link angles. For algebraic convenience however, three link angles (β_L, β_R and α) are used, as shown in Figure 4.2a. (The subscript *'L'* denotes that the value is for the left-hand end of the linkage, while the subscript *'R'* denotes that the value is for the right-hand end.) These angles are functions of the geometry of the linkage, the vertical position y and angle θ of the load centre-of-mass, and the vertical position y_s and angle θ_s of the ambulance floor.

With reference to Figure 4.2a, three equations for these angles can be written:

Vertically

$$f + h + y - y_s = L_2 \sin(\alpha - \theta_s) + L_1 \sin(\beta_L + \theta_s) + (e + e_e)\sin\theta + h\cos\theta\,. \qquad (4.1)$$

For the chain $CABDC$ formed by the pitch arms

$$L_1 \sin\beta_L + 2e\sin(\theta - \theta_s) = L_1 \sin\beta_R\,, \qquad (4.2)$$

and

$$L_1 \cos\beta_L + 2e\cos(\theta - \theta_s) + L_1 \cos\beta_R = 2L_2 \cos\alpha\,. \qquad (4.3)$$

These three equations are solved simultaneously by using the secant method to find β_L, β_R and α as detailed in Appendix B1.1a.

b) Link Angle Rates

The rates of change of the link angles with respect to time ($\dot{\beta}_L, \dot{\beta}_R$ and $\dot{\alpha}$) can be determined as a function of the stretcher load rates ($\dot{y}$ and $\dot{\theta}$) and ambulance floor rates ($\dot{y}_s$ and $\dot{\theta}_s$). This is done by differentiating Equations 4.1,4.2 and 4.3 (as described in Appendix B1.1b) and yields

$$\begin{bmatrix} \dot{\beta}_L \\ \dot{\beta}_R \\ \dot{\alpha} \end{bmatrix} = \begin{bmatrix} \frac{\partial \beta_L}{\partial y} & \frac{\partial \beta_L}{\partial \theta} & \frac{\partial \beta_L}{\partial y_s} & \frac{\partial \beta_L}{\partial \theta_s} \\ \frac{\partial \beta_R}{\partial y} & \frac{\partial \beta_R}{\partial \theta} & \frac{\partial \beta_R}{\partial y_s} & \frac{\partial \beta_R}{\partial \theta_s} \\ \frac{\partial \alpha}{\partial y} & \frac{\partial \alpha}{\partial \theta} & \frac{\partial \alpha}{\partial y_s} & \frac{\partial \alpha}{\partial \theta_s} \end{bmatrix} \begin{bmatrix} \dot{y} \\ \dot{\theta} \\ \dot{y}_s \\ \dot{\theta}_s \end{bmatrix}. \tag{4.4}$$

c) Link Angle Accelerations

With reference to Appendix B1.1c, the accelerations of the link angles ($\ddot{\beta}_L, \ddot{\beta}_R$ and $\ddot{\alpha}$) can be found by differentiation of Equation 4.4 which gives

$$\begin{bmatrix} \ddot{\beta}_L \\ \ddot{\beta}_R \\ \ddot{\alpha} \end{bmatrix} = \begin{bmatrix} \frac{\partial \beta_L}{\partial y} & \frac{\partial \beta_L}{\partial \theta} & \frac{\partial \beta_L}{\partial y_s} & \frac{\partial \beta_L}{\partial \theta_s} \\ \frac{\partial \beta_R}{\partial y} & \frac{\partial \beta_R}{\partial \theta} & \frac{\partial \beta_R}{\partial y_s} & \frac{\partial \beta_R}{\partial \theta_s} \\ \frac{\partial \alpha}{\partial y} & \frac{\partial \alpha}{\partial \theta} & \frac{\partial \alpha}{\partial y_s} & \frac{\partial \alpha}{\partial \theta_s} \end{bmatrix} \begin{bmatrix} \ddot{y} \\ \ddot{\theta} \\ \ddot{y}_s \\ \ddot{\theta}_s \end{bmatrix} + \begin{bmatrix} \frac{d}{dt}\left(\frac{\partial \beta_L}{\partial y}\right) & \frac{d}{dt}\left(\frac{\partial \beta_L}{\partial \theta}\right) & \frac{d}{dt}\left(\frac{\partial \beta_L}{\partial y_s}\right) & \frac{d}{dt}\left(\frac{\partial \beta_L}{\partial \theta_s}\right) \\ \frac{d}{dt}\left(\frac{\partial \beta_R}{\partial y}\right) & \frac{d}{dt}\left(\frac{\partial \beta_R}{\partial \theta}\right) & \frac{d}{dt}\left(\frac{\partial \beta_R}{\partial y_s}\right) & \frac{d}{dt}\left(\frac{\partial \beta_R}{\partial \theta_s}\right) \\ \frac{d}{dt}\left(\frac{\partial \alpha}{\partial y}\right) & \frac{d}{dt}\left(\frac{\partial \alpha}{\partial \theta}\right) & \frac{d}{dt}\left(\frac{\partial \alpha}{\partial y_s}\right) & \frac{d}{dt}\left(\frac{\partial \alpha}{\partial \theta_s}\right) \end{bmatrix} \begin{bmatrix} \dot{y} \\ \dot{\theta} \\ \dot{y}_s \\ \dot{\theta}_s \end{bmatrix}. \tag{4.5}$$

4.3.2 Cylinder Analysis

a) Cylinder Kinematics

Using the notation of Figure 4.2b, the cylinder extensions (δ_L and δ_R) and cylinder force moment arms (r_L and r_R) can be written in terms of the link angles. This is outlined below.

For the left-hand end of the linkage, the cylinder extension δ_L is given by the difference between the instantaneous cylinder length l_L and the initial cylinder length l_0. ie.

$$\delta_L = l_L - l_0 . \tag{4.6}$$

The cylinder force moment arm r_L about pivot *C* is given by

$$r_L = l_1 \sin(\psi_L + \beta_L) . \tag{4.7}$$

Similarly, for the right-hand end of the linkage, the cylinder extension δ_R is given by

$$\delta_R = l_R - l_0 , \tag{4.8}$$

and the cylinder force moment arm r_R about pivot *D* is given by

$$r_R = l_1 \sin(\psi_R + \beta_R) . \tag{4.9}$$

The instantaneous cylinder lengths (l_L and l_R) and cylinder angles (ψ_L and ψ_R) can be expressed in terms of the link angles (β_L, β_R and α), as shown in Appendix B1.2.

b) Cylinder Forces

The force of each cylinder (F_L or F_R) is a function of the difference between the initial cylinder force $(p_0 - p_{at})A_c$, and the change in force due to cylinder displacement ($k\delta$). Since the suspension is undamped in this analysis, the cylinder forces are independent of cylinder velocity $\dot{\delta}$.

From this then, the cylinder force F_L (shown in Figure 4.2b) is given by

$$F_L = (p_{L0} - p_{at})A_c - k_L \delta_L , \tag{4.10}$$

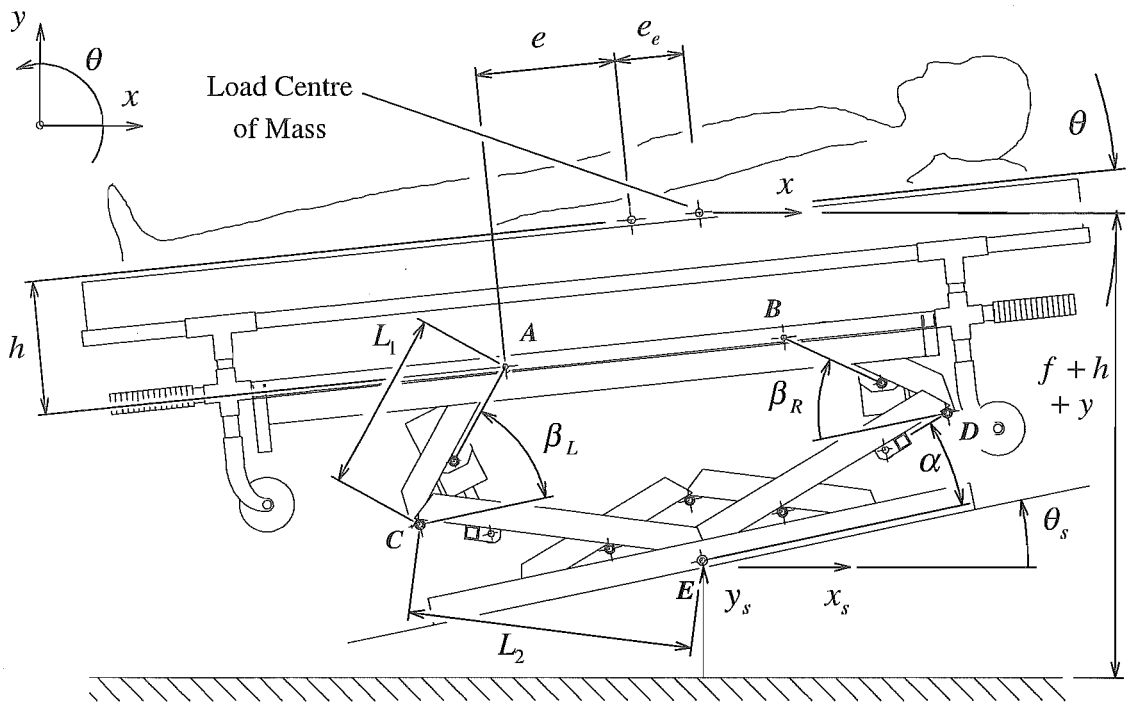

Figure 4.2a *Notation for Suspension Kinematic Analysis*

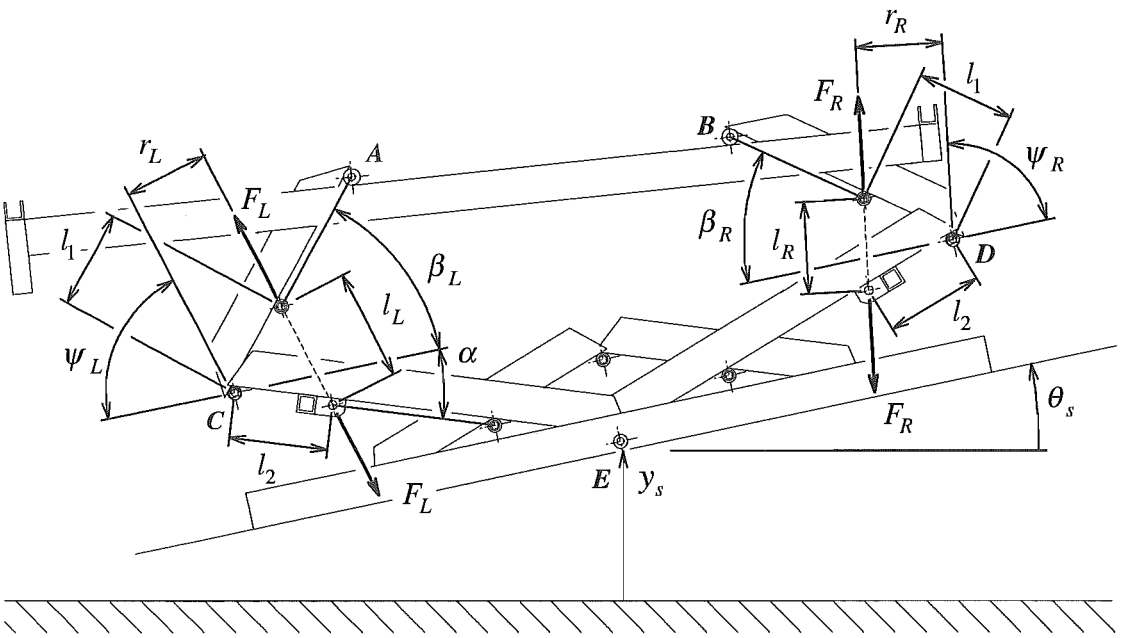

Figure 4.2b *Notation for Cylinder Analysis*

where the stiffness of the left-hand cylinder k_L can be defined by using Equation 3.4 as

$$k_L = \frac{\gamma p_{L0} A_c^2}{V_{c0} + V_t} \left(\frac{1}{1 + \frac{A_c \delta_L}{V_{c0} + V_t}} \right)^{\gamma+1}.$$

Similarly, the cylinder force F_R on the right-hand end of the linkage is given by

$$F_R = (p_{R0} - p_{at}) A_c - k_R \delta_R, \tag{4.11}$$

where

$$k_R = \frac{\gamma p_{R0} A_c^2}{V_{c0} + V_t} \left(\frac{1}{1 + \frac{A_c \delta_R}{V_{c0} + V_t}} \right)^{\gamma+1}.$$

The initial cylinder pressure (p_{L0} or p_{R0}) is dependent on the mass of the patient (m_{pat}) and the load offset (e_c), as detailed in Appendix B2.4.

4.3.3 Dynamics

The response of the suspension to ambulance floor vibration is analysed by first determining the suspension linkage forces. Equations of motion for the load are then written in terms of these forces. This is outlined below.

a) Link Forces

The four top frame suspension forces A_x, A_y, B_x and B_y, which act at the pivots A and B shown in Figure 4.3, are functions of the dynamics of the linkage. This is analysed assuming:

- The light aluminium alloy links are of negligible mass compared to the mass of the load.
- The links are rigid. This is justifiable given that the behaviour of the suspension is studied at relatively low frequencies.

As the linkage is planar, only three independent equations (4.12, 4.13 and 4.14) can be written can be for the linkage in terms of the forces A_x, A_y, B_x and B_y.

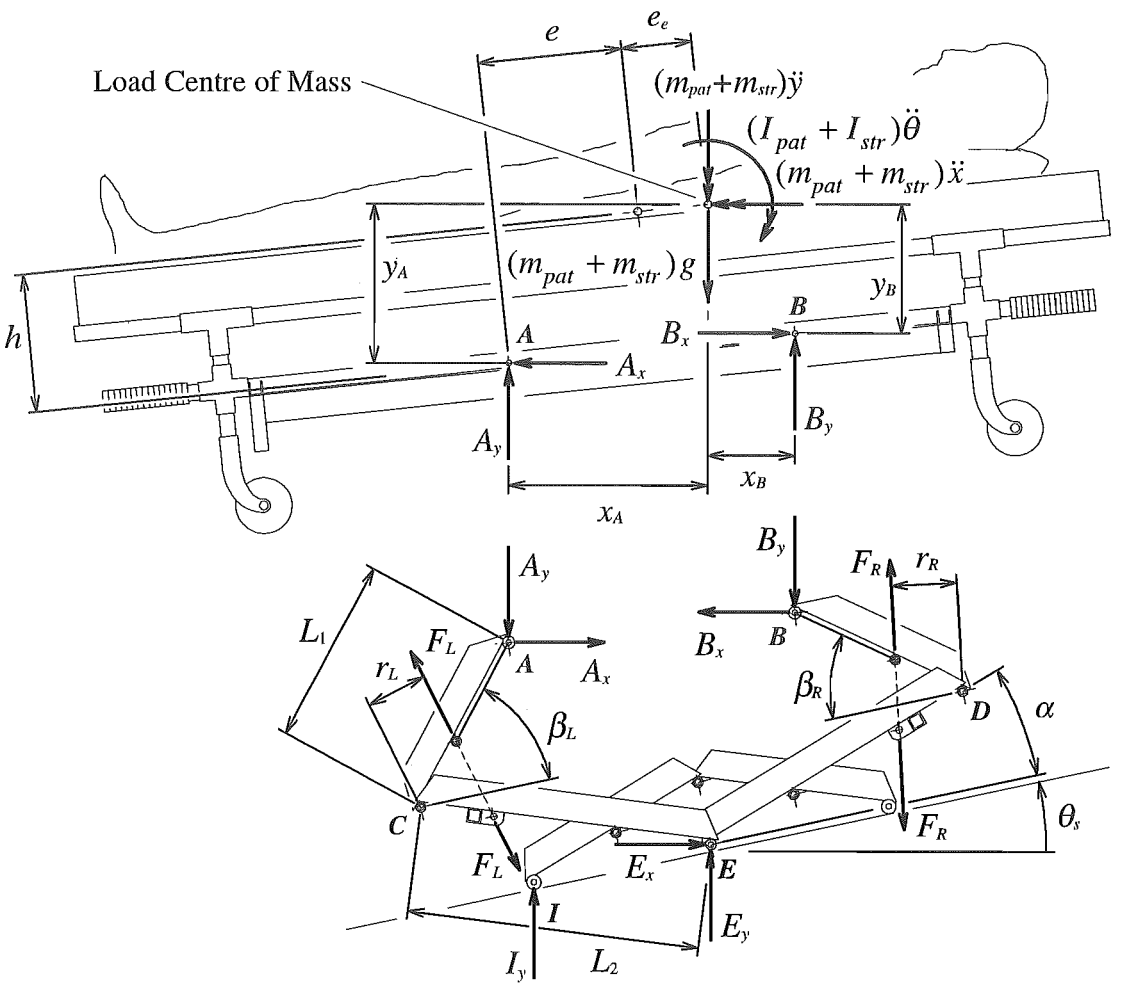

***Figure 4.3** Suspension Load and Linkage Free Body Diagrams*

For the left-hand pitch link *AC* shown in Figure 4.3, taking moments about *C*

$$A_x L_1 \sin(\beta_L + \theta_s) + A_y L_1 \cos(\beta_L + \theta_s) = F_L r_L . \tag{4.12}$$

Similarly, for the right-hand pitch link *BD*, taking moments about *D*

$$B_x L_1 \sin(\beta_R - \theta_s) + B_y L_1 \cos(\beta_R - \theta_s) = F_R r_R . \tag{4.13}$$

Finally, for the linkage as a whole (with reference to Appendix B2.1)

$$\begin{aligned}
&A_x(L_2\sin(\alpha-\theta_s)+L_1\sin(\beta_L+\theta_s))\\
&+B_x(L_2\sin(\alpha+\theta_s)+L_1\sin(\beta_R-\theta_s))\\
&-A_y(L_2\cos(\alpha-\theta_s)-L_1\cos(\beta_L+\theta_s))\\
&-B_y(L_2\cos(\alpha+\theta_s)-L_1\cos(\beta_R-\theta_s))=0.
\end{aligned} \tag{4.14}$$

b) Load Equations of Motion

Three equations of motion can be written for the load free body diagram of Figure 4.3. These equations are in terms of the load coordinates x, y and θ, and the forces A_x, A_y, B_x and B_y.

In the x direction

$$A_x - B_x + (m_{pat} + m_{str})\ddot{x} = 0. \tag{4.15}$$

In the y direction

$$-A_y - B_y + (m_{pat} + m_{str})\ddot{y} = -(m_{pat} + m_{str})g. \tag{4.16}$$

In the θ direction

$$A_x y_A - B_x y_B + A_y x_A - B_y x_B + (I_{pat} + I_{str})\ddot{\theta} = 0, \tag{4.17}$$

where x_A, x_B, y_A and y_B are defined in Appendix B2.2.

c) Coupling of Coordinates

Although three equations of motion (4.15, 4.16 and 4.17) have been written for the load in terms of three coordinates (x, y and θ), only two coordinates are required as the suspension has just two degrees of freedom (y and θ).

To eliminate the horizontal coordinate, $\ddot{x}$ can be expressed as a function of $\ddot{y}$ and $\ddot{\theta}$. As detailed in Appendix B2.3, this is done by writing x as a function of y and θ, and then differentiating twice with respect to time to give

$$\ddot{x} = \ddot{x}_s + L_2(\dot{\alpha} - \dot{\theta}_s)^2 \cos(\alpha - \theta_s) - L_1(\dot{\beta}_L + \dot{\theta}_s)^2 \cos(\beta_L + \theta_s)$$
$$-\dot{\theta}^2((e+e_e)\cos\theta - h\sin\theta) - \ddot{\theta}_s(L_2 \sin(\alpha - \theta_s) + L_1 \sin(\beta_L + \theta_s))$$
$$+[L_2 \sin(\alpha - \theta_s) \quad -L_1 \sin(\beta_L + \theta_s)]\begin{bmatrix} \frac{\partial \alpha}{\partial y_s} & \frac{\partial \beta_L}{\partial y_s} \\ \frac{\partial \alpha}{\partial \theta_s} & \frac{\partial \beta_L}{\partial \theta_s} \\ \frac{d}{dt}\left(\frac{\partial \alpha}{\partial y}\right) & \frac{d}{dt}\left(\frac{\partial \beta_L}{\partial y}\right) \\ \frac{d}{dt}\left(\frac{\partial \alpha}{\partial \theta}\right) & \frac{d}{dt}\left(\frac{\partial \beta_L}{\partial \theta}\right) \\ \frac{d}{dt}\left(\frac{\partial \alpha}{\partial y_s}\right) & \frac{d}{dt}\left(\frac{\partial \beta_L}{\partial y_s}\right) \\ \frac{d}{dt}\left(\frac{\partial \alpha}{\partial \theta_s}\right) & \frac{d}{dt}\left(\frac{\partial \beta_L}{\partial \theta_s}\right) \end{bmatrix}^T \begin{bmatrix} \ddot{y}_s \\ \ddot{\theta}_s \\ \dot{y} \\ \dot{\theta} \\ \dot{y}_s \\ \dot{\theta}_s \end{bmatrix}$$
$$+\ddot{y}\left(L_2 \frac{\partial \alpha}{\partial y}\sin(\alpha - \theta_s) - L_1 \frac{\partial \beta_L}{\partial y}\sin(\beta_L + \theta_s)\right) \tag{4.18}$$
$$-\ddot{\theta}\left((e+e_e)\sin\theta + h\cos\theta - L_2 \frac{\partial \alpha}{\partial \theta}\sin(\alpha - \theta_s) + L_1 \frac{\partial \beta_L}{\partial \theta}\sin(\beta_L + \theta_s)\right).$$

The first term in this expression ($\ddot{x}_s$) represents the horizontal acceleration of the ambulance floor. This is of interest when studying the behaviour of the suspension during ambulance braking or acceleration.

4.3.4 Method of Solution

a) System Equations

We now have seven equations (4.12-4.18). Three of these are for the linkage (4.12-4.14), three are for the load (4.15-4.17), and one expresses $\ddot{x}$ as a function of $\ddot{y}$ and $\ddot{\theta}$ (4.18). These equations are in terms of seven unknowns - four unknown suspension forces (A_x, A_y, B_x, B_y), and three unknown accelerations ($\ddot{x}$, $\ddot{y}$, $\ddot{\theta}$). In matrix form these are:

$$\mathbf{Ff} = \mathbf{w}, \tag{4.19}$$

which can be written in full as

$$\begin{bmatrix} F_{41} & 0 & F_{43} & 0 & 0 & 0 & 0 \\ 0 & F_{52} & 0 & F_{54} & 0 & 0 & 0 \\ F_{61} & F_{62} & F_{63} & F_{64} & 0 & 0 & 0 \\ 1 & -1 & 0 & 0 & m_{pat}+m_{str} & 0 & 0 \\ 0 & 0 & -1 & -1 & 0 & m_{pat}+m_{str} & 0 \\ y_A & -y_B & x_A & -x_B & 0 & 0 & I_{pat}+I_{str} \\ 0 & 0 & 0 & 0 & 1 & F_{76} & F_{77} \end{bmatrix} \begin{bmatrix} A_x \\ B_x \\ A_y \\ B_y \\ \ddot{x} \\ \ddot{y} \\ \ddot{\theta} \end{bmatrix} = \begin{bmatrix} F_L r_L \\ F_R r_R \\ 0 \\ 0 \\ -(m_{pat}+m_{str})g \\ 0 \\ {}^1w_7+{}^2w_7 \end{bmatrix},$$

where the first row corresponds to Equation 4.12, the second row to Equation 4.13, and so on.

The elements F_{ij}, ${}^1w_7$, and ${}^2w_7$ of this equation are given in Appendix B2.5.

This system of equations can be solved by matrix inversion to find $\mathbf{f}$. ie.

$$\mathbf{f} = [A_x \quad B_x \quad A_y \quad B_y \quad \ddot{x} \quad \ddot{y} \quad \ddot{\theta}]^T = \mathbf{F}^{-1}\mathbf{w}. \tag{4.20}$$

b) Method of Integration

After first defining an ambulance floor input ($y_s, \theta_s, \dot{y}_s, \dot{\theta}_s, \ddot{y}_s$, $\ddot{\theta}_s$) and initial values for $y, \theta, \dot{y}$ and $\dot{\theta}$, the motion of the stretcher is determined by integrating $\ddot{y}$ and $\ddot{\theta}$ (as given by Equation 4.20) by using either of Matlab's numerical integration functions (*ode23* or *ode45*).

4.3.5 Suspension Natural Frequencies

By linearising the equations presented thus far, algebraic expressions for the suspension natural frequencies in bounce and pitch can be found:

For bounce

$$f_y = \frac{\omega_y}{2\pi} = \frac{1}{2\pi}\sqrt{\frac{2k}{m_{pat}+m_{str}}\left(\left(\frac{f}{l_0}\right)\left(\frac{l_1}{L_1}\right)\left(\frac{l_2}{L_2}\right)\right)^2 - \frac{g}{f}\left(1-\left(\frac{f}{l_0}\right)^2\left(\frac{l_1}{L_1}\right)\left(\frac{l_2}{L_2}\right)\right)}. \tag{4.21}$$

For pitch

$$f_\theta = \frac{\omega_\theta}{2\pi} = \frac{1}{2\pi}\sqrt{\frac{2k}{(I_{pat}+I_{str})}\left(\left(\frac{e}{c-e}\right)\left(\frac{l_1}{L_1}\right)\left(\frac{l_2}{L_2}\right)\left(\frac{cb+a(c-e)}{l_0}\right)\right)^2 - \frac{(m_{pat}+m_{str})ge(cb+a(c-e))}{(I_{pat}+I_{str})(a+b)(c-e)^2}\left(b-e\left(\frac{l_1}{L_1}\right)\left(\frac{l_2}{L_2}\right)\left(\frac{cb+a(c-e)}{l_0^2}\right)\right)}. \quad (4.22)$$

The derivation of these equations is presented in Appendix C.

Both of these equations are independent of the length L_3 of the stabilising arms *FI* and *FJ* (Figure 4.1a). This indicates that the method by which the lower arms (*CE* and *DE*) are constrained to be at the same angle α is unimportant as far as the fundamental behaviour of the suspension is concerned.

For a patient of average mass and inertia (68 kg and 11.3 kgm^2 respectively, Appendix A3) the suspension natural frequencies are

$f_y = 0.46$ Hz (bounce),

$f_\theta = 0.46$ Hz (pitch).

In the absence of the 1.123 litre auxiliary tanks (ie. $V_t = 0$) the suspension natural frequencies increase to

$f_y(V_t = 0) = 1.54$ Hz (bounce),

$f_\theta(V_t = 0) = 1.44$ Hz (pitch).

Based on Equations 4.21 and 4.22, Figure 4.4 shows that the suspension pitch and bounce natural frequencies reduce with increasing patient mass. This is consistent with the trend given by Equation 3.6. Importantly, the reductions are small and this means that the level of isolation provided by the suspension will alter little - whether the patient be a small child or an unusually heavy adult. The reduction in pitch natural frequency is a little greater than that for bounce, as patient inertia is proportional to (patient mass)$^{5/3}$ (Appendix A3).

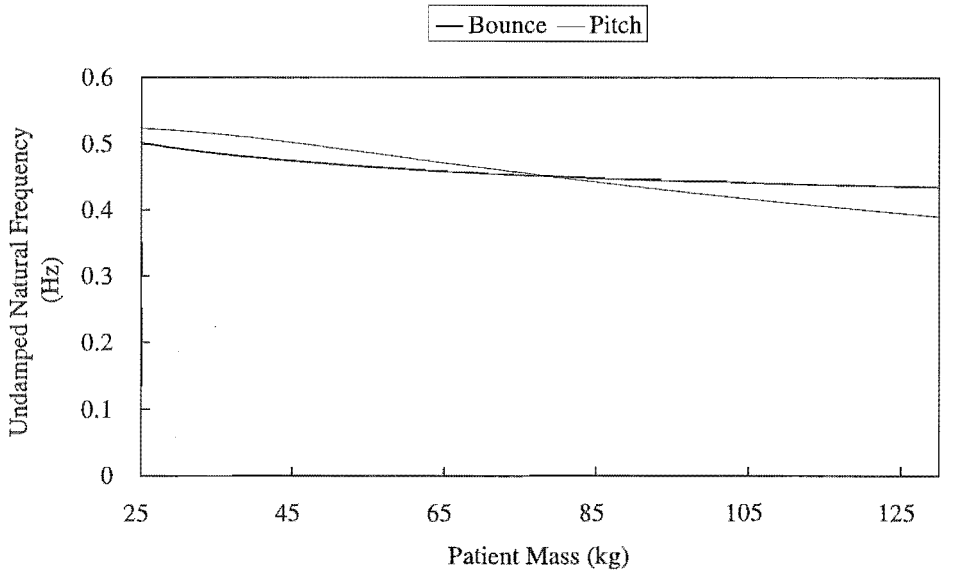

***Figure 4.4** The Variation of Suspension Natural Frequencies with Patient Mass*

4.4 SUSPENSION FORCES AND RESTORING RATES

4.4.1 Suspension Forces

Both Equations 4.21 and 4.22 have two components - the first in terms of the spring stiffness k, and the second in terms of the acceleration due to gravity g. The latter term is a function of the suspension static forces (ie. the isolator static force $(p_0 - p_{at})A_c$ and the load weight force $(m_{pat} + m_{str})g$). It has the effect of reducing natural frequency as its sign is negative. When the suspension is at equilibrium the isolator provides the force required to counteract the weight force of the stretcher and patient, as indicated by Equations B36 and B37. However, when the suspension is displaced, these static isolator and weight forces are no longer in balance. This imbalance causes a force and/or torque to be applied to the stretcher. The magnitude of this force and/or torque varies with suspension deflection. In a kinematically simpler suspension, such as a mass supported on a vertical spring, the static component of spring force (which is given by the product of static deflection and spring stiffness) is equal to the load weight force, irrespective of the deflection of the suspension.

Because the suspension has low stiffness springs, the static component of cylinder force $p_0 A_c$ is large compared to the dynamic component of cylinder force $k\delta$. Consequently, the predicted suspension natural frequencies were found to be very sensitive to assumptions regarding the direction of the static force component. From the point of view of designing a suspension that would behave in accordance with theory, pinning

cylinders to the links was preferred to fixing rubber air bags directly to the links. (The direction of the forces provided by the latter arrangement could not be readily determined, Chapter 3, Section 3.4.3).

4.4.2 Suspension Restoring Rates

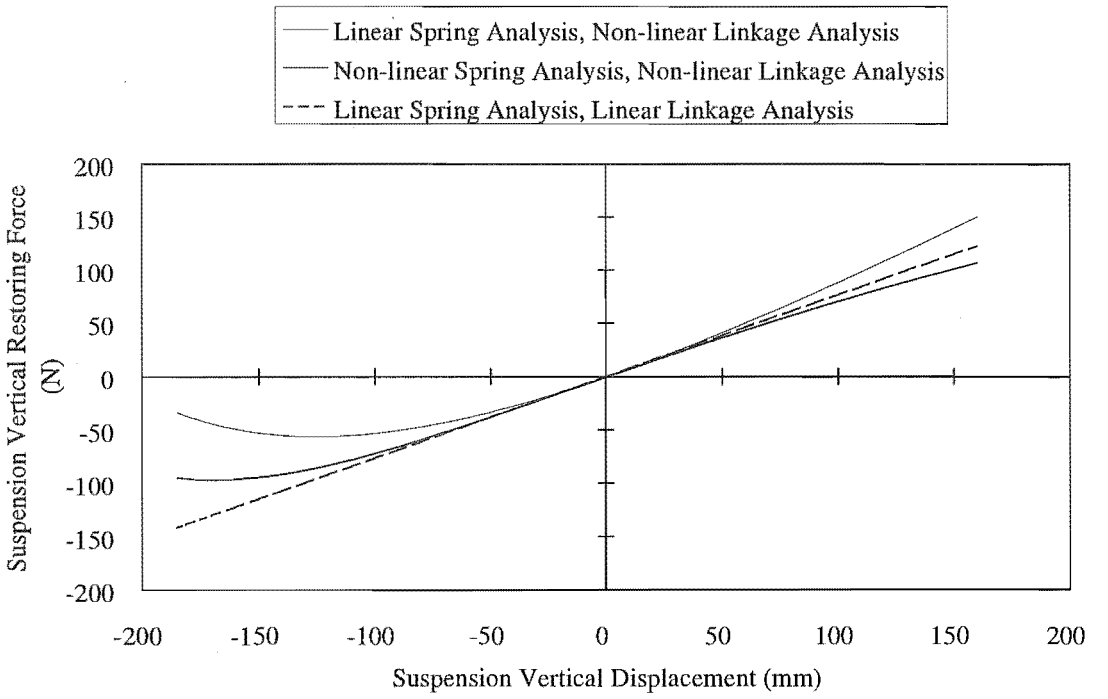

***Figure 4.5** The Suspension Vertical Restoring Force Characteristic*
($m_{pat} = 68\ kg,\ e_e = 0$)

a) Restoring Rate in Bounce

The vertical restoring force of the suspension is a function of the kinematics of the linkage and the force/deflection characteristic of the isolators. To investigate the contribution of linkage kinematics to suspension restoring force alone, the pneumatic spring stiffness can be linearised (Equation 3.5). When this is done, the linkage kinematics are found to give rise to a restoring rate which reduces in suspension compression as shown by the thin curve of Figure 4.5 (ie. the linkage has a softening characteristic). In a suspension with a higher natural frequency this softening characteristic would be less marked [82].

As a consequence of the linkage non-linearity, suspension free vibration from a large initial amplitude occurs at a frequency which is lower than the nominal frequency and displacements of the suspension in compression are greater than those in extension.

Figure 4.6 shows the simulated free vibration response of the suspension from initial displacements of 120 mm and 60 mm, using the linear spring and non-linear linkage analysis. When the initial displacement is large (120 mm), the period of oscillation is 2.55 seconds (which indicates a frequency of 0.39 Hz) and the displacement in compression exceeds that in extension by 33%. When the initial displacement is smaller (60 mm), behaviour is more linear with the displacements in compression and extension differing by only 12% and the frequency of oscillation being 0.44 Hz. (The nominal natural frequency is 0.46 Hz.)

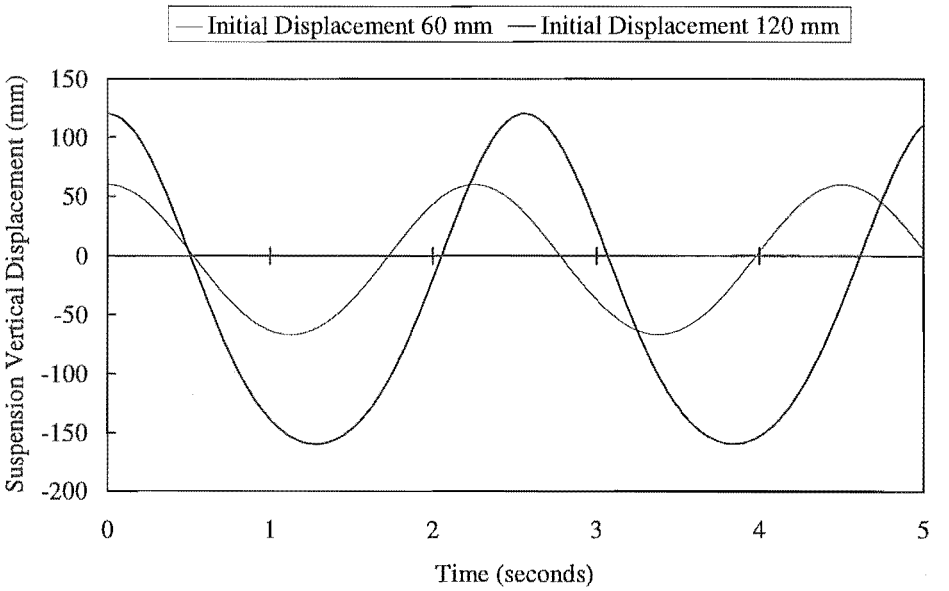

Figure 4.6 *Simulated Suspension Free Vibration From 60 mm and 120 mm (non-linear linkage analysis, linear spring analysis,* $m_{pat} = 68$ *kg,* $e_e = 0$*)*

In practice, the softening characteristic attributable to the linkage is offset somewhat by the hardening nature of the pneumatic isolators (Equation 3.4), as shown by the bold curve of Figure 4.5. Accordingly, for the bulk of the suspension stroke (±100 mm say), the restoring force varies almost linearly with suspension displacement as evidenced by comparison with the dashed line of the figure. The drop-off in restoring force is greatest for the lowest 25 mm of suspension travel (ie. -185 to -165 mm). This part of the stroke is used for loading only and is not available for (or important to) isolation.

Suspensions which have a hardening rate in both compression and extension can be considered desirable from the point of view of (1) reducing the required stroke, and (2) preventing hard contact with the bump/rebound buffers. The softening characteristic of the stretcher suspension described above is therefore undesirable. In designing the linkage, the softening characteristic was minimised by mounting the cylinders at an angle (Section 3.4.4). The angle of the cylinders was chosen by plotting in a spreadsheet

the theoretical suspension force versus displacement relationship for a given cylinder angle. The cylinder angle that gave the most linear relationship was chosen by iteration.

A hardening characteristic could be achieved on the stretcher suspension by fitting rubber air bellows in place of the cylinders, as these can give an increasing area (and hence stiffness) in compression. Some bellows can also give a hardening characteristic in extension [80]. As noted in Section 4.4.1, this would introduce some uncertainty into the analysis of the suspension. This would not be of practical concern as the desired suspension characteristics could be obtained by using an experimental approach (ie. by measuring the suspension natural frequencies and restoring rate, and then altering the surge tank volume and mounting angle of the bellows as required).

b) Restoring Rate in Pitch

The suspension restoring torque in pitch varies almost perfectly linearly with stretcher angle θ. This is because the reduction in restoring moment from the end of the linkage in compression is offset by the increase in restoring moment from the end of the linkage in extension.

4.5 SIMULATION EXAMPLES

In this section, the results of some simulations are presented. These simulations were carried out using the non-linear linkage and non-linear spring stiffness equations presented in Section 4.3 of this chapter. The purpose of the results presented here is not to investigate expected isolation performance. Rather, their purpose is to illustrate some of the key dynamic characteristics of the suspension. Response of the suspension to realistic inputs and expected isolation levels are considered in later chapters.

4.5.1 Coupling

a) Kinematic Coupling

While pure suspension bounce motions are possible when $e_c = 0$, pitch induces vertical and horizontal vibration. The levels of these induced vibrations are very low, and to the first-order of accuracy pitch and bounce are uncoupled (Appendix C). Figure 4.7 shows the simulated pitch, bounce, and horizontal free vibration responses of the suspension from an initial rotation (θ) of 5°. Since the pitch and linear motions have different units, it is not possible to compare them directly. Hence, the left-hand vertical axis of the figure has units of degrees and is used for pitch, while the right-hand axis has units of mm and is used for the linear displacements vertically (y) and horizontally (x).

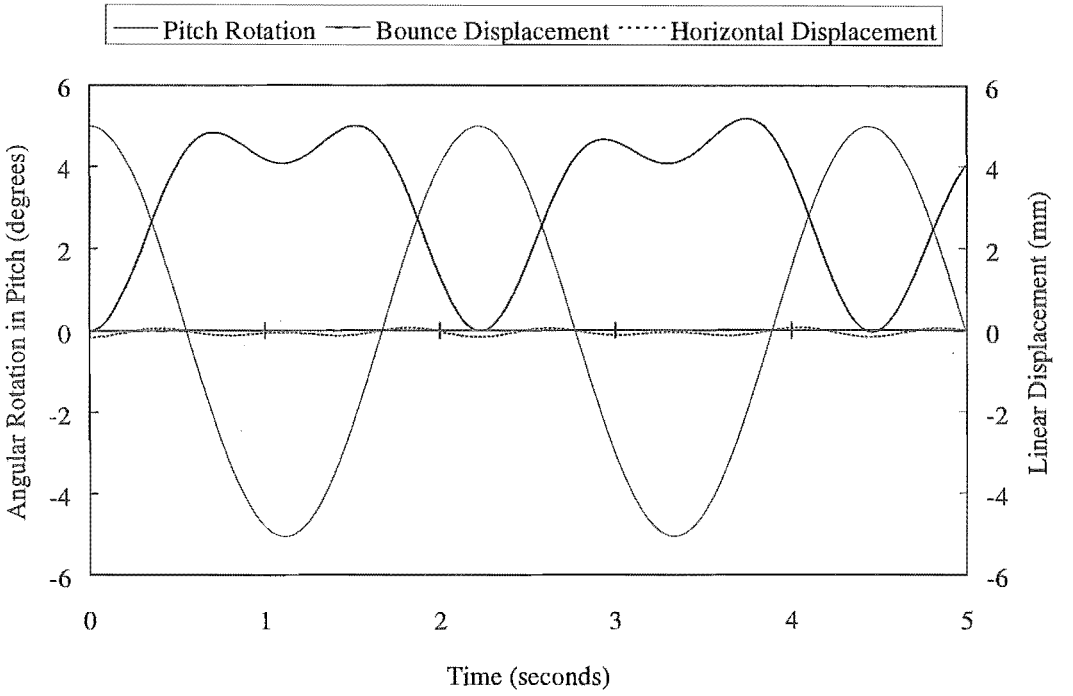

***Figure 4.7** Kinematic Coupling of Vibration Modes: Suspension Free Vibration From Initial Rotation of 5° (m_{pat} = 68 kg, e_e = 0)*

b) Coupling Due To Load Offset

When the load is not located centrally ($e_e \neq 0$), the static pressures of the isolators are different and there is first-order coupling between the pitch and bounce vibration modes. Figure 4.8 shows the pitch resulting from an initial vertical suspension displacement of 100 mm when the load offset is 100 mm.

It can be seen that the pitch vibration levels (as plotted on the right-hand axis) are substantial and reach a peak amplitude of 8°. These amplitudes are at a maximum in the region of minimum vertical vibration (and vice-versa). When the simulation is performed over a longer time period beating is observed, although not at the frequency of ($f_\theta - f_y$) predicted by linear theory. This is because the period of oscillation in bounce is amplitude dependent. (The period of oscillation in pitch is also amplitude dependent, although to a much lesser extent.)

The degree of coupling between bounce and pitch increases with increasing offset of the load e_e.

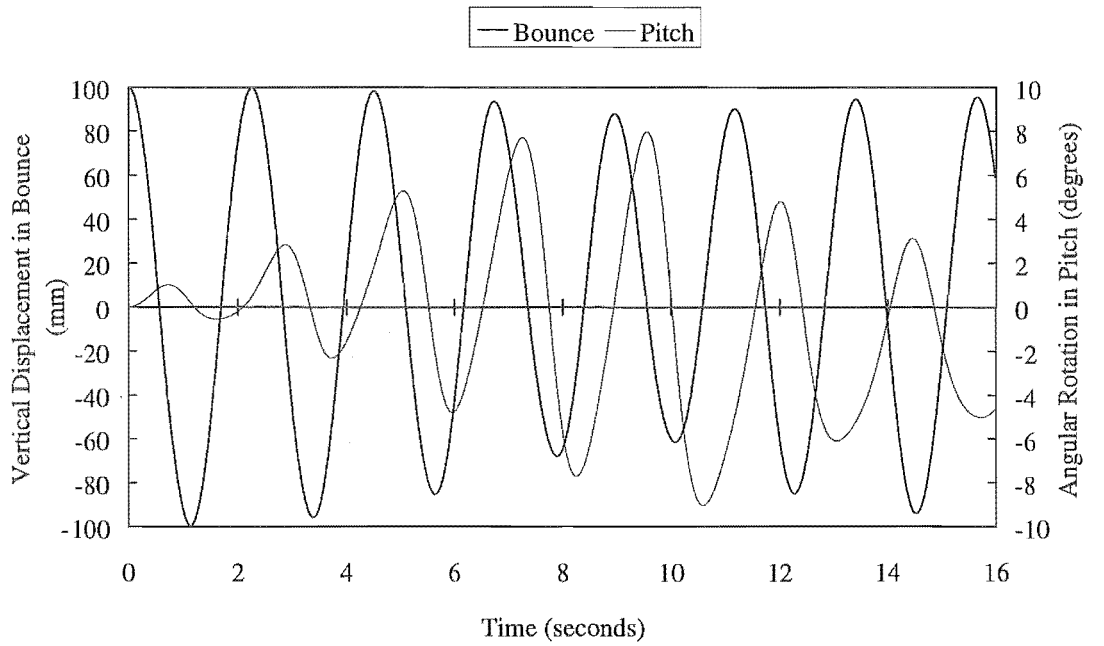

***Figure 4.8** Coupling of Pitch and Bounce Resulting From Eccentric Loading: Suspension Free Vibration From Initial Vertical Displacement of 100 mm ($m_{pat} = 68\ kg,\ e_e = 100\ mm$)*

c) The Significance of Coupling

Coupling is not unique to the stretcher suspension, but is common to many multi-degree-of-freedom suspensions. In automobiles with passive suspensions for example, there is coupling between pitch and bounce - the degree of which depends upon the weight and distribution of passengers and luggage.

As far as isolation behaviour of the stretcher suspension is concerned, the presence of coupling simply means that pure bounce of the ambulance floor will result not only in patient bounce but also pitch. Similarly, floor pitch will result not only in patient pitch but also bounce. In practice, floor inputs are a combination of random bounce and pitch motions and the patient will be subject to both bounce and pitch - irrespective of whether there is coupling or not.

Generally, ambulance floor bounce motions are more significant than pitch [46]. Any coupling in the stretcher suspension therefore results in more patient pitch than would otherwise be the case. Whether this is desirable or not depends largely upon the relative pitch/bounce tolerance levels of the patient concerned. Tolerance data reported by MIRA [57], and discussed by Leyshon and Stammers [46], suggests that the patient is more sensitive to bounce than pitch. Some coupling might therefore be an advantage, since the energy associated with bounce inputs would not go entirely into patient

bounce, but partly into bounce and partly into pitch. The level of patient bounce would therefore be reduced at the expense of an increase in pitch. Experimental tests would be useful to investigate this.

Irrespective of the exact nature of pitch/bounce tolerance levels and the degree to which coupling is either harmful or beneficial, the actual level of coupling between bounce and pitch in the stretcher suspension will be low since:

- The springs are height levelled individually. If the springs were passive (such as in the majority of automobiles), or height levelled together (ie. using only one sensor), then the degree of coupling would be greater.
- It would be natural to locate the patient centrally on the stretcher. (The stretcher and patient must be lifted into the ambulance, and a centrally positioned patient would mean that both ambulance personnel would carry a similar load.)
- The top frame of the suspension is slightly offset so that for a patient of average mass the springs are evenly loaded. (The mid-point and centre-of-mass of the human body are not in the same place, Appendix A3).

In the simulation and experimental work presented in the remainder of this thesis, the effects of coupling have been largely ignored. From the point of view of improving suspension performance, studying coupling is not particularly useful. This is because the amount of coupling is largely a function of the form of the linkage and the loading conditions - it is not something that can readily be altered or adjusted by attention to detail design. It is true, however, that the effects of large amounts coupling would need to be checked experimentally before considering the suspension for production.

4.5.2 Forced Vibration

a) Bounce

Figure 4.9 shows the simulated response of the suspended stretcher to a vertical floor input of ±75 mm at 4 Hz. The motion can be considered to be made up of two parts - the natural frequency response (which has a period of $(f_y)^{-1}$ seconds), and the response due to the input which is at 4 Hz and of lesser amplitude.

In practice, damping causes the part of the response which is at the natural frequency to decay with time to leave only the response due to the input.

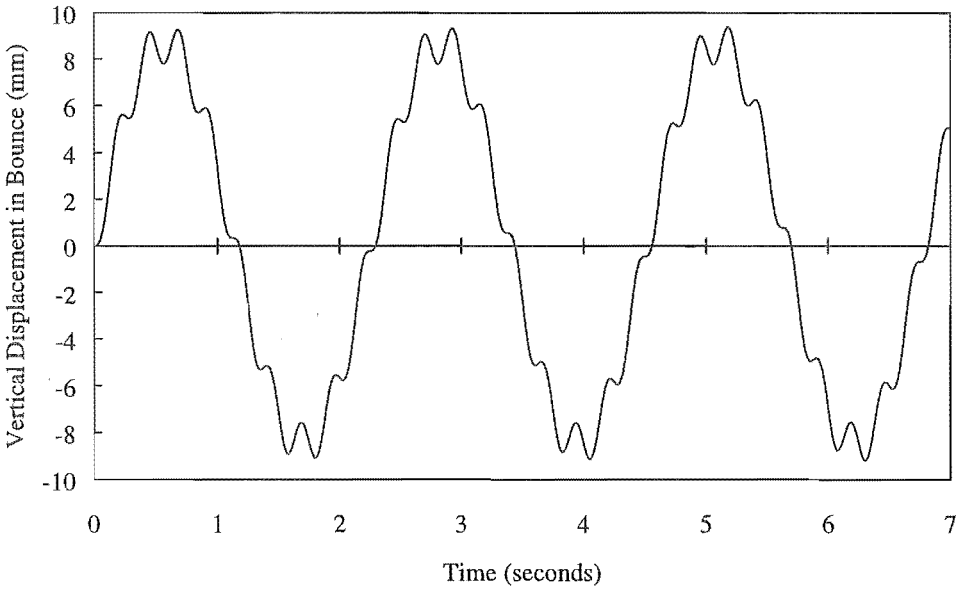

***Figure 4.9** Forced Vibration in Bounce: Vertical Input of ±75 mm @ 4 Hz ($m_{pat} = 68\ kg,\ e_e = 0$)*

b) Pitch

The pitch response of the suspension to a rotation of the ambulance floor is shown in Figure 4.10. In the example considered, the input amplitude is ±3° at a frequency of 4 Hz and the centre of rotation of the floor is at pivot E. As can be seen, the waveform of the response is somewhat different to that for bounce (Figure 4.9). This is because the suspension load is situated well above floor level. (The distance between the centre of rotation of the floor at E and the suspension load is given by $f+h \cong 650$ mm, Figure 4.1a). This is explained further below.

When the floor pitches, the load itself experiences inputs in three directions - vertical, horizontal, and rotational (pitch). As an indication of magnitude, the vertical and horizontal components are (to the first-order of accuracy):

$$\text{vertical acceleration} = (f + h)\dot{\theta}_s^{\,2}, \tag{4.23}$$

$$\text{horizontal acceleration} = (f + h)\ddot{\theta}_s. \tag{4.24}$$

These simple equations (which are based on the well known expressions for the tangential and radial accelerations of a point moving about a fixed origin) were not used in the analysis of suspension motion. They are included here only to clarify the nature of the vertical and horizontal accelerations involved.

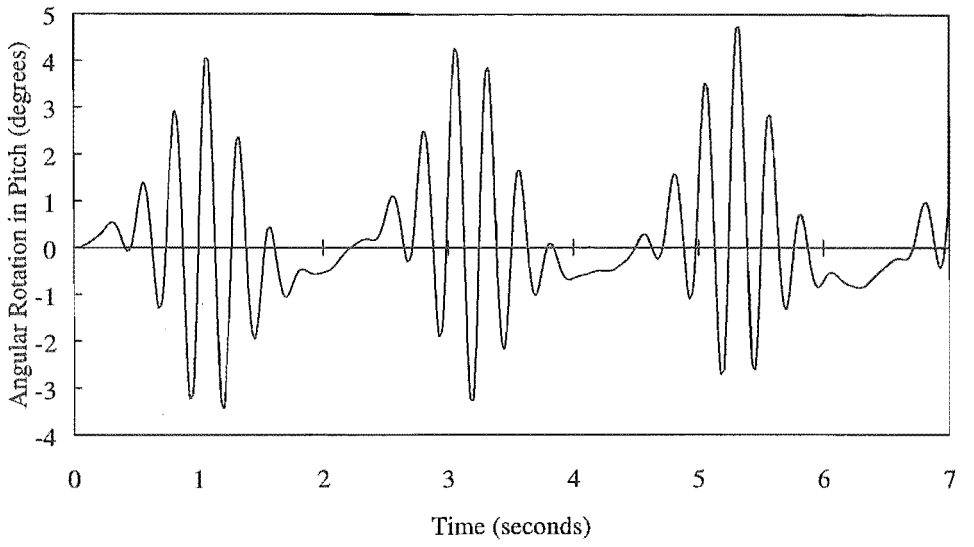

Figure 4.10 *Forced Vibration in Pitch: Pitch Input of ±3° @ 4 Hz*
(m_{pat} =68 kg, e_e =0)

The vertical component of input serves to excite the bounce mode of the suspension. As a result, the suspension is at its design height only at 0, $(f_y)^{-1}$, $2(f_y)^{-1}$, $3(f_y)^{-1}$ ... seconds (ie. 0, 2.15, 4.32, 6.47... seconds). At these times the pitch and load centres of the suspension coincide (Section 3.3.1b) and the pitch response of the stretcher is observed to be a minimum. (The distance between the load and the pitch-centre varies with *y* and is zero when the suspension is at its design height.)

In contrast, when the bounce response is large in amplitude (maximums occur at $\frac{1}{2}(f_y)^{-1}$, $\frac{3}{2}(f_y)^{-1}$, $\frac{5}{2}(f_y)^{-1}$ ... seconds) there is a large distance between the suspension load and the instantaneous centre-of-pitch of the linkage. Consequently, the horizontal component of input causes a pitching moment to be applied to the load. This pitching moment is directly proportional to:

- The magnitude of the horizontal input. (This is in turn proportional to the pitch acceleration of the ambulance floor $\ddot{\theta}_s$, Equation 4.24.)
- The instantaneous distance between the suspension load and the centre-of-pitch of the suspension - the larger this distance, the larger the pitching moment resulting from the horizontal input will be.

Additional simulations have shown that for small amplitude floor rotations (less than approximately 2°) the vertical component of input is small and there is little suspension bounce. Accordingly, the changes in the instantaneous pitch-centre relative to the load are sufficiently small that the pitching moment caused by horizontal acceleration is very small. The pitch waveform is then similar to that for bounce (Figure 4.9). That is, pitch

of the suspension load results mainly from the pitch component of input rather than from the horizontal component of input.

4.5.3 Stability During Braking

Figure 4.11 shows the response of the suspension when the floor input is ±50 mm vertically at 4 Hz and the ambulance is braking at 0.4g. This level of deceleration is higher than what would typically be used in stopping the ambulance. (According to von Gierke and Goldman [49], the level of deceleration of a 'comfortable' stop in an automobile is 0.25g, while a more rapid stop of 0.45g is 'very undesirable'.) As the suspension is loaded symmetrically, suspension pitch is due entirely to braking. From the figure, the maximum pitch angle is 2.1° which indicates that situating the pitch and load centres to coincide is effective in stabilising the suspension during braking.

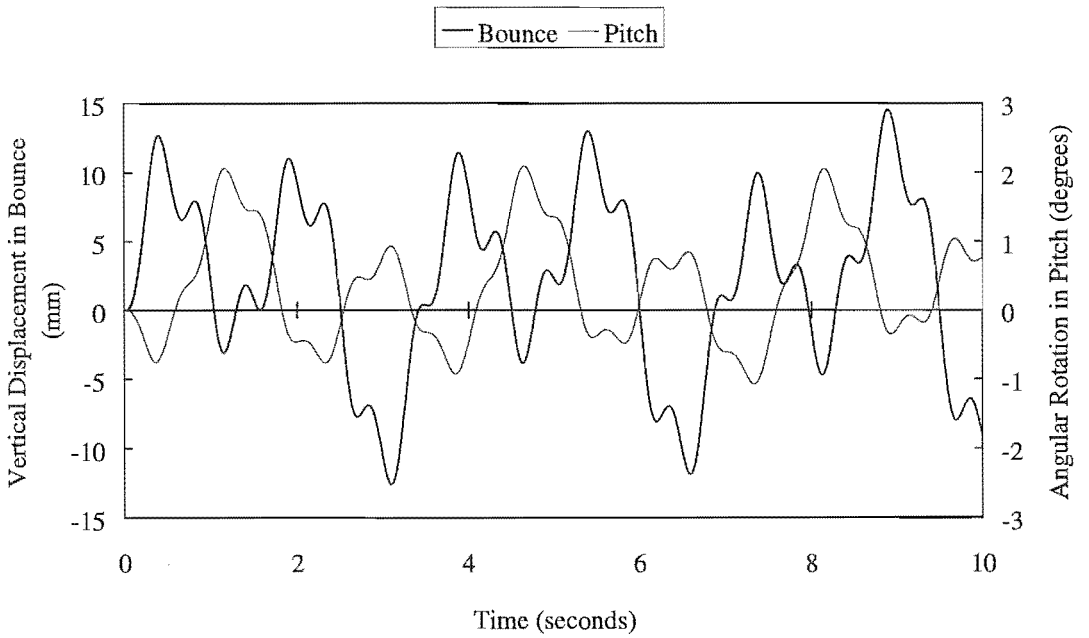

***Figure 4.11** Pitch Induced by Ambulance Braking: Suspension Response to Vertical Input of ±50 mm @ 4 Hz While Braking @ 0.4g (m_{pat} = 68 kg, e_e = 0)*

CHAPTER 5

Pneumatic Damping

5.1 INTRODUCTION

Damping is required in a suspension to limit resonance at the natural frequency, but it is detrimental to the isolation of inputs above the cross-over frequency. In a pneumatic suspension, damping can be achieved by introducing a flow restriction into the connection between the cylinder (or bellows) and the surge tank.

Two types of restriction are considered in this chapter: the capillary and the orifice. In the first part of this chapter, the key features of damping with capillary and orifice restrictions are introduced by way of a literature review. This review, as far as the author is aware, is the most comprehensive to date on pneumatic damping. It is of a general nature and does not consider the specifics of the stretcher suspension application. Particular attention is paid to the effects of using a compressible fluid for damping rather than an incompressible fluid such as oil.

The latter part of this chapter considers pneumatic damping for the stretcher suspension and compares the merits of orifice and capillary restrictors. Comparisons are made by numerically simulating the response of the suspension in an ambulance travelling over a minor road. Both patient acceleration and the sensitivity of isolation levels to changes in patient mass are used as indicators of suspension performance.

5.2 CAPILLARY DAMPING

5.2.1 Flow Through a Capillary

A capillary restriction can be formed in a number of ways. Typically, parallel plates [83], tubes [84], or sections of foam [12] are used. When the flow of air through a capillary is laminar, the equations modelling it can be linearised and analysis is simple. This is shown in the following section.

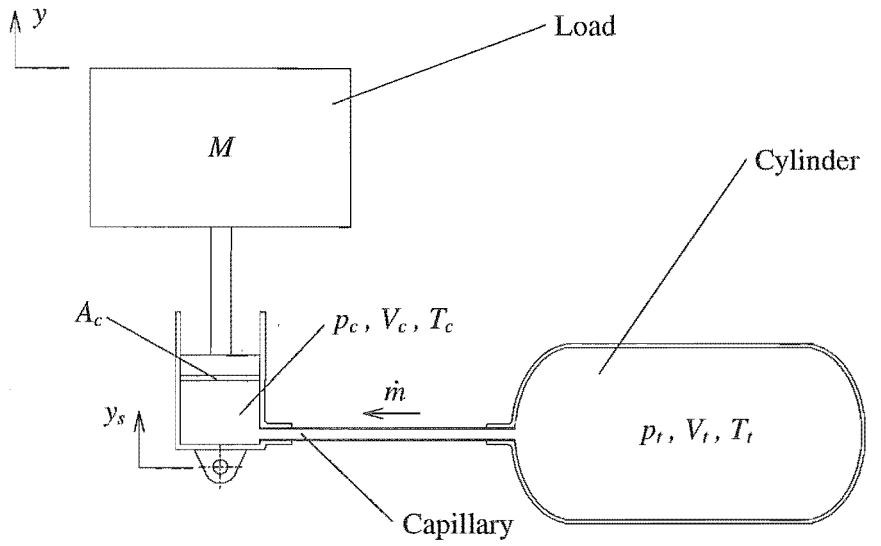

***Figure 5.1** Capillary-Damped Pneumatic Isolator*

Using the notation of Figure 5.1, and assuming isothermal flow (which is reasonable given that laminar flow implies low flow velocities), the mass flow rate of air $\dot{m}$ from the tank to the cylinder (through the capillary) is given by Massey [85] as

$$\dot{m} = \frac{C_R}{2RT_t}(p_t^{\,2} - p_c^{\,2}). \tag{5.1}$$

For the case where the flow of air is in the opposite direction (cylinder to tank), the mass flow rate is given by

$$\dot{m} = \frac{C_R}{2RT_c}(p_t^{\,2} - p_c^{\,2}). \tag{5.2}$$

Note that only air flow within the capillary is assumed to be isothermal: the same assumption has not been made for the thermodynamic processes occurring within the cylinder and tank. For this reason there are two capillary flow equations - one for the case where the air entering the capillary is at tank temperature (Equation 5.1), and one for the case where the air is at cylinder temperature (Equation 5.2).

The tank pressure can be written as

$$p_t \cong p_0 + \Delta p_t,$$

and the cylinder pressure as

$$p_c \cong p_0 + \Delta p_c,$$

where p_0 is the static (equilibrium) pressure, and Δp_t and Δp_c are the small changes in the tank and cylinder pressures resulting from piston displacement. When these expressions are substituted into Equation 5.1 (or 5.2), and second-order small quantities are ignored, the mass flow rate can be written as

$$\dot{m} = \frac{C_R}{RT_0} p_0 (p_t - p_c). \tag{5.3}$$

This linear equation applies irrespective of flow direction.

For a restriction formed by a tube of diameter d_c, and length L_c, the capillary resistance C_R is given by

$$C_R = \frac{\pi d_c^{\,4}}{128 \mu L_c}. \tag{5.4}$$

5.2.2 Analysis of Capillary-Damped Isolators

Following on from the work of Shearer [86], who used capillary resistances connected to auxiliary tanks to provide damping for a servo-controlled pneumatic ram, Cavanaugh [83] derived the third order equation and then the transmissibility of a constant area, double-acting capillary-damped spring. His equation when applied to a single-acting spring (using the notation of Figure 5.1) is

$$\begin{aligned}\left(\frac{V_{c0}}{V_{c0}+V_t}\frac{V_t}{\gamma C_R p_0}\right)\frac{d^3y}{dt^3} + \frac{d^2y}{dt^2} + \left(\frac{V_t}{V_{c0}+V_t}\frac{A_c^{\,2}}{MC_R}\right)\frac{dy}{dt} + \left(\frac{\gamma p_0 A_c^{\,2}}{M(V_{c0}+V_t)}\right)y \\ = \left(\frac{V_t}{V_{c0}+V_t}\frac{A_c^{\,2}}{MC_R}\right)\frac{dy_s}{dt} + \left(\frac{\gamma p_0 A_c^{\,2}}{M(V_{c0}+V_t)}\right)y_s.\end{aligned} \tag{5.5}$$

After defining the tank/cylinder volume ratio as

$$N = \frac{V_t}{V_{c0}},$$

and the damping ratio ξ by

$$\xi = \left(\frac{V_t}{\gamma C_R p_0}\right)\frac{\omega_n}{2},$$

Equation 5.5 can be written as

$$\left(\frac{1}{1+N}\frac{2\xi}{\omega_n^3}\right)\frac{d^3y}{dt^3}+\left(\frac{1}{\omega_n^2}\right)\frac{d^2y}{dt^2}+\left(\frac{2\xi}{\omega_n}\right)\frac{dy}{dt}+y=\left(\frac{2\xi}{\omega_n}\right)\frac{dy_s}{dt}+y_s, \tag{5.6}$$

where the natural frequency ω_n is defined in Section 3.5.1 of Chapter 3.

From this, the transmissibility $T(\omega)$ can be determined:

$$T(\omega)=\sqrt{\frac{1+\left(2\xi\left(\frac{\omega}{\omega_n}\right)\right)^2}{\left(1-\left(\frac{\omega}{\omega_n}\right)^2\right)^2+\left(2\xi\left(\frac{\omega}{\omega_n}\right)\right)^2\left(1-\frac{1}{1+N}\left(\frac{\omega}{\omega_n}\right)^2\right)^2}}. \tag{5.7}$$

Equation 5.7 indicates that the level of damping and stiffness of a capillary-damped system are frequency dependent and that the restriction size influences not only damping but also system natural frequency. This is shown in Figure 5.2 and can be explained as follows:

a) Effect of Frequency

At low excitation frequencies, the effective system volume is that of the tank and cylinder, and the isolator stiffness k is low.

$$k(\omega \to 0)=\frac{\gamma p_0 A_c^2}{V_{c0}+V_t}.$$

At higher frequencies, there is minimal flow between the cylinder and tank and the tank is effectively blocked off from the cylinder. As a result, the isolator behaves as a stiffer system with little damping.

$$k(\omega \to \infty)=\frac{\gamma p_0 A_c^2}{V_{c0}}.$$

Cavanaugh [83] shows that this undamped behaviour at high frequencies is advantageous and gives rise to an attenuation rate of 40 dB/decade, whereas the attenuation rate for a conventional isolation system (linear spring and viscous damper in parallel) is 20 dB/decade.

b) Effect of Capillary Resistance

When the capillary resistance is low, the isolator behaves as a low frequency system which is virtually undamped. Conversely, if the capillary resistance is high, the surge tank has virtually no effect; the isolator stiffness is high; and there is very little damping. The optimum restriction area lies somewhere between these two extremes and can be determined analytically.

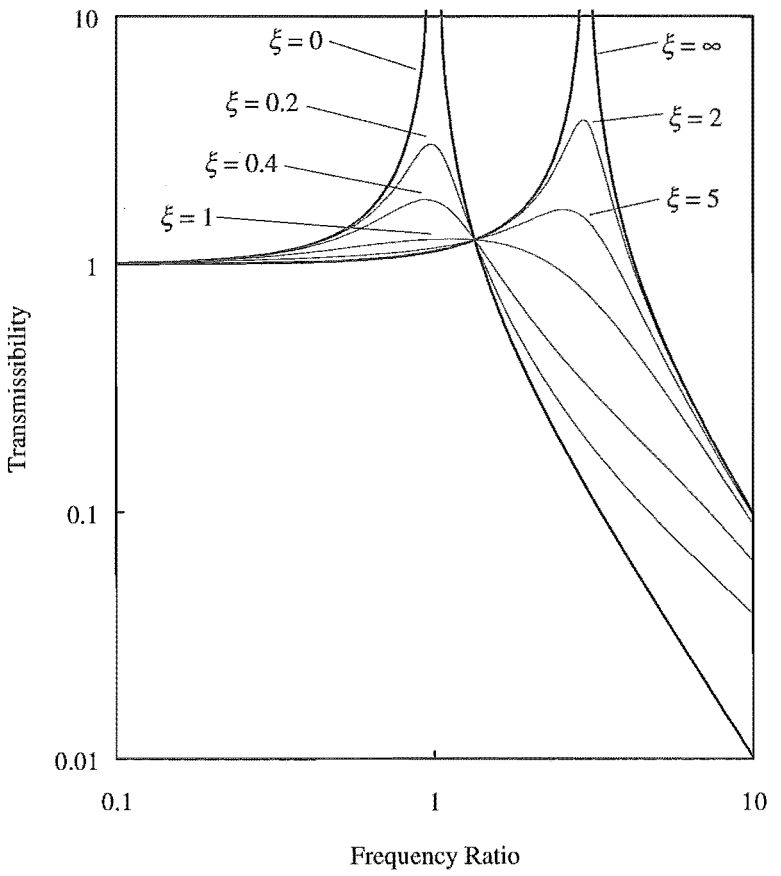

***Figure 5.2** Transmissibility of a Capillary-Damped Pneumatic Isolator (obtained using Equation 5.7)*

Note that Figure 5.2 is not intended to represent any real isolation system - it is included only to illustrate the dual frequency nature of isolation systems which employ a compressible damping fluid.

A capillary-damped isolator can be modelled by an equivalent system which consists of two linear springs and a viscous damper (as shown in Figure 5.3). The spring stiffnesses are given by

$$k_1 = \frac{\gamma p_0 A_c^{\,2}}{V_{c0}},$$

$$k_2 = \frac{\gamma p_0 A_c^{\,2}}{V_t},$$

and the damping coefficient is given by

$$c_e = \frac{A_c^{\,2}}{C_R}.$$

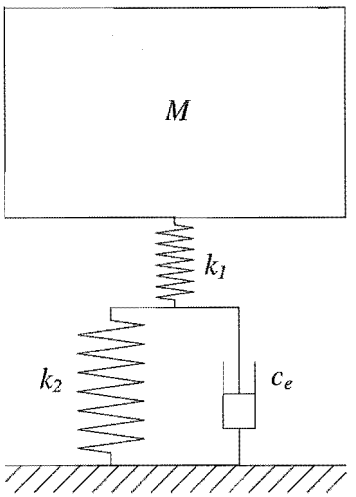

***Figure 5.3** Alternative Model of a Capillary-Damped Isolator*

5.2.3 Characteristics and Applications

Possibly for the reason that flow of air through a capillary can be adequately modelled by a linear equation (5.3), earlier analytical pneumatic damping papers deal almost exclusively with the capillary restriction rather than the orifice. A summary of some of these papers is given below.

Soliman et al [87] have analysed capillary-damped flexible rubber bellows and took into account the stiffness of the rubber and the change in isolator area with deflection.

Excellent agreement was obtained between the experimental and theoretical frequency responses.

For best damping, the ratio of cylinder/surge tank volume should be small so that there is good coupling between piston movement and mass flow rate through the capillary. This is discussed by Cellucci et al [13].

Gee-Clough and Waller [88] have noted that the dual frequency characteristics of self-damped pneumatic springs are the wrong way round, since at low excitation frequencies the effective spring stiffness is low, while at high frequencies the effective stiffness is high. (Ideally, stiffness would be high at low excitation frequencies to reduce amplification at resonance, but low at high excitation frequencies). They present an improvement by using an inertia block and two isolators connected by a capillary. This system gave good control of resonance and excellent high frequency isolation, although the requirement of a substantial additional mass could be a practical disadvantage.

Esmailzadeh has proposed and analysed a capillary-damped pneumatic automobile suspension [89], and presented transmissibilities for unsprung and sprung masses in terms of the key air-spring design parameters. A technique for finding the optimum air-spring parameters is given along with a design example. In a later paper [90], he considers the use of two isolators connected by a capillary (in a manner somewhat similar to that of Gee-Clough and Waller [88]) which gave improved isolation. The second of the isolators was connected between the wheel and road surface. In both studies excellent agreement was obtained between theoretical and experimental results.

In another paper considering air springs for automotive use, Bhave [91] modelled the effect of connecting front and rear air springs with a capillary and showed that improved isolation was possible. The use of additional independent springs would be mandatory for such a system to be stable.

Bachrach and Riven [84] analysed a constant area capillary-damped pneumatic spring using the complex stiffness approach. This gave a clearer picture of the effects of tank/cylinder volume ratio and capillary dimensions. They showed that the dimensions of the capillary affect only the frequency at which maximum damping occurs, and that the maximum loss factor depends only on the tank/cylinder volume ratio. Bachrach and Riven [92] also investigated augmentation of car tyre damping by connecting the tyre, with a capillary, to an additional compliant chamber integral with the wheel.

5.3 ORIFICE DAMPING

5.3.1 Flow Through an Orifice

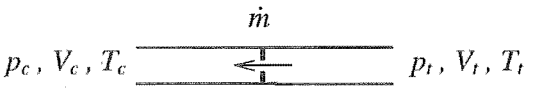

Figure 5.4 Orifice Restriction

Four equations are required to define the mass flow rate through the orifice restriction of Figure 5.4 as two flow directions and two flow regimes (subsonic or choked) are possible. These are equations are given below (after Massey [85]):

For $p_t \geq p_c$ ($\dot{m}$ positive)

$$\text{and } \frac{p_c}{p_t} \geq \left(\frac{2}{\gamma+1}\right)^{\left(\frac{\gamma}{\gamma-1}\right)} \text{ (subsonic flow)}$$

$$\dot{m} = \frac{C_d A_{or} p_t}{\sqrt{T_t}} \sqrt{\frac{2\gamma}{R(\gamma-1)}\left(\left(\frac{p_c}{p_t}\right)^{\left(\frac{2}{\gamma}\right)} - \left(\frac{p_c}{p_t}\right)^{\left(\frac{\gamma+1}{\gamma}\right)}\right)}, \tag{5.8}$$

$$\text{or for } \frac{p_c}{p_t} < \left(\frac{2}{\gamma+1}\right)^{\left(\frac{\gamma}{\gamma-1}\right)} \text{ (choked flow)}$$

$$\dot{m} = C_d A_{or} p_t \sqrt{\frac{\gamma}{RT_t}\left(\frac{2}{\gamma+1}\right)^{\left(\frac{\gamma+1}{\gamma-1}\right)}}. \tag{5.9}$$

For $p_t < p_c$ ($\dot{m}$ negative) and

$$\frac{p_t}{p_c} \geq \left(\frac{2}{\gamma+1}\right)^{\left(\frac{\gamma}{\gamma-1}\right)} \text{ (subsonic flow)}$$

$$\dot{m} = \frac{-C_d A_{or} p_c}{\sqrt{T_c}} \sqrt{\frac{2\gamma}{R(\gamma-1)} \left(\left(\frac{p_t}{p_c}\right)^{\left(\frac{2}{\gamma}\right)} - \left(\frac{p_t}{p_c}\right)^{\left(\frac{\gamma+1}{\gamma}\right)} \right)}, \tag{5.10}$$

or for $\frac{p_t}{p_c} < \left(\frac{2}{\gamma+1}\right)^{\left(\frac{\gamma}{\gamma-1}\right)}$ (choked flow)

$$\dot{m} = -C_d A_{or} p_c \sqrt{\frac{\gamma}{RT_c} \left(\frac{2}{\gamma+1}\right)^{\left(\frac{\gamma+1}{\gamma-1}\right)}}. \tag{5.11}$$

Equations 5.8 and 5.10 can be simplified by using the binomial expansion to give

$$\dot{m} = sign(p_t - p_c) C_d A_{or} \sqrt{\frac{2p_0}{RT_0} |p_t - p_c|}, \tag{5.12}$$

where $sign(p_t - p_c) = +1$ if $p_t - p_c > 0$, or
$sign(p_t - p_c) = -1$ if $p_t - p_c < 0$.

5.3.2 Analysis of Orifice-Damped Isolators

The characteristics of a pneumatic isolator fitted with an orifice restriction are similar to those of a capillary-damped system (ie. dual frequency nature, Section 5.2.2a,b), except that the level of damping is amplitude-dependent - small amplitude vibrations being virtually undamped. For an orifice $\dot{m} \propto \sqrt{p_t - p_c}$ (Equation 5.12), whereas for a capillary $\dot{m} \propto p_t - p_c$ (Equation 5.3). As a result, the analysis of an orifice-damped spring is more complicated than that of a capillary-damped system. According to Baker [93], orifice sizes are generally determined experimentally rather than analytically.

Hedrick [94], in a paper reviewing the use of active suspensions for railway vehicles, mentions that for small displacements the orifice-damped pneumatic spring can be modelled by an equivalent system of 2 linear springs and a viscous damper, as shown in Figure 5.3. In light of Equations 5.8 and 5.10, this would appear to be an inadequate approach if accurate results were required.

Evidence of this is provided by Koyanagi [95] who shows that the design of an orifice-damped pneumatic isolator is unsatisfactory by linear methods (particularly at low

frequencies), and that the non-linear characteristic of the orifice restriction is detrimental to isolation performance. To overcome these problems, Koyanagi linearises the orifice characteristic by using what he calls a 'disk valve controlled variable nozzle'. Experimental results are presented which show that amplitude-independent displacement transmissibility is achieved with this modified orifice arrangement. The agreement between theoretical and experimental results is very good. In a second paper [96], the application of this damping system to a rail vehicle is considered.

Andersen [97] analyses both laminar and orifice flow restrictions for use in damping pneumatic systems. He shows that the damping force provided by an orifice is proportional to spring static pressure p_0, and so adapts to suit the mass of the load M. Chalmers [38] and Gvineriya et al [98] mention this also. In contrast, the capillary restriction gives a damping force which varies little with load. Light loads therefore tend to be overdamped and heavy loads underdamped.

5.3.3 Characteristics and Applications

Chalmers [38] has used an orifice-damped pneumatic isolator in parallel with a hysteretic rubber damper in the Chalmers Truck Suspension. This arrangement proved effective, and eliminated the need for conventional hydraulic dampers. Chalmers comments that this is an advantage since hydraulic dampers transmit shock and require maintenance/replacement at intervals. The Chalmers suspension was arranged to give reduced damping in compression by opening two additional orifices. Others [98,99] have used similar arrangements to provide different orifice areas in compression and rebound.

Gvineriya et al [98] have simulated the behaviour of an orifice-damped pneumatic spring for use with coaches. They consider both the experimental and theoretical frequency response of a design with two auxiliary chambers, and show that this arrangement can provide good control of both sprung and unsprung resonances.

Vogel and Claar [99] detail a pneumatic suspension for an on-highway truck sleeper bunk which uses constant area pneumatic isolators fitted with orifice restrictors. They refer to their system as being slow-active, although it is better described as being self-levelling and passive according to the semantics of Sharp and Crolla [100]. Results of non-linear numerical simulations for free vibration of the system are presented. The equations modelling the isolators are then linearised and the response of the system to sinusoidal inputs is investigated.

5.4 STRETCHER SUSPENSION DAMPING

The foregoing literature review does not make it clear, for any given isolation application, which of the restrictors would be best: the orifice (which gives a non-linear characteristic whereby small-amplitude vibrations are virtually undamped), or the capillary (which gives a more linear characteristic). In particular, it is not obvious which type of restrictor is best for the stretcher suspension. Moreover, while a number of papers analyse pneumatically damped isolators by considering free vibration and/or response to sinusoidal inputs, none appear to consider response to realistic random inputs. This is necessary for a proper comparison of the two restriction types because of the non-linearity of the orifice damping method.

In the remaining sections of this chapter, capillary and orifice restrictors are compared for use in the stretcher suspension. This is done by simulating the response of the suspension to vibrations of the ambulance floor. Importantly, realistic random motion of the ambulance floor is used rather than sinusoidal motion. In this respect, the modelling work which follows represents an improvement over the previous pneumatic damping research reviewed in Sections 5.2 and 5.3.

5.5 MODELLING

The mathematical model used to investigate stretcher suspension damping is described in this section. The objectives of the modelling and simulation work are to:

- Compare the relative merits of the capillary and orifice as damping restrictions.
- Determine the best type of restriction for the stretcher suspension.
- Determine a suitable restriction size for the stretcher suspension.

5.5.1 Stretcher Suspension

The focus of the work in this chapter is on pneumatic damping. Other aspects of suspension behaviour are not of direct interest. Accordingly, some simplifications have been made to the suspension model presented in Chapter 4. (This simpler model is intended only to provide a basis for evaluating pneumatic damping methods - it is not used for investigating the effect of other suspension parameters, or behaviours such as coupling, stability during braking etc.) The simplifications to the model of Chapter 4 are:

- The bounce mode only is considered ($\theta = \theta_s = 0$). This simplifies analysis markedly over the general case where pitch is considered also.
- The suspension is assumed to be loaded symmetrically ($e_e = 0$).

- A linear equation is used to determine the angle of the pitch links β. (With only a very small loss of accuracy, $\sin\beta$ and $\cos\beta$ are calculated from the linear kinematic Equations C11 and C12 of Appendix C, rather than the exact non-linear Equations 4.1-4.3 of Chapter 4. This approach gives a worthwhile reduction in the time required to simulate the system. Other kinematic quantities are calculated using the exact non-linear equations of Chapter 4.)

After making these simplifications to the equations of Chapter 4, the vertical acceleration of the load $\ddot{y}$ can be expressed explicitly in terms of p_c, y, and y_s as

$$\ddot{y} = \frac{2(p_c - p_{at})A_c}{(m_{pat} + m_{str})} \left(\frac{r}{L_1 \cos\beta + \dfrac{eL_1 \sin\beta}{a + b + (y - y_s)}} \right) - g . \tag{5.13}$$

This equation neglects non-pneumatic forms of suspension damping such as friction in the linkage pivots. In addition, the effects of contact with bump stops are not included in the equation. During road tests of the prototype suspension, which was not fitted with bump stops, the ±160 mm working space proved to be ample and was not exceeded - even over poor surfaces (Chapter 8). The bump stops that would be incorporated in a production version of the suspension would therefore be contacted infrequently and only over very poor surfaces.

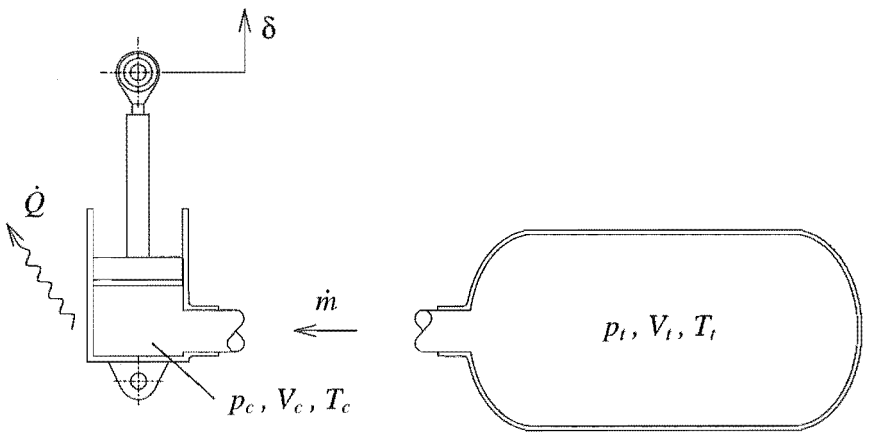

Figure 5.5 Notation for the Tank and Cylinder Analysis

5.5.2 Pneumatic Isolator

The pneumatic isolator is analysed using the notation of Figure 5.5 and the data below:

$V_t = 1.123\text{x}10^{-3}\ \text{m}^3$
$V_{c0} = 0.1559\text{x}10^{-3}\ \text{m}^3$
$A_c = 3.117\text{x}10^{-3}\ \text{m}^2$

a) Tank

The first law of thermodynamics for unsteady flow applied to the tank gives

$$-\dot{m}h_t = \frac{d}{dt}\int_{V_t} u_t \rho_t dV_t \,. \tag{5.14}$$

For a perfect gas, the specific enthalpy h_t of the air in the tank is given by

$$h_t = c_p T_t \,, \tag{5.15}$$

the specific internal energy u_t by

$$u_t = c_v T_t \,, \tag{5.16}$$

and the density ρ_t by,

$$\rho_t = \frac{p_t}{RT_t} \,. \tag{5.17}$$

After noting that

$$\gamma = \frac{c_p}{c_v} \,, \tag{5.18}$$

Equation 5.14 together with Equations 5.15-5.18 give the mass flow rate of air $\dot{m}$ exiting the tank as

$$\dot{m} = \frac{-V_t}{\gamma RT_t}\dot{p}_t \,. \tag{5.19}$$

b) Cylinder

The air entering the cylinder can be assumed to be at the temperature of the tank air T_t. This is valid if a capillary restriction is used (since the flow will be isothermal, Section 5.2.1), and also if an orifice restriction is used (since flow will be adiabatic).

The first law applied to the cylinder gives

$$\dot{m}h_t - p_c\dot{V}_c - \dot{Q} = \frac{d}{dt}\int_{V_c} u_c\rho_c dV_c \,. \tag{5.20}$$

The energy dissipated by damping, which is given by $\dot{m}c_p(T_c - T_t)$, is assumed to be lost as heat at the rate of $\dot{Q}$ from the component downstream of the restriction. For positive $\dot{m}$ this component is the cylinder.

After substituting $\dot{Q} = \dot{m}c_p(T_c - T_t)$ into 5.20, and using the perfect gas relationships of 5.15-5.17 (but applied to the cylinder), the mass flow rate of air into the cylinder is given by

$$\dot{m} = \frac{1}{\gamma RT_c}(\gamma p_c\dot{V}_c + V_c\dot{p}_c) \,. \tag{5.21}$$

c) Rates of Pressure Change

For the case where a capillary restriction is used, the rate of change of tank pressure ($\dot{p}_t$) can be found in terms of the instantaneous air temperatures (T_t, T_c) and pressures (p_t, p_c) by equating the capillary equation (Equation 5.1 or 5.2) to the tank mass flow rate equation (Equation 5.19). Similarly, when an orifice is used, the rate of change of tank pressure is determined by equating Equation 5.8 (or 5.9,5.10,5.11) to the tank mass flow rate equation (5.19). For both types of restriction, the rate of change of cylinder pressure ($\dot{p}_c$) is found in terms of the rate of change of tank pressure ($\dot{p}_t$) by using Equations 5.19 and 5.21.

These rates of change of pressure are given in Appendix D for both restriction types, along with equations which define the cylinder volume and the tank and cylinder air masses and temperatures.

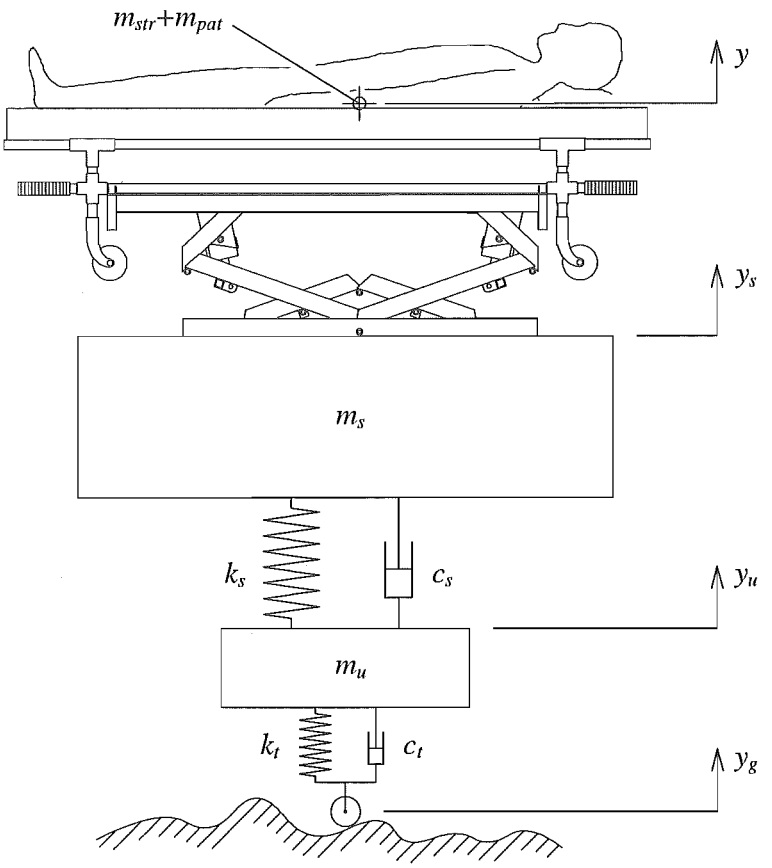

***Figure 5.6** Ambulance 1/4 Vehicle Model*

5.5.3 Ambulance

The ambulance suspension is represented by the 1/4 vehicle model shown in Figure 5.6. Justification for the use of 1/4 vehicle models in general is given by Sharp and Crolla [100]. The 1/4 vehicle model is permissible in this application because only vertical inputs are investigated and the stretcher suspension is mounted directly over the rear ambulance wheel arch.

The parameters used here are based on the data given by Geary [42], and a scaled up version of the passenger vehicle model used by Sharp and Hassan [101].

a) Ambulance Suspension Data

$m_s = 512$ kg
$m_u = 67.5$ kg
$c_s = 2180$ Ns/m
$c_t = 179$ Ns/m
$k_s = 58.5$ kN/m
$k_t = 392$ kN/m

b) Unsprung Mass Acceleration

For the case where the tyre is in contact with the road (ie. $y_g + y_{ts} - y_u \geq 0$), the acceleration of the unpsrung mass $\ddot{y}_u$ is given by

$$\ddot{y}_u = \frac{c_t(\dot{y}_g - \dot{y}_u) - c_s(\dot{y}_u - \dot{y}_s) + k_t(y_g + y_{ts} - y_u) - k_s(y_u - y_s)}{m_u} - \frac{(m_{pat} + m_{str} + m_s + m_u)}{m_u} g. \tag{5.22}$$

For the case where the tyre has lifted off the road (ie. $y_g + y_{ts} - y_u < 0$),

$$\ddot{y}_u = \frac{-c_s(\dot{y}_u - \dot{y}_s) - k_s(y_u - y_s) - (m_{pat} + m_{str} + m_s + m_u)g}{m_u}, \tag{5.23}$$

where the tyre static deflection is given by

$$y_{ts} = \frac{(m_u + m_s + m_{str} + m_{pat})}{k_t} g. \tag{5.24}$$

c) Sprung Mass Acceleration

The acceleration of the sprung mass $\ddot{y}_s$ is given by

$$\ddot{y}_s = \frac{c_s(\dot{y}_u - \dot{y}_s) + k_s(y_u - y_s) - (m_{pat} + m_{str})\ddot{y}}{m_s}. \tag{5.25}$$

5.5.4 Road Profile

The road profile was generated using the inverse Fourier Transform from the power spectral density of road displacement given by Robson [102]:

$$S(\upsilon) = \kappa \upsilon^{-w}. \tag{5.26}$$

For the work described here, the values of the road roughness coefficient κ and spectral slope index w are:

$\kappa = 500\text{x}10^{-8}$ m^2/(cycle/m)$^{(-w+1)}$ for a minor road, and
$w = 2.5$.

This model is valid for $0.01 < \upsilon < 10$ cycle/m [102]. In total, 3201 sine waves with wavelengths in the range 0.375-100m were summed. Each wave was associated with a random phase angle by using Matlab's *rand* function. The profile ordinates were spaced at 187.5 mm, which gave a road length of 600m. In the modelling work presented here, the ambulance speed was 54 km/h which gave a travelling time of 40 seconds with disturbances in the range 0.15-40 Hz.

5.5.5 Method of Solution

The derivatives $[\dot{y}_u \quad \dot{y}_s \quad \dot{y} \quad \ddot{y}_u \quad \ddot{y}_s \quad \ddot{y} \quad \dot{p}_c \quad \dot{p}_t \quad \dot{m}]$, as given by the equations in the foregoing, are integrated numerically using Matlab's *ode23* function to determine $[y_u \quad y_s \quad y \quad \dot{y}_u \quad \dot{y}_s \quad \dot{y} \quad p_c \quad p_t \quad m]$. Appendix E contains additional detail on this.

5.6 SIMULATION RESULTS

The simulation results below were generated using two types of input: sinusoidal and random. The random inputs were generated by using the ambulance and road models described above.

To begin with, the results of the sinusoidal input simulations are presented.

5.6.1 Suspension Response to Sinusoidal Vibration

a) Capillary Damping

In accordance with theory, simulations have shown that the displacement transmissibility of the suspension, when fitted with a capillary damper, is independent of load. The form of the transmissibility is similar to that shown in Figure 5.2. Note that the graph shows only the form of the transmissibility (ie. dual frequency) - the actual values on the graph do not represent the transmissibility of the stretcher suspension.

b) Orifice Damping

Figure 5.7 shows the simulated displacement transmissibility of the stretcher suspension when loaded with a patient of average mass and fitted with a 2.0 mm orifice restriction. Sinusoidal displacement inputs of amplitude ±150 mm, ±50 mm, and ±10 mm are used. In contrast to the case where a capillary restriction was used, the response of the suspension is clearly dependent upon the input amplitude, with the smallest amplitude input (±10 mm) being the least damped. When the input amplitude is large (±150 mm), the dual frequency nature of the suspension is evident. Nominally, the vertical natural frequencies of the suspension are 0.46 Hz (no damping restriction) and 1.54 Hz (fully-closed damping restriction), as given in Section 4.3.5 of Chapter 4.

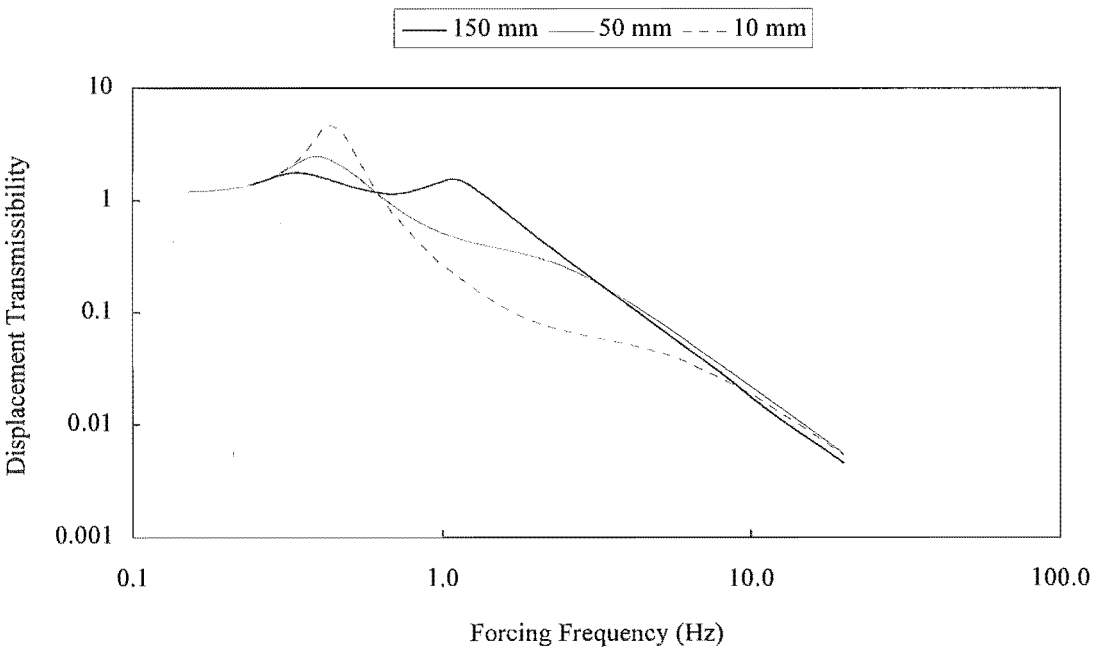

***Figure 5.7** Simulated Suspension Displacement Transmissibility Using an Orifice Restrictor (m_{pat} = 68 kg, 2.0 mm orifice)*

At above 10 Hz, the suspension displacement transmissibility is largely unaffected by input displacement amplitude. This is because suspension damping is minimal at high frequencies, as explained in Section 5.2.2.

5.6.2 Suspension Response to Ambulance Floor Vibration

a) Effect of Restriction Size

Figure 5.8 shows the variation of peak and r.m.s. patient accelerations with orifice size when the suspension is mounted on the ambulance model shown in Figure 5.6 and 600 m of minor road is traversed at 15 m/s (54 km/h). As orifice size is reduced, damping is increased and suspension isolation performance is seen to worsen. The trend using a capillary restriction is similar and is not shown here.

While r.m.s. acceleration is a good indicator of isolation performance [103], a single high acceleration could be harmful to an injured patient so the peak values of acceleration have been considered also. For the results shown here, the method of suspension performance evaluation (r.m.s. or peak) appears to be unimportant. That is, both measures indicate the same isolation performance trends for different restriction types and sizes.

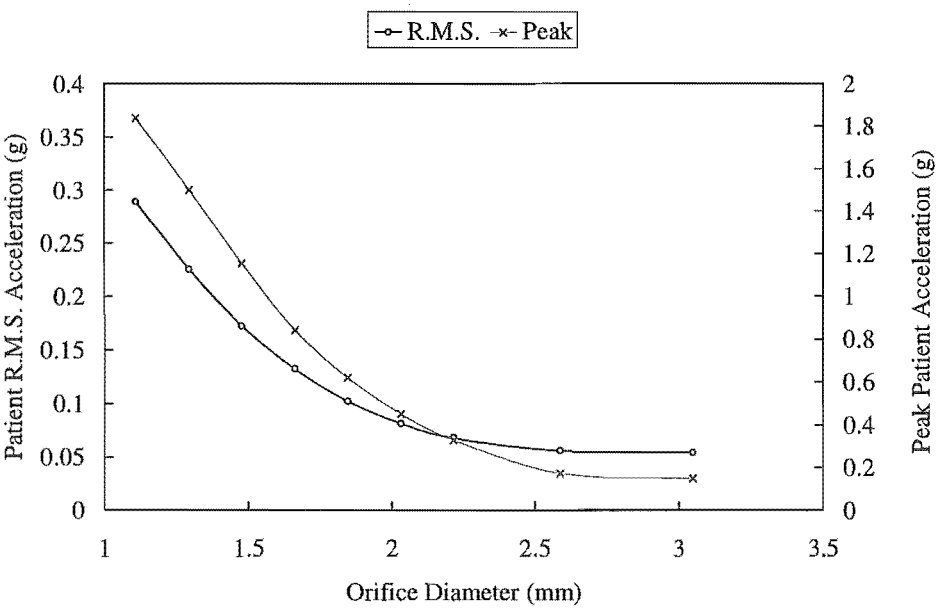

Figure 5.8 The Effect of Orifice Diameter on Suspension Isolation Performance ($m_{pat} = 68\ kg$)

Because spectral accelerations of the ambulance floor are relatively low in magnitude at frequencies around the stretcher suspension natural frequency (Figure 5.11), high

damping to limit stretcher suspension resonance is not required. Accordingly, the best value of damping is the lowest that is sufficient to prevent the suspension from exceeding its maximum stroke capability. In this regard, having a suspension with a suitably long stroke is of key importance in obtaining good isolation as it permits a lower value of damping to be used.

Table 5.1 Damping Restriction Performance Comparison

Restriction Type	*Capillary*	*Orifice*
Restriction size	$C_R = 0.235$ pm^5/Ns	$d_{or} = 3.0$ mm
Patient r.m.s. acceleration (g)	0.051	0.054
Patient peak acceleration (g)	0.14	0.15

b) Effect of Restriction Type

Table 5.1 gives the capillary and orifice restrictor sizes which result in the lowest level of r.m.s. and peak patient accelerations for a patient of average mass. These restrictor sizes were determined on the basis of using the full suspension stroke. This was thought to be a reasonable approach given that the combination of road roughness and travelling speed considered in this simulation work give rise to ambulance floor vibrations that are greater than would be experienced in a typical ambulance journey (as evidenced by comparison of Figure 5.10 with Figure 8.2).

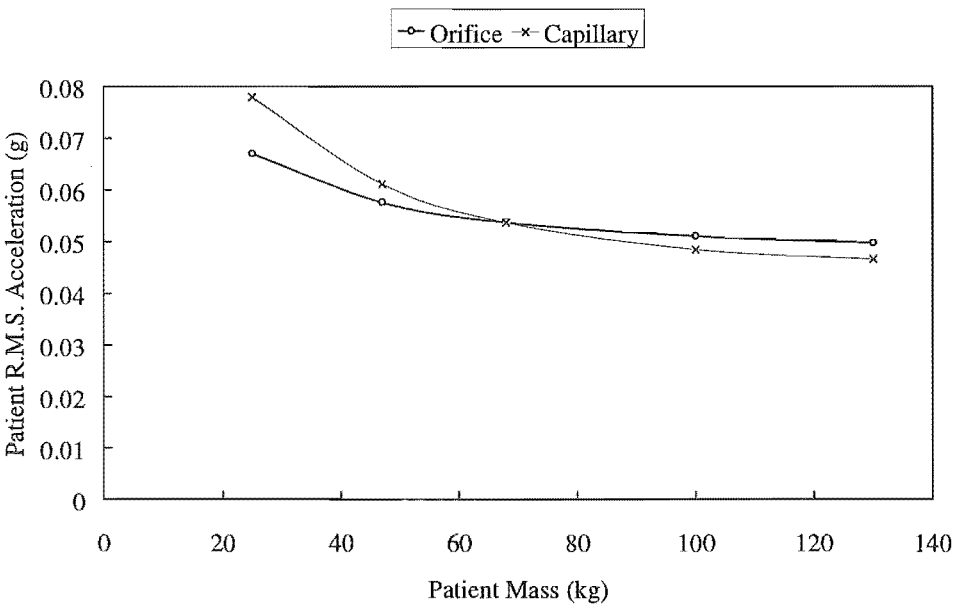

***Figure 5.9** The Sensitivity of Capillary and Orifice Damping Methods to Load Change (capillary coefficient $C_R = 0.121$ pm^5/Ns, 3.0 mm orifice)*

As table 5.1 shows, suspension isolation when using the capillary damper is superior to that when using the orifice damper by a little less than 5%.

Figure 5.9 compares patient r.m.s. accelerations for the two restriction types as a function of patient mass. It confirms that the orifice damping method is less sensitive to changes in load than the capillary damping method. For the results presented the figure, the capillary restrictor coefficient was set to 0.121 pm^5/Ns so that, for a patient of average mass, the r.m.s. accelerations of the patient were the same for both restriction types. This makes clearer the effect of load change on the relative performance of the two damping methods.

5.6.3 Restriction Type Evaluation and Selection

a) Stretcher Suspension Application

The performance of the two restriction types is very similar, with the capillary exhibiting slightly superior isolation and the orifice better insensitivity to changes in load.

Because the level of damping required for the suspension is low, the mass flow rate of air through the capillary restriction is high. Consequently, a large cross sectional flow diameter d_c is required in order to ensure laminar flow ($R_e = \frac{4\dot{m}}{\pi d_c \mu}$ less than 2000). This would mean that the capillary restriction would be physically bulky. In practice, an arrangement using foam restrictors or multiple tubes in parallel might be used (eg. 384 tubes, 0.5 mm in diameter, and 1.35 m long used in parallel give $C_R = 0.235$ pm^5/Ns and a maximum Reynolds number of 2000 for the simulated journey considered here). Alternatively, the restrictor could be reduced in size a little in the knowledge that high acceleration inputs would not result in laminar flow.

In contrast, the orifice restriction is compact and easy to manufacture. On this basis it was chosen for experimental work in preference to the capillary - a diameter of around 3.0 mm being suitable.

b) General Evaluation

The stretcher suspension application of pneumatic damping is not a good one for making general observations on the relative merits of orifice and capillary restrictions. This is because the required level of damping is modest.

Table 5.2 Damping Restriction Performance Comparison
(for a reduced working space of 37.4 mm r.m.s.)

Restriction Type	*Capillary*	*Orifice*
Restriction size	$C_R = 4.87$ pm^5/Ns	$d_{or} = 1.8$ mm
Patient r.m.s. acceleration (g)	0.086	0.13
Patient peak acceleration (g)	0.27	0.84

However, for the case where the suspension r.m.s. working space is arbitrarily reduced to 37.4 mm, and the level of damping is increased accordingly, the capillary restriction gives the better isolation as shown in Table 5.2 - particularly of peak floor vibrations. This example is of course unrealistic, as in practice the suspension stiffness would be increased if the working space was reduced. The results of the table do however suggest that the linear characteristic provided by the capillary restriction might be preferable to the non-linear characteristic provided by the orifice.

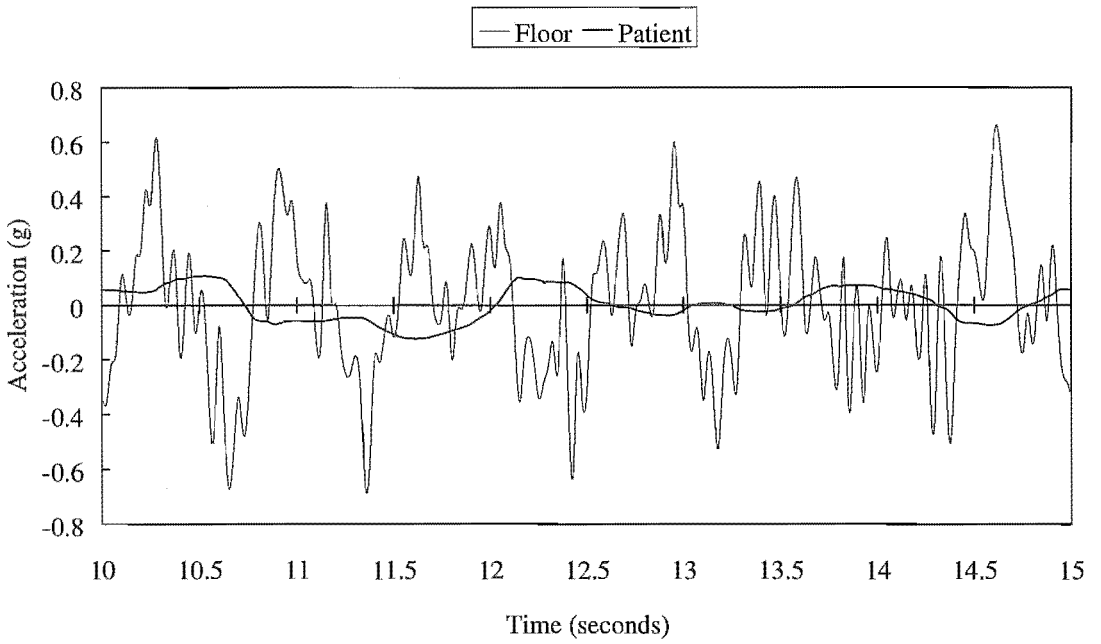

***Figure 5.10** Ambulance Floor and Patient Vertical Accelerations*
(m_{pat} = 68 kg, 3.0 mm orifice)

5.7 SUSPENSION PERFORMANCE

5.7.1 Bounce

When a 3.0 mm diameter orifice is used in the stretcher suspension the patient is well-isolated, as shown in Figure 5.10. In Figure 5.11, ambulance floor and suspended stretcher acceleration spectra (r.m.s.) are compared. (These spectra were calculated from the acceleration power spectral density given by Matlab's *psd* function). It can be seen that good isolation of high frequency vibrations is achieved and that the dominant floor vibrations at 1.6 Hz are well isolated. The response of the suspension is predominantly at its low natural frequency of 0.46 Hz and amplification of floor vibrations below 0.65 Hz is evident. The net effect of the suspension is however clearly beneficial with r.m.s. acceleration reduced from 0.28g to 0.054g , and peak acceleration from 0.98g to 0.15g.

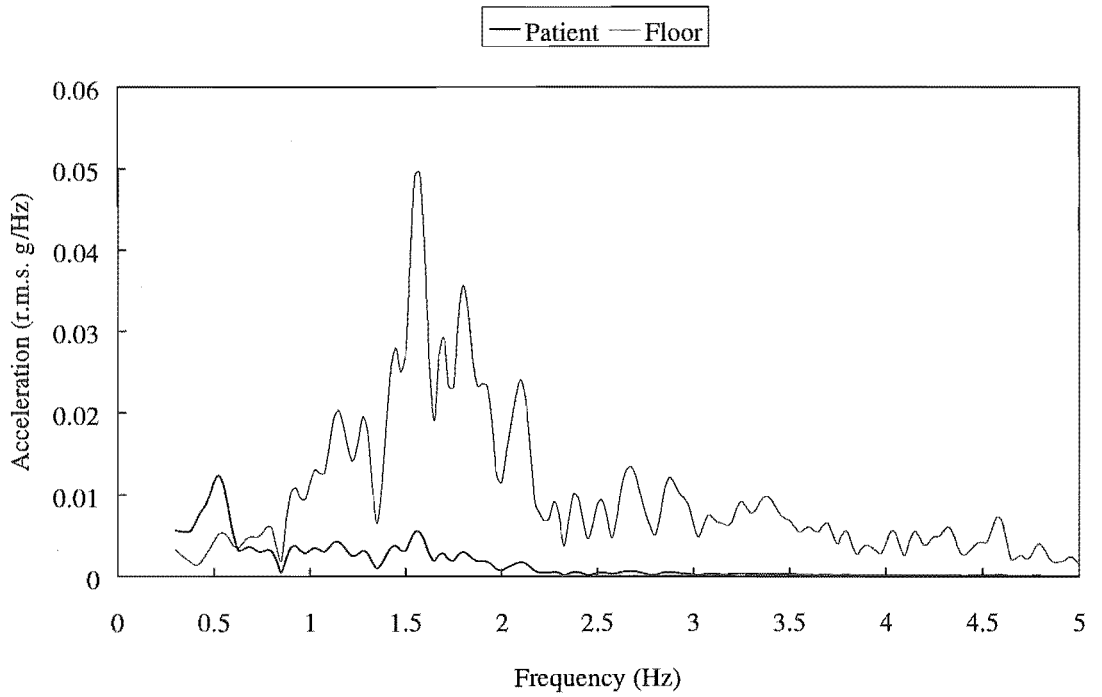

***Figure 5.11** Ambulance Floor and Patient Bounce Acceleration Spectra (m_{pat} = 68 kg, 3.0 mm orifice)*

In practice, the actual levels of isolation will be inferior to these simulated values due in part to the effects of linkage and cylinder friction. This is discussed further in Chapter 7.

5.7.2 Pitch

The results presented thus far have considered only damping of the vertical mode of the suspension. However, using the linear analysis of Appendix C, Equation 5.27 can be derived. It defines the relative magnitude of the pitch and bounce damping ratios (ξ_y:ξ_θ) as a function of the linkage geometry, the load mass and inertia, and the suspension natural frequencies. For a patient of average mass, this expression is equal to 1.18 which indicates that the level of damping of both modes is similar.

$$\frac{\xi_y}{\xi_\theta} = \frac{\omega_\theta}{\omega_y}\left(\frac{I_{pat} + I_{str}}{m_{pat} + m_{str}}\right)\left(\frac{(a+b)\sqrt{L_1^2 - b^2}}{eb + (a+b)\sqrt{L_1^2 - b^2}}\right) \tag{5.27}$$

The level of suspension damping is dictated by the requirement in bounce, because the bounce working space is a little less than that in pitch (relative to typical ambulance floor input levels).

5.8 SUMMARY

In this chapter, the results of a literature review on pneumatic damping have indicated the following:

- Self-damped pneumatic springs have a dual frequency character.
- The capillary restriction gives a linear damping characteristic.
- The orifice restriction gives a non-linear characteristic whereby small amplitude vibrations are virtually undamped.
- The orifice restriction gives a damping force which adapts to suit the mass of the load. (Damping force increases with load.)
- The capillary restriction gives a damping force which varies little with load. (Heavy loads therefore tend to be underdamped and light loads overdamped.)

By simulation, the performance of the stretcher suspension when using orifice and capillary damping restrictions has been studied. The key results of these simulations are:

- A high level of damping is not necessary since
  - the available suspension working space is generous,
  - vibrations of the ambulance floor are modest at frequencies near the suspension natural frequency.
- The performance of the suspension is similar when using either of the two restriction types.
- The orifice restriction has been chosen for installation in the suspension as it is compact and readily manufactured.
- The stretcher suspension theoretically provides good levels of isolation when fitted with a 3.0 mm orifice restriction (eg. r.m.s. patient acceleration reduced by a factor of 5 compared to the case where the stretcher sits directly on the ambulance floor).

CHAPTER 6

Semi-Active Pneumatic Damping

6.1 INTRODUCTION

According to the simulation results of the previous chapter, the suspension is theoretically capable of providing good levels of isolation above approximately 1.0 Hz. However, amplification of floor vibrations at frequencies below the cross-over frequency (approximately 0.65 Hz) is inevitable (Figure 5.11).

In this chapter, reducing amplification of these low frequency floor vibrations by using adjustable orifice restrictors is studied. Both switchable (2-state) and continuously variable orifice control strategies are considered.

To begin with, approaches to active suspension control are briefly reviewed.

6.2 ACTIVE SUSPENSIONS

A passive suspension typically has components which can store energy (springs) or dissipate energy (dampers) as shown in Figure 6.1. The force produced by these components is inherently limited to being a function of the relative motion between the input and the load.

On the other hand, active suspensions (which employ a controllable force actuator in place of one or all of the passive suspension elements) can generate a force which is independent of suspension relative motion - energy can be dissipated or added to the system at will.

Although the bulk of publications considering active suspension/isolation systems are relatively recent, Karnopp et al [104] refer to patents granted in the 1920's for shock absorbers in which a seismic mass was intended to activate hydraulic valving. Ruzicka's 1968 state-of-the-art paper [105] mentions an active suspension developed in 1938. Of these early systems, most of the practical examples tended to simply provide continuous self-levelling action. This allowed a lower natural frequency to be used without resulting in large static deflections due to load changes or sustained acceleration.

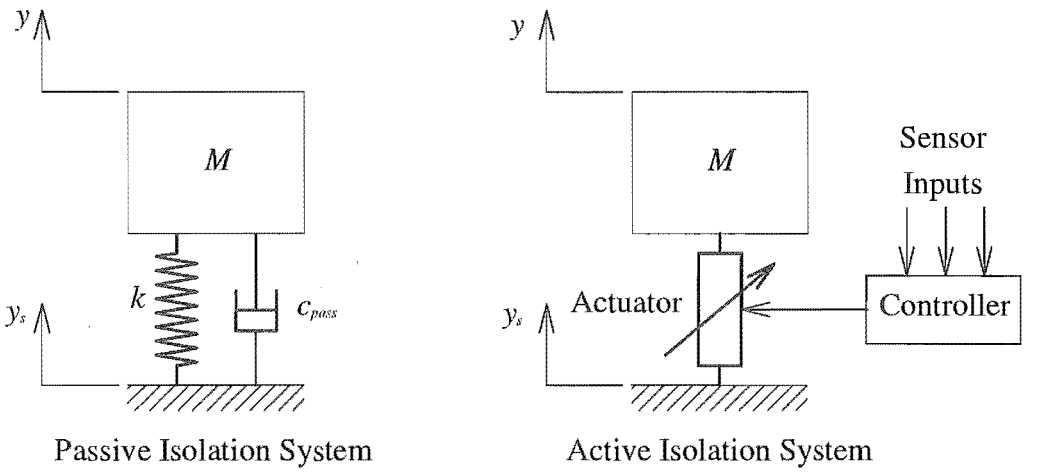

***Figure 6.1** Schematic of Passive and Active Suspension Systems*

More recent active suspension developments are reviewed by Goodall and Kortüm [106], and Pollard and Simons [107], both of whom focus mainly on rail vehicle applications. Sharp and Crolla [100], and Claar II and Vogel [108] consider automotive suspension applications. Nagai [109] has reviewed both automotive and rail active suspension research, looking mainly at work done in Japan, while a classified bibliography of advanced suspensions for ground vehicles has been prepared Elbeheiry et al [110]. Some contemporary texts also include a discussion active suspensions - Bastow and Howard [3], and Gillespie [103] being examples.

6.2.1 Classification of Active Suspensions

The review of Sharp and Crolla [100] is particularly thorough and includes a comprehensive discussion of road and suspension modelling techniques; advanced automotive suspensions; and suspension control strategies. It classifies advanced automotive suspensions in the following way:

a) Active

In a (fully) active suspension, the passive suspension elements are replaced by a force actuator - commonly a hydraulic ram. The control bandwidth of the actuator extends substantially beyond the wheelhop frequency, which is typically near 10 Hz.

b) Semi-Active

A semi-active suspension can be a considered as a simplification of a fully-active suspension as the force actuator can only dissipate energy rather than supplying it as well. A spring in parallel with the force dissipater (adjustable damper) is required to support the load. A number of devices capable of providing a controllable dissipative force have appeared in the literature. These include a hydraulic damper fitted with an adjustable flow restriction [111], a hydraulic damper utilising an electro-rheological fluid [112], and an electromagnetically actuated friction device [113].

A simplification of the semi-active approach is to switch between two or more discrete damping settings rather than to vary the damping force continuously.

c) Slow-Active

Slow-active systems can be thought of as fully-active systems with a reduced control bandwidth - commonly around 3 Hz. This bandwidth is sufficient to control the vehicle sprung mass resonances in bounce, pitch, and roll. Two approaches are used to provide the suspension force. One is to use a rigid actuator (such as a hydraulic ram, or electric motor and leadscrew) in series with a spring. At frequencies above the control bandwidth, the actuator is rigid. The other approach is to use an inherently flexible actuator such as a pneumatic ram.

The power requirements of slow-active and fully-active suspensions can be reduced markedly by employing a passive spring in parallel with the actuator. The actuator needs then to respond to dynamic forces only.

Crolla and Nour [114] compare these suspension control strategies in terms of power requirements and performance. The performance of the semi-active and slow-active approaches are shown to be comparable, but inferior, to the fully-active case. The use of a switchable damper is reported to offer a performance somewhat better than a system with a passive damper, but not as good as the more complex approaches. The power requirements of the fully-active and slow-active approaches were found to be similar.

6.2.2 Active and Advanced Pneumatic Suspensions

Although a number of slow-active and advanced suspensions using pneumatic components have been proposed, modelled, and in some cases tested experimentally, there appear to be few examples in commercial use. Some of the literature in this area is reviewed below.

a) Rail Vehicle Applications

Cho and Hedrick [32] have investigated using single-acting pneumatic actuators in parallel with passive pneumatic springs for improved lateral isolation of passenger carriages. Their results show that a 50% improvement in r.m.s. acceleration was achieved using a control bandwidth of 3 Hz. Good levels of isolation were also measured by Jindai et al [34] who built and tested a $(^1/_5)^{th}$ scale rail passenger car fitted with double-acting pneumatic actuators.

A novel control approach is described by Klinger and Calzado [35] who developed an on/off pneumatic suspension. This suspension used a double-acting pneumatic actuator, the upper and lower chambers of which were connected via a solenoid valve which could close to provide a stiff actuator or open to provide damping (by restricting air flow between the chambers). A 3-position/4-way valve was used to control air flow in and out of the actuator chambers. In using solenoid valves and on/off control, this system could be less costly than suspensions utilising servo-valves and continuous control. The simulated performance of the system was reported to be comparable to that of a fully-active hydraulic suspension.

b) Automotive Applications

Esmailzadeh [115] has studied the performance of a servo-valve controlled pneumatic suspension intended for automobiles. A rubber bellow actuator was used, and passive damping was provided by fitting capillary resistances in the line between the actuator and an auxiliary tank. Results of the study indicated good agreement between linear theory and experiments. Very good isolation was realised for a broad range of frequencies.

A low bandwidth, servo-valve controlled, pneumatic seat suspension intended for use in off-road vehicles and earth moving machines is described by Stein [116]. Experimental results are presented which compare the performance of the seat in active and passive modes. A marked improvement in isolation when using active control is evident - particularly at frequencies around the natural frequency of the passive system. The primary obstacle to commercial production is regarded as being the price of the sensors.

Sharp and Hassan [117] have simulated the performance of a slow-active pneumatic suspension in which actuator pressure was controlled with an air pump driven by a d.c. motor rather than by a servo-valve and high pressure air supply. This approach was reported to give advantages with respect to capital cost, maintenance, and particularly energy consumption.

Decker et al [118] describe briefly an experimental system developed by Bosch which used a pneumatic spring with several auxiliary volumes. By switching between the volumes the spring stiffness could be varied dynamically, although careful consideration of the switching processes was required to prevent disturbing oscillations from occurring.

A much simpler approach to improving pneumatic suspension performance has been implemented by automobile manufacturers such as Toyota and Mitsubishi. The system of Toyota, which was developed for the 1986 Soarer, used 3-state switchable hydraulic dampers and 2-chamber pneumatic springs at each wheel station [29,30]. The springs could be arranged to give three distinct rates by operating on the main chamber, the auxiliary chamber, or both chambers. Alteration to the settings of the suspension were made to suit vehicle speed and road roughness, and/or to limit vehicle attitude changes during manoeuvring. The system of Mitsubishi appears to be substantially similar, although only two damping rates and two spring rates are used [31]. These systems are better regarded as being passive and adaptive rather than active.

6.2.3 Semi-Active Pneumatic Damping

On the basis of Section 6.2.1 it would appear that a semi-active pneumatic suspension might offer improved performance over a passive pneumatic suspension, but without the power requirements associated with the slow-active control approach. The implementation of the semi-active control approach using pneumatic devices does not appear to have been considered however - this observation being made on the basis of a reasonably thorough, but not comprehensive, literature search.

The performance of the stretcher suspension when fitted with adjustable (semi-active) damping restrictors has been studied by simulation - the primary objective being to reduce amplification of floor vibrations below 0.65 Hz without impairing the isolation of higher frequency inputs. This is discussed further in the remainder of this chapter.

6.3 ADJUSTABLE PNEUMATIC DAMPER CONTROL

6.3.1 Skyhook Damping

It is possible to determine a good strategy for adjusting the stretcher suspension damping restrictors by studying the simple mechanical isolation systems shown in Figure 6.2. Transmissibilities for these systems are presented in Figure 6.3.

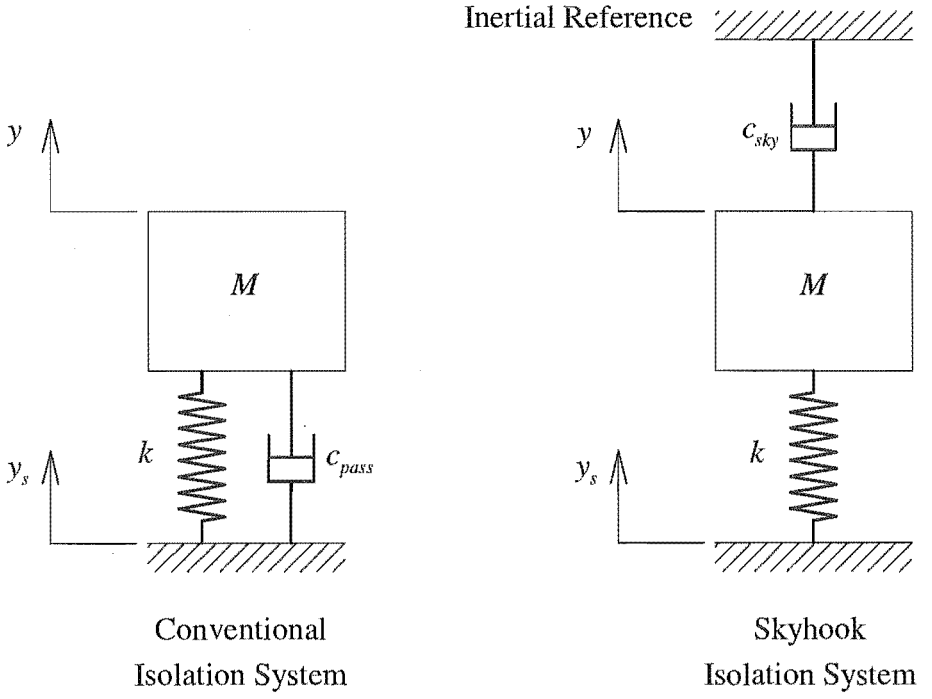

***Figure 6.2** Schematic of Conventional and Skyhook Isolation Systems*

As shown by Figure 6.3, the level of damping in a conventional linear isolation system is a compromise between providing good control of resonance (high damping) and good high frequency isolation (low damping) - both cannot be optimised simultaneously. On the other hand, in a so-called skyhook system (where the damper is attached to a fixed point in space rather than between the input and the load) good high and low frequency performance can be realised. With skyhook (or absolute) damping, the damping force is generated in proportion to the absolute velocity of the suspended mass $\dot{y}$. The force generated by a conventionally connected damper is in proportion to the suspension relative velocity ($\dot{y} - \dot{y}_s$).

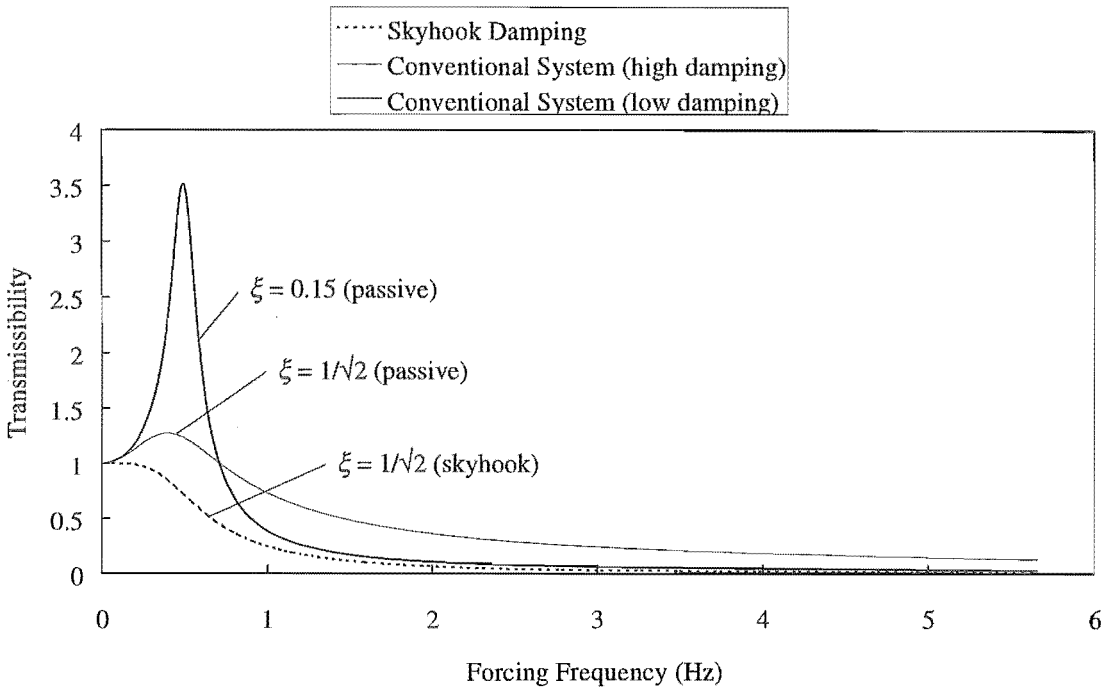

***Figure 6.3** Transmissibilities of Conventional and Skyhook Isolation Systems*

It can be shown mathematically (by using linear optimal control theory) that the skyhook damping approach is optimal in terms of minimising quadratic performance indices containing the suspension deflection ($y - y_s$) and the acceleration of the load ($\ddot{y}$) [104,106]. These indices represent the working space and isolation performance of the suspension respectively. Intuitively, the skyhook approach is advantageous since damping forces will be generated only when required (ie. when the mass moves). Damping forces in a conventional isolator are generated whenever the input moves relative to the mass.

Although attaching the damper to a fixed point in space is generally not physically possible, an active suspension can be made to mimic the behaviour of the skyhook system by appropriate control of the actuator force.

6.3.2 Control Strategy

Figure 6.4 shows the method used to implement the skyhook damping strategy in the stretcher suspension model. For clarity, the linkage of the suspension is omitted and only one of the two isolators is shown.

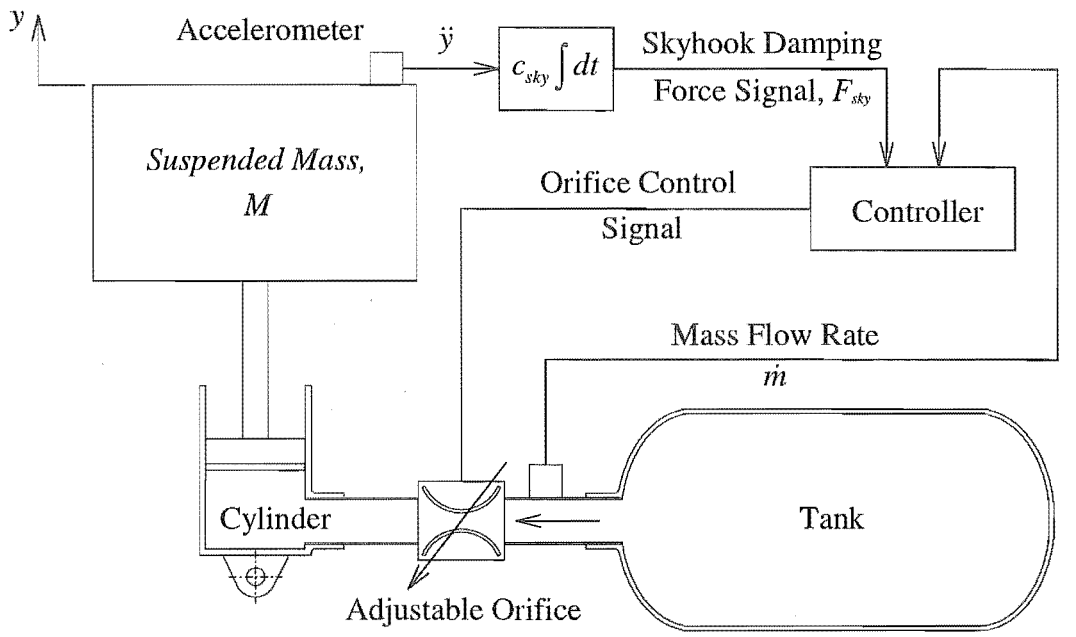

***Figure 6.4** Implementation of Skyhook Damping for the Stretcher Suspension*

The skyhook damping force ($F_{sky} = c_{sky}\dot{y}$) is determined by integrating the signal from an accelerometer mounted on the suspended load. The mass flow $\dot{m}$ between cylinder and tank is also measured.

The orifice area is then controlled (open loop) as follows:

a) $\dot{m}$ and $\dot{y}$ same sign (energy to be dissipated)

When the mass flow rate ($\dot{m}$) and the absolute velocity of the load ($\dot{y}$) are of the same sign, then energy is required to be dissipated from the system. In this case the orifice area is set to give the skyhook damping force F_{sky}. (ie. demand damping force F_d = skyhook damping force, F_{sky}).

b) $\dot{m}$ and $\dot{y}$ opposite sign (energy required)

When the mass flow rate ($\dot{m}$) and the absolute velocity of the load ($\dot{y}$) are of opposite sign, then energy is required of the damper. Since this is not possible the orifice is opened fully. (ie. demand damping force $F_d = 0$).

In order to track the skyhook force continuously, an actuator (as used in a fully-active or slow-active suspension) rather than a controllable damper would be required.

The open loop control approach, as proposed here for the stretcher suspension, is commonly used for adjustable dampers and it can be preferable to closed loop force feedback control. (With force feedback control, the damper is adjusted according to the error between the measured and demand damping forces). For example, Besinger et al [119] have compared by experiment open and closed loop control of an adjustable hydraulic damper. They found that an open loop controller provided the best suspension performance (by virtue of a faster response with less phase delay) and noted that it would be less costly to instrument than a controller using force feedback. Force feedback control was considered to have advantages only if the damper was subject to large temperature variations or significant wear.

6.3.3 Orifice Control Law

The equation required to set the orifice area A_{or} for a given mass flow rate $\dot{m}$ and suspended mass absolute velocity $\dot{y}$ can be determined from the analysis of Chapter 5. This is detailed below, with the assumptions that:

- Isolator temperature changes are negligible (ie. $\Delta T_t \cong \Delta T_c \cong 0$). This implies that $T_t \cong T_c \cong T_0$.
- Products of small pressure and volume terms are negligible (ie. $\Delta V_c \dot{p}_c \cong 0$ and $\Delta p_c \dot{V}_c \cong 0$). This implies that $V_c \dot{p}_c \cong V_{c0} \dot{p}_c$ and $p_c \dot{V}_c \cong p_0 \dot{V}_c$.

The vertical equation of motion for the stretcher and patient (Equation 5.13) can be rearranged so that it is explicit in terms of the cylinder pressure p_c. ie:

$$p_c = \frac{(m_{pat} + m_{str})(\ddot{y} + g)}{2A_c} \left(\frac{L_1 \cos\beta + \dfrac{eL_1 \sin\beta}{a + b + (y - y_s)}}{r} \right) + p_{at}. \tag{6.1}$$

This equation can be linearised by first substituting for $L_1 \sin\beta$, $L_1 \cos\beta$ and r (by using Equations C11, C12 and C21/22 respectively), and then ignoring the products of the small displacements y and y_s. This involves considerable algebra. The atmospheric pressure p_{at} can be eliminated by using the static load and pressure Equations B36/37 and B38/39. These steps yield the cylinder pressure as

$$p_c = \frac{(m_{pat} + m_{str})}{2A_c R_y} \ddot{y} - \frac{(m_{pat} + m_{str})g}{2A_c R_y f} \left(1 - R_y \left(\frac{f}{l_0} \right) \right) (y - y_s) + p_0, \tag{6.2}$$

where R_y is the ratio of cylinder displacement δ to vertical suspension displacement y. This ratio is given by

$$R_y = \frac{f}{l_0}\frac{l_1}{L_1}\frac{l_2}{L_2}, \tag{6.3}$$

and is equal to the reciprocal of the spring installation ratio, as defined in Section 3.4.4 of Chapter 3.

A second independent equation for the cylinder pressure p_c can found by considering the mass flow rate through the orifice. This is done by rearranging Equation 5.12 to give

$$p_t - p_c = sign(p_t - p_c)\left(\frac{\dot{m}}{C_d A_{or}}\right)^2 \frac{RT_0}{2p_0}. \tag{6.4}$$

The tank pressure can be eliminated from this equation by using 5.19 to yield

$$-\frac{\gamma RT_0}{V_t}\int \dot{m}dt + p_0 - p_c = sign(p_t - p_c)\left(\frac{\dot{m}}{C_d A_{or}}\right)^2 \frac{RT_0}{2p_0}, \tag{6.5}$$

where the equilibrium pressure p_0 on the left-hand side of this equation is the constant of integration.

The integral of the mass flow rate $\dot{m}$ on the left-hand side of Equation 6.5 can be evaluated by linearising 5.21 to give

$$\dot{m} = \frac{1}{\gamma RT_0}(\gamma p_0 \dot{V}_c + V_{c0}\dot{p}_c), \tag{6.6}$$

which after integration becomes

$$\int \dot{m}dt = \frac{1}{\gamma RT_0}(\gamma p_0 V_c + V_{c0}p_c) + \text{constant}, \tag{6.7}$$

where the constant of integration is eliminated by noting that at $t = 0$, $p_c = p_0$, $V_c = V_{c0}$ and $\int \dot{m}dt = 0$ so that

$$\int \dot{m}dt = \frac{1}{\gamma RT_0}\left((\gamma p_0 A_c R_y (y - y_s) + V_{c0}(p_c - p_0)\right). \tag{6.8}$$

After substituting this expression for $\int \dot{m}dt$ into Equation 6.5, and using Equation 6.2 to eliminate the cylinder pressure p_c, the equation of motion for the stretcher and load can be written as

$$\begin{aligned}&(m_{pat} + m_{str})\ddot{y}\\ &+ sign(p_t - p_c)A_c R_y \frac{V_t}{V_t + V_{c0}} \frac{RT_0}{p_0}\left(\frac{\dot{m}}{C_d A_{or}}\right)^2\\ &+\left(\left(\frac{2\gamma p_0 A_c^{\,2} R_y^{\,2}}{V_t + V_{c0}}\right) - \frac{(m_{pat} + m_{str})g}{f}\left(1 - R_y \frac{f}{l_0}\right)\right)(y - y_s) = 0.\end{aligned} \tag{6.9}$$

The first term in this equation represents the load inertial force, the second represents the damping force, and the third represents the effective spring force.

To determine the manner in which the orifice area should be varied, the suspension damping force is equated to the demand damping force F_d. ie.

a) if $\dot{y}\dot{m} \geq 0$ *(energy to be dissipated,* $F_d = F_{sky}$*)*

$$c_{sky}\dot{y} = sign(p_t - p_c)A_c R_y \frac{V_t}{V_t + V_{c0}} \frac{RT_0}{p_0}\left(\frac{\dot{m}}{C_d A_{or}}\right)^2. \tag{6.10}$$

Making this equation explicit in A_{or} indicates that the orifice area should be set according to

$$A_{or} = sign(p_t - p_c)\frac{\dot{m}}{C_d}\sqrt{\frac{V_t}{V_t + V_{c0}} \frac{RT_0}{p_0} \frac{sign(p_t - p_c)A_c R_y}{c_{sky}\dot{y}}}. \tag{6.11}$$

b) if $\dot{y}\dot{m} < 0$*, (energy required,* $F_d = 0$*)*

$$0 = sign(p_t - p_c)A_c R_y \frac{V_t}{V_t + V_{c0}} \frac{RT_0}{p_0}\left(\frac{\dot{m}}{C_d A_{or}}\right)^2. \tag{6.12}$$

Making this equation explicit in A_{or} indicates that the orifice area should be set to have an infinite area. Since this is not physically possible, the orifice area is set to its maximum value:

$$A_{or} = A_{or,\max}. \tag{6.13}$$

6.3.4 Modelling

The performance of the suspension when using this orifice control strategy is studied by using the ambulance, road, stretcher suspension, and isolator models described in Section 5.5 of Chapter 5. Only the vertical mode of the suspension is considered (no pitch) and, in this initial study, ideal behaviour of the variable-orifice restriction is assumed (ie. the orifice area is considered to vary according to equations 6.11 and 6.13 with no phase lag). All of the simulations have been carried out using a patient mass of 68 kg.

6.4 SIMULATION RESULTS

6.4.1 Continuously Variable Damping

a) Damping Force Variation

Figure 6.5 compares the skyhook, demand, and actual damping forces for four seconds of the simulated journey. The actual damping force is seen to track the demand damping force closely - the differences being attributable to kinematic and thermodynamic non-linearities which are included in the linkage and isolator models but not in the equations used to set the orifice area (6.11, 6.13).

Figure 6.6 shows the variation of orifice area for the same 4 seconds of the simulated journey. When the damping restriction is opened fully ($\dot{y}\dot{m} < 0$, power required) the actual damping force is close to zero. It has been found satisfactory to use a maximum orifice area of 16.8 mm^2, this resulting in minimal pressure drop across the restriction when it is opened fully (Figure 6.7).

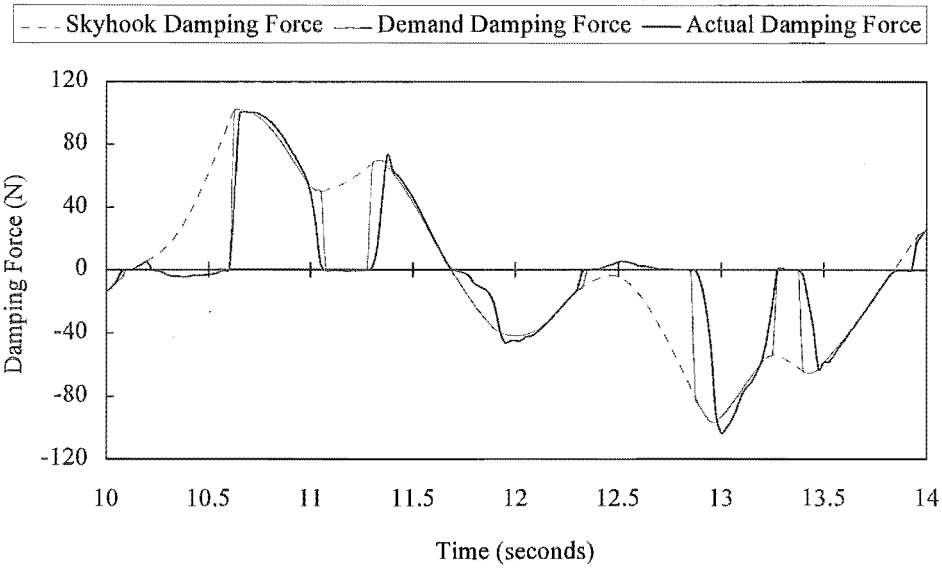

***Figure 6.5** Simulated Skyhook, Demand, and Actual Damping Forces (c_{sky} = 307 Ns/m)*

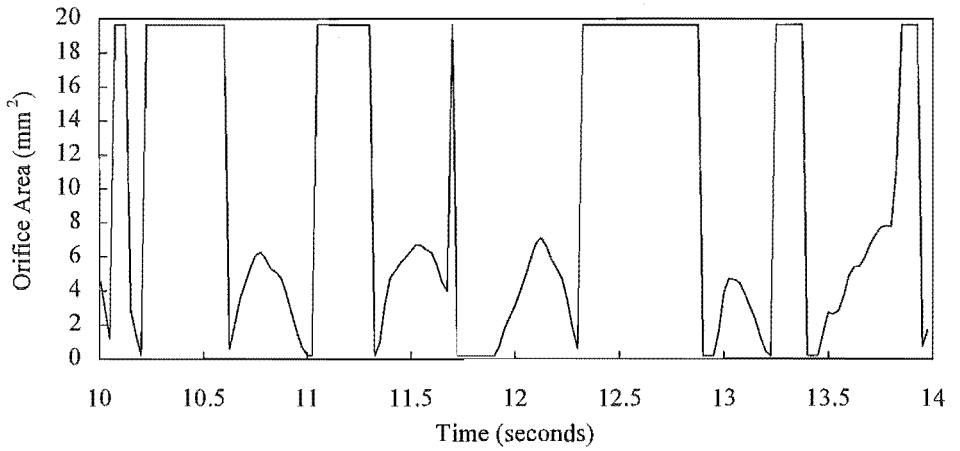

***Figure 6.6** Simulated Orifice Area (c_{sky} = 307 Ns/m)*

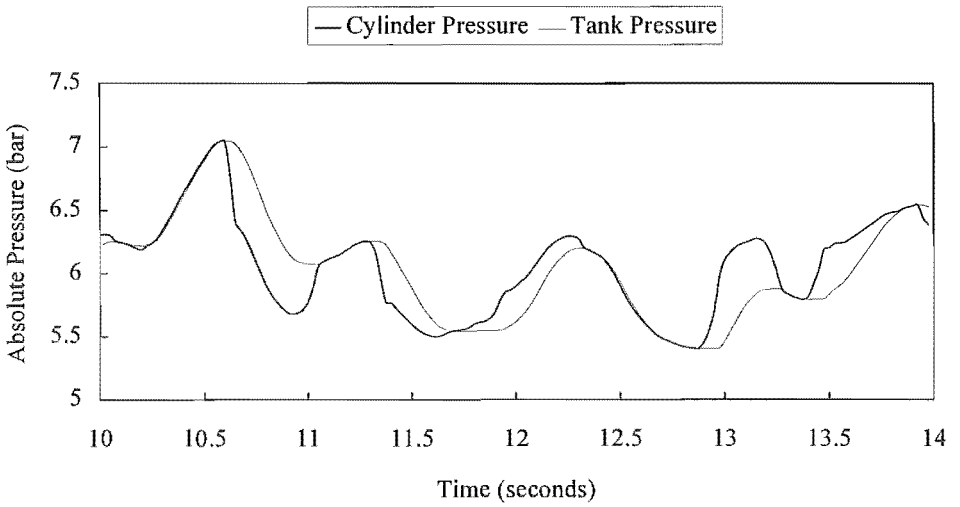

***Figure 6.7** Simulated Tank and Cylinder Pressures (c_{sky} = 307 Ns/m)*

b) Damping Gain

The performance of the suspension was evaluated for a range of damping gains (c_{sky}), some of which are given in Table 6.1. As shown, the r.m.s. acceleration of the stretcher was found to be minimum when using a damping gain of 307 Ns/m - this value implying a damping ratio ξ_{sky} of 0.53. The working space of the suspension tended to reduce for values of gain which gave improved r.m.s. isolation. High values of gain (eg. c_{sky} = 878 Ns/m) were found to completely eliminate amplification of floor vibrations at low frequencies, but were associated with poorer isolation of higher frequencies.

***Table 6.1** The Effect of Damping Gain (c_{sky}) on Suspension Performance*

Damping Gain c_{sky} *(Ns/m)*	*Damping Ratio* ξ_{sky}	*Stretcher R.M.S. Acceleration (g)*	*Suspension R.M.S. Working Space (mm)*
87.8	0.15	0.0453	57.1
249	0.43	0.0380	47.9
307	0.53	0.0377	47.5
468	0.80	0.0384	47.7
878	1.50	0.0431	49.8

6.4.2 Switchable Damping

A simplification to the continuously variable damping strategy considered thus far is to switch between two discrete damping states. The control algorithm for this approach can be found by simplifying Equations 6.11 and 6.13 and is given below.

$$\text{high damping (small orifice) if } (p_t - p_c)\dot{y} > 0$$
$$\text{low damping (large orifice) if } (p_t - p_c)\dot{y} \leq 0$$

6.4.3 Comparison of Systems

The isolation performance of the suspension when using a passive (fixed size) orifice, a 2-state switchable orifice, and a continuously variable orifice have been compared. The optimal orifice sizes for the passive and switchable systems are given in Table 6.2. These sizes were chosen on the basis of using the same r.m.s. working space of 47.5 mm

as the continuously variable system (operating with the optimal gain of 307 Ns/m, Table 6.1).

***Table 6.2** Passive, Switchable, and Continuously Variable Damping Configurations (for an r.m.s. working space of 47.5 mm)*

Orifice Control Method	*Minimum Orifice Area (mm^2)*	*Maximum Orifice Area (mm^2)*	*Damping Gain c_{sky} (Ns/m)*
Passive (fixed size)	4.09	4.09	-
Switchable	3.25	11.8	-
Continuously variable	0.17	16.8	307

Figure 6.8 compares the acceleration transmissibilities for the three damping methods. These transmissibilities were calculated using Matlab's *tfe* function. It is evident that the suspension when fitted with the continuously variable damper provides the best isolation, and that the advantages of this damping approach are most significant at low frequencies (where amplification of floor vibrations occur). While the switchable damper appears to offer a small improvement over the passive damper in reducing amplification at resonance, isolation above around 2 Hz is worse.

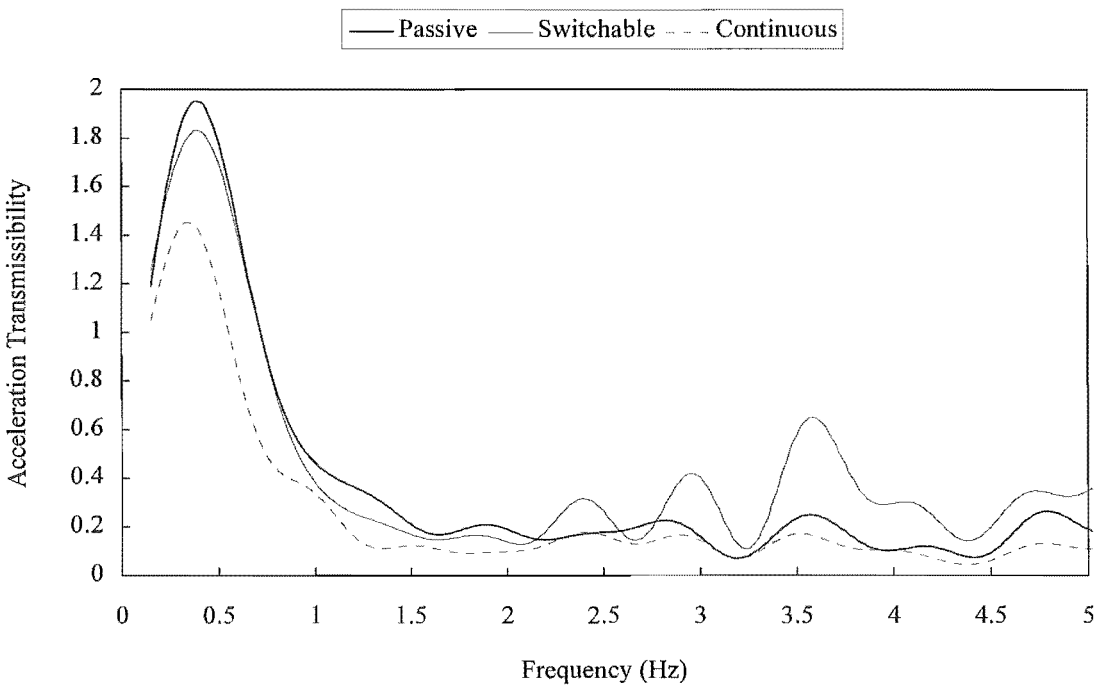

***Figure 6.8** Stretcher Suspension Acceleration Transmissibilities for the Passive, Switchable, and Continuously Variable Damping Methods*

Table 6.3 The Performance of the Passive, Switchable, and Continuously Variable Damping Methods compared to the Unisolated Case

Damping Method	*R.M.S. Isolation*		*Peak Isolation*	
	Stretcher R.M.S. Acceleration (g)	*% of Unisolated*	*Stretcher Peak Acceleration (g)*	*% of Unisolated*
Unisolated	0.278	100	0.97	100
Passive	0.064	23	0.29	30
Switchable	0.056	20	0.27	28
Continuous	0.038	14	0.11	11

In Table 6.3, the r.m.s. and peak accelerations of the stretcher associated with the three damping methods are compared to the r.m.s and peak accelerations of the ambulance floor (unisolated case). It is evident that good levels of isolation are provided by the stretcher suspension, irrespective of which damping method is used. The advantage of the switchable damper over the passive damper appear to be modest in terms of both improvements to peak and r.m.s. isolation. On the other hand, the continuously variable damper gives a marked improvement over the passive damper - particularly in reducing peak vibrations of the stretcher.

6.5 PROSPECTS FOR IMPLEMENTATION

6.5.1 Hardware

In fitting a continuously variable damper to the stretcher suspension, an economical and reliable method of measuring mass flow rate and achieving a restriction with a variable area would need to be chosen. Some possibilities are introduced below.

a) Measurement of Mass Flow Rate

The mass flow rate could be determined in a number of ways. Perhaps the best would be to use a temperature-sensitive microbridge sensor which would give an output voltage proportional to air flow. Such sensors are available at reasonable cost and are used for the likes of medical ventilation/anaesthesia control, gas analysers, and gas meters. Alternatively, a differential pressure transducer could be used to measure the pressure drop across the damping restriction. By knowing the instantaneous restriction area the mass flow rate could then be calculated using Equations 5.8-5.11, although a look-up table based on experimental data might be preferable to provide greater accuracy.

b) Adjustable Orifice Restriction

A simple approach to achieving an adjustable flow restriction would be to use (say) three on/off solenoid valves in combination. This would provide eight (2^3) discrete damping settings. Alternatively, a continuously variable area could be achieved by using a step-motor to drive a rotary valve. To reduce response time, the geometry of the valve port could be arranged to go from fully-open to fully-closed in a quarter turn (or similar).

6.5.2 Adaptation

a) Adaptation to Running Conditions

It is now well established that a key advantage of active suspensions is that their parameters can be (slowly) adjusted to suit the running conditions by using a 'microcomputer supervisor' [100]. This is in contrast to passive systems whose parameters must be chosen to cope with the largest inputs, meaning that their performance over better surfaces is compromised.

For the stretcher suspension, the best value of damping gain (307 Ns/m) applies only to the particular floor input used in the simulations. In practice, the damping gain would be adjusted to suit the prevailing floor vibrations (which for a particular ambulance would vary with road roughness and ambulance speed). While this would place some additional demands on the controller, no additional instrumentation or hardware would be required.

b) Sensitivity to Load Changes

The method presented thus far for controlling the damping restriction makes no allowance for the weight of the patient, and all of the modelling work has assumed a patient mass of 68 kg. It is a relatively simple matter, however, to modify the control equation (6.11) so that the damping force increases with load. This is done as follows:

> Rather than expressing the desired skyhook damping force in terms of the damping coefficient c_{sky} (which has a value which is best for only one particular patient mass), the skyhook damping force is expressed in terms of the damping ratio ξ_{sky} which we choose to be a constant that is independent of mass. Equation 6.10 then becomes

$$2(m_{pat}+m_{str})\omega_y\xi_{sky}\dot{y} = sign(p_t-p_c)A_cR_y\frac{V_t}{V_t+V_{c0}}\frac{RT_0}{p_0}\left(\frac{\dot{m}}{C_dA_{or}}\right)^2. \qquad (6.14)$$

Making this equation explicit in A_{or} (in the manner of 6.11) then yields

$$A_{or} = sign(p_t-p_c)\frac{\dot{m}}{C_d}\sqrt{\frac{V_t}{V_t+V_{c0}}\frac{RT_0}{p_0}\frac{sign(p_t-p_c)A_cR_y}{2(m_{pat}+m_{str})\omega_y\xi_{sky}\dot{y}}}. \qquad (6.15)$$

For a patient of average mass, controlling the orifice damper according to this equation would give the suspension an identical performance to that presented in Section 6.4. For other patient masses, the performance would be similar - any differences being due to suspension non-linearities which are not allowed for in the equation and/or the small change in suspension natural frequency that occurs as patient mass is altered (Figure 4.4).

6.5.3 Evaluation

The results of the simple simulations presented here suggest that semi-active pneumatic damping of the stretcher suspension would give improved isolation. However, the acceptable levels of isolation afforded by the use of a fixed size orifice make the additional cost and complexity associated with the implementation of the semi-active approach unwarranted. In addition, the improvements obtained by using a controllable damper would be less marked than the simulation results suggest, as the model has assumed ideal damping valve behaviour.

It is possible however, that the semi-active pneumatic damping method might usefully be applied in other isolation applications where the requirements of simplicity and low cost were less of a priority. To this end, further study of the characteristics of semi-active pneumatic damping might prove worthwhile. Such a study could include investigation of the following by simulation:

- The sensitivity of the optimal value of c_{sky} to input vibration level.
- The importance of adjusting c_{sky} to suit the load.
- The importance of cylinder/tank volume ratio.
- The degradation in performance due to valve dynamics.
- The effects of control bandwidth.
- The performance relative to other suspension systems (eg. fully-active hydraulic, slow-active pneumatic).

Experiments would be useful - particularly in determining if open loop control of the orifice would be satisfactory.

6.6 SUMMARY

Key points of this chapter are summarised below:

- Active suspensions have advantages over passive suspensions, and skyhook damping provides the opportunity to limit amplification at resonance without compromising the isolation of higher frequencies.
- The results of simple simulations (in which ideal restriction behaviour is assumed) suggest that the stretcher suspension would provide better isolation using a semi-active pneumatic damper than when using a passive damper.
- In theory, the stretcher suspension provides good levels of isolation with a passive damper, so that the incorporation of the more sophisticated semi-active damping approach would not appear to be justified.
- The semi-active pneumatic damping method might be usefully applied in other applications, and would benefit from further theoretical and experimental study.

CHAPTER 7

Laboratory Tests

7.1 INTRODUCTION

A laboratory shaking table has been used to measure suspension acceleration transmissibilities in bounce and pitch. A range of inputs have been used, and the effects of both pneumatic damping level and patient mass have been investigated.

In this chapter, the shaker table is described and the suspension acceleration measurement and processing methods are reported. Test results are then presented, discussed, and compared with theoretical results. Particular attention is paid to the detrimental effects of Coulomb damping.

7.2 SHAKER TABLE

The Department of Mechanical Engineering at the University of Canterbury had no shaker tables suitable for the purpose of stretcher suspension testing. Financial and time constraints ruled out the design and construction of a servo-controlled, hydraulically actuated machine capable of providing inputs typical of an ambulance floor. It was therefore decided to build a simple direct-drive mechanical shaker capable of providing sinusoidal inputs only. As a result, study of the experimental response of the suspension to random inputs was limited to road testing (Chapter 8).

7.2.1 Actuation Method

Of the mechanical table actuation methods considered, the round cam was chosen for its simplicity and ability to provide sinusoidal motion. The key features of using a round cam-driven shaker are introduced by considering the simple single-cam system of Figure 7.1. The right-hand side of the figure shows a free body diagram for the system. Although simple, this system has the key features of the actual table used for testing which is shown in Figures 7.2a-e.

The vertical acceleration of the table load ($\ddot{y}_s$) is given by Equation 7.1. It indicates that sinusoidal motion of the vibrated mass is realised only if the camshaft speed is constant. ie. $\ddot{\theta}_c = 0$.

$$\ddot{y}_s = -r_s\dot{\theta}_c \sin\theta_c + r_s\ddot{\theta}_c \cos\theta_c . \tag{7.1}$$

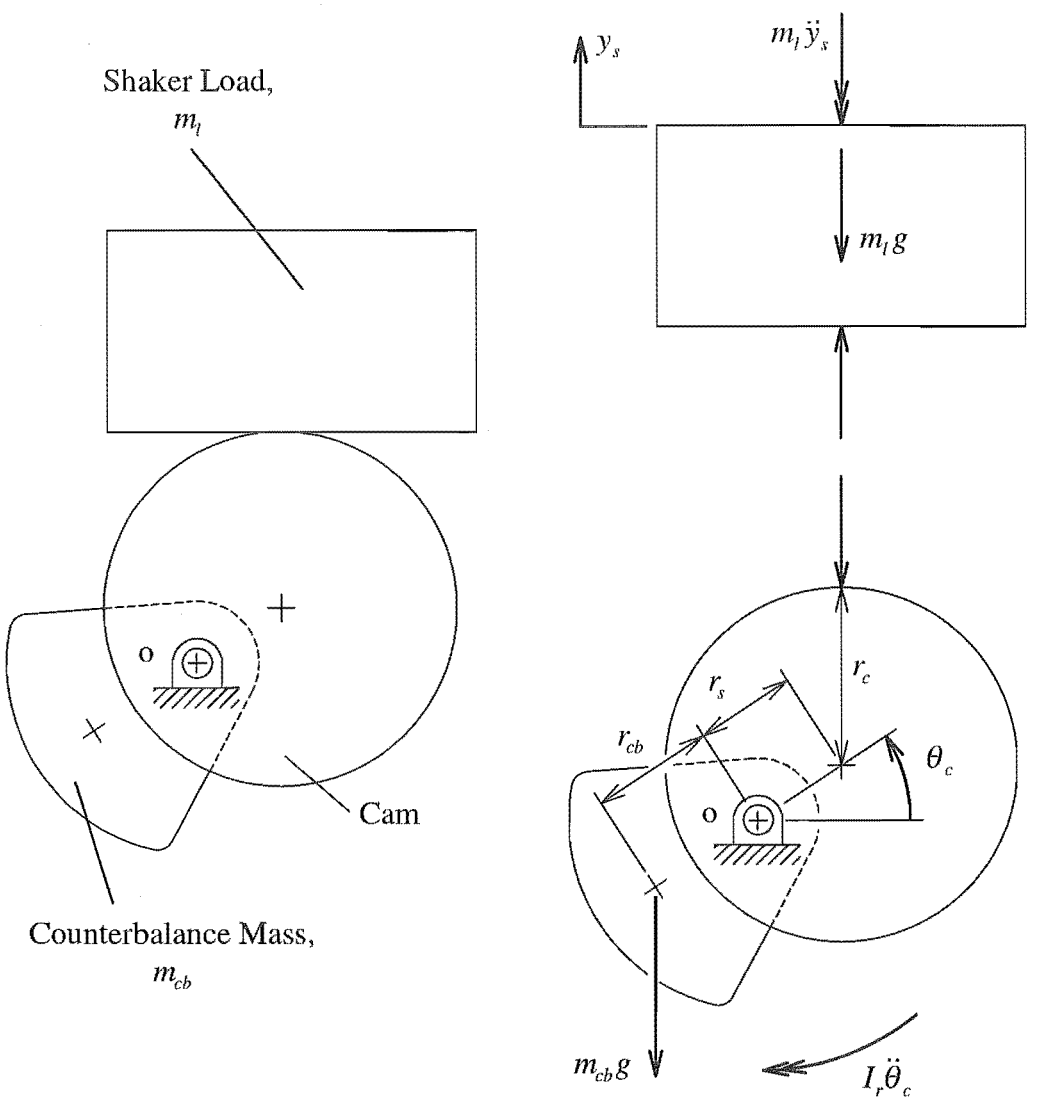

***Figure 7.1** A Simple Cam-Actuated Shaker (shown with a free body diagram)*

By taking moments about the camshaft axis 'o', and neglecting friction and other losses, the camshaft angular acceleration can be found:

$$\ddot{\theta}_c = \frac{(r_{cb}m_{cb} - r_s m_l)g\cos\theta_c - m_l\ddot{y}_s r_s \cos\theta_c}{I_r} . \tag{7.2}$$

This equation shows that the unwanted acceleration ($\ddot{\theta}_c$) of the system is a result of:

- A component of torque resulting from static imbalance (the first term in the numerator of Equation 7.2).
- A component of torque resulting from the acceleration ($\ddot{y}_s$) of the load (the second term in the numerator of Equation 7.2). This component peaks twice per cam revolution as $\ddot{y}_s$ is a function of $\sin\theta_c$ and $\sin\theta_c\cos\theta_c = \frac{1}{2}\sin(2\theta_c)$.

Accordingly, the speed fluctuations of the system (a function of the magnitude of $\ddot{\theta}_c$) can be reduced to acceptable levels by arranging for the system to be statically balanced (ie. $r_s m_l - r_{cb} m_{cb} = 0$), and/or by increasing the flywheel effect provided by the inertia (I_r) of the cam, camshaft, and counterbalance assembly.

7.2.2 Mechanical Embodiment

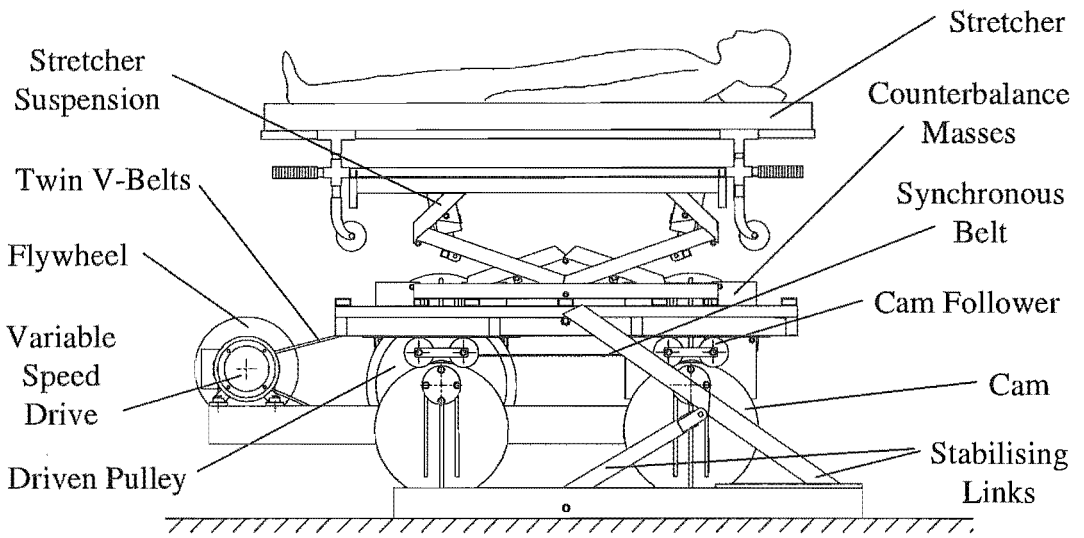

***Figure 7.2a** The Laboratory Shaker Table (shown configured for vertical inputs)*

Figure 7.2a shows an elevation of the shaker table used for testing. Manufacturing drawings for the table can be found in Appendix G.

The structural steel table platform is actuated by two cams (450 mm diameter) whose eccentricity can be independently adjusted to give bounce, pitch, or a combination of these motions. For pure bounce motion, the cams are set to have the same stroke. For pure pitch, the cams are set to have equal and opposite strokes. Any other combination

of cam strokes results in a combination of pitch and bounce. The cams drive the table through cam followers which rest on the cams. These followers eliminate sliding contact at the cam/table interfaces and consist of nylon rollers which are held in a steel frame and run on deep groove ball bearings.

The cams are driven through a twin V-belt reduction (7.39:1) by a 2 pole, 4 kW variable speed AC drive. An optical tachometer measures shaker table speed. Speed fluctuations of the machine (due to the acceleration of the load and table, Section 7.2.1) are reduced by attaching a flywheel to the motor output shaft. Static balance of the machine is achieved by fitting counterbalance masses at 180° to the cams. The eccentricity and mass of the counterbalances are altered to suit the cam stroke and patient mass respectively.

To permit continuous stroke adjustment of the machine, both the cams and counterbalances are attached to the camshafts by friction joints - each held together by 4 M12 bolts torqued to 80 Nm. During adjustment, a locking pin is fitted through the machine frame and into the driven pulley to prevent rotation of the camshafts.

The reversing nature of the torque on the machine led to the following choice of transmission components:

- A synchronous toothed belt drive rather than a chain drive to couple the cams.
- Friction locking rings rather than keys to attach:
  - the cam and counterbalance hubs to the camshafts
  - the flywheel/pulley assembly to the motor output shaft
  - the synchronous belt pulleys to the camshaft

A stabilising mechanism consisting of two hinged links prevents longitudinal, lateral, roll, and yaw motions of the table while leaving the bounce and pitch freedoms unconstrained. The stainless steel axles of the links run in 16 mm diameter molybdenum disulphide impregnated nylon bushes.

The 50 mm diameter camshafts use deep groove ball bearings which are attached to a base frame fabricated from structural steel sections. This is bolted to the concrete laboratory floor with 12 M10 bolts. Fixed to the base frame with two wing nuts is a safety guard consisting of wire mesh on a steel frame. This guard is mounted on wheels and can be rolled away to allow access to the machine during adjustment.

Figure 7.2b *Laboratory Shaker Table*

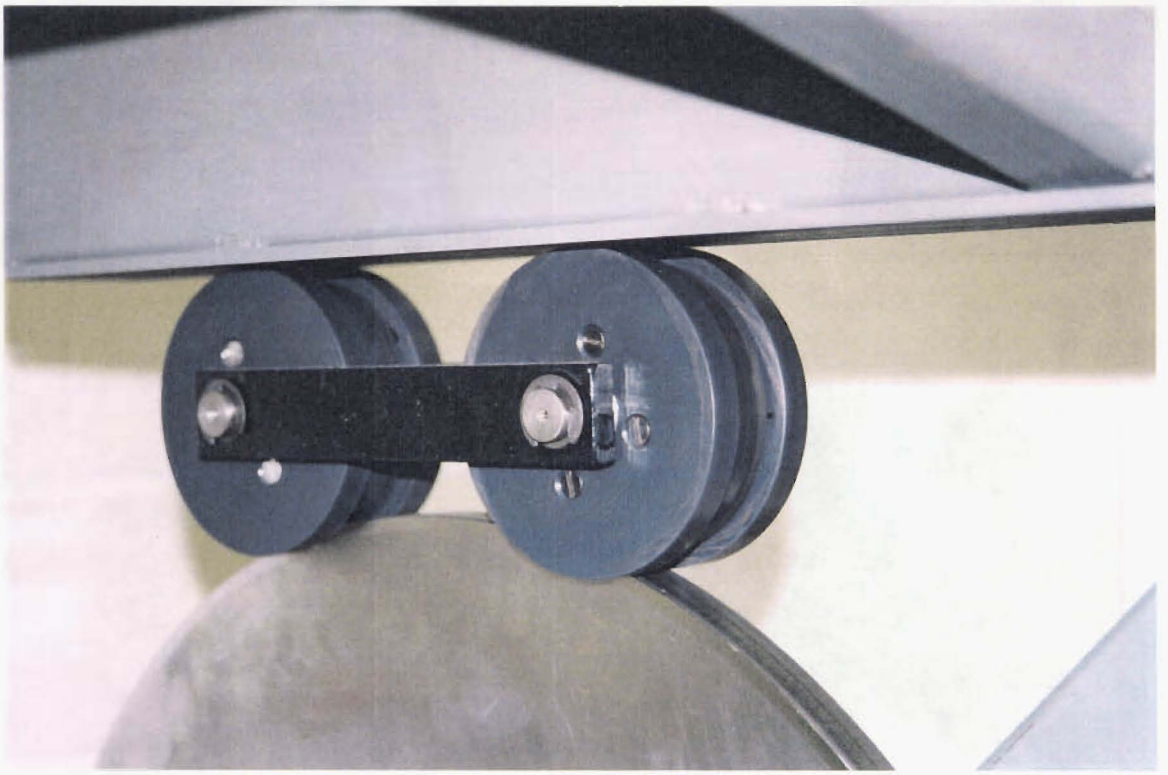

Figure 7.2c *Cam Followers*

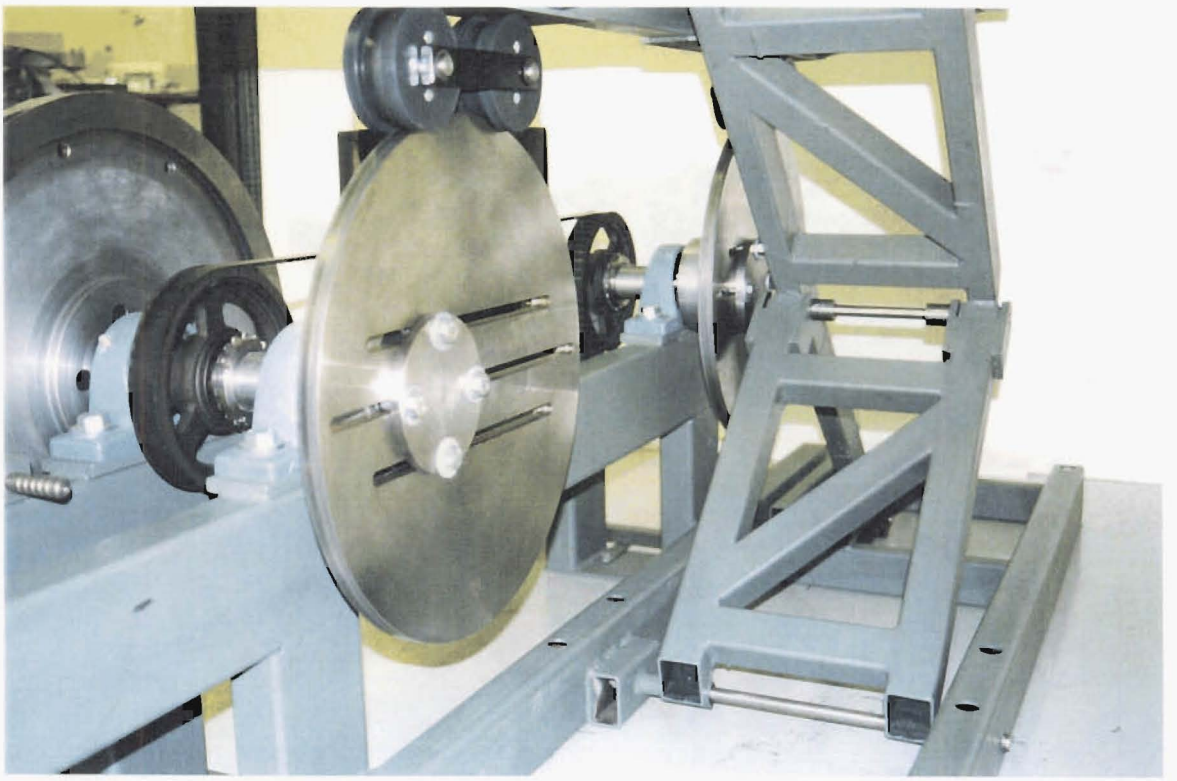

Figure 7.2d Cam and Stabilising Links

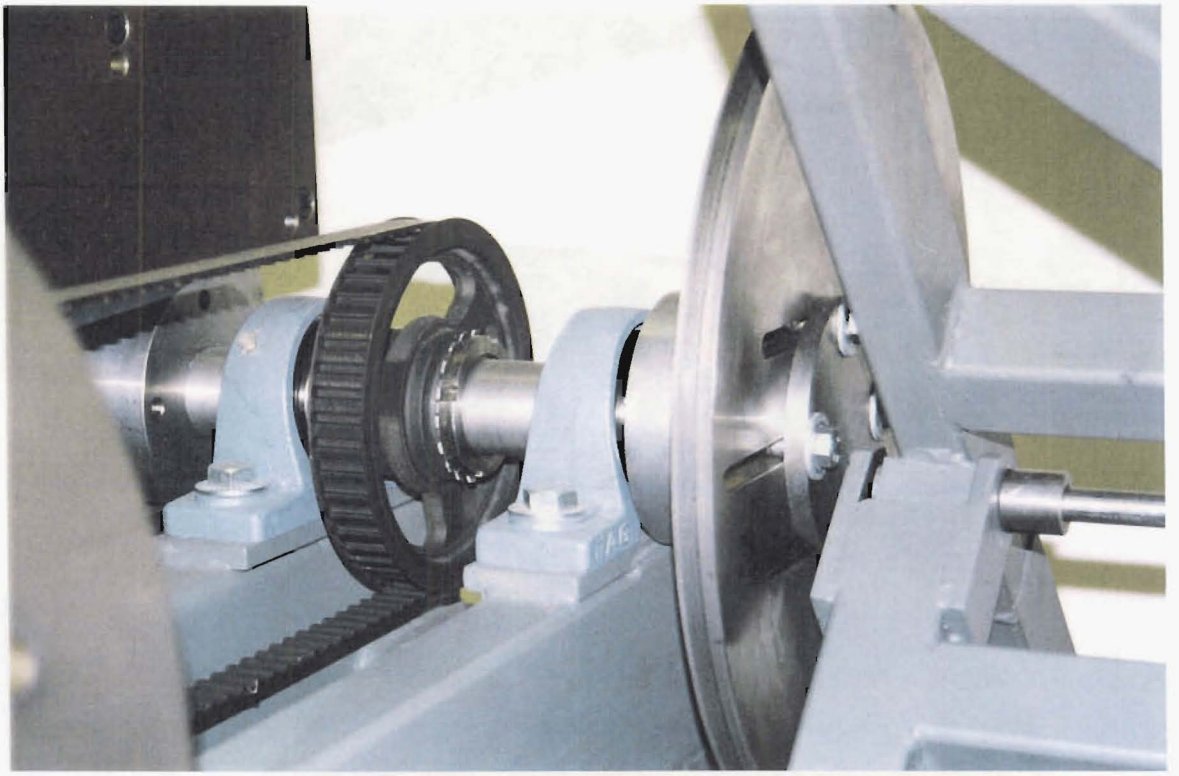

Figure 7.2e Camshaft

7.2.3 Performance

Performance data for the shaker table is shown in Table 7.1. As the table is not fixed mechanically to the cams, maximum acceleration is limited to 1g. This exceeds the typical levels of ambulance floor vibration and is adequate for the purposes of ambulance stretcher suspension testing.

Table 7.1 Shaker Table Performance Data

Maximum table payload	175 kg
Maximum table acceleration	1g
Vertical stroke range	0-±145 mm
Pitch angle range	0-19°
Frequency range	0.27-12.0 Hz

The machine is low in cost and simple. Although time consuming to adjust (eg. 20 minutes to alter table stroke), it has proven to operate reliably and effectively.

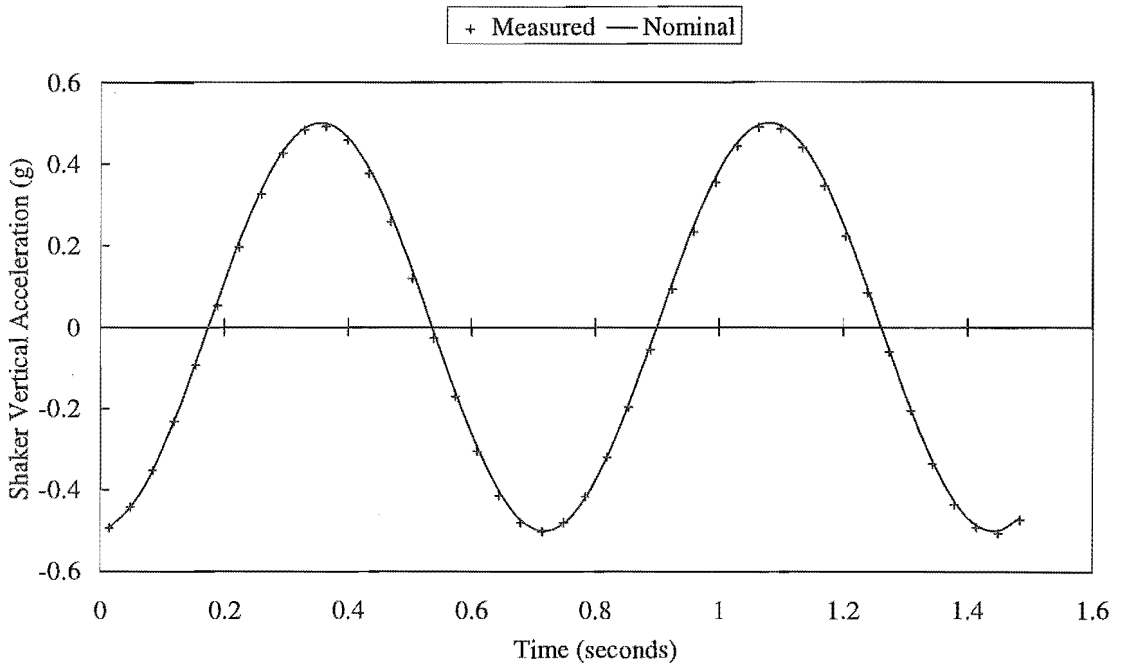

***Figure 7.3** Experimental Validation of Shaker Motion (vertical input of 0.50g @ 1.38 Hz)*

7.2.4 Experimental Validation

Figure 7.3 shows the measured acceleration of the table when the shaker is set to give a vertical input of 0.50g (±65 mm @ 1.38 Hz). Also shown on the figure is the nominal ideal/sinusoidal acceleration. The excellent level of agreement between the nominal and measured accelerations is typical of that for all of the other inputs used. (During suspension testing, table motion was measured after making any changes to its speed or stroke). This indicates that using the flywheel and counterbalance masses was effective in balancing the machine and ensuring (virtually) sinusoidal motion.

7.3 ACCELERATION MEASUREMENT AND PROCESSING

The items of equipment used for acceleration measurement and processing are shown in Figure 7.4 and detailed in Tables 7.2 and 7.3.

7.3.1 Accelerometers and Accelerometer Amplifiers

a) Bounce Test Acceleration Measurement

For bounce testing, a single Brüel & Kjær (BK) piezoelectric accelerometer was fixed centrally to the underside of the suspension top frame. This was connected to a charge amplifier. Initially a BK Systel ACS charge amplifier was used, but this failed part way through testing and was replaced by a BK 2624. The low frequency cut-off of both of the amplifiers was set to 0.03 Hz to ensure proper measurement of the lowest frequency vibrations at 0.3 Hz (Table 7.4). This resulted in some low frequency drift of the acceleration signal which was removed in software (Section 7.3.4). Further information on the measurement of low frequency vibrations using piezoelectric accelerometers is given by Brüel and Kjær [120].

Before each test the calibration of the accelerometer was checked by subjecting it to a known shaker table acceleration.

b) Pitch Test Acceleration Measurement

Two strain gauge accelerometers were used for pitch testing. These were fixed to the underside of the suspension top frame and spaced at 450 mm (longitudinally). Calibration checks were made at the start and end of each day of testing by using the inversion method [121].

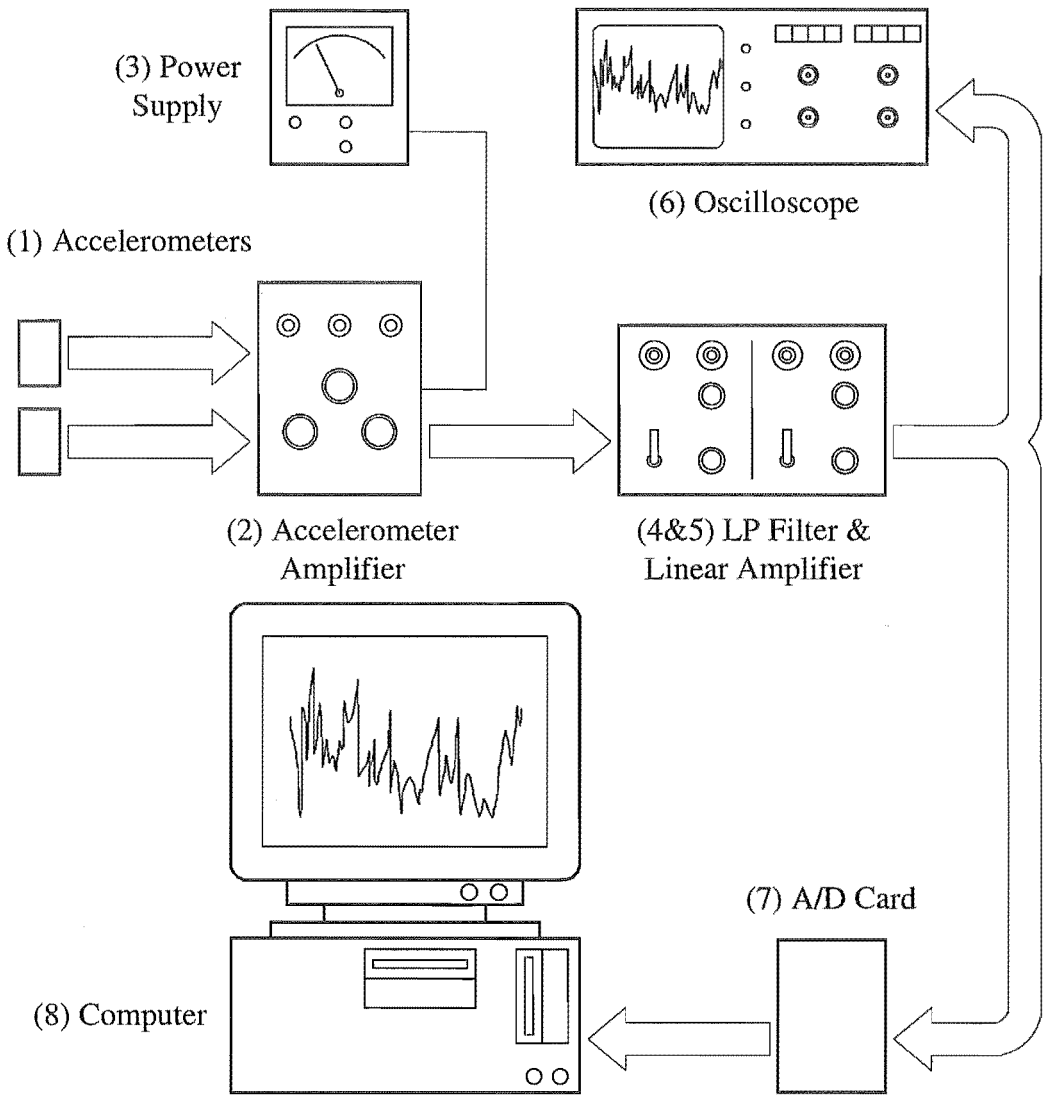

***Figure 7.4** Acceleration Measurement and Processing*

***Table 7.2** Acceleration Measurement Hardware*

Item	*Bounce Tests*	*Pitch Tests*
1	Piezoelectric accelerometer (BK 4338)	Strain gauge accelerometer (Kyowa BA-20L)
2	Charge amplifier (BK Systel AC3 or BK 2624)	Dynamic strain amplifier (Kyowa DPM-6E)
3	DC power supply (Topward TPS-2000)	DC power supply (Topward TPS-2000)

Strain gauge accelerometers have a frequency response which extends down to d.c. (ie. static) and so were well suited to the test work undertaken (which was at low frequencies). Unlike the piezoelectric accelerometer and charge amplifier combination, the use of a strain gauge accelerometer and amplifier is associated with minimal signal drift. In light of this, it would have been better to use a strain gauge based accelerometer for bounce testing.

7.3.2 Signal Conditioning in Hardware

To remove extraneous higher frequency (shock) components, the accelerometer amplifier output voltage was low-pass (LP) filtered using a cut-off frequency of at least five times the shaker frequency. These high frequency components were thought to result from impacting due to bush/bearing clearances in the stretcher suspension and shaker table [122]. The signal was then amplified using an adjustable gain linear amplifier to a level suitable for A/D conversion.

Table 7.3 Signal Processing Hardware

Item	*Description*
4	LP Butterworth filter (4^{th} order)
5	Linear amplifier (with adjustable gain and offset)
6	Oscilloscope (Phillips PM3217, 2 channel)
7	12 bit A/D card (PC LabCard, model PCL-812 PG)
8	Computer (IBM PC compatible 386)

For pitch testing, the acceleration signal voltage was the sum of the acceleration due to gravity and the dynamic acceleration of the stretcher suspension. The d.c. part of this signal (ie. that due to gravity) was subtracted from the total signal before amplification by using the adjustable offset feature of the amplifier. This gave improved resolution of the dynamic part of the signal after A/D conversion.

7.3.3 Signal Sampling and Storage

Data was sampled and stored using a PC fitted with a 12 bit A/D card. Data acquisition software was written in Turbo Pascal 5.0. For each test, the sampling frequency was set at 200 times the shaker table frequency and the record length was 1000 points. This gave sampling of 5 complete cycles of vibration.

7.3.4 Signal Post-Processing in Software

a) Filtering

Matlab® was used for further processing of the acceleration data as summarised below:

- A/D conversion errors and momentary overload of the charge amplifier occurred sporadically. The erroneous data points associated with these problems were replaced with the mean of the data points either side of the errors.
- The low frequency drift evident in some of the lower frequency bounce test data was removed by using a 12th order high-pass (HP) Butterworth filter.
- Hardware filtering was insufficient to remove the high frequency components in some of the tests carried out at high frequencies and high accelerations. For these tests the data was further filtered in software using a 12th order LP Butterworth filter.

Figure 7.5 shows a typical suspension acceleration signal before and after filtering in software.

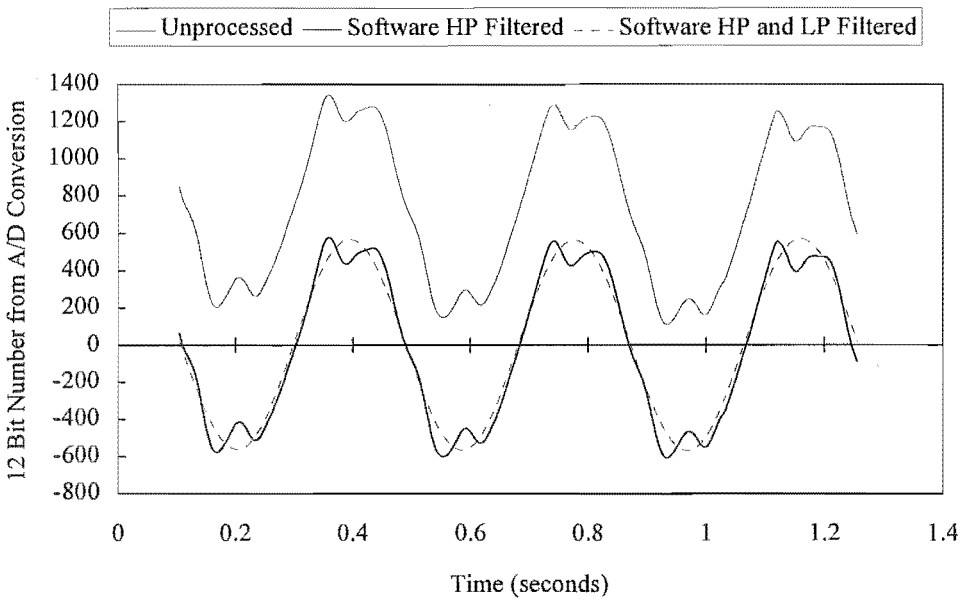

Figure 7.5 *Typical Suspension Acceleration Signal Before and After Software Filtering (vertical input of 0.50g @ 2.63 Hz, stretcher load 68 kg, orifice diameter 3.5 mm)*

b) Calculation of Transmissibility

Bounce transmissibilities were calculated by first determining the stretcher suspension acceleration amplitude $(\ddot{y}_{s,\max} - \ddot{y}_{s,\min})/2$, and then dividing by the known input from

the shaker table. For the first few tests, the shaker table input was determined from its measured acceleration trace. After a number of tests, however, it became evident that there was excellent agreement between the measured and nominal table accelerations (Section 7.2.4). Following this, the input from the table was calculated directly from its speed and stroke.

Pitch transmissibilities were calculated in the same way except that suspension angular acceleration was determined by calculating the difference between the suspension accelerometer signals and then dividing by their distance of separation (450 mm).

7.4 BOUNCE TESTS

7.4.1 Tests Performed

Bounce transmissibilities were measured for three acceleration levels denoted by A (0.50g), B (0.052g), and C (0.036g) in Table 7.4. For each acceleration level, testing was carried out at nine frequencies. The maximum vertical shaker displacement used was ±100 mm and the minimum was ±3.5 mm.

Table 7.4 Bounce Test Data: Shaker Table Frequencies (Hz)

Test No.	*Shaker Displacement Amplitude (mm)*	***Test Series A*** *Shaker Vertical Acceleration 0.50g*	***Test Series B*** *Shaker Vertical Acceleration 0.052g*	***Test Series C*** *Shaker Vertical Acceleration 0.036g*
1	100	1.11	0.36	0.30
2	65	1.39	0.45	0.37
3	42	1.72	0.55	0.46
4	27	2.15	0.69	0.58
5	18	2.63	0.85	0.70
6	12	3.22	1.04	0.86
7	8	3.94	1.27	1.06
8	5	4.98	1.61	1.34
9	3.5	5.96	1.92	1.60

For each of these inputs, three stretcher loads (patient masses) were used: 34 kg, 68 kg, and 102 kg. These loads consisted of steel plates bolted to the stretcher and were centrally located to prevent coupling between bounce and pitch. For the load

representing a patient of average mass, four damping levels were used as indicated by Table 7.5. In total 162 bounce tests were performed.

***Table 7.5** Bounce Test Data: Stretcher Suspension Loads and Damping Orifice Sizes*

Patient Mass (kg)	*No Orifice*	*3.5 mm Diameter Orifice*	*2.0 mm Diameter Orifice*	*1.0 mm Diameter Orifice*
34		●		
68	●	●	●	●
102		●		

Square edged orifices were used for damping. These were preferred to sharp edged orifices as they have a discharge coefficient ($C_d = 0.82$) which is independent of flow direction and varies little with pressure drop [97,123]. Each orifice consisted of a 16 mm diameter mild steel disk (1.75 mm wide) in which a hole of the required size was drilled centrally. Both sides of the disks were surface ground to give sharp corners at the hole entry/exit. The disks were fitted directly into the pneumatic cylinder ports and O-ring seals were used to prevent air leakage between the sides of the disks and the internal walls of the ports.

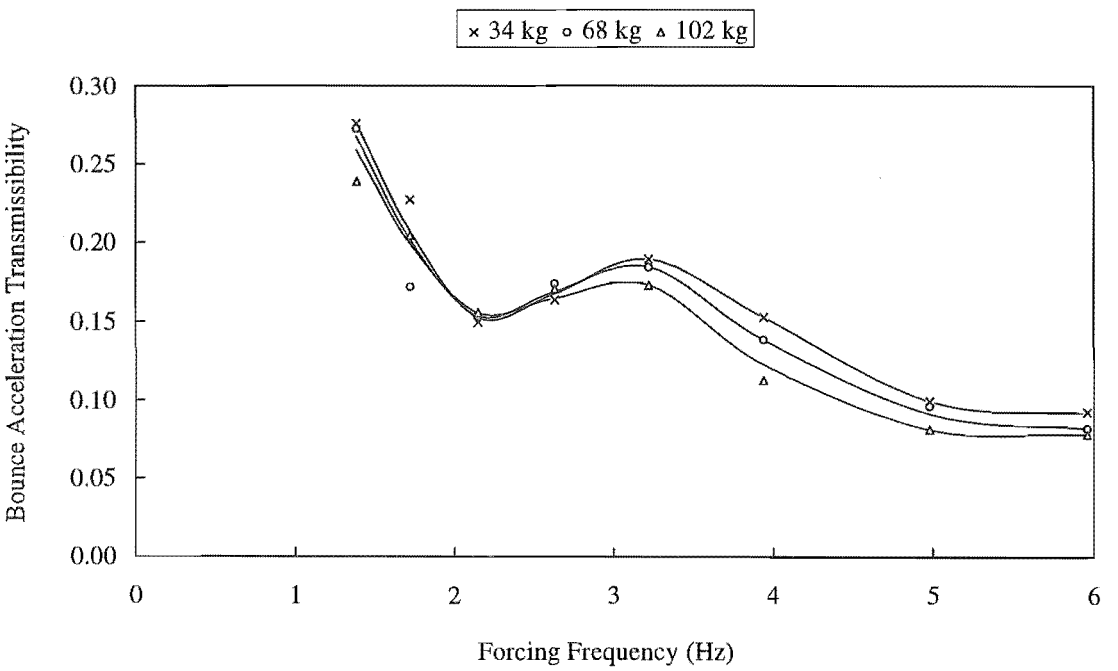

***Figure 7.6** The Effect of Patient Mass on Bounce Acceleration Transmissibility for Test Series A (0.50g), 3.5 mm Orifice*

7.4.2 Bounce Test Results

Experimental bounce acceleration transmissibilities are shown in Figures 7.6-7.9. Smooth curves have been drawn through the experimental data points which are marked by symbols. Numerical transmissibility values are tabulated in Appendix F.

a) Tests Series A (0.50g)

Figures 7.6 and 7.7 show the response of the suspension at frequencies above resonance. Irrespective of patient mass, very good levels of isolation are achieved when using a 3.5 mm orifice, as indicated by Figure 7.6. For example, above 1.4 Hz isolation exceeds 70%, while above 5.2 Hz isolation exceeds 90%. For increased levels of pneumatic damping (ie. smaller orifice sizes) suspension performance in the frequency range considered worsens, as shown by Figure 7.7. The local maximum in transmissibility which occurs at 3.2 Hz is thought to be caused by a resonance attributed to excessive clearance in the linear bearing of the suspension stabilising arm.

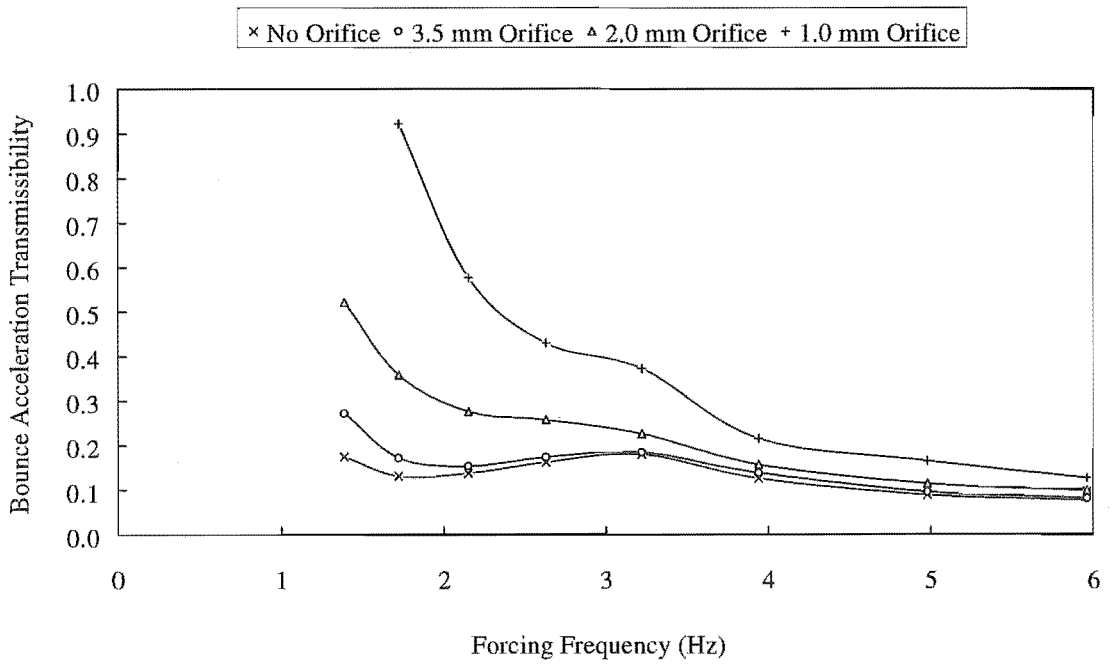

***Figure 7.7** The Effect of Orifice Size on Bounce Acceleration Transmissibility for Test Series A (0.50g), 68 kg Patient*

b) Test Series B (0.052g)

Test Series B includes shaker frequencies down to the suspension natural frequency, as shown in Figures 7.8 and 7.9. Figure 7.8 indicates that the suspension natural frequency is approximately 0.45 Hz and largely independent of mass.

In Figure 7.9 the effects of damping level are examined. For excitation frequencies in the region of the suspension natural frequency, increased damping is beneficial in reducing amplification. At frequencies above the cross-over frequency (0.65 Hz), best isolation is obtained by using a low level of damping. Both of these trends are consistent with theory. When the highest level of damping is used (1.0 mm orifice), the suspension resonates at its higher natural frequency (as evidenced by the transmissibility peak at around 1 Hz). This indicates that the suspension is tending to operate on the cylinder volume only. When the 2.0 mm orifice is used the suspension has transmissibility peaks at both natural frequencies.

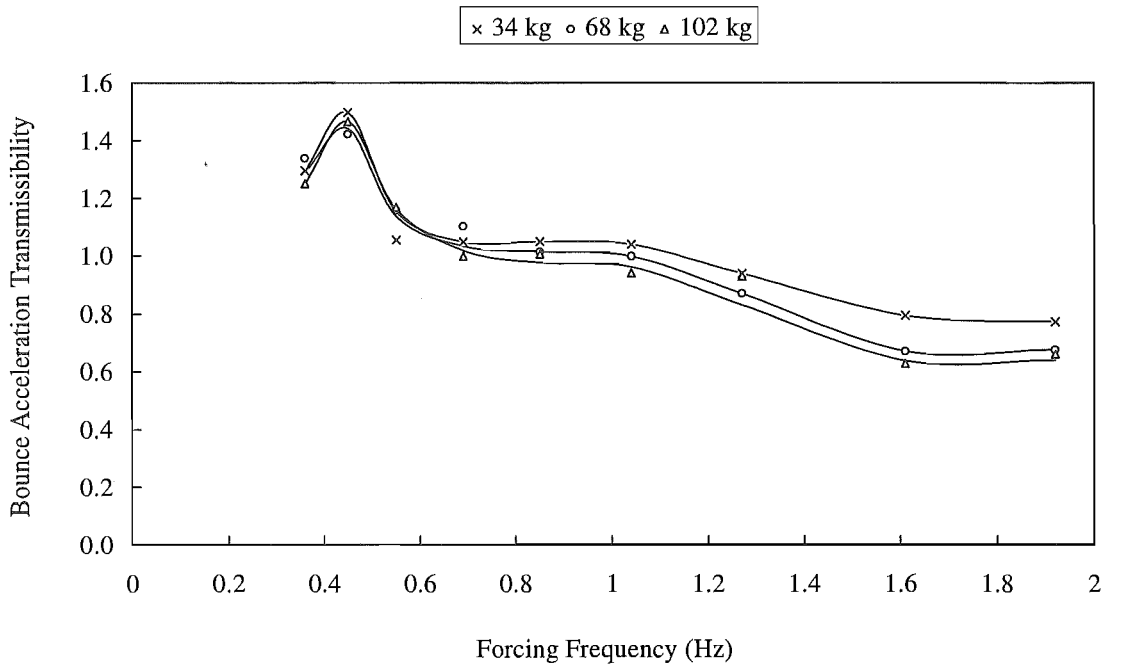

Figure 7.8 *The Effect of Patient Mass on Bounce Acceleration Transmissibility for Test Series B (0.052g), 3.5 mm Orifice*

c) Test Series C (0.036g)

The transmissibility results for input C are shown in tabular form in Appendix F only. They are not displayed graphically here because the measured levels of isolation were very poor. This is thought to be the result of Coulomb damping which is discussed in the following section.

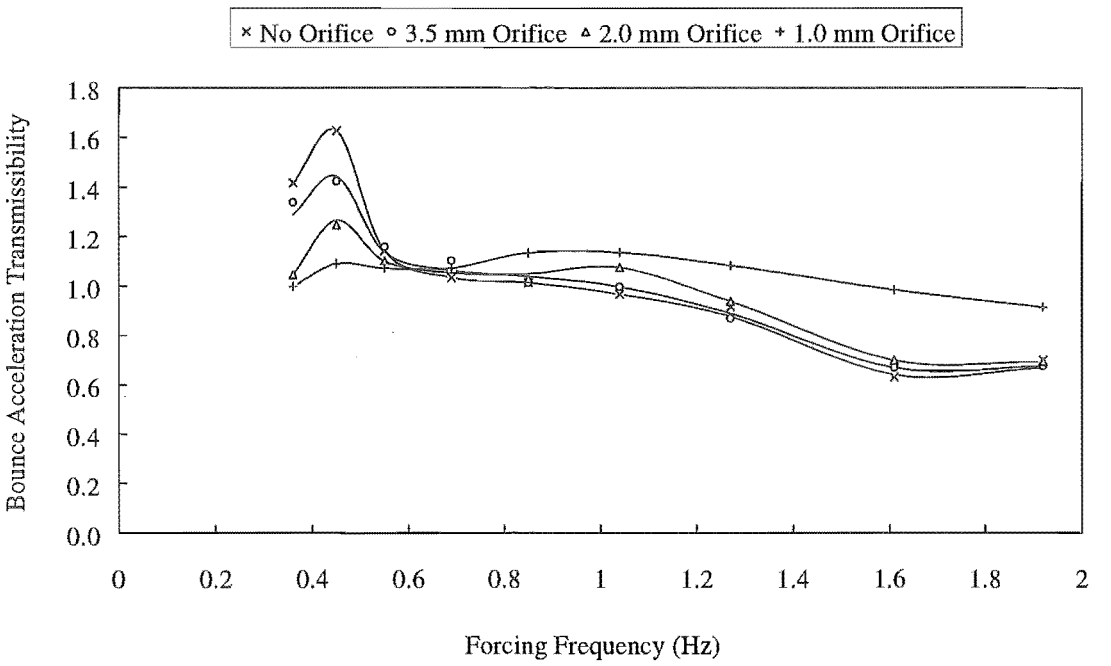

***Figure 7.9** The Effect of Orifice Size on Bounce Acceleration Transmissibility for Test Series B (0.052g), 68 kg Patient*

7.5 COULOMB DAMPING

7.5.1 Introduction

Coulomb (or dry friction) damping can be considered as a constant force which opposes the relative motion of two surfaces in sliding contact. When the direction of relative motion changes so too does the direction of the force. Consequently, the equations of motion for a system with Coulomb damping are discontinuous, and two equations must be used - one for either direction of motion. Early work which analysed the vibration of Coulomb damped systems was done by Jacobsen [124] who used an equivalent viscous damping approach to derive an approximate solution. Later, Den Hartog [125] derived an exact solution to the problem. Both of these authors assumed a constant normal force. Crede and Ruzicka [126] summarise the properties of a number of damping methods, including Coulomb damping, by presenting acceleration and displacement transmissibilities, while Anderson [97] considers the properties of a pneumatic isolation system with Coulomb damping.

7.5.2 Characteristics

Coulomb damping is detrimental to the performance of suspensions because no movement of the suspension can occur for inputs which are insufficient to cause the Coulomb damping force to be exceeded [3,103]. As the input acceleration is increased in magnitude, Coulomb damping has less influence on isolation levels. This trend is evident in the experimental results shown in Figures 7.6-7.9, where best isolation is for the highest acceleration inputs.

Stammers and Leyshon [45,68] note that the transmissibilities for their suspension, and for the suspension of Blok [69], exhibit poorer isolation than simple theory would predict at high frequencies. The transmissibilities considered here show a similar trend, as evidenced by Figure 7.10 which compares experimental and simulated transmissibilities for Test Series A. The simulated transmissibility was generated using the model described in Chapter 5 and does not take into account Coulomb damping. The greatest difference (as a proportion) between the experimental and simulated transmissibilities occurs at high frequencies.

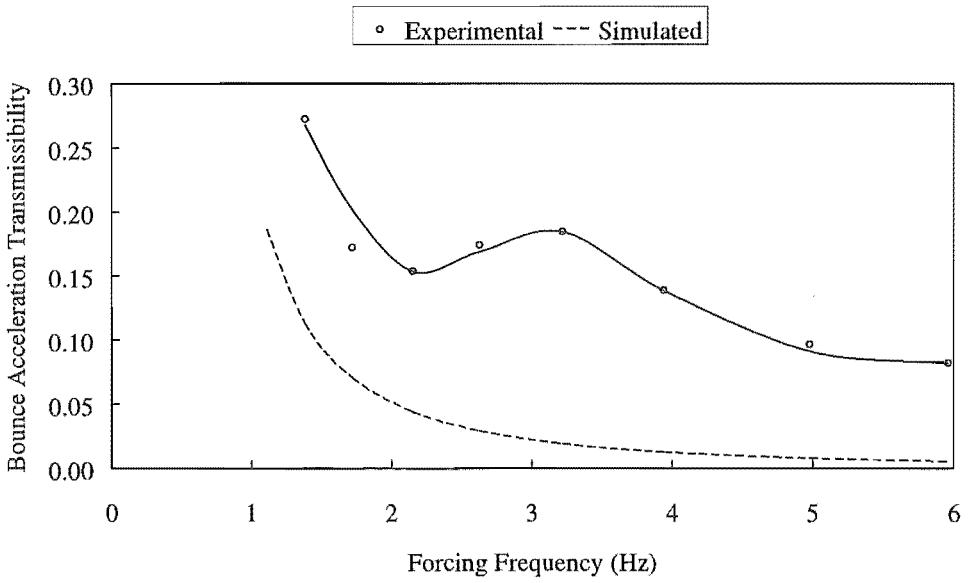

***Figure 7.10** Experimental and Simulated Bounce Acceleration Transmissibilities for Test Series A (68 kg patient, 3.5 mm orifice)*

It is at high frequencies that Coulomb damping has the most deleterious effect on isolation. This is discussed by Crede and Ruzicka [126] who show that acceleration transmissibility approaches a constant value at high frequencies. This is because spring forces reduce at high frequencies by virtue of a decrease in isolator displacement. The Coulomb damping force is, however, independent of frequency and so dictates the response of the isolated load. With reference to [126], the limiting value of acceleration

transmissibility (T_{lim}) is a function of the input acceleration ($\ddot{y}_s$), the suspended mass ($m_{pat}+m_{str}$), and the Coulomb damping force (F_c), as given below

$$T_{\text{lim}} = \frac{4}{\pi}\frac{F_c}{(m_{pat}+m_{str})\ddot{y}_s}. \tag{7.3}$$

This equation predicts a lower limiting value of transmissibility (T_{lim}) for higher frequency inputs - a trend which occurs in the results of Figures 7.6-7.9.

Figures 7.6 and 7.8 show the effects of change in mass on suspension performance. They indicate that there is a slight improvement in high frequency isolation for greater stretcher loads. On the basis of Equation 7.3, this suggests that the Coulomb damping force does not increase linearly with suspension load.

7.5.3 Simulation Model

In the stretcher suspension, Coulomb damping results from friction in the linkage pivots and cylinder seals. This can be included in the simulation model of Chapter 5 by introducing an additional term into the equation defining stretcher vertical acceleration (5.13). A term modelling pivot and cylinder seal viscous friction is also added, as shown in Equation 7.4 below:

$$\begin{aligned}\ddot{y}(m_{pat}+m_{str}) = 2(p_c - p_{at})A_c\left(\frac{r}{L_1\cos\beta + \dfrac{eL_1\sin\beta}{a+b+(y-y_s)}}\right) - (m_{pat}+m_{str})g \\ +\text{sign}(\dot{y}_s-\dot{y})F_c + c_b(\dot{y}_s-\dot{y}).\end{aligned} \tag{7.4}$$

where $sign(\dot{y}_s-\dot{y}) = +1$ if $\dot{y}_s-\dot{y}>0$ or
$sign(\dot{y}_s-\dot{y}) = -1$ if $\dot{y}_s-\dot{y}<0$.

In the modelling work described here, the values of the Coulomb and viscous damping constants (F_c and c_b respectively) are for a patient of average mass. Other patient masses are not considered.

a) Coulomb Damping

A constant value for the Coulomb damping force (F_c) of 22 N is used. This was obtained experimentally by measuring the force required to initiate displacement of the suspension from its equilibrium position.

Modelling Coulomb damping by a constant in this way is a common approach which gives results that are in good agreement with experiments in this instance. However, a more accurate model would take into account the effects below:

- The contribution from the linkage bushes to the total Coulomb damping force is a function of the normal force on the bushes. This normal force varies with suspension dynamic load.
- The static coefficient of friction will probably be greater than the kinetic coefficient.
- Cylinder seal damping models often include a term in the pressure difference across the actuator (eg. Bowns and Ballard [127]).

b) Viscous Damping

A viscous damping coefficient (c_b) of 150 Ns/m is used (critical damping ratio = 0.22). While this value appears high, it gives good agreement between the simulated and theoretical results.

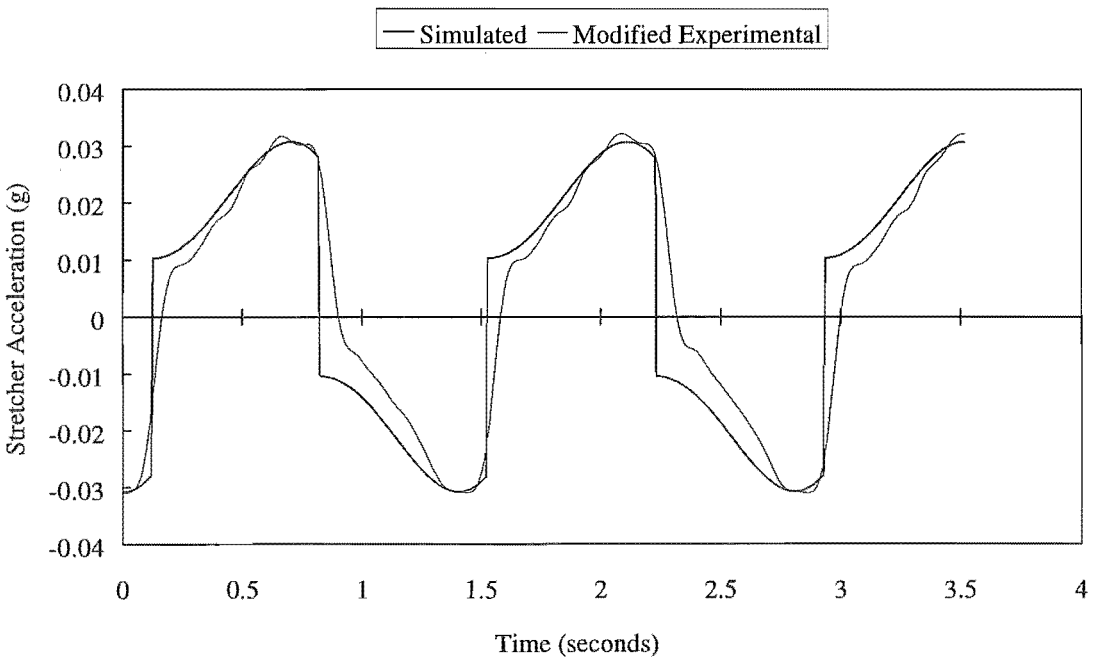

***Figure 7.11** Experimental and Simulated Stretcher Bounce Accelerations for Input C5 (68 kg patient, 3.5 mm orifice)*

7.5.4 Simulation Results

Figure 7.11 compares an experimental and simulated stretcher acceleration record. The experimental acceleration has been reduced a little in magnitude (scaled) so that it has the same amplitude as the simulated acceleration. This was done to better illustrate the good agreement between the acceleration waveforms. In the example shown, a low acceleration input (C5, 0.036g @ 0.70 Hz) is used so that the effects of Coulomb damping are more noticeable. The step changes in the simulated acceleration occur when the suspension relative velocity (and Coulomb damping force) change direction. The experimental acceleration curve is not perfectly vertical during this change in suspension velocity sign - possibly due in part to the effects of LP filtering.

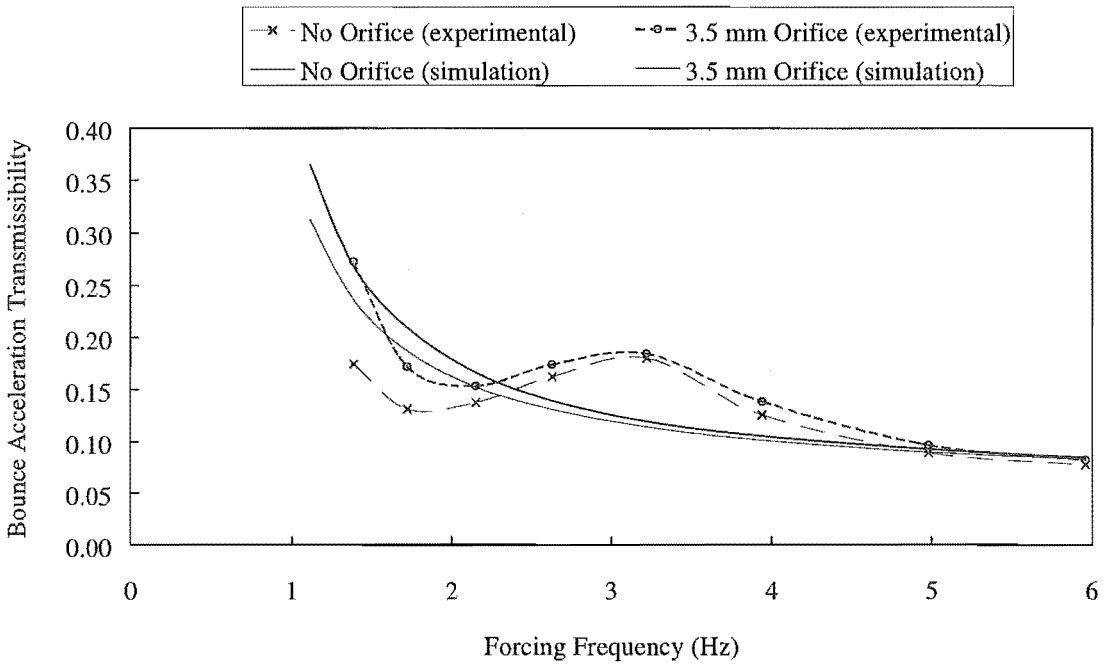

***Figure 7.12** Experimental and Simulated Stretcher Bounce Transmissibilities for Test Series A (68 kg patient, no orifice and 3.5 mm orifice)*

Figures 7.12 and 7.13 compare the experimental and simulated transmissibilities for Test Series A. Good agreement is evident, irrespective of the level of pneumatic damping. This indicates that the model for Coulomb and viscous damping is reasonable, and that these damping methods are important to the performance of the suspension.

As the stretcher suspension has a low stiffness and low level of added (pneumatic) damping, the harmful effects of Coulomb damping are particularly noticeable. This is illustrated in Figure 7.14 which shows the simulated suspension forces for an input of 0.50g at 1.39 Hz (input A2).

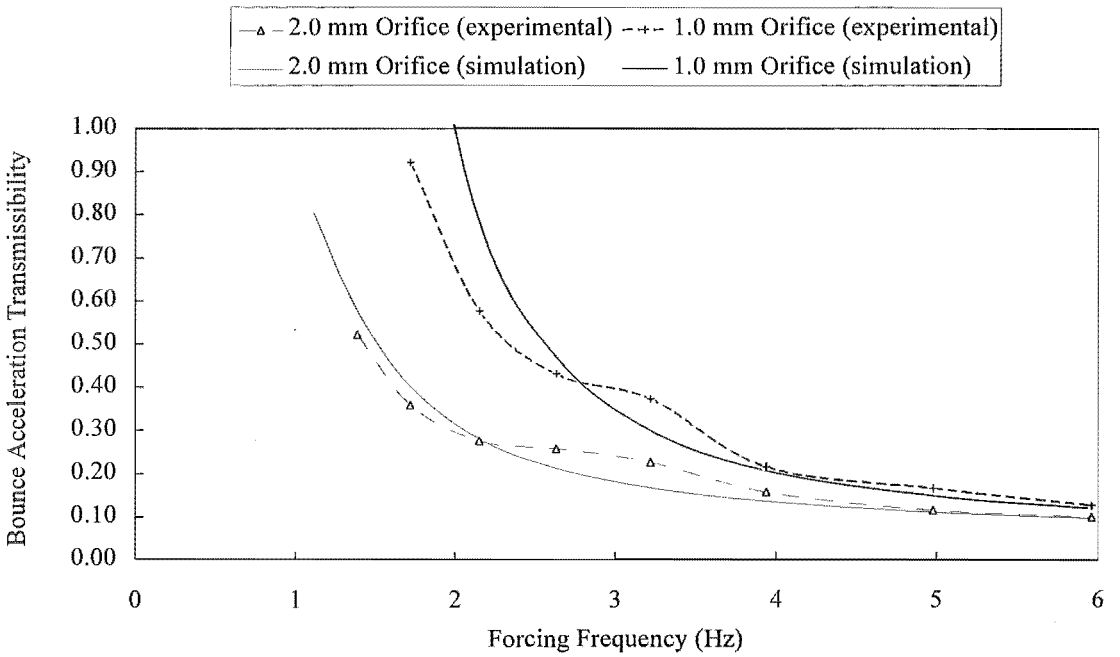

Figure 7.13 *Experimental and Simulated Stretcher Bounce Transmissibilities for Test Series A (68 kg patient, 2.0 mm and 1.0 mm orifices)*

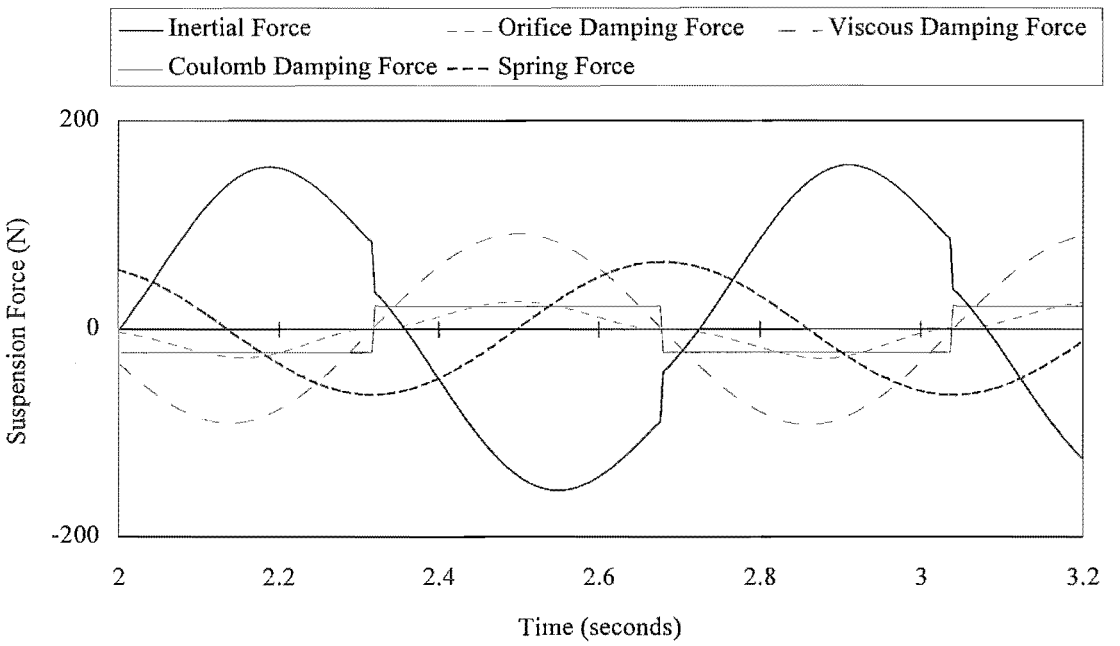

Figure 7.14 *Simulated Suspension Forces for Input A2 (68 kg patient, 3.5 mm orifice)*

7.6 PITCH TESTS

7.6.1 Tests Performed

Pitch transmissibilities were measured using two shaker table angular acceleration levels. These are denoted by D (3.28 rad/s^2) and E (1.87 rad/s^2) in Table 7.6. For each acceleration level, testing was carried out at nine frequencies. The maximum table angular rotation was ±14.91° and the minimum was ±0.53°.

Table 7.6 Pitch Test Data: Shaker Table Frequencies (Hz)

Test No.	*Shaker Angular Rotation Amplitude (degrees)*	***Test Series D** Shaker Pitch Acceleration 3.28 rad/s^2*	***Test Series E** Shaker Pitch Acceleration 1.87 rad/s^2*
1	14.91	0.59	0.45
2	9.80	0.73	0.55
3	6.36	0.91	0.69
4	4.10	1.14	0.86
5	2.73	1.39	1.05
6	1.82	1.70	1.29
7	1.21	2.09	1.58
8	0.76	2.64	1.99
9	0.53	3.15	2.38

All pitch testing was carried out using a stretcher loaded with steel weights. These weights were distributed to represent a patient of average mass and inertia (Equation A13, Appendix A3). This meant that the springs were evenly loaded ($e_e = 0$) and that pitch and bounce were uncoupled. The suspension was tested with no pneumatic damping, and with 3.5, 3.0, 2.0, and 1.0 mm diameter orifices to give a total of 90 tests.

7.6.2 Pitch Test Results

Figures 7.15 and 7.16 show the experimental pitch transmissibilities for Test Series D and E respectively. As shown in Figure 7.15, the initial reduction in transmissibility with increasing frequency is very good for the lowest four values of damping. At high frequencies, the reduction is markedly less and there is a resonance between 1.55 and

1.7 Hz. This resonance is also evident in Figure 7.16. The reason for this resonance is not known.

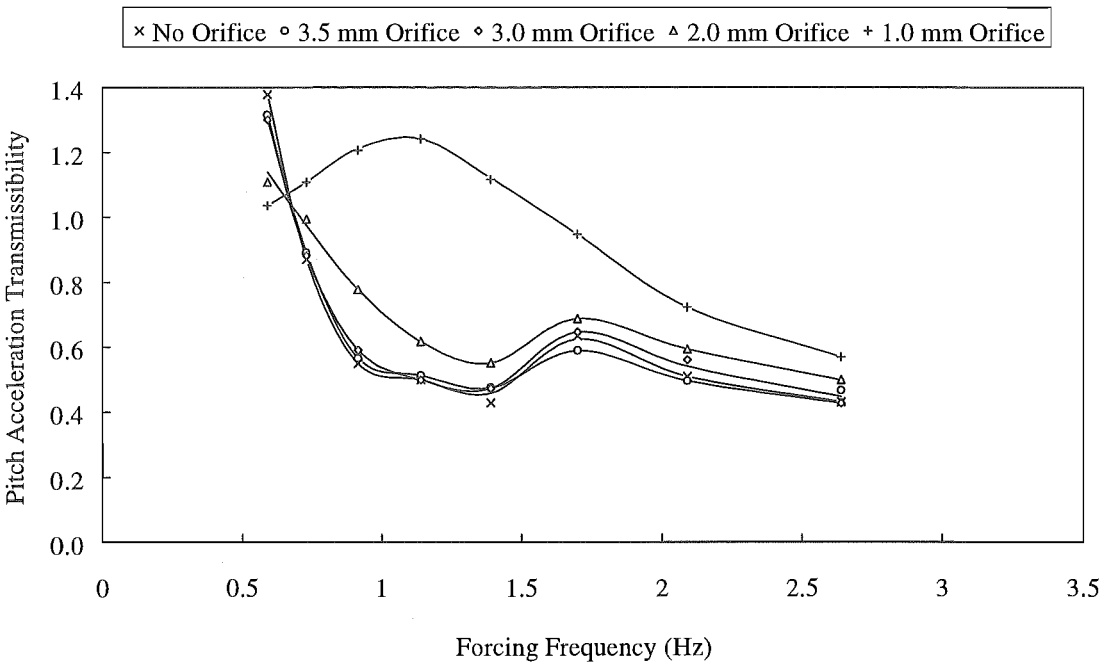

***Figure 7.15** The Effect of Orifice Size on Pitch Angular Acceleration Transmissibility for Test Series D (3.28 rad/s^2), 68 kg Patient*

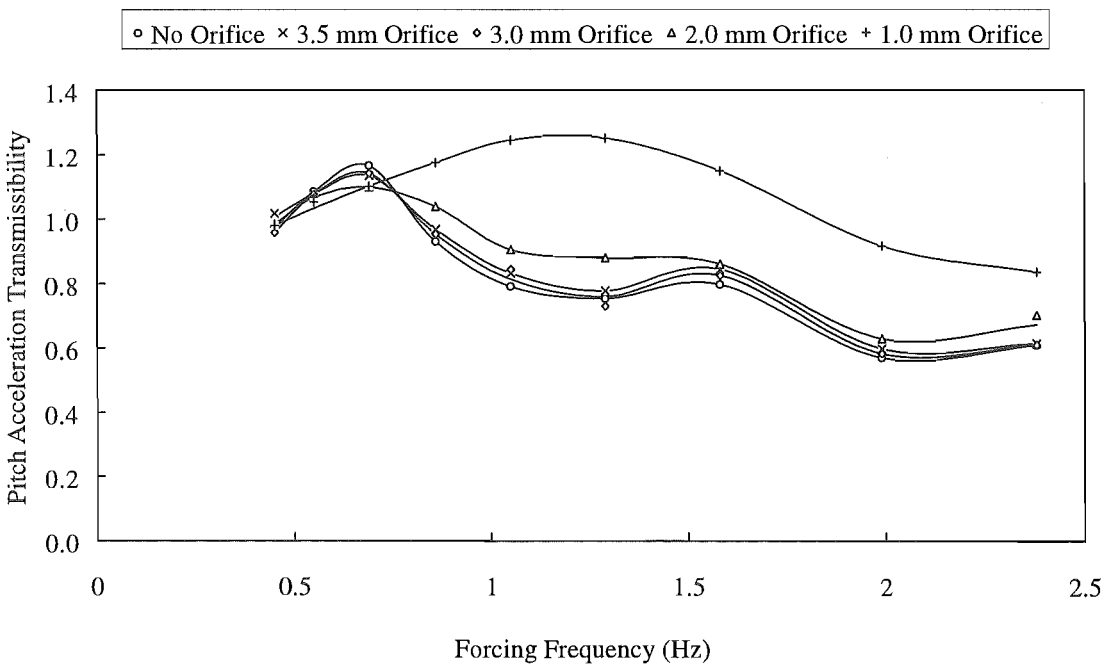

***Figure 7.16** The Effect of Orifice Size on Pitch Angular Acceleration Transmissibility for Test Series E (1.87 rad/s^2), 68 kg Patient*

On the basis of Figure 7.15, the suspension pitch natural frequency is somewhat less than 0.6 Hz. This is consistent with the theoretical value of 0.46 Hz. However, the peak transmissibility of Figure 7.16 is at 0.65 Hz. This suggests that the pitch natural frequency increases above its design value for lower acceleration inputs. While the bounce test results showed that the bounce natural frequency was very close to its theoretical value, insufficient tests were done to properly assess any effects that input size might have. If further tests were to be done, the effect of input size on bounce natural frequency should be investigated.

The effects of pneumatic damping level are consistent with theory in that increased damping gives reduced amplification at resonance but poorer isolation above the cross-over frequency. For the highest level of pneumatic damping, peak transmissibility is between 1.1 and 1.2 Hz which would suggest that there is minimal flow between the cylinders and tanks.

The levels of isolation shown in Figures 7.15 and 7.16 are relatively poor in comparison with what could be expected theoretically. This is thought to be due in part to the effects of Coulomb damping (Section 7.5). Evidence of this is that pitch isolation is better for the higher input (D), and that the transmissibilities tend to a constant value at high frequencies.

7.6.3 Suggestions for Future Testing

All of the pitch test results above are for a 68 kg patient. The decision not to investigate the effects of using other patient masses was made on the basis of the bounce test results - these showed that the bounce transmissibility and natural frequency varied little with patient mass. It can therefore be concluded that the change in the stiffness of the springs with load is in accordance with theory (ie. the spring stiffness increases with absolute spring pressure, Equation 3.5, Section 3.5.1). This being the case, the pitch transmissibility would also be expected to be largely independent of load (in accordance with the Equation 4.22 and Figure 4.4). If further tests were to be carried out on the suspension, experimental confirmation of this should be sought by using different patient masses.

As the suspension has been loaded symmetrically for the tests described here, coupling has not been investigated. In future testing, it might be worthwhile to look at the effects of coupling - preferably using bounce as well as pitch inputs.

Additional testing is required to clarify why some features of the pitch results were not in accordance with theory. In particular, explanations for the following behaviours should be sought by further testing:

- The occurrence of a secondary pitch resonance between 1.55 and 1.7 Hz.
- The increase in pitch natural frequency for low input accelerations.

7.7 SUMMARY

Key results of the suspension tests described in this chapter are summarised below:

- Bounce isolation is good for high acceleration inputs. eg. For a 3.5 mm damping orifice and a shaker vertical acceleration of 0.50g, the levels of isolation are:
  - better than 70% above 1.4 Hz,
  - better than 90% above 5.2 Hz.
- The bounce natural frequency and bounce acceleration transmissibility vary little with patient mass.
- The bounce natural frequency is close to its theoretical value.
- The effects of pneumatic damping are consistent with theory in the following respects:
  - a small orifice (ie. high damping) reduces amplification of inputs below the cross-over frequency,
  - above the cross-over frequency a low level of damping gives best isolation,
  - for the highest level of damping (1.0 mm orifice) the suspension operates on its higher natural frequency.
- The presence of Coulomb friction has a detrimental effect on isolation. ie.
  - low magnitude accelerations are poorly isolated,
  - acceleration transmissibility reaches a limiting value at high frequencies.
- Further tests are required to clarify the value of the pitch natural frequency and how this changes with input level (if at all). Additional tests are also required to investigate the reasons for the secondary pitch resonance between 1.55 and 1.7 Hz.

CHAPTER 8

Road Tests

8.1 INTRODUCTION

Suspension road tests were carried out in cooperation with the Christchurch Ambulance Service (Order of St John). An ambulance based on a Chevrolet chassis was used. This had a natural frequency in bounce of approximately 1.8 Hz (Figures 8.3 and 8.4). Quantitative assessment of the isolation provided by the stretcher suspension was made by recording ambulance floor and stretcher vibrations. Metal weights were bolted to the stretcher to simulate a patient of average mass and inertia ($e_e = 0$, no coupling). Qualitative assessments of suspension performance were made by two healthy males.

Rather than using an orifice diameter of 3.0 mm (which was predicted as suitable by the simulations of Chapter 5), all testing was carried out using an orifice diameter of 3.5 mm. This was done to take into account the non-pneumatic forms of damping which were neglected in the simulations, but whose effects were noticeable in the results of the laboratory tests.

8.2 QUANTITATIVE TESTING

8.2.1 Instrumentation

Four accelerometers (one Kyowa AS-10B additional to those used for the laboratory tests) were employed. Two of these were fixed to the stretcher frame - one at the centre-of-mass of the load, and the other 473 mm towards the head of the stretcher (ie. toward the front of the ambulance). The other two accelerometers were fixed to the suspension base frame directly below those on the stretcher.

Fixing the accelerometers directly to the stretcher frame ignores any effect that the mattress might have on patient isolation. Leyshon and Stammers [46] have investigated the transmissibility of the mattress and a standard York 2 stretcher. They report that the mattress is useful for alleviating mechanical shock, although it provides no isolation below 20 Hz. Peak amplification is 3.2 at around 12 Hz.

Figure 8.1 *Suspension Installed in Ambulance for Testing.*

Floor and stretcher bounce were determined by using the centrally located accelerometers. In order to compare test results with the earlier work of Leyshon and Stammers [46], stretcher pitch was defined as the linear difference in acceleration between the head and centre-of-mass of the patient. It was calculated by first multiplying the difference between the stretcher accelerometer signals by 750 mm (the assumed distance from head to centre-of-mass), and then dividing by their distance of separation (473 mm). Floor pitch was similarly defined.

Accelerations were sampled and stored using the data acquisition system described in Chapter 7 (Section 7.3). This was driven through an inverter by 12 volt batteries. No LP hardware filters were used. The sampling frequency was set at 100 Hz and the number of samples per channel was 4000, giving a test duration of 40 seconds. This equates to a distance of 778 m for an ambulance speed of 70 km/h. A longer testing time would have been preferred, but was not possible using the data acquisition system described. (The Turbo Pascal complier imposes a 64 kb limit on the size of a single data structure, and each data point requires 4 bytes of memory).

8.2.2 Road Description

All of the tests were carried out on relatively straight sections of road. Table 8.1 describes the road surfaces which are ranked in order of increasing quality (as indicated by induced floor vertical r.m.s. accelerations, Table 8.2). The ambulance speeds are also given.

Table 8.1 Road Descriptions and Ambulance Speeds

Road	*Description*	*Speed (km/h)*
A	Suburban road in a residential area having a poor surface with short wavelength irregularities.	50
B	Rural road with a poor surface and a railway crossing.	53
C	Typical rural road.	95
D	Suburban section of single-lane motorway with a good surface.	70
E	Typical suburban single-lane road with a reasonable surface.	50
F	Suburban section of State Highway with two lanes and a good surface.	50

8.2.3 Bounce Test Results

a) Floor Bounce

In Figure 8.2, floor and stretcher vertical accelerations are compared for an especially rough section of road A (the worst road). For this road, short wavelength irregularities caused significant motion of the ambulance floor at its natural frequency (ie. resonance of the ambulance sprung mass). This is emphasised by Figure 8.3 which compares the floor and stretcher acceleration spectra in the range 0-10 Hz and shows that vertical acceleration of the ambulance floor peaks at around 1.8 Hz.

There is also a significant higher frequency component of floor vibration which occurs at around 15 Hz (Figure 8.2). This is possibly associated with resonance of the unsprung mass. Both Leyshon and Stammers [46] and Snook and Pacifico [59] (who tested the Dutch 'floating stretcher' of Blok [69]) also measured significant vibration at this frequency.

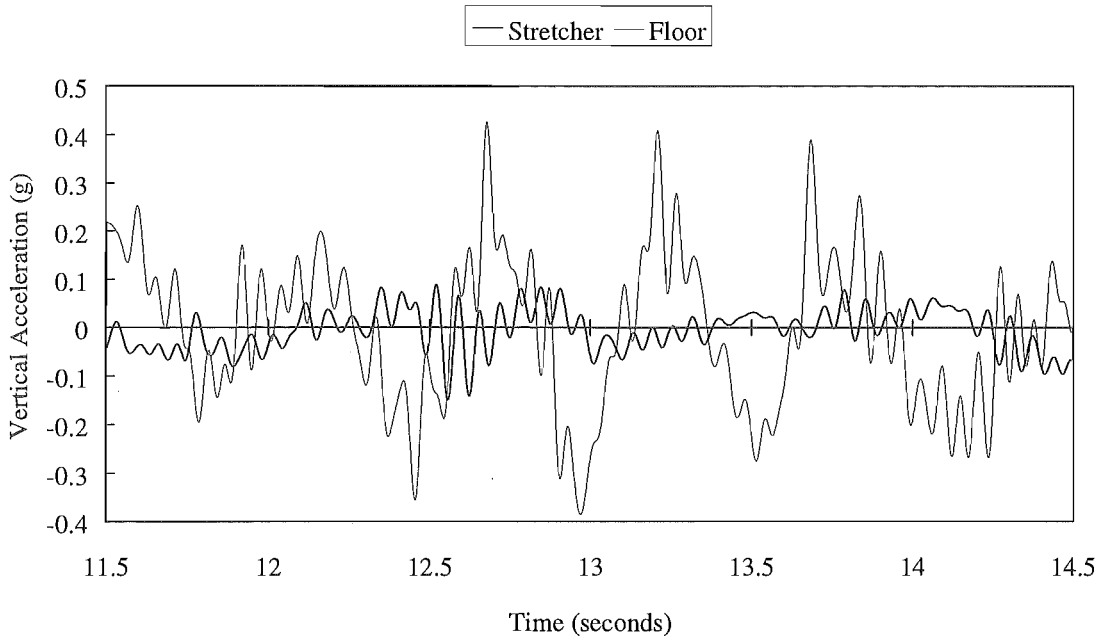

***Figure 8.2** Floor and Stretcher Vertical Accelerations (Road A)*

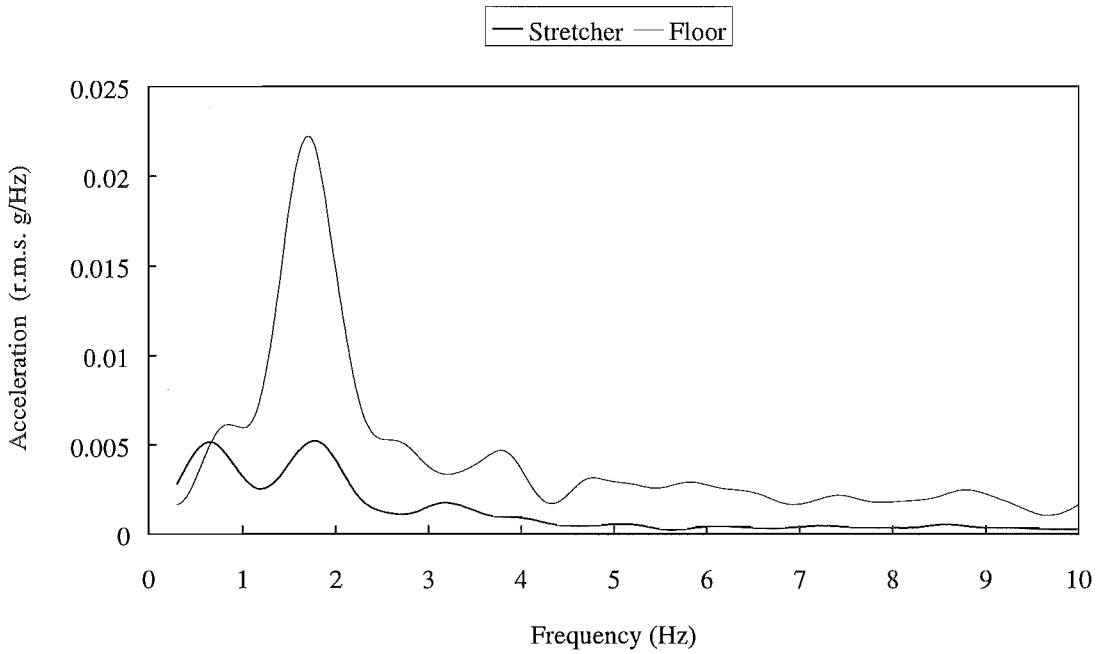

***Figure 8.3** Ambulance Floor and Stretcher Bounce Acceleration Spectra (Road A)*

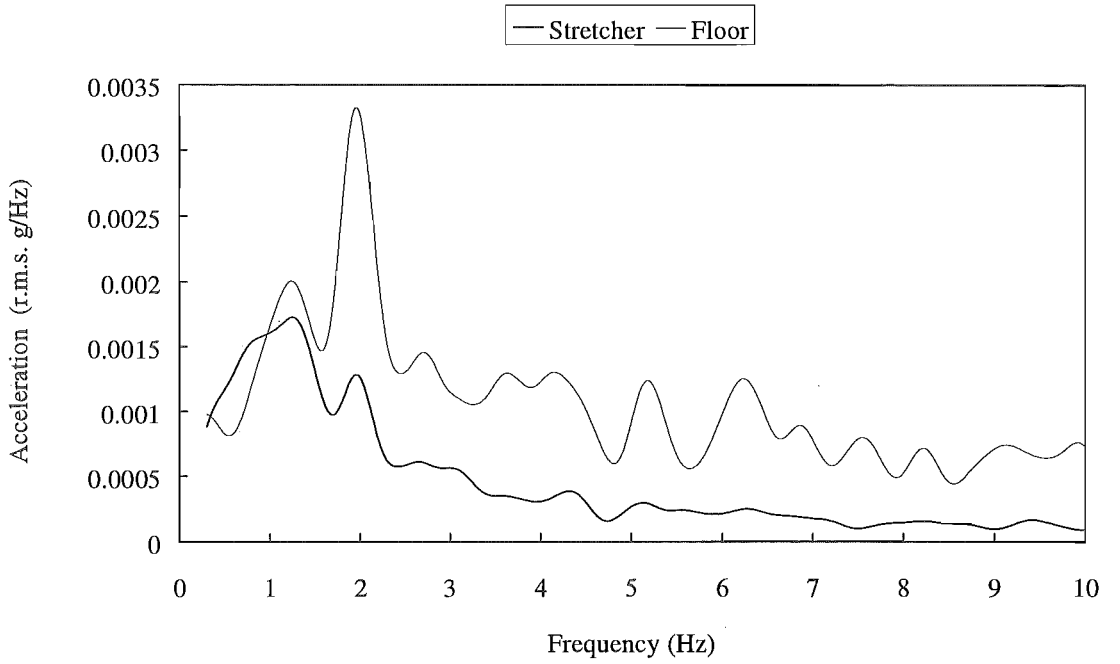

Figure 8.4 *Ambulance Floor and Stretcher Bounce Acceleration Spectra (Road E)*

b) Stretcher Bounce

Both Figures 8.2 and 8.3 show that the stretcher suspension provides good levels of isolation - particularly of the high-magnitude low-frequency floor vibrations which occur at around 1.8 Hz. Peak spectral accelerations of the stretcher occur in the region of the natural frequency of the stretcher suspension (0.46 Hz), and also in the region of peak input from the floor at 1.8 Hz (Figure 8.3). The nature of the floor and stretcher bounce acceleration spectra over a road with a better surface (E) are similar, as shown in Figure 8.4.

Both roads A and E had a relatively high pavement texture due to the use of uniformly sized crushed chips. This pavement texture is typical of New Zealand suburban roads.

c) Transmissibilities

Figure 8.5 compares the suspension bounce transmissibilities for roads A and E. It is evident that the suspension is effective down to low frequencies - amplification occurring only below 1 Hz. For the road with the poorer surface (A), peak suspension transmissibility occurs at around 0.5 Hz, the cross-over frequency is 0.75 Hz, and good isolation (50% or better) is achieved above 1 Hz. For the road of better quality (E), the cross-over frequency is a little higher at 1 Hz and isolation in excess of 50% is achieved

only at frequencies greater than 1.8 Hz. Amplification at stretcher suspension resonance is greater for the rougher road (A).

The differences between the stretcher suspension transmissibilities over roads A and E are greatest at low frequencies (below around 4 Hz). This is thought to be due to the greater relative difference between the floor vibration magnitudes at low frequencies. (Above 2.5 Hz the relative difference between the floor vibration magnitudes for the two roads reduces, as shown in Figures 8.3 and 8.4).

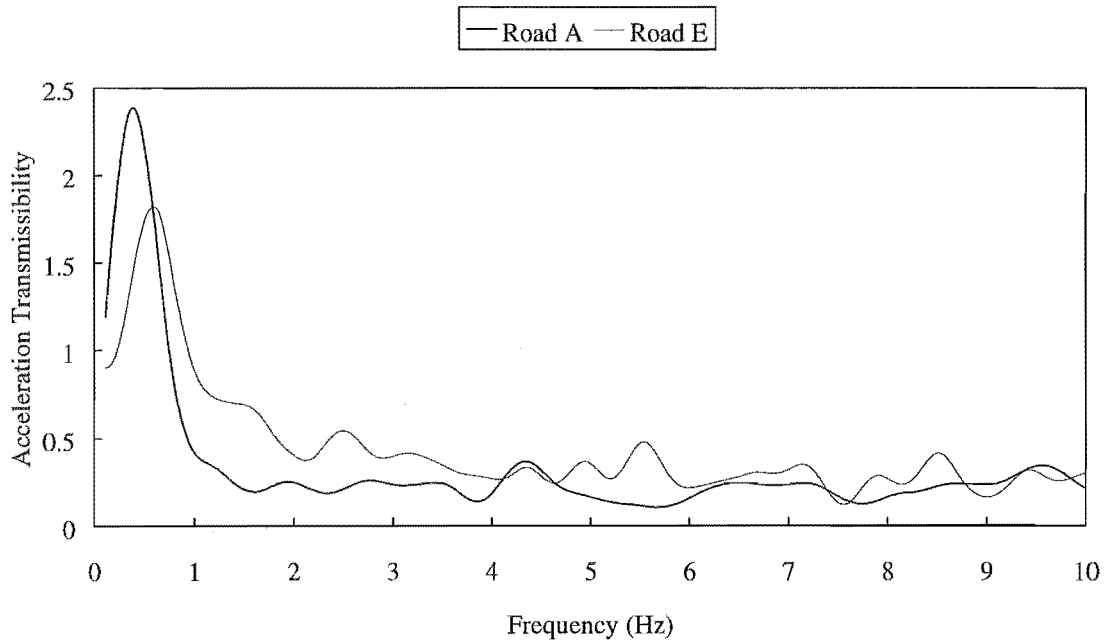

***Figure 8.5** Stretcher Suspension Bounce Acceleration Transmissibilities (Roads A and E)*

The character of the transmissibilities shown in Figure 8.5 are consistent with the effects of Coulomb damping in that:

- Best isolation is achieved when the input is higher (road A).
- Amplification at resonance is greater when the input is higher (road A).
- At higher frequencies the transmissibilities approach a constant value (of 0.24).

d) Reductions in Peak and R.M.S. Accelerations

The reduction in peak and r.m.s. floor vibrations achieved using the stretcher suspension are summarised in Table 8.2. These values were calculated after first removing the high frequency components from the acceleration data by using a LP software filter (24^{th} order Butterworth) with a cut-off of 12 Hz. (The supine patient is most sensitive to lower frequency vibrations as discussed in Chapter 2, so that isolation of frequencies

above around 10 Hz is less important.) If higher frequency components are considered, bigger reductions in r.m.s. and peak accelerations are realised (Table 8.3).

While Table 8.2 shows that the best reductions in floor r.m.s. vibrations are achieved over the worst surfaces (65% reduction for road A), good levels of isolation are achieved for all of the roads and the minimum reduction is 45% (road E). Reductions in peak vibrations are a little better than r.m.s. reductions, and range from 58% to 83%. There appears to be no correlation between the peak floor acceleration and the level of peak reduction achieved.

Table 8.2 Reductions in Peak and R.M.S. Floor Bounce Accelerations (0-~12 Hz)

Road	*Floor Peak Accel. (g)*	*Stretcher Peak Accel. (g)*	*Reduction in Peak Accel. (%)*	*Floor R.M.S. Accel. (g)*	*Stretcher R.M.S. Accel. (g)*	*Reduction in R.M.S. Accel. (%)*
A	0.478	0.170	64	0.131	0.046	65
B	0.381	0.117	69	0.077	0.033	57
C	0.525	0.089	83	0.060	0.028	54
D	0.237	0.081	66	0.050	0.025	50
E	0.191	0.080	58	0.038	0.021	45
F	0.250	0.055	78	0.037	0.018	52

e) Evaluation of Bounce Isolation

The vertical isolation provided by the suspension compares favourably to that provided by the systems of Blok [69] and Leyshon and Stammers [46].

Blok's stretcher suspension reduced ambulance floor r.m.s. accelerations by 42% [59]. This value was calculated by taking into account frequencies up to 60 Hz and cannot be compared directly with the results of Table 8.2. However, when the results of Table 8.2 are re-calculated without LP filtering (ie. taking into account components up to 50 Hz), the suspension described here is shown to provide the better isolation - the reductions in r.m.s. acceleration being approximately 1.7 times better than for those of Blok's system (Table 8.3).

Table 8.3 Reductions in R.M.S. Floor Bounce Accelerations (0-50 Hz)

Road	*Floor R.M.S. Accel. (g)*	*Stretcher R.M.S. Accel. (g)*	*Reduction in R.M.S. Accel. (%)*
A	0.243	0.061	75
E	0.162	0.043	73

Leyshon and Stammers [46] measured vertical floor vibration in an ambulance over four surfaces and by defining patient tolerance margins (based on the research of Oliver and Gibson [57]) found that isolation was needed most between 1.5 and 4 Hz. They report that the transmissibility of their suspension was 0.87 at 1.5 Hz, and 0.32 at 4 Hz. As shown in Table 8.4, the suspension described in this thesis provides better isolation in this important 1.5-4 Hz range and can be considered superior to the suspension of Stammers and Leyshon. At higher frequencies, where good isolation is not so important, the suspension of Leyshon and Stammers provides the better isolation. The good isolation at 1.5 Hz provided by the suspension described here is a function of its low natural frequency.

***Table 8.4** Comparison of Suspension Bounce Transmissibilities (ignoring amplification of stretcher and mattress)*

Freq. (Hz)	*Leyshon and Stammers Suspension [46]*	*Suspension Described in This Thesis*	
		Road A	*Road E*
1.5	0.87	0.36	0.65
4	0.32	0.21	0.32
10	0.12-0.15	0.24	0.24

f) Limitations of the Comparisons

The data on suspension performance presented in the section above, while providing a very useful guide to the relative performance of the three suspension systems, cannot be regarded as more than indicative. This is because the same floor input was not used for all of the tests. (The floor vibration depends in part on the travelling speed, road roughness, and ambulance chassis design.) In practice, comparisons based on using the same floor input would be inconvenient and time consuming and would require (1)

access to all three suspension systems, and (2) a means of generating repeatable random input.

8.2.4 Pitch Test Results

a) Pitch Measurements

During pitch testing an amplifier failed which left only three useful accelerometers. Simultaneous measurements of floor and stretcher pitch were thus not possible, and each road was traversed twice - once to measure stretcher pitch, and once to measure floor pitch. This test method was not ideal but probably satisfactory for the purposes of initial suspension evaluation.

b) Floor Pitch

In Figure 8.6, ambulance floor bounce and pitch accelerations are compared for road B. The nature of the comparisons for the other roads are similar and are not shown here. Floor pitch is seen to vary little with frequency. In contrast to bounce, there is no substantial low frequency peak. This, perhaps, can be explained in part by the roads used - none had significant long-wave irregularities.

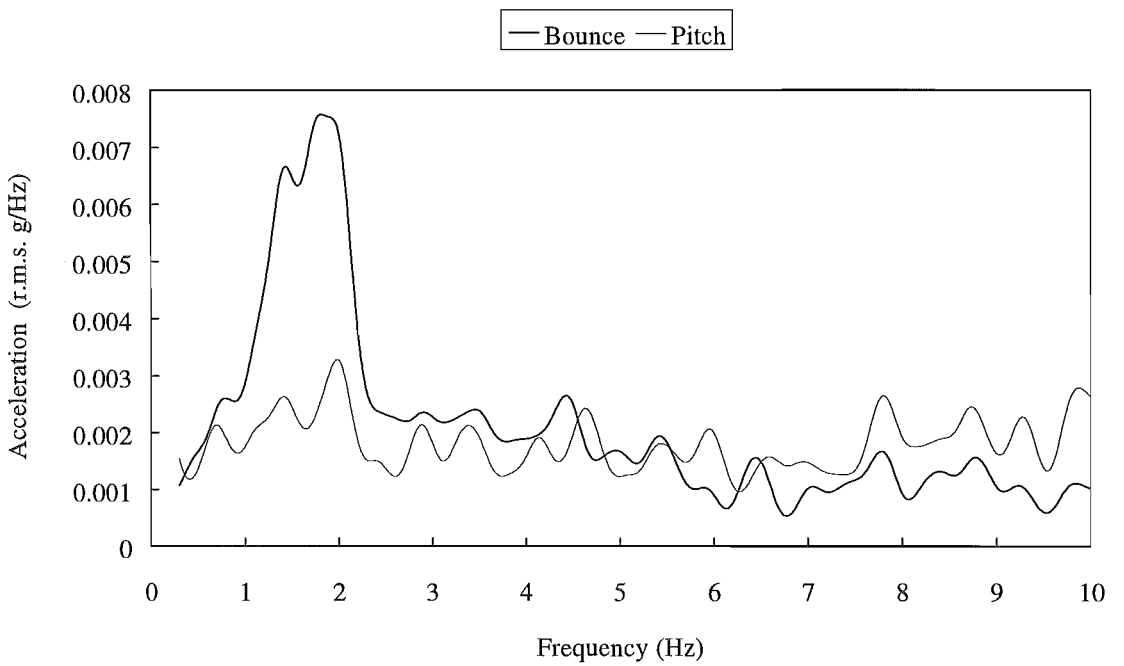

Figure 8.6 Ambulance Floor Bounce and Pitch Acceleration Spectra (Road B)

In the range 4-6 Hz, floor pitch and bounce are similar in magnitude. At higher frequencies floor pitch is greater than floor bounce. This would indicate that above 6 Hz acceleration of the ambulance floor above the front wheels is substantially greater than at the rear. (The ambulance wheelbase is in the order of 3 m, and pitch is defined as the difference in floor acceleration at a distance of 750 mm). By way of comparison, Leyshon and Stammers [46] measured floor pitch greater in magnitude to bounce only at higher frequencies (above 8.5 Hz). At less than 8.5 Hz, floor pitch levels approached the levels of bounce only over rough surfaces at low frequencies (around 1 Hz).

It is not clear why, at above 2-3 Hz, the levels of floor pitch are high compared to bounce for the tests described here. Possibly, transducer or processing errors may have been involved. Alternatively, the effect may simply be related to the character of the ambulance suspension. Repeated tests would be required to establish this - preferably using the same ambulance as well as an ambulance with a different chassis.

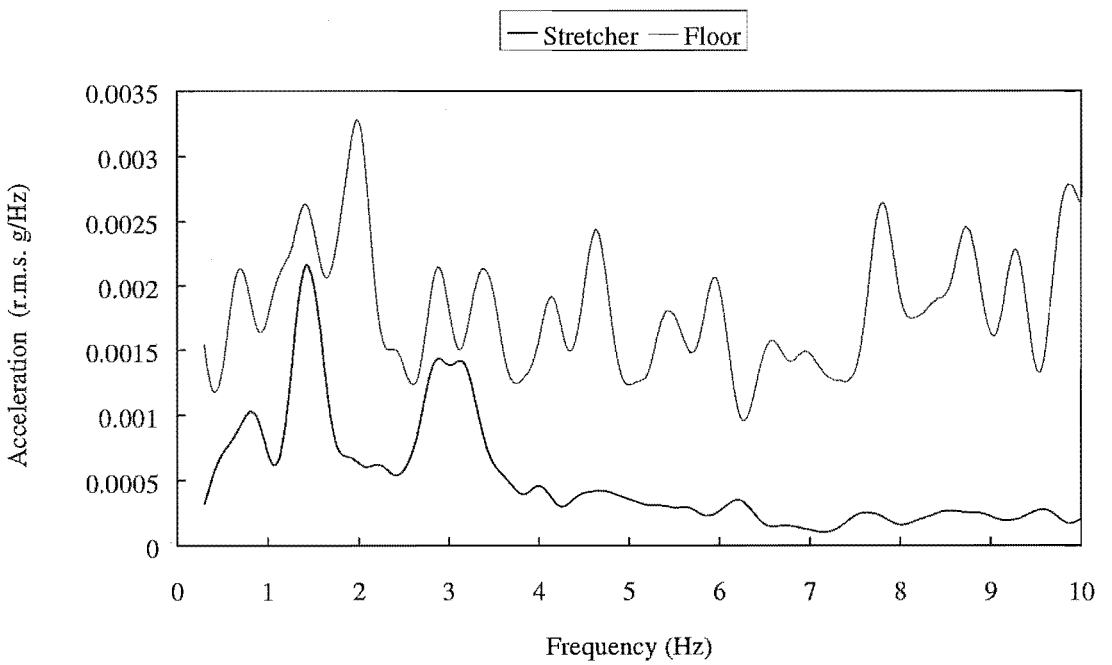

***Figure 8.7** Ambulance Floor and Stretcher Pitch Acceleration Spectra (Road B)*

c) Pitch Isolation

Floor and stretcher pitch acceleration spectra are compared in Figure 8.7 for road B. Spectra comparing floor and stretcher pitch for the other roads are similar. Excellent isolation is evident across the full range of frequencies considered and there is no amplification below the theoretical cross-over frequency of 0.65 Hz. (While this lack of

low frequency amplification is surprising, it is consistent with the pitch transmissibility for a journey over a smooth road shown by Leyshon and Stammers [46].)

A peak in stretcher pitch can be observed at 0.75 Hz. This is likely to be associated with the natural frequency response of the stretcher suspension. There are also peaks at 1.5 Hz and 3 Hz which correspond to peaks in floor input.

On the basis of the floor and stretcher pitch r.m.s. accelerations given in Table 8.5, it can be concluded that isolation of floor pitch does not improve with floor vibration level. The same trend was noted by Leyshon and Stammers [46] who measured little isolation over a bumpy road, while on a better quality road transmissibility was 0.25 between 3.5 Hz and 6 Hz. For both roads pitch isolation was less than bounce isolation. The authors commented that the suspension gave a good ride subjectively, which would indicate that floor pitch is less important than bounce. Tolerance margins in pitch and bounce were presented which provided numerical evidence of this.

***Table 8.5** Reductions in R.M.S. Floor Pitch Accelerations (0-~12 Hz)*

Road	*Floor R.M.S. Accel. (g)*	*Stretcher R.M.S. Accel. (g)*	*Reduction in R.M.S. Accel. (%)*
A	0.080	0.029	64
B	0.064	0.019	70
C	0.088	0.013	85
D	0.088	0.014	84
E	0.053	0.015	72
F	0.062	0.014	78

While the actual levels of pitch isolation shown in Table 8.5 are very good, they should not be confidently regarded as accurate until confirmed by repeated tests. This is because of the possibility of errors in the measurements of floor pitch (Subsection b).

8.2.5 Comparison of Patient Pitch and Bounce

Figure 8.8 compares stretcher pitch and bounce for the journey over road B. As shown, the largest vibrations experienced by the suspended patient are in bounce and these occur at a frequency below around 2.5 Hz. Pitch vibrations below this frequency are of lesser magnitude. At above around 4 Hz, the patient is subject to very little vibration in

either pitch or bounce and the acceleration levels of both modes are similar. The trends shown in this figure are representative of the relative stretcher pitch and bounce accelerations for the other roads.

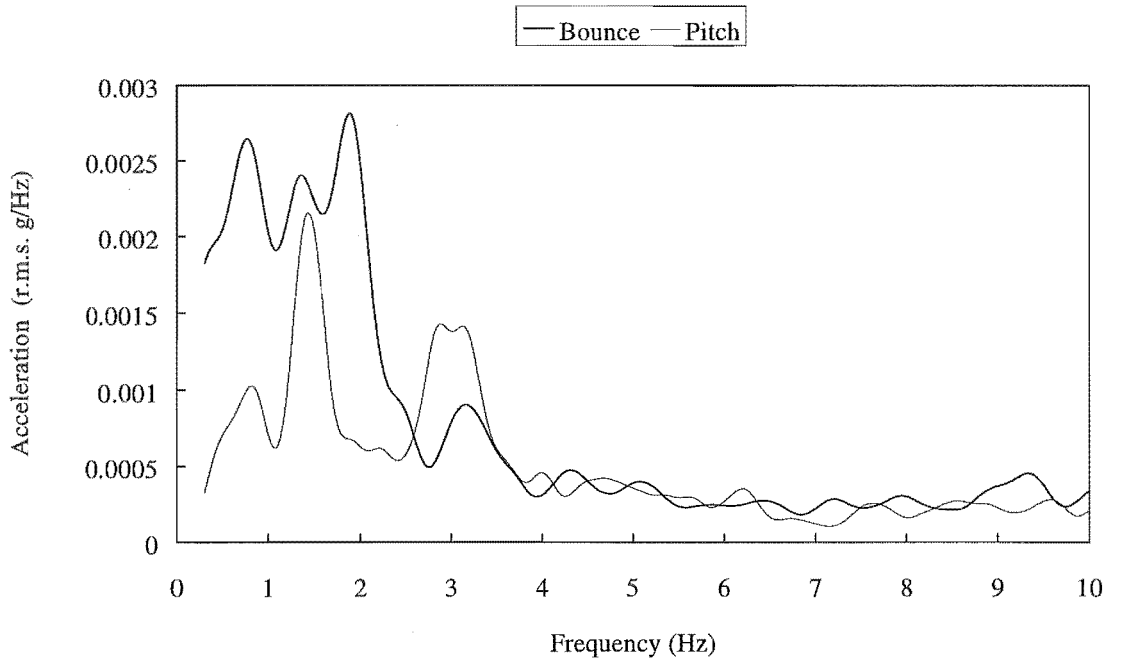

Figure 8.8 Stretcher Bounce and Pitch Acceleration Spectra (Road B)

8.3 SUBJECTIVE EVALUATION

8.3.1 Ride Quality

Assessments of the ride quality of the suspension were made by two subjects who took short journeys on the suspended stretcher in the University of Canterbury environs. The isolation provided by the suspension was very noticeable and vibration was difficult to detect. One of those using the suspension noted an impression of 'uncanny smoothness'. Good isolation of floor motion resulting from speed humps (judder bars) was noted. While the movements of the stretcher relative to the roof associated with these irregularities did not appear to be disconcerting, longer duration tests would be required to confirm this. (Some researchers working with stretcher suspensions have reported that the visible movement of the roof relative to the stretcher can cause the patient distress.)

Pitch of the suspended stretcher was not readily detectable and observation of the stretcher during operation suggested that floor bounce was the dominant input mode. This may have been partly a function of the road surface, which did not appear to excite significant ambulance floor pitch. Deliberately high levels of ambulance deceleration during braking did not result in significant stretcher pitch.

The suspension linkage proved to be insufficiently stiff both laterally and in roll. This was particularly a problem when cornering and could be detected when lying on the stretcher.

8.3.2 Additional Observations

The suspension stroke of ±160 mm in bounce proved to be ample and was not exceeded during road testing. Deflections over the roughest road (road A) were ±27.4 mm r.m.s. and ranged between peaks of 69 mm in extension and 86 mm in compression. This indicates that the lower effective stiffness associated with large suspension deflections (as discussed in Chapter 4, Section 4.4.2) is not important to suspension behaviour over typical roads.

The low level of pneumatic damping provided by the 3.5 mm diameter orifice appeared to be suitable. Appreciable damping forces (indicated by an audible flow of air through the orifice) were developed only for the largest suspension displacements.

Leakage from the pneumatic circuit was negligible. (The ride height of the suspension did not alter significantly during the course of testing which lasted 1.5 hours.)

In spite of the detrimental effects of Coulomb damping, very good levels of isolation have been realised - possibly because the largest amplitude floor vibrations are at lower frequencies (where Coulomb damping has less effect). At higher frequencies, where the effects of Coulomb damping are increasingly significant, good isolation is less important as (1) the floor input is reduced, and (2) patient tolerance levels are higher. In addition, the deleterious effects of Coulomb damping are less evident for high acceleration inputs (rough roads), and it is over rough roads that isolation is most required.

As the laboratory tests were carried out using higher acceleration inputs than were experienced during road testing, it was expected that the detrimental effects of Coulomb damping would be more noticeable in the road test results. This proved not to be the case, however, and the road test transmissibilities were similar to, or better than, the laboratory transmissibilities (eg. Figures 7.8 and 8.5). It can therefore be concluded that

the detrimental effects of Coulomb damping are less marked for realistic ambulance floor inputs than for sinusoidal inputs.

8.4 SUMMARY

The results of road tests described in this chapter show that the suspension provides a marked reduction in floor vibrations transmitted to the stretcher.

- In bounce:
  - isolation is obtained for input frequencies above 1 Hz,
  - at 4 Hz, suspension transmissibility is in the range 0.21-0.32,
  - floor r.m.s. accelerations are reduced by between 45% and 65%,
  - best isolation is realised for rougher roads.
- In pitch the measured levels of isolation are very good, but are possibly optimistic. Repeated pitch tests are intended.
- Subjectively, the suspension gives a very good ride and vibration is difficult to detect. The lateral/roll stiffness of the linkage is, however, too low - this is particularly evident when cornering.
- The detrimental effects of friction appear to be less important for random inputs compared to the case where sinusoidal inputs are used (Chapter 7).

CHAPTER 9

Summary and Recommendations

9.1 INTRODUCTION

9.1.1 Summary of Project Aims

This project had two main aims. The first was to design, build, and test a prototype two degree-of-freedom stretcher suspension using pneumatic springs. Improvements to existing suspensions were sought in terms of providing better isolation and reducing cost, weight, and bulk. The second aim was to investigate and compare the properties of pneumatic damping restrictions. Restrictions investigated were the capillary, the orifice, and the adjustable orifice.

9.1.2 Summary of Research Activities

Work on this project began by reviewing the problem of patient vibration in ambulances and highlighting the drawbacks of currently used stretcher suspension systems. Following this, a requirement specification was established and work began on designing a new suspension. As part of the design process, analysis was carried out to establish the link lengths that would give the suspension the required kinematic properties and natural frequencies. Detail design followed and drawings for manufacture were prepared. Additional theoretical work was carried out to investigate some basic suspension behaviours including coupling and stability during braking.

Pneumatic damping was chosen for the suspension and two damping restrictions were compared - the capillary and the orifice. Comparisons were made first by way of a literature review, and then by modelling and simulation. Further simulations were carried out to determine what advantages might arise from using a semi-active pneumatic damper.

For experimental tests, a simple mechanical shaker table was built and a computer-based data acquisition system was set up. Tests were carried out on the suspension using a variety of shaker inputs, and the effects of using different patient masses and damping levels were investigated. After the tests, some additional modelling work was done to compare the theoretical and experimental transmissibilities of the suspension.

Road trials of the suspension were carried out in an ambulance over a number of different road surfaces. Both bounce and pitch of the floor and stretcher were recorded and then processed to give an indication of the isolation performance of the suspension.

9.2 RESULTS OF STUDY

The aims of this project have been largely met both in terms of designing an improved suspension and also in terms of investigating pneumatic damping methods. A summary of the key research results is given below.

9.2.1 Theoretical

1. Simulations investigating undamped suspension behaviour have shown:
   - The suspension static forces are large compared to the forces resulting from spring deflection. Consequently, suspension behaviour is very sensitive to the directions of these static forces and how they change with suspension deflection. The key significance of this is in terms of analysis and design: if design work were to be carried out using analysis which failed to properly model the static forces, then the suspension would not have the desired natural frequencies. In certain circumstances, the suspension would also be unstable and tend to collapse for large downward displacements. However, as the suspension described in this thesis was designed after making proper allowance for the static forces, it behaves in the intended manner.
   - The kinematics of the suspension linkage give rise to a vertical stiffness which reduces in compression (softening characteristic). While this reduction is not desirable, it is offset in part by the hardening rate of the pneumatic springs. Accordingly, for typical suspension movements the effective variation of stiffness with displacement is small enough not to be important to suspension behaviour.
   - Pure stretcher pitch induces stretcher bounce. For the case where the load is located centrally, this is a higher-order effect. However, when the load is offset from the linkage centre there is first-order coupling and the patient is likely to be subject to more pitch and less bounce than would otherwise be the case (the dominant motion of the ambulance floor is in bounce). Additional experiments would be required to determine the effects that this would have on patient comfort.
   - As the load is situated above the floor, pure floor pitch induces horizontal vibration of the load. Consequently, when the instantaneous pitch and

load centres are non-coincident, large floor pitch amplitudes cause significant pitching of the load. For typical ambulance floor pitch inputs this effect is not noticeable.

- Arranging for the load and suspension pitch centres to coincide is effective in preventing undue stretcher pitch during ambulance braking or acceleration.

2. Damping in a pneumatic suspension can be conveniently achieved by fitting a restriction between the spring and an auxiliary tank. A literature review of pneumatic damping methods (believed to be the most comprehensive to date) has summarised typical pneumatic damping applications and highlighted the following properties of two damping restrictions:
   - The capillary restriction gives a linear damping characteristic.
   - The orifice restriction gives a non-linear characteristic whereby small amplitude vibrations are virtually undamped.

   Simulations have shown that the level of damping required in the stretcher suspension is low and that the orifice restriction is the most suitable (since it gives a damping force which better adapts to changes in load than the capillary). As far as the author is aware, these simulations are the first for which a realistic random input (rather than a simple sinusoidal input) has been used study the performance of pneumatic dampers.

3. The use of continuously variable pneumatic dampers in suspensions does not appear to have been considered. Simulations have shown that fitting a variable orifice restrictor (controlled according to the skyhook damping policy) to the stretcher suspension gives improved isolation compared to fitting a fixed area orifice restriction (eg. 41% reduction in stretcher r.m.s. vertical acceleration). Although theoretically promising, the use of a semi-active damper on the stretcher suspension would not appear worthwhile given that good levels of isolation are achieved using a passive damper. The more sophisticated damping method might however be usefully applied in other isolation applications - particularly where a low cost was not so important. Additional simulation work followed by experiments would be required to develop a practical system. Also, the performance and cost-effectiveness of the system would need to be compared to other types of suspension (eg. fully-active hydraulic and slow-active pneumatic).

9.2.2 Design

The suspension described in this thesis (and shown in Figure 8.1) has the following features:

- Two degrees of freedom - one in bounce and the other in pitch.
- Low natural frequencies. (Nominally, the natural frequencies in pitch and bounce are 0.46 Hz).
- Generous working space. (The stroke in bounce is ±160 mm and the stroke in pitch is ±9.5°).
- A load-independent ride height. (This is achieved by using a simple pneumatic circuit).
- Load-independent natural frequencies.
- Damping which adapts to suit the load. (This is provided by a 3.5 mm diameter orifice restriction which is fitted into the pneumatic circuit).
- Coincident pitch and load centres which prevent undue stretcher pitch during ambulance braking or acceleration.
- The ability to carry patients weighing 30-130 kg.
- The ability to accept a standard wheeled stretcher.
- The ability to collapse to a height which allows easy roll on/off loading/unloading of the stretcher.
- The ability to fit around an ambulance wheel arch. This allows two stretchers to be carried in the ambulance - one over either wheel arch.
- Low weight. The weight of the suspension is approximately 24.5 kg (without air supply). This would be reduced a little if rubber bellows were used instead of cylinders. If air was to be supplied from a tank, rather than a compressor, the unit would be entirely self-sufficient and could be readily transferred between ambulances.
- Low cost. (Simple structural aluminium sections and standard pneumatic components are used in the suspension).
- Ease of use. To operate the suspension, the ambulance attendant would be required to:
    - Roll the stretcher over the suspension.
    - Clamp the stretcher to the suspension (clamps were not fitted to the prototype described here, but would be required in a production version).
    - Toggle the switch on the height levelling circuit from the 'down' position to the 'up' position.

  Lowering the suspension would be a reverse of this procedure.

While only some of the features listed above are unique to the pneumatic suspension, it is believed that the overall package represents an improvement over existing designs -

particularly with respect to low weight, low cost, and the ability to be located around an ambulance wheel-arch. To a significant degree, these improvements were made possible by using pneumatic springs. As these adapt to load, they relieved the linkage of providing any load-adaptive function. (The linkage could therefore be designed to be more compact than would otherwise have been possible).

9.2.3 Experimental

a) Confirmation of Theory

1. Both shaker and road test results confirm that the bounce natural frequency is very close to its design value of 0.46 Hz. Additional tests are required to confirm the exact value of the pitch natural frequency.

2. Shaker tests using patient masses of 34 kg, 68 kg, and 102 kg confirm that the bounce natural frequency varies little with load. Suspension transmissibility also varies little with load. These results indicate that the stiffness of the pneumatic springs adapts to suit load in accordance with theory.

b) Bounce Performance

1. Shaker tests show that the suspension provides very good isolation of high acceleration inputs. When subject to a 0.50g sinusoidal bounce input, isolation is better than 70% above 1.4 Hz and better than 90% above 5.2 Hz. The levels of isolation reduce for lower acceleration inputs.

2. Road tests show that the suspension provides bounce isolation levels which compare very favourably with those of existing suspensions - particularly at low frequencies where good isolation is most needed. For example, the suspension described by Stammers and Leyshon [46] had a vertical transmissibility of 0.87 at 1.5 Hz and 0.32 at 4 Hz (averaged over four surfaces). Corresponding transmissibilities for the suspension described here are 0.36-0.65 at 1.5 Hz and 0.21-0.32 at 4 Hz. (The lower figure is for measurements made over a poor road, and the higher figure for measurements over a good road.)

3. The suspension reduces vertical r.m.s. vibration of the patient by between 45% and 65%. The best reductions occur over the worst roads.

c) Pitch Performance

1. Pitch isolation of sinusoidal inputs is satisfactory although inferior to both bounce isolation and theoretical predictions.

2. The levels of pitch isolation in an ambulance were very good. Reductions in r.m.s acceleration were between 64% and 78%, and the pitch transmissibility was less than unity across the full range of frequencies considered (0-10 Hz). These are very good results, but would appear to be optimistic given the disappointing isolation measured using shaker inputs.

d) Problems

1. Some problems were encountered with the pneumatic circuit used for height levelling. For high rates of lift, the suspension would overshoot the required height. For cases where the suspension was not evenly loaded, the circuit failed to give a level suspension.

2. Both laboratory and road tests have shown that isolation of high frequency and/or low acceleration inputs is detrimentally affected by Coulomb damping in the suspension bushes. Simulations, which have compared the performance of the suspension with and without Coulomb damping, have emphasised this.

3. The lateral and roll stiffness of the linkage is insufficient and would need to be improved in a production version.

9.3 RECOMMENDATIONS FOR FURTHER WORK

9.3.1 Further Testing

The results of the road and laboratory tests are encouraging and suggest that a production version of the stretcher suspension could provide an improved alternative to current systems. Further testing is required, however, to clarify the following aspects of pitch behaviour:

- The value of the pitch natural frequency and how this alters (if at all) with input size.
- The effects of patient mass on pitch natural frequency and transmissibility.
- The effect of input type on pitch isolation. (While excellent isolation was recorded during road tests, the isolation of shaker inputs was somewhat disappointing).

For the most part, the experimental work described in this thesis has been limited to simply confirming basic properties of the suspension and providing initial indications of its performance. Naturally, more extensive testing would be required prior to finalising a production design. In particular, the effects of significant coupling between bounce and pitch would need to be checked. Also, the advantages of using a two degree-of-freedom linkage rather than a bounce-only linkage would need be assessed. If providing pitch isolation proved not to be important, then a scissor linkage of the type used by previous students (Figure 2.3) would be a simpler and less costly alternative.

9.3.2 Suspension Modifications

Improvements to the present design can clearly be made in moving to a production model. Key changes are discussed below:

1. To reduce friction, the nylon bushes used in the linkage pivots could be replaced by rolling element bearings.

2. To further reduce friction, rubber bellows (fixed directly to the pitch and lower arms) could be used in preference to the cylinders. Bellows of the convolution type would be the best choice, as the alternative rolling diaphragm (reversible sleeve) type tend to be less able to stroke through an arc and/or accommodate misalignment - particularly in the smaller sizes that would be suitable for the stretcher suspension application. While the use of bellows might preclude accurate suspension analysis, an experimental approach to determining the best spring mounting angle and surge tank volume could be used. In order to achieve a sufficiently low natural frequency, attention would need to be given to offsetting the hardening rate of the bellows with the softening rate of the linkage.

3. Any reductions in friction resulting from the modifications above would reduce the problem of overshoot during suspension height levelling. This improvement, coupled with using the base frame rather than the top frame to actuate the height trip valves, might then make the existing circuit satisfactory. If this proved not to be so, continuously acting height levelling systems would need to be considered. Potentially suitable systems would include:
    - The mechanically-actuated height levelling valves used in truck suspensions, which are available at modest cost. These might require some modification, as they are designed for the control of larger springs than used in the stretcher suspension.

- Solenoid actuated valves utilising the signals from linear displacement transducers.

Such continuously acting systems would result in increased air consumption and possibly cost.

4. The problem of insufficient linkage stiffness, both laterally and in roll, is partly the result of having to offset the top frame so that the suspension can be positioned to fit around the wheel arch. While there is little that can be done to reduce the linkage offset (without compromising the suspensions favourable position), it is thought that a marked increase in stiffness is possible by using larger structural sections for the links.

5. Although a weight penalty would be involved, the use of steel for the linkage might be a better alternative to aluminium given that it undergoes less distortion when welded.

6. A more accurate approach to the alignment of the pivots is required. This could be achieved by bolting rather than welding the bushes to the linkage. If rolling element bearings were used, bolting would be the natural attachment method.

References

1. **Humphrey, E.** (editor in chief), Ambulance. *Encyclopedia International*, Grolier Incorporated, New York, Vol. 1, 1975, pp 341.

2. **Newcomb, T.P.** and **Spur, R.T.** *A technical history of the motor car.* Adam Hilger, Bristol and New York, 1989.

3. **Bastow, D.** and **Howard, G.P.** *Car suspension and handling.* Third edition, Pentech Press, London, 1993.

4. **MIRA.** *MIRA-Car 2000.* 1993.

5. **Daniels, J.R.** *The car of the future.* London: Economic Intelligence Unit, November 1989.

6. **Seiffert, U.** and **Walzer, P.** *Automobile technology of the future.* 1989, (Translated from German by Jaeckel, H.R., Warrendale Pa., SAE, 1991).

7. **Godden, W.G.** and **Aslam, M.** and **Scalise, T.** Seismic isolation of an electron microscope. *Seventh World Conference on Earthquake Engineering*, Turkey, 8, 1980, pp 69-76.

8. **Waller, R.A.** and **Benham, P.P.** Fatigue machine mounted on air springs. *Engineering*, 8, March 1963, pp 338-339.

9. **Anon.** Air-tight products for seating systems. *International Journal of Applied Pneumatics*, 5, December 1993, pp 26.

10. **Anon.** Luxury lesson in control. *Automation and control*, Journal of the Institute of Measurement and Control (NZ) Ltd., October 1996, pp 30.

11. **Vu, H.V.** and **Torby, B.J.** Pneumatic vibration isolation of a table traversed by a moving load. *Vibration Isolation, Acoustics, and Damping in Mechanical Systems*, ASME, DE-Vol.62, 1993, pp 39-42.

12. **Cellucci, T.A.** and **Williams, R.** Tuned damping of steel tables offers submicron stability. *Laser Focus World*, July 1992, pp 117-122.

13. **Cellucci, T.A.** and **Houghton, B.** Vibration control without sticker shock. *Machine Design*, November 12, 1993, pp 38- 42.

14. **Green, G.L.** Accurate positional servo for use with pneumatically supported masses and vibrationally isolated tables. *Rev. Sci. Instrum*, 58(7), July 1987, pp 1303-1305.

15. **Hundal, M.S.** Literature review - pneumatic shock absorbers and isolators. *Shock and Vibration Digest*, 12, No. 9, 1980, pp 17-21.

16. **Hundal, M.S.** Analysis of performance of pneumatic impact absorbers. *Trans. ASME, Journal of Mechanical Design*, 100, April 1978, pp 236-241.

17. **Sainsbury, J.H.** Air suspension for road vehicles. *Proc. Instn Mech. Engrs Auto. Div.*, No. 3, 1957-58, pp 75-101.

18. **Anon.** Airide springs. *Automobile Engineer*, June 1958, pp 208-210.

19. **Anon.** Dunlop air suspension. *Automobile Engineer*, May 1958, pp 168-174.

20. **Berry, W.S.** The air coil spring - A new factor in Rambler suspension. *SAE Transactions*, Vol. 66, 1958, pp 471-474.

21. **Hansen, K.H.** and **Bertsch, J.F.** and **Denzer, R.E.** 1958 Chevrolet level air suspension. *SAE Transactions*, Vol. 66, 1958, pp 483-490.

22. **McFarland, F.R.** and **Peckham, E.G.** and **Dietrich, E.** The Buick Air Poise suspension. *SAE Transactions*, Vol. 66, 1958, pp 466-470.

23. **O'Shea, C.F.** The Ford approach to air suspension. *SAE Transactions*, Vol. 66, 1958, pp 475-482.

24. **Perkins, R.W.** Oldsmobile New-Matic ride. *SAE Transactions*, Vol. 66, 1958, pp 491-495.

25. **Polhemus, V.D.** and **Kehoe (Jr), L.J.** and **Cowin, F.H.** and **Milliken, S.L.** Cadillac's air suspension for the Eldorado Brougham. *SAE Transactions*, Vol. 66, 1958, pp 346-356.

26. **Chance, B.K.** 1984 Continental Mark VII/Lincoln Continental electronically-controlled air suspension (EAS) system. *SAE Transactions* No. 840342, Vol. 93, 1984.

27. **Anon.** Range Rover: Limousine-refinement with all-terrain capability. *Automotive Engineer*, October/November 1992, pp 20-21.

28. **Anon.** Land Rover Range Rover. *Automotive Engineering*, December 1992, pp 51-52.

29. **Hirose, M.** and **Matsushige, S.** and **Kamiya, K.** Toyota electronic modulated air suspension system for the 1986 Soarer. *IEEE Transactions on Industrial Electronics*, Vol. 35, No. 2, May 1988, 193-200.

30. **Tanashaki, H.** and **Shindo, K.** and **Nogami, T.** and **Oonuma, T.** Toyota electronic modulated air suspension for the 1986 Soarer. *SAE Transactions*, No. 870541, Vol. 96, 1987.

31. **Mizuguchi, M.** and **Suda, T.** and **Chikamori, S.** and **Kobayashi, K.** Chassis electronic control systems for the Mitsubishi 1984 Galant. *SAE Transactions*, No. 840258, Vol. 93, 1984.

32. **Cho, D.** and **Hedrick, J.K.** Pneumatic actuators for vehicle active suspensions. *Trans. ASME, Journal of Dynamic Systems, Measurement, and Control*, Vol. 107, March 1985, pp 67-72.

33. **Higaki, H.** and **Fujimori, S.** and **Horike, Y.** and **Yasui, T.** and **Koyanagi, S.** and **Okamoto, I.** and **Terada, K.** An active pneumatic tilting system for railway cars. *The Dynamics of Vehicles on Roads and Tracks*, Proc. 12th Symposium, 1991, pp 254-268.

34. **Jindai, K.** and **Kasai, K.** and **Terada, K.** and **Kakehi, Y.** and **Iwasaki, F.** Fundamental study on semi-actively controlled pneumatic servo suspensions for rails cars. Contributed by the Rail Transportation of the ASME for presentation at the *Joint ASME/IEEE Railroad Conference*, April 28-30, 1981, Atlanta, Georgia.

35. **Klinger, D.L.** and **Calzado, A.J.** A pneumatic on-off vehicle suspension system. *Trans. ASME, Journal of Dynamic Systems, Measurement and Control*, June 1977, pp 130-136.

36. **Schönfeld, K.** and **Geiger, H.** and **Hesse, K.** Electronically controlled air suspension (ECAS) for commercial vehicles. SAE Technical Paper No. 912671, 1991.

37. **Anon.** Trends in CV suspension and vibration diagnostics. *Automotive Engineer*, June/July 1992. pp 15-16.

38. **Chalmers, W.G.** Chalmers series 1200 air/rubber truck tandem. SAE Technical Paper No. 852345, 1985.

39. **The Press** *(Christchurch, N.Z.)*, Fuel blamed for engine failures. Saturday, September 7, 1996, pp 8.

40. **Observer** *(Christchurch, N.Z.)*, Ducato popular choice. September 4, 1995, pp 28.

41. **The Press** *(Christchurch, N.Z.)*, The Order of St John. Tuesday, July 20, 1993, pp 26-27.

42. **Geary, L.** *Ambulances*. Ian Henry Publications, Hornchurch, 64 transport series, 11, 1984.

43. **Anon.** Ambulances: a break with conservatism? *Automotive Engineer*, February/March 1994, pp 37-38.

44. **Snook, R.** Medical aspects of ambulance design. *British Medical Journal*, 3, 1972, pp 574-578.

45. **Stammers, C.W.**, and **Leyshon, D.** Ambulance stretcher suspension. *Proc. Instn Mech. Engrs*, Vol. 199, No. D2, 1985, pp 151-160.

46. **Leyshon, D.R.**, and **Stammers, C.W.** The development and performance of an ambulance stretcher suspension. *Proc. Instn Mech. Engrs*, Vol. 200, No. D4, 1986, pp 249-257.

47. **Oliver, R.J.** and **Holt, A.J.** Evaluation of ride and performance characteristics of six ambulances. MIRA report K 13042, 1979.

48. **Wasserman, D.E.** Human vibration standards. *Sound and Vibration*, July 1991, pp 30-32.

49. **von Gierke, H.E.** and **Goldman, D.E.** Effects of shock and vibration on man. *Shock and Vibration Handbook*, third edition, (edited by Harris, C.M.), McGraw-Hill, 1988, Chapter 44.

50. **International Organisation for Standardisation.** Acoustics, vibration and shock: handbook on international standards for acoustics, mechanical vibration and shock. International Organisation for Standardisation, Geneva, 1980.

51. **Howarth, V.C.H.,** and **Griffin, M.J.** The frequency dependence of subjective reaction to vertical and horizontal whole-body vibration at low magnitudes. *Journal of the Acoustical Society of America*, Vol. 83, No. 4, April 1988, pp 1406-1413.

52. **Matthews, J.** The measurement of tractor ride comfort. *SAE Transactions*, No. 730795, Vol. 82, 1973.

53. **Guignard, J.C.** Human response to intense low-frequency noise and vibration. *Proc. Instn Mech. Engrs*, Vol. 182, Pt 1, No. 3, 1967-68, pp 55-59.

54. **Miwa, T.** and **Yonekawa, Y.** Evaluation of methods for vibration effect, Part 9: Response to sinusoidal vibration at lying posture. *Ind. Health*, No. 7, 1969, pp 116-126.

55. **Reiher, H.** and **Meister, F.J.** Forsch. auf dem Gebiete des Ingenieurwesens II, 11, 1931, pp 381; ibid III, 1, 1932, pp 177; ibid VI, 3, 1938, pp 116.

56. **Chen, Y.** and **Gao, Li.** A study of reduced comfort boundary of human exposure to whole-body vibration at lying posture. SAE Technical Paper No. 901647, 1990.

57. **Oliver, R.J.** and **Gibson, P.D.G.** The sensitivity of supine stretcher-borne human subjects to vibration in three translational and two rotational modes. MIRA report K 13010, 1978.

58. **Stammers, C.W.** Protecting the patient from floor vibration. *Ambulance Service Journal*, Vol. 20, No. 3, 1991, pp 13-14.

59. **Snook, R.** and **Pacifico, R.** Ambulance ride: fixed or floating stretcher? *British Medical Journal*, 2, 1976, pp 405-407.

60. **Cullen, C.H.** and **Douglas, W.K.** and **Danziger, A.M.** Mortality of the ambulance ride. *British Medical Journal*, 3, 1967, pp 438.

61. **Pichard, E.** *et al.* Les accélérations et les vibrations dans la pathologie liée au transport sanitaire. *Revue des Corps de Santé*, 11(5), 1970, pp 611-635.

62. **Waddell, G.** and **Scott, P.D.R.** and **Lees, N.W.** and **Ledingham, I.McA.** Effects of ambulance transport in critically ill patients. *British Medical Journal*, 1, 1975, pp 386-389.

63. **Waddell, G.** Movement of critically ill patients within hospital. *British Medical Journal*, 2, 1975, pp 417-419.

64. **Wheble, V.H.** Ambulance transport: a question of patient comfort. *Engineering in Medicine*, Vol. 16, No. 1, 1987, pp 47-50.

65. **Trunkey, D.B.** Trauma. *Scientific American*, Vol. 249, No. 2, 1983, pp 20-27.

66. **Bothwell, P.W.** Design for ambulances. *British Medical Journal*, 2, 1968, pp 366.

67. **London, P.S.** The design of ambulances. *Proc. Instn Mech. Engrs*, Vol. 182, Pt 2A, No. 7, 1967-68, pp 188-199.

68. **Stammers, C.W.** and **Leyshon, D.** Ambulance stretchers: design for vibration isolation. *Tenth ASME Conference on Mechanical Vibration and Noise*, Cincinatti, Ohio, September 10-13, 1985, Paper 85-DET-45.

69. **Blok, S.** Improvement of vibration isolation in transports by bearings flats. *Journal of the Society of Environmental Engineers*, 12, No. 59, December 1973, pp 3-8.

70. **Dalyell, T.** Bath chairs and bumpy ambulances. *New Scientist*, November 22, 1984, pp 46.

71. **Black, J.** Ambulance stretcher suspension. European Patent No. 88305088.3, September 1983.

72. **Sutton, R.A.** Vibration isolation of patients in ambulances. Project Report No. 29, Department of Mechanical Engineering, University of Canterbury, 1986.

73. **Wylie, B.** Vibration isolation of patients in ambulances. Project Report No. 54, Department of Mechanical Engineering, University of Canterbury, 1989.

74. **Pettigrew, K.B.** Vibration isolation of patients in ambulances. Project Report No. 68, Department of Mechanical Engineering, University of Canterbury, 1991.

75. **Raine, J.K.** and **Henderson, R.J.** A vibration isolating stretcher suspension. *Proc. IPENZ Annual Conference*, Hamilton, February 1993, pp. 221-232.

76. **Sharp, R.** Which way for vehicle suspension? *Automotive Engineer*, June/July 1994, pp 2,66.

77. **Craighead, I.A.** An active suspension system for an ambulance stretcher. *Proc. Instn Mech. Engrs Conf. on Advanced Suspensions*, Paper No. C426/88, 1988, pp 59-67.

78. **Horning, R.W.** and **Schubert, D.W.** Air suspension and active vibration-isolation systems. *Shock and Vibration Handbook*, third edition, (editor Harris C.M.), McGraw-Hill, 1987, Chapter 33.

79. **Barber, A.** *Pneumatic Handbook.* seventh edition, Elsevier Science Publishers Limited, 1989.

80. **Firestone.** *Airstroke® actuators and Airmount® isolators - engineering manual and design guide*, EMDG 596, printed in U.S.A., 1996.

81. **Campbell, C.** *New directions in suspension design*, Robert Bently Inc., 1981.

82. **Giles, J.G.** *Steering, suspension and tyres.* Iliffe Books Ltd., London, 1968.

83. **Cavanaugh, R.D.** Air suspension and servo-controlled isolation systems. *Shock and Vibration Handbook*, Vol. 2, (editors Harris C.M. and Crede C.E.), New York, McGraw-Hill, 1961, Chapter 33.

84. **Bachrach, B.I.** and **Riven, E.** Analysis of a damped pneumatic spring. *Journal of Sound and Vibration*, 86(2), 1983, pp 191-197.

85. **Massey, B.S.** *Mechanics of Fluids.* fifth edition, Van Nostrand Reinhold (International), 1988.

86. **Shearer, J.L.** Study of pneumatic processes in the continuous control of motion with compressed air - II. *Trans. ASME*, 78, February 1956, pp 243-249.

87. **Soliman, J.I.** and **Tajer-Ardabili, D.** Self-damped pneumatic isolator for variable frequency excitation. *Journal of Mechanical Engineering Science*, 8, No. 3, 1966, pp 284-293.

88. **Gee-Clough, D.** and **Waller, R.A.** An improved self-damped pneumatic isolator. *Journal of Sound and Vibration*, 8(3), 1968, pp 364-376.

89. **Esmailzadeh, E.** Compact self-damped pneumatic isolators for road vehicles. *Trans. ASME, Journal of Mechanical Engineering Design*, 102, April 1980, pp 270-277.

90. **Esmailzadeh, E.** Optimisation of pneumatic vibration isolation system for vehicle suspension. *Trans. ASME, Journal of Mechanical Design*, 100, July 1978, pp 500-506.

91. **Bhave, S.Y.** Effect of connecting the front and rear air suspensions of a vehicle on the transmissibility of road undulation inputs. *Vehicle System Dynamics*, 21, 1992, pp 225-245.

92. **Bachrach, B.I.** and **Riven, E.** Pneumatic damping of vehicle tyres to improve ride quality. *SAE Transactions*, No. 840746, Vol. 93, 1984.

93. **Baker, J.K.** *Vibration Isolation.* Engineering Design Guides, 13, Oxford University Press for the Design Council, 1975.

94. **Hedrick, J.K.** Railway Vehicle Active Suspensions. *Vehicle System Dynamics*, 10, 1981, pp 267-283.

95. **Koyanagi, S.** The development of the air spring with variable nozzle. *Quarterly report of the RTRI*, 31, No. 3, August 1990, pp 122-127.

96. **Koyanagi, S.** A design method for the vibration isolation system of an air spring suspended vehicle. *Quarterly report of the RTRI*, 32, No. 1, March 1991, pp 2-7.

97. **Andersen, B. W.** *The Analysis and Design of Pneumatic Systems.* John Wiley and Sons, 1967.

98. **Gvineriya, K.I.** and **Dzhokhadze, G.D.** and **Kiselev, B.A.** and **Kozlova, I.V.** and **Fomchenko, V.M.** Calculation of the constructional parameters of a pneumatic damper for suspension units of the type used in automobiles. *Vestnik Mashinostroeniya*, No. 3, 1989, pp 16-19.

99. **Vogel, J.M.** and **Claar II, P.W.** Development of a slow-acting active control pneumatic suspension system for heavy vehicle applications. SAE Technical Paper No. 912675, 1991.

100. **Sharp, R.S.** and **Crolla, D.A.** Road vehicle suspension system design - a review. *Vehicle System Dynamics*, 16, 1987, pp 167-192.

101. **Sharp, R.S.** and **Hassan, S.A.** An evaluation of passive automobile suspension systems with variable stiffness and damping parameters. *Vehicle System Dynamics*, 15, 1986, pp 335-350.

102. **Robson, J.D.** Road surface description and vehicle response. *International Journal of Vehicle Design*, 1, 1979, pp 25-35.

103. **Gillespie, T.D.** *Fundamentals of Vehicle Dynamics.* SAE Inc, Warrendale, U.S.A, 1992.

104. **Karnopp, D.** and **Crosby, M.J.** and **Harwood, R.A.** Vibration control using semi-active force generators. *Trans. ASME, Journal of Engineering for Industry*, May 1974, pp 619-626.

105. **Ruzicka, J.E.** Active vibration and shock control. *SAE Transactions*, No. 680747, 1968.

106. **Goodall, R.M.** and **Kortüm, W.** Active controls in ground transportation - a review of the state-of-the-art and future potential. *Vehicle System Dynamics*, 12, 1983, pp 225-257.

107. **Pollard, M.G.** and **Simons, N.J.A.** Passenger comfort - the role of active suspensions. *Proc. Instn Mech. Engrs*, Vol. 198D, No. 11, pp 161-175.

108. **Claar II, P.W.** and **Vogel, J.M.** A review of active suspension control for on and off-highway vehicles. *SAE Transactions*, No. 892482, Vol. 98, 1982.

109. **Nagia, M.** Recent researches on active suspensions for ground vehicles. *JSME International Journal*, Series C, Vol. 36, No. 2, 1993, pp 161-170.

110. **Elbeheiry, E.M.** and **Karnopp, D.C.** and **Elaraby, M.E.** and **Abdelraaouf, A.M.** Advanced ground vehicle suspension systems - a classified bibliography. *Vehicle System Dynamics*, 24, 1995, pp 231-258.

111. **Parker, G.A.** and **Lau, K.S.** A novel valve for semi-active vehicle suspension systems. *Proc. Instn Mech. Engrs Conf. on Advanced Suspensions*, Paper No. C427/88, 1988, pp 69-74.

112. **Pinkos, A.** and **Shtarkman, E.** and **Fitzgerald, T.** An actively damped passenger car suspension system with low voltage electro-rheological magnetic fluid. SAE Technical Paper No. 930268, 1993.

113. **Ryba, D.** Semi-active damping with an electromagnetic force generator. *Vehicle System Dynamics*, 22, 1993, pp 79-95.

114. **Crolla, D.A.** and **Nour, Aboul A.M.A.** Theoretical comparisons of various active suspension systems in terms of performance and power requirements. *Proc. Instn Mech. Engrs Conf. on Advanced Suspensions*, Paper No. C420/88, 1988, pp 1-9.

115. **Esmailzadeh, E.** Servovalve-controlled pneumatic suspensions. *Journal of Mechanical Engineering Science*, Vol. 21, No. 1, 1979, pp 7-18.

116. **Stein, G.J.** Results of investigation of an electropneumatic active vibration control system for a driver's seat. *Proc. Instn Mech. Engrs*, Vol. 209, Pt D, 1985, pp 227-234.

117. **Sharp, R.S.** and **Hassan, S.A.** Performance predictions for a pneumatic active car suspension system. *Proc. Instn Mech. Engrs*, Vol. 202, No. D4, 1988, pp 243-250.

118. **Decker, H.** and **Schramm, W.** and **Kallenbach, R.** A practical approach towards advanced semi-active suspension systems. *Proc. Instn Mech. Engrs Conf. on Advanced Suspensions*, Paper No. C430/88, 1988, pp 93-99.

119. **Besinger, F.H.** and **Cebon, D.** and **Cole, D.J.** Force control of a semi-active damper. *Vehicle System Dynamics*, 24, 1995, pp 695-723.

120. **Brüel & Kjær.** *Charge Amplifier Type* 2624 - *Instructions and Applications.* B&K Instruments, Orboe Print, Copenhagen, Denmark, January 1970.

121. **Harris, C.M.** Measurement techniques. *Shock and Vibration Handbook*, third edition, (edited by Harris, C.M.), McGraw-Hill, 1988, Chapter 15.

122. **Unholtz, K.** Vibration testing machines. *Shock and Vibration Handbook*, third edition, (edited by Harris, C.M.), McGraw-Hill, 1988, Chapter 25.

123. **Grace, H.P.** and **Lapple, C.E.** Discharge coefficients for small-diameter orifices and flow nozzles. *Trans. ASME*, 73, July 1951, pp 639-647.

124. **Jacobsen, L.S.** Steady forced vibration as influenced by damping. *Trans. ASME*, 1930, pp 169-181.

125. **Den Hartog, J.P.** Forced vibrations with combined coulomb damping and viscous friction. *Trans. ASME*, 1931, pp 107-115.

126. **Crede, C.E.** and **Ruzicka, J.E.** Theory of vibration isolation. *Shock and Vibration Handbook*, third edition, (edited by Harris C.M.), McGraw-Hill, 1988, Chapter 30.

127. **Bowns, D.E.** and **Ballard, R.L.** Digital computation for the analysis of pneumatic actuator systems. *Proc. Instn Mech. Engrs*, Vol. 186, 1972/73, pp 881-889.

APPENDIX A

Suspension and Load Data

In this appendix, the geometry of the suspension is defined. The mass and inertia of the load are also given.

A1 Linkage Geometry

a) Link Lengths

With reference to Figure 4.1a, the link lengths which define the suspension geometry are

$$\begin{aligned} e &= 257.5 \text{ mm}, \\ h &= 247.8 \text{ mm}, \\ L_1 &= 331.5 \text{ mm}, \\ L_2 &= 525.5 \text{ mm}, \\ L_3 &= 172.0 \text{ mm}. \end{aligned} \tag{A1}$$

b) Distances at Design Height

The distances b, c, a and f (shown in Figure 4.1a), which apply when the linkage is at its design height, can be calculated from the link lengths above. By similar triangles

$$b = \frac{hL_1}{\sqrt{e^2 + h^2}} = 230 \text{ mm}, \tag{A2}$$

$$c = \frac{e(b+h)}{h} = 496.2 \text{ mm}, \tag{A3}$$

and by Pythagoras

$$a = \sqrt{L_2^{\,2} - c^2} = 173.0 \text{ mm}, \tag{A4}$$

and finally

$$f = a + b = 403.0 \text{ mm}. \tag{A5}$$

c) Link Angles

Using Figure 4.1b, the suspension link angles at the design height are

$$\beta_0 = \sin^{-1}\left(\frac{b}{L_1}\right) = 43.93°, \tag{A6}$$

$$\alpha_0 = \sin^{-1}\left(\frac{a}{L_2}\right) = 19.22°. \tag{A7}$$

A2 Cylinder Location

The positions of the cylinder mounting points l_1 and l_2 are shown in Figure 4.1b and have the values

$$l_1 = 132.5 \text{ mm}, \tag{A8}$$

$$l_2 = 132.5 \text{ mm}. \tag{A9}$$

Using the cosine rule, the cylinder length at design height is given by

$$l_0 = \sqrt{l_1^2 + l_2^2 - 2l_1 l_2 \cos(\alpha_0 + \beta_0)},$$

and also by the cosine rule we can write (for the triangle ACE)

$$\cos(\alpha_0 + \beta_0) = \frac{L_1^2 + L_2^2 - (e^2 + f^2)}{2L_1 L_2},$$

therefore

$$l_0 = \sqrt{l_1^2 + l_2^2 - \frac{l_1}{L_1}\frac{l_2}{L_2}(L_1^2 + L_2^2 - (e^2 + f^2))} = 138.8 \text{ mm}. \tag{A10}$$

The cylinder angle with the ambulance floor (ψ_0) can be found from

$$\psi_0 = \cos^{-1}\left(\frac{l_2 \cos\alpha_0 - l_1 \cos\beta_0}{l_0}\right), \text{ or}$$

$$\psi_0 = \sin^{-1}\left(\frac{l_2 \sin\alpha_0 + l_1 \sin\beta_0}{l_0}\right),$$

to yield

$$\psi_0 = 77.65°. \tag{A11}$$

The moment arm r_0 of the cylinders is given by

$$r_0 = l_1 \sin(\psi_0 + \beta_0),$$

and using the identity

$$\sin(\psi_0 + \beta_0) \equiv \sin\psi_0 \cos\beta_0 + \sin\beta_0 \cos\psi_0,$$

with the foregoing equations for $\sin^{-1}\psi_0$ and $\cos^{-1}\psi_0$ we can write

$$r_0 = \frac{l_1}{L_1}\frac{l_2}{L_2}\left(\frac{cb + a(c-e)}{l_0}\right) = 112.9 \text{ mm}. \tag{A12}$$

A3 Load Data

a) Load Mass

The mass of the load is given by the sum of the mass of the patient (m_{pat}) and the mass of the stretcher (m_{str}) where

$m_{str} = 25$ kg,
$m_{pat} = 30$-130 kg [45].

The average mass of a patient can be taken as 68 kg [45].

b) Load Inertia

The inertia of the human body (I_{pat}) at an offset of ε_{pat} from the body centre-of-mass is given by [45] as

$$I_{pat} = 0.01 m_{pat}^{\left(\frac{5}{3}\right)} + m_{pat}\varepsilon_{pat}^2 . \tag{A13}$$

The centre-of-mass of the human body lies at a distance of $\frac{42.5}{100} h_{pat}$ from the crown of the head. The height of the human body (h_{pat}) is given by

$$h_{pat} = 0.42 m_{pat}^{\left(\frac{1}{3}\right)} . \tag{A14}$$

These equations should be considered approximate, as human body proportions vary widely [45].

The stretcher is modelled as a uniform beam of length l_{str} whose inertia (I_{str}) at an offset (ε_{str}) from the stretcher centre-of-mass is given by

$$I_{str} = \frac{m_{str} l_{str}^2}{12} + m_{str}\varepsilon_{str}^2 , \tag{A15}$$

where l_{str} = 1.84 m.

APPENDIX B

Suspension Analysis

In this appendix, suspension analysis details omitted from the summary presented Chapter 4 are given. In the interests of clarity, some equations are repeated from Chapter 4. These are referred to using the equation numbers of Chapter 4.

B1 KINEMATICS

B1.1 Linkage Kinematics

a) Link Angles

Section 4.3.1 of Chapter 4 gives three equations for the link angles (β_L, β_R, α) shown in Figure 4.2a:

$$f + h + y - y_s = L_2 \sin(\alpha - \theta_s) + L_1 \sin(\beta_L + \theta_s) + (e + e_e)\sin\theta + h\cos\theta, \quad (4.1)$$

$$L_1 \sin\beta_L + 2e\sin(\theta - \theta_s) = L_1 \sin\beta_R, \quad (4.2)$$

$$L_1 \cos\beta_L + 2e\cos(\theta - \theta_s) + L_1 \cos\beta_R = 2L_2 \cos\alpha. \quad (4.3)$$

These equations can be solved simultaneously to yield a polynomial in $\sin\beta_L$ as follows:

From Equation 4.2 and the trigonometric identity

$$\cos\beta_R \equiv \sqrt{1 - \sin^2\beta_R},$$

we can write

$$\cos\beta_R \equiv \sqrt{1 - \left(\sin\beta_L + \frac{2e\sin(\theta - \theta_s)}{L_1}\right)^2}.$$

Substituting the above with $\cos\beta_L \equiv \sqrt{1-\sin^2\beta_L}$ into 4.3 gives

$$L_1\sqrt{1-\sin^2\beta_L} + 2e\cos(\theta-\theta_s) + L_1\sqrt{1-\left(\sin\beta_L + \frac{2e\sin(\theta-\theta_s)}{L_1}\right)^2} = 2L_2\cos\alpha\,. \tag{B1}$$

Using the trigonometric identities

$$\sin(\alpha-\theta_s) \equiv \sin\alpha\cos\theta_s - \sin\theta_s\cos\alpha\,,$$

$$\sin(\beta_L+\theta_s) \equiv \sin\beta_L\cos\theta_s + \sin\theta_s\cos\beta_L\,,$$

$$\cos\beta_L \equiv \sqrt{1-\sin^2\beta_L}\,,$$

$$\sin\alpha \equiv \sqrt{1-\cos^2\alpha}\,,$$

in 4.1 gives

$$\begin{aligned} f+h+y-y_s = {} & L_2\left(\cos\theta_s\sqrt{1-\cos^2\alpha} - \sin\theta_s\cos\alpha\right) \\ & + L_1\left(\sin\beta_L\cos\theta_s + \sin\theta_s\sqrt{1-\sin^2\beta_L}\right) \\ & + (e+e_e)\sin\theta + h\cos\theta. \end{aligned} \tag{B2}$$

Substituting $\cos\alpha$ from B1 into B2 gives a polynomial in $\sin\beta_L$. This is solved numerically for $\sin\beta_L$ (and hence β_L) by using the secant method. β_R is calculated by back substitution of β_L into 4.2, and α by back substitution of β_L and β_R into 4.3.

b) Link Angle Rates

The link angle rates $\dot{\mathbf{v}}$ (where $\dot{\mathbf{v}} = [\dot{\beta}_L \quad \dot{\beta}_R \quad \dot{\alpha}]^T$) can be expressed as functions of the suspension load and ambulance floor rates $\dot{\mathbf{u}}$ (where $\dot{\mathbf{u}} = [\dot{y} \quad \dot{\theta} \quad \dot{y}_s \quad \dot{\theta}_s]^T$) by determining the inverse Jacobian ($\mathbf{J}^{-1}$) for the suspension. This gives an equation of the form

$$\dot{\mathbf{v}} = \mathbf{J}^{-1}\dot{\mathbf{u}}\,, \tag{B3}$$

or in full

$$\begin{bmatrix} \dot{\beta}_L \\ \dot{\beta}_R \\ \dot{\alpha} \end{bmatrix} = \begin{bmatrix} \frac{\partial \beta_L}{\partial y} & \frac{\partial \beta_L}{\partial \theta} & \frac{\partial \beta_L}{\partial y_s} & \frac{\partial \beta_L}{\partial \theta_s} \\ \frac{\partial \beta_R}{\partial y} & \frac{\partial \beta_R}{\partial \theta} & \frac{\partial \beta_R}{\partial y_s} & \frac{\partial \beta_R}{\partial \theta_s} \\ \frac{\partial \alpha}{\partial y} & \frac{\partial \alpha}{\partial \theta} & \frac{\partial \alpha}{\partial y_s} & \frac{\partial \alpha}{\partial \theta_s} \end{bmatrix} \begin{bmatrix} \dot{y} \\ \dot{\theta} \\ \dot{y}_s \\ \dot{\theta}_s \end{bmatrix}. \tag{4.4}$$

The inverse Jacobian ($\mathbb{J}^{-1}$) can be determined by implicit partial differentiation of each of the three kinematic equations (4.1, 4.2, 4.3) with respect to y, θ, y_s and θ_s. This yields 12 equations, which in matrix form are

$$\begin{bmatrix} L_1 \cos(\beta_L + \theta_s) & 0 & L_2 \cos(\alpha - \theta_s) \\ L_1 \cos\beta_L & -L_1 \cos\beta_R & 0 \\ L_1 \sin\beta_L & L_1 \sin\beta_R & -2L_2 \sin\alpha \end{bmatrix} \begin{bmatrix} \frac{\partial \beta_L}{\partial y} & \frac{\partial \beta_L}{\partial \theta} & \frac{\partial \beta_L}{\partial y_s} & \frac{\partial \beta_L}{\partial \theta_s} \\ \frac{\partial \beta_R}{\partial y} & \frac{\partial \beta_R}{\partial \theta} & \frac{\partial \beta_R}{\partial y_s} & \frac{\partial \beta_R}{\partial \theta_s} \\ \frac{\partial \alpha}{\partial y} & \frac{\partial \alpha}{\partial \theta} & \frac{\partial \alpha}{\partial y_s} & \frac{\partial \alpha}{\partial \theta_s} \end{bmatrix}$$

$$= \begin{bmatrix} 1 & -(e+e_e)\cos\theta + h\sin\theta & -1 & -L_1 \cos(\beta_L + \theta_s) + L_2 \cos(\alpha - \theta_s) \\ 0 & -2e\cos(\theta - \theta_s) & 0 & 2e\cos(\theta - \theta_s) \\ 0 & -2e\sin(\theta - \theta_s) & 0 & 2e\sin(\theta - \theta_s) \end{bmatrix}, \tag{B4}$$

or

$$\mathbf{P}\mathbf{J}^{-1} = \mathbf{Q}, \tag{B5}$$

which can be solved for $\mathbb{J}^{-1}$ to give

$$\mathbf{J}^{-1} = \mathbf{P}^{-1}\mathbf{Q}. \tag{B6}$$

c) Link Angle Accelerations

The acceleration of the link angles ($\ddot{\beta}_L, \ddot{\beta}_R, \ddot{\alpha}$) can be determined from B3 using the product rule for differentiation to yield

$$\ddot{\mathbf{v}} = \mathbf{J}^{-1}\ddot{\mathbf{u}} + \dot{\mathbf{J}}^{-1}\dot{\mathbf{u}}, \tag{B7}$$

or in full

$$\begin{bmatrix} \ddot{\beta}_L \\ \ddot{\beta}_R \\ \ddot{\alpha} \end{bmatrix} = \begin{bmatrix} \frac{\partial \beta_L}{\partial y} & \frac{\partial \beta_L}{\partial \theta} & \frac{\partial \beta_L}{\partial y_s} & \frac{\partial \beta_L}{\partial \theta_s} \\ \frac{\partial \beta_R}{\partial y} & \frac{\partial \beta_R}{\partial \theta} & \frac{\partial \beta_R}{\partial y_s} & \frac{\partial \beta_R}{\partial \theta_s} \\ \frac{\partial \alpha}{\partial y} & \frac{\partial \alpha}{\partial \theta} & \frac{\partial \alpha}{\partial y_s} & \frac{\partial \alpha}{\partial \theta_s} \end{bmatrix} \begin{bmatrix} \ddot{y} \\ \ddot{\theta} \\ \ddot{y}_s \\ \ddot{\theta}_s \end{bmatrix} + \begin{bmatrix} \frac{d}{dt}\left(\frac{\partial \beta_L}{\partial y}\right) & \frac{d}{dt}\left(\frac{\partial \beta_L}{\partial \theta}\right) & \frac{d}{dt}\left(\frac{\partial \beta_L}{\partial y_s}\right) & \frac{d}{dt}\left(\frac{\partial \beta_L}{\partial \theta_s}\right) \\ \frac{d}{dt}\left(\frac{\partial \beta_R}{\partial y}\right) & \frac{d}{dt}\left(\frac{\partial \beta_R}{\partial \theta}\right) & \frac{d}{dt}\left(\frac{\partial \beta_R}{\partial y_s}\right) & \frac{d}{dt}\left(\frac{\partial \beta_R}{\partial \theta_s}\right) \\ \frac{d}{dt}\left(\frac{\partial \alpha}{\partial y}\right) & \frac{d}{dt}\left(\frac{\partial \alpha}{\partial \theta}\right) & \frac{d}{dt}\left(\frac{\partial \alpha}{\partial y_s}\right) & \frac{d}{dt}\left(\frac{\partial \alpha}{\partial \theta_s}\right) \end{bmatrix} \begin{bmatrix} \dot{y} \\ \dot{\theta} \\ \dot{y}_s \\ \dot{\theta}_s \end{bmatrix}, \tag{4.5}$$

where the time derivative of the inverse Jacobian ($\dot{\mathbf{J}}^{-1}$) is found by differentiating B5 to give

$$\mathbf{P}\dot{\mathbf{J}}^{-1} + \dot{\mathbf{P}}\mathbf{J}^{-1} = \dot{\mathbf{Q}}, \tag{B8}$$

or in full

$$\begin{bmatrix} \mathbf{P} \end{bmatrix} \begin{bmatrix} \dot{\mathbf{J}}^{-1} \end{bmatrix} + \begin{bmatrix} -L_1(\dot{\beta}_L + \dot{\theta}_s)\sin(\beta_L + \theta_s) & 0 & -L_2(\dot{\alpha} - \dot{\theta}_s)\sin(\alpha - \theta_s) \\ -L_1\dot{\beta}_L \sin\beta_L & L_1\dot{\beta}_R \sin\beta_R & 0 \\ L_1\dot{\beta}_L \cos\beta_L & L_1\dot{\beta}_R \cos\beta_R & -2L_2\dot{\alpha}\cos\alpha \end{bmatrix} \begin{bmatrix} \mathbf{J}^{-1} \end{bmatrix}$$

$$= \begin{bmatrix} 0 & \dot{\theta}((e+e_e)\sin\theta + h\cos\theta) & 0 & L_1(\dot{\beta}_L + \dot{\theta}_s)\sin(\beta_L + \theta_s) \\ & & & -L_2(\dot{\alpha} - \dot{\theta}_s)\sin(\alpha - \theta_s) \\ 0 & 2e(\dot{\theta} - \dot{\theta}_s)\sin(\theta - \theta_s) & 0 & -2e(\dot{\theta} - \dot{\theta}_s)\sin(\theta - \theta_s) \\ 0 & -2e(\dot{\theta} - \dot{\theta}_s)\cos(\theta - \theta_s) & 0 & 2e(\dot{\theta} - \dot{\theta}_s)\cos(\theta - \theta_s) \end{bmatrix}, \tag{B9}$$

which can be solved for $\dot{\mathbf{J}}^{-1}$ to give

$$\dot{\mathbf{J}}^{-1} = \mathbf{P}^{-1}\dot{\mathbf{Q}} - \mathbf{P}^{-1}\dot{\mathbf{P}}\mathbf{J}^{-1}. \tag{B10}$$

B1.2 Cylinder Kinematics

Equations 4.6-4.9 of Chapter 4 give the cylinder extensions (δ_L, δ_R) and cylinder force moment arms (r_L, r_R) in terms of the instantaneous cylinder lengths (l_L, l_R) and angles (ψ_L, ψ_R). These cylinder lengths and angles are defined below.

From Figure 4.2b, the instantaneous length l_L of the left-hand cylinder is given by the cosine rule as

$$l_L = \sqrt{l_1^2 + l_2^2 - 2l_1 l_2 \cos(\alpha + \beta_L)}, \tag{B11}$$

and the angle of the cylinder (relative to the ambulance floor) is given by

$$\psi_L = \cos^{-1}\left(\frac{l_2 \cos\alpha - l_1 \cos\beta_L}{l_L}\right). \tag{B12}$$

Similarly, for the right-hand cylinder

$$l_R = \sqrt{l_1^2 + l_2^2 - 2l_1 l_2 \cos(\alpha + \beta_R)}, \tag{B13}$$

and

$$\psi_R = \cos^{-1}\left(\frac{l_2 \cos\alpha - l_1 \cos\beta_R}{l_R}\right). \tag{B14}$$

B2 DYNAMICS

B2.1 Linkage Forces

As the suspension base frame is at an angle θ_s to the horizontal, it is convenient to analyse the linkage forces using the rotated coordinate system (x', y') shown in Figure B1. The top frame forces (A_x', B_x', A_y', B_y') of this rotated coordinate system are related to the forces (A_x, B_x, A_y, B_y) of the (x, y) coordinate system by

$$
\begin{aligned}
A_x' &= A_x \cos\theta_s - A_y \sin\theta_s, \\
B_x' &= B_x \cos\theta_s + B_y \sin\theta_s, \\
A_y' &= A_x \sin\theta_s + A_y \cos\theta_s, \\
B_y' &= -B_x \sin\theta_s + B_y \cos\theta_s.
\end{aligned}
\tag{B15}
$$

As discussed in Chapter 3 (Section 3.3.2c), the roller at *J* (Figure B1) is inoperative and the moment on the stabilising links (*FI* and *FJ*) is reacted entirely at *I*.

From Figure B1, taking moments about *E*:

$$
\begin{aligned}
&I_y' L_3 \cos\alpha + A_x'(L_2 \sin\alpha + L_1 \sin\beta_L) + B_y'(L_2 \cos\alpha - L_1 \cos\beta_R) \\
&= B_x'(L_2 \sin\alpha + L_1 \sin\beta_R) + A_y'(L_2 \cos\alpha - L_1 \cos\beta_L).
\end{aligned}
\tag{B16}
$$

The unknown force in this equation (I_y') can be eliminated by considering the free body diagram of Figure B2:

Taking moments about *E* for all of the links shown in the free body diagram gives

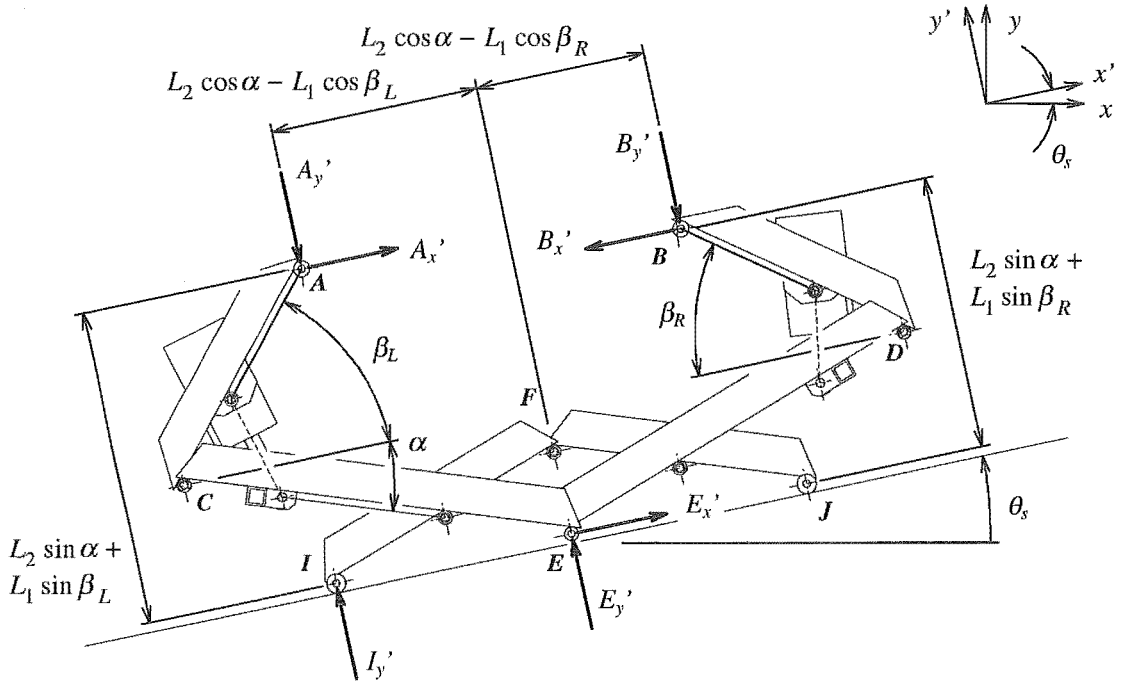

***Figure B1** Suspension Linkage Free Body Diagram*

$$I_y' L_3 \cos\alpha + A_x'(L_2 \sin\alpha + L_1 \sin\beta_L) + H_x' \frac{L_3}{2} \sin\alpha$$
$$= A_y'(L_2 \cos\alpha - L_1 \cos\beta_L) + H_y' \frac{L_3}{2} \cos\alpha. \quad \text{(B17)}$$

Taking moments about *F* for link *FJ* yields

$$H_x' \frac{L_3}{2} \sin\alpha + H_y' \frac{L_3}{2} \cos\alpha = 0. \quad \text{(B18)}$$

Taking moments about *G* for the link chain *IFJ* yields

$$I_y' \frac{L_3}{2} \cos\alpha = H_y' L_3 \cos\alpha. \quad \text{(B19)}$$

Eliminating H_x' and H_y' from B17 using B18 and B19 gives

$$I_y' L_3 \cos\alpha = 2A_y'(L_2 \cos\alpha - L_1 \cos\beta_L) - 2A_x'(L_2 \sin\alpha + L_1 \sin\beta_L). \quad \text{(B20)}$$

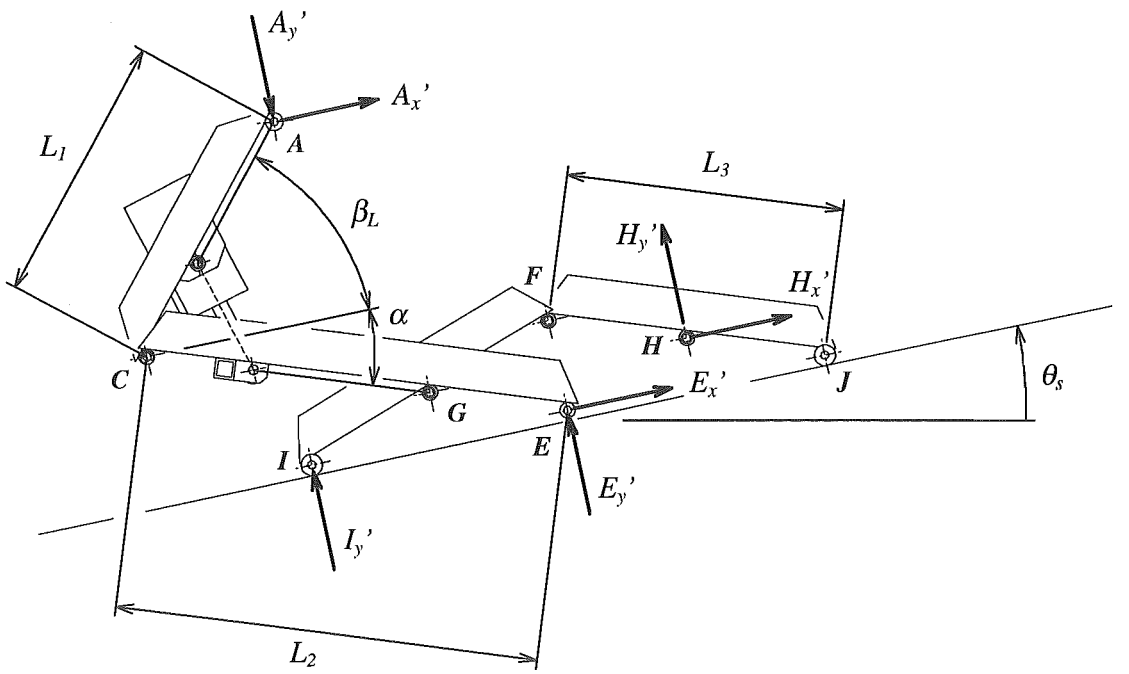

***Figure B2** Free Body Diagram for Left-Hand Side of Linkage*

Solving B16 and B20 simultaneously to eliminate I_y' gives

$$\begin{aligned} &A_x'(L_2\sin\alpha + L_1\sin\beta_L) + B_x'(L_2\sin\alpha + L_1\sin\beta_R) \\ &- A_y'(L_2\cos\alpha - L_1\cos\beta_L) - B_y'(L_2\cos\alpha - L_1\cos\beta_R) = 0. \end{aligned} \tag{B21}$$

This equation can be expressed in terms of the forces of the coordinate system (x,y) by using Equation B15 and the addition formulas (B22,B23) below. This then yields Equation 4.14 of Chapter 4.

$$\begin{aligned} \sin(\beta_L \pm \theta_s) &\equiv \sin\beta_L\cos\theta_s \pm \sin\theta_s\cos\beta_L, \\ \sin(\beta_R \pm \theta_s) &\equiv \sin\beta_R\cos\theta_s \pm \sin\theta_s\cos\beta_R, \\ \sin(\alpha \pm \theta_s) &\equiv \sin\alpha\cos\theta_s \pm \sin\theta_s\cos\alpha. \end{aligned} \tag{B22}$$

$$\begin{aligned} \cos(\beta_L \pm \theta_s) &\equiv \cos\beta_L\cos\theta_s \mp \sin\theta_s\sin\beta_L, \\ \cos(\beta_R \pm \theta_s) &\equiv \cos\beta_R\cos\theta_s \mp \sin\theta_s\sin\beta_R, \\ \cos(\alpha \pm \theta_s) &\equiv \cos\alpha\cos\theta_s \mp \sin\theta_s\sin\alpha. \end{aligned} \tag{B23}$$

B2.2 Force Moment Arms

The moment arms (x_A, x_B, y_A, y_B) of the top frame forces (A_x, B_x, A_y, B_y) shown in Figure 4.3 and used in Equation 4.17 are given by

$$\begin{bmatrix} x_A \\ x_B \\ y_A \\ y_B \end{bmatrix} = \begin{bmatrix} \cos\theta & -\sin\theta & \cos\theta \\ \cos\theta & \sin\theta & -\cos\theta \\ \sin\theta & \cos\theta & \sin\theta \\ -\sin\theta & \cos\theta & \sin\theta \end{bmatrix} \begin{bmatrix} e \\ h \\ e_e \end{bmatrix}. \tag{B24}$$

B2.3 Coupling Of Coordinates

From Figure 4.2a

$$x = x_s - L_2\cos(\alpha - \theta_s) + L_1\cos(\beta_L + \theta_s) + (e + e_e)\cos\theta - h\sin\theta - e_e. \tag{B25}$$

Differentiating this once with respect to time gives velocity in the x direction:

$$\dot{x} = \dot{x}_s + L_2(\dot{\alpha} - \dot{\theta}_s)\sin(\alpha - \theta_s) - L_1(\dot{\beta}_L + \dot{\theta}_s)\sin(\beta_L + \theta_s) - \dot{\theta}((e + e_e)\sin\theta + h\cos\theta),$$

(B26)

where the link angle rates are given by Equation 4.4.

Differentiating again gives acceleration in the x direction:

$$\begin{aligned}\ddot{x} = \ddot{x}_s &+ L_2(\ddot{\alpha} - \ddot{\theta}_s)\sin(\alpha - \theta_s) + L_2(\dot{\alpha} - \dot{\theta}_s)^2\cos(\alpha - \theta_s) \\ &- L_1(\ddot{\beta}_L + \ddot{\theta}_s)\sin(\beta_L + \theta_s) - L_1(\dot{\beta}_L + \dot{\theta}_s)^2\cos(\beta_L + \theta_s) \\ &- \dot{\theta}^2((e + e_e)\cos\theta - h\sin\theta) \\ &- \ddot{\theta}((e + e_e)\sin\theta + h\cos\theta).\end{aligned} \quad \text{(B27)}$$

The accelerations of the link angles ($\ddot{\beta}_L, \ddot{\beta}_R, \ddot{\alpha}$) can be eliminated from this equation by using Equation 4.5 to give Equation 4.18 of Chapter 4 (which is in terms of $\ddot{y}$ and $\ddot{\theta}$).

B2.4 Cylinder Static Pressures

The static cylinder pressures can be found directly from the dynamic equations.

From Equation 4.15, setting $\ddot{x} = 0$:

$$A_{x0} = B_{x0}. \quad \text{(B28)}$$

From 4.16, setting $\ddot{y} = 0$:

$$-A_{y0} - B_{y0} = -(m_{pat} + m_{str})g. \quad \text{(B29)}$$

From 4.17, setting $\ddot{\theta} = 0$:

$$A_{x0}y_{A0} - B_{x0}y_{B0} + A_{y0}x_{A0} - B_{y0}x_{B0} = 0, \quad \text{(B30)}$$

where the moment arms ($x_{A0}, x_{B0}, y_{A0}, y_{B0}$) of the forces ($A_{x0}, B_{x0}, A_{y0}, B_{y0}$) are given by B24 after setting $\theta = 0$. ie.

$$\begin{bmatrix} x_{A0} \\ x_{B0} \\ y_{A0} \\ y_{B0} \end{bmatrix} = \begin{bmatrix} 1 & 0 & 1 \\ 1 & 0 & -1 \\ 0 & 1 & 0 \\ 0 & 1 & 0 \end{bmatrix} \begin{bmatrix} e \\ h \\ e_e \end{bmatrix}. \tag{B31}$$

By eliminating A_{x0} and B_{x0} from Equation B30 using B28, and using the result in Equation B29 (after substituting for the force moment arms of B31), the vertical static forces at the top frame can be expressed as

$$A_{y0} = \frac{(m_{pat} + m_{str})g}{2}\left(\frac{e - e_e}{e}\right), \tag{B32}$$

$$B_{y0} = \frac{(m_{pat} + m_{str})g}{2}\left(\frac{e + e_e}{e}\right). \tag{B33}$$

From Equation 4.14, using $\beta_L = \beta_{L0}$, $\beta_R = \beta_{R0}$, and $\alpha = \alpha_0$, we can write for the load:

$$A_{y0}e + B_{y0}e - A_{x0}(a+b) - B_{x0}(a+b) = 0. \tag{B34}$$

Substituting for A_{y0} and B_{y0} from B32 and B33 respectively gives the horizontal static forces at the top frame as

$$A_{x0} = B_{x0} = \frac{(m_{pat} + m_{str})g}{2}\left(\frac{e}{a+b}\right). \tag{B35}$$

Using B32, B33, and B35 in 4.12 and 4.13 gives the cylinder static forces F_{L0} and F_{R0} as

$$F_{L0} = \frac{\frac{(m_{pat} + m_{str})g}{2}\left(\frac{(e - e_e)(c-e)}{e} + \frac{eb}{a+b}\right)}{r_0}, \tag{B36}$$

$$F_{R0} = \frac{\frac{(m_{pat} + m_{str})g}{2}\left(\frac{(e + e_e)(c-e)}{e} + \frac{eb}{a+b}\right)}{r_0}. \tag{B37}$$

The cylinder static pressures are given in terms of these forces by

$$p_{L0} = \frac{F_{L0}}{A_c} + p_{at}, \tag{B38}$$

$$p_{R0} = \frac{F_{R0}}{A_c} + p_{at}. \tag{B39}$$

B2.5 Equations of Motion

The elements of the matrix $\mathbb{F}$ and column vector $\mathbb{w}$ of Equation 4.19 are given below:

$$\begin{aligned} F_{41} &= L_1 \sin(\beta_L + \theta_s), \\ F_{43} &= L_1 \cos(\beta_L + \theta_s), \\ F_{52} &= L_1 \sin(\beta_R - \theta_s), \\ F_{54} &= L_1 \cos(\beta_R - \theta_s). \end{aligned} \tag{B40}$$

$$\begin{aligned} F_{61} &= +(L_2 \sin(\alpha - \theta_s) + L_1 \sin(\beta_L + \theta_s)), \\ F_{62} &= +(L_2 \sin(\alpha + \theta_s) + L_1 \sin(\beta_R - \theta_s)), \\ F_{63} &= -(L_2 \cos(\alpha - \theta_s) - L_1 \cos(\beta_L + \theta_s)), \\ F_{64} &= -(L_2 \cos(\alpha + \theta_s) - L_1 \cos(\beta_R - \theta_s)). \end{aligned} \tag{B41}$$

$$F_{76} = L_1 \frac{\partial \beta_L}{\partial y} \sin(\beta_L + \theta_s) - L_2 \frac{\partial \alpha}{\partial y} \sin(\alpha - \theta_s). \tag{B42}$$

$$F_{77} = (e + e_e)\sin\theta + h\cos\theta - L_2 \frac{\partial \alpha}{\partial \theta} \sin(\alpha - \theta_s) + L_1 \frac{\partial \beta_L}{\partial \theta} \sin(\beta_L + \theta_s). \tag{B43}$$

$$\begin{aligned} {}^1w_7 = {} & \ddot{x}_s + L_2(\dot{\alpha} - \dot{\theta}_s)^2 \cos(\alpha - \theta_s) - L_1(\dot{\beta}_L + \dot{\theta}_s)^2 \cos(\beta_L + \theta_s) \\ & -\dot{\theta}^2((e + e_e)\cos\theta - h\sin\theta) - \ddot{\theta}_s(L_2 \sin(\alpha - \theta_s) + L_1 \sin(\beta_L + \theta_s)). \end{aligned} \tag{B44}$$

$$
{}^{2}w_{7} = \begin{bmatrix} L_2 \sin(\alpha - \theta_s) & -L_1 \sin(\beta_L + \theta_s) \end{bmatrix}
\begin{bmatrix}
\dfrac{\partial \alpha}{\partial y_s} & \dfrac{\partial \beta_L}{\partial y_s} \\
\dfrac{\partial \alpha}{\partial \theta_s} & \dfrac{\partial \beta_L}{\partial \theta_s} \\
\dfrac{d}{dt}\left(\dfrac{\partial \alpha}{\partial y}\right) & \dfrac{d}{dt}\left(\dfrac{\partial \beta_L}{\partial y}\right) \\
\dfrac{d}{dt}\left(\dfrac{\partial \alpha}{\partial \theta}\right) & \dfrac{d}{dt}\left(\dfrac{\partial \beta_L}{\partial \theta}\right) \\
\dfrac{d}{dt}\left(\dfrac{\partial \alpha}{\partial y_s}\right) & \dfrac{d}{dt}\left(\dfrac{\partial \beta_L}{\partial y_s}\right) \\
\dfrac{d}{dt}\left(\dfrac{\partial \alpha}{\partial \theta_s}\right) & \dfrac{d}{dt}\left(\dfrac{\partial \beta_L}{\partial \theta_s}\right)
\end{bmatrix}^{T}
\begin{bmatrix} \ddot{y}_s \\ \ddot{\theta}_s \\ \dot{y} \\ \dot{\theta} \\ \dot{y}_s \\ \dot{\theta}_s \end{bmatrix}. \qquad \text{(B45)}
$$

APPENDIX C

Natural Frequencies

C1 INTRODUCTION

In this appendix the suspension natural frequencies in bounce and pitch are determined by linearising the equations presented in Chapter 4. Reference is also made to the equations of Appendix B.

In linearising, the following applies:

- $\sin\theta \approx \theta$ and $\cos\theta \approx 1$ for small θ (and similarly for small $\Delta\beta_L, \Delta\beta_R$ and $\Delta\alpha$).
- Products of the small quantities $y, \theta, \Delta\beta_L, \Delta\beta_R$ and $\Delta\alpha$ are ignored.

As only free vibration behaviour is of interest in determining natural frequencies, the ambulance floor is considered to be fixed in space (ie. $y_s = \theta_s = 0$). For simplicity of analysis, the load centre-of-mass is assumed to be centrally located ($e_e = 0$).

C2 KINEMATICS

C2.1 Link Angles

The link angles (β_L, β_R, α) of Figure 4.2a can be written as the sum of the equilibrium angle (denoted by the subscript '0') and the (small) change in angle. ie.

$$\begin{aligned} \beta_L &= \beta_0 + \Delta\beta_L, \\ \beta_R &= \beta_0 + \Delta\beta_R, \\ \alpha &= \alpha_0 + \Delta\alpha. \end{aligned} \tag{C1}$$

Substituting these expressions into Equations 4.1,4.2 and 4.3 gives

$$f + h + y = L_2 \sin(\alpha_0 + \Delta\alpha) + L_1 \sin(\beta_0 + \Delta\beta_L) + e\sin\theta + h\cos\theta, \tag{C2}$$

$$L_1 \sin(\beta_0 + \Delta\beta_L) + 2e\sin\theta = L_1 \sin(\beta_0 + \Delta\beta_R), \tag{C3}$$

$$L_1\cos(\beta_0+\Delta\beta_L)+2e\cos\theta+L_1\cos(\beta_0+\Delta\beta_R)=2L_2\cos(\alpha_0+\Delta\alpha)\,. \qquad \text{(C4)}$$

After using the identities

$$\sin(\beta_0+\Delta\beta_L)\equiv\sin\beta_0\cos\Delta\beta_L+\sin\Delta\beta_L\cos\beta_0\,,$$
$$\sin(\beta_0+\Delta\beta_R)\equiv\sin\beta_0\cos\Delta\beta_R+\sin\Delta\beta_R\cos\beta_0\,,$$
$$\sin(\alpha_0+\Delta\alpha)\equiv\sin\alpha_0\cos\Delta\alpha-\sin\Delta\alpha\cos\alpha_0\,,$$

in Equations C2,C3 and C4, and linearising the results, we can write (with reference to the static geometry of Figure 4.1a)

$$y=c\Delta\alpha+(c-e)\Delta\beta_L+e\theta\,, \qquad \text{(C5)}$$

$$\Delta\beta_R-\Delta\beta_L=\frac{2e\theta}{c-e}\,, \qquad \text{(C6)}$$

$$b\Delta\beta_L+b\Delta\beta_R-2a\Delta\alpha=0\,. \qquad \text{(C7)}$$

Solving C5,C6 and C7 simultaneously yields the change in link angles as a function of y and θ:

$$\Delta\beta_L=\frac{ya}{cb+a(c-e)}-\frac{e\theta}{c-e}\,, \qquad \text{(C8)}$$

$$\Delta\beta_R=\frac{ya}{cb+a(c-e)}+\frac{e\theta}{c-e}\,, \qquad \text{(C9)}$$

$$\Delta\alpha=\frac{yb}{cb+a(c-e)}\,. \qquad \text{(C10)}$$

To the first order of accuracy, pitching can be considered to be a function of the angles of the top links only (β_L,β_R). This is because the change in angle ($\Delta\alpha$) of the lower arms (*CE,DE*) is independent of the angle (θ) of the load (Equation C10).

C2.2 Common Trigonometric Expressions

Expressions in terms of the sine and cosine of the angles β_L,β_R and α occur frequently in the analysis which follows. They can be found by using Equation C1 with Equations C8,C9 and C10, and are written below:

$$L_1 \sin\beta_L = b + \frac{ya(c-e)}{cb + a(c-e)} - e\theta, \tag{C11}$$

$$L_1 \cos\beta_L = (c-e) - \frac{yab}{cb + a(c-e)} + \frac{be\theta}{c-e}, \tag{C12}$$

$$L_1 \sin\beta_R = b + \frac{ya(c-e)}{cb + a(c-e)} + e\theta, \tag{C13}$$

$$L_1 \cos\beta_R = (c-e) - \frac{yab}{cb + a(c-e)} - \frac{be\theta}{c-e}, \tag{C14}$$

$$L_2 \sin\alpha = a + \frac{ybc}{cb + a(c-e)}, \tag{C15}$$

$$L_2 \cos\alpha = c - \frac{yab}{cb + a(c-e)}. \tag{C16}$$

C3 CYLINDER ANALYSIS

C3.1 Cylinder Kinematics

a) Cylinder Extensions

Referring to Figure 4.2b, the instantaneous length of the left-hand cylinder l_L is given by Equation B11 as

$$l_L = \sqrt{l_1^2 + l_2^2 - 2l_1 l_2 \cos(\alpha + \beta_L)}. \tag{B11}$$

After substituting in the trigonometric Equations C11, C12, C15 and C16, this equation becomes

$$l_L = \sqrt{l_0^2 + 2y(a+b)\frac{l_1}{L_1}\frac{l_2}{L_2} - 2e\theta\frac{l_1}{L_1}\frac{l_2}{L_2}\left(\frac{cb + a(c-e)}{c-e}\right)}.$$

Using the binomial expansion and ignoring second-order and higher terms gives

$$l_L = l_0 + \frac{y(a+b)}{l_0}\frac{l_1}{L_1}\frac{l_2}{L_2} - \frac{e\theta}{l_0}\frac{l_1}{L_1}\frac{l_2}{L_2}\left(\frac{cb+a(c-e)}{c-e}\right). \tag{C17}$$

Similarly, the instantaneous right-hand cylinder length l_R is given by

$$l_R = l_0 + \frac{y(a+b)}{l_0}\frac{l_1}{L_1}\frac{l_2}{L_2} + \frac{e\theta}{l_0}\frac{l_1}{L_1}\frac{l_2}{L_2}\left(\frac{cb+a(c-e)}{c-e}\right). \tag{C18}$$

The cylinder elongations are given by Equations 4.6 and 4.8 as

$$\delta_L = l_L - l_0, \tag{4.6}$$

$$\delta_R = l_R - l_0, \tag{4.8}$$

from which we can write (using C17 and C18)

$$\delta_L = \frac{y(a+b)}{l_0}\frac{l_1}{L_1}\frac{l_2}{L_2} - \frac{e\theta}{l_0}\frac{l_1}{L_1}\frac{l_2}{L_2}\left(\frac{cb+a(c-e)}{c-e}\right), \tag{C19}$$

$$\delta_R = \frac{y(a+b)}{l_0}\frac{l_1}{L_1}\frac{l_2}{L_2} + \frac{e\theta}{l_0}\frac{l_1}{L_1}\frac{l_2}{L_2}\left(\frac{cb+a(c-e)}{c-e}\right). \tag{C20}$$

b) Cylinder Moment Arms

The left-hand cylinder moment arm r_L (as shown in Figure 4.2b) is given by Equation 4.7 as

$$\begin{aligned} r_L &= l_1 \sin(\psi_L + \beta_L) \\ &\equiv l_1 \sin\psi_L \cos\beta_L + l_1 \sin\beta_L \cos\psi_L. \end{aligned} \tag{4.7}$$

Using the geometry of Figure 4.2b we can write

$$\sin\psi_L = \frac{l_2 \sin\alpha + l_1 \sin\beta_L}{l_L},$$

$$\cos\psi_L = \frac{l_2 \cos\alpha - l_1 \cos\beta_L}{l_L}.$$

After using C11, C12, C14 and C16 with the above, the left-hand cylinder moment can be expressed as

$$r_L = \frac{\frac{l_1}{L_1}\frac{l_2}{L_2}\left(cb + a(c-e) + \frac{e\theta(ab - c(c-e))}{c-e} + \frac{y(a+b)(c(c-e)-ab)}{cb + a(c-e)}\right)}{l_0 + \delta_L}. \quad \text{(C21)}$$

Similarly, the right-hand cylinder moment arm can be expressed as

$$r_R = \frac{\frac{l_1}{L_1}\frac{l_2}{L_2}\left(cb + a(c-e) - \frac{e\theta(ab - c(c-e))}{c-e} + \frac{y(a+b)(c(c-e)-ab)}{cb + a(c-e)}\right)}{l_0 + \delta_R}. \quad \text{(C22)}$$

C3.2 Cylinder Forces

As the suspension is assumed to be loaded symmetrically ($e_e = 0$), the left- and right-hand cylinder static forces (F_{L0} and F_{R0}) will be the same. They can be determined from Equation B36/37 after substituting for r_0 using Equation A12 to yield

$$F_{L0} = F_{R0} = \frac{(m_{pat} + m_{str})g}{2}\left(\frac{l_0}{f}\right)\left(\frac{L_1}{l_1}\right)\left(\frac{L_2}{l_2}\right). \quad \text{(C23)}$$

C4 DYNAMICS

C4.1 Link Forces

After setting the ambulance floor angle θ_s to zero in Equations 4.12, 4.13 and 4.14, the following equations for the link forces (shown in Figure 4.3) can be written:

For the pitch arms

$$A_x L_1 \sin\beta_L + A_y L_1 \cos\beta_L = F_L r_L, \quad \text{(C24)}$$

$$B_x L_1 \sin\beta_R + B_y L_1 \cos\beta_R = F_R r_R, \quad \text{(C25)}$$

and for the linkage as a whole

$$A_x(L_2\sin\alpha + L_1\sin\beta_L) + B_x(L_2\sin\alpha + L_1\sin\beta_R)$$
$$- A_y(L_2\cos\alpha - L_1\cos\beta_L) - B_y(L_2\cos\alpha - L_1\cos\beta_R) = 0. \quad \text{(C26)}$$

C4.2 Load Equations of Motion

As given by Equations 4.15-4.17, the equations of motion for the load are:

In the x direction

$$A_x - B_x + (m_{pat} + m_{str})\ddot{x} = 0\,. \quad \text{(C27)}$$

In the y direction

$$-A_y - B_y + (m_{pat} + m_{str})\ddot{y} = -(m_{pat} + m_{str})g\,. \quad \text{(C28)}$$

In the θ direction

$$A_x y_A - B_x y_B + A_y x_A - B_y x_B + (I_{pat} + I_{str})\ddot{\theta} = 0\,, \quad \text{(C29)}$$

where the moment arms (x_A, x_B, y_A, y_B) given by Equation B24 can be linearised to give

$$\begin{bmatrix} x_A \\ x_B \\ y_A \\ y_B \end{bmatrix} = \begin{bmatrix} 1 & -\theta \\ 1 & \theta \\ \theta & 1 \\ -\theta & 1 \end{bmatrix} \begin{bmatrix} e \\ h \end{bmatrix}. \quad \text{(C30)}$$

C4.3 Coupling of Coordinates

When the ambulance floor is horizontal ($\theta_s = 0$), Equation B25 gives the horizontal displacement of the centre-of-mass of the load (x) as

$$x = -L_2\cos\alpha + L_1\cos\beta_L + e\cos\theta - h\sin\theta\,, \quad \text{(C31)}$$

which, after using C16 and C12, reduces to

$$x = \frac{be\theta}{c-e} - h\theta, \tag{C32}$$

but Equation A3 gives

$$c = \frac{e(b+h)}{h},$$

so that

$$x = 0, \tag{C33}$$

and

$$\dot{x} = 0, \tag{C34}$$

and

$$\ddot{x} = 0. \tag{C35}$$

C4.4 Natural Frequencies

Equations C24-C29 and Equation C35 can be solved simultaneously to determine expressions for the suspension natural frequencies. The amount of algebra required for this solution process can be reduced markedly by noting that, for the symmetrically loaded case ($e_e = 0$), bounce and pitch are uncoupled. This allows the bounce and pitch natural frequencies to be determined separately, as detailed in the remainder of this appendix.

a) Bounce Natural Frequency

For pure bounce motion the suspension top frame does not rotate. This means that we can set $\theta = 0$ and $\ddot{\theta} = 0$. The system of equations (C24-C29 and C35) is then solved as follows:

Using C35 in C27 yields

$$A_x = B_x. \tag{C36}$$

Using this result along with Equation C30 in C29 gives

$$A_y = B_y . \tag{C37}$$

After using C36, C37 and C11-C16 in C26, we can write

$$A_x = A_y \frac{e}{a+b+y} . \tag{C38}$$

The unknown force A_x can be eliminated from this equation by using C24, which yields

$$A_y = \frac{F_L r_L}{L_1 \cos\beta_L + \dfrac{e}{a+b+y} L_1 \sin\beta_L} . \tag{C39}$$

This expression for the suspension vertical force when substituted into the vertical equation of motion (C28) gives the stretcher acceleration as

$$\ddot{y} = \frac{2F_L}{(m_{pat}+m_{str})} \left(\frac{r_L}{L_1 \cos\beta_L + \dfrac{eL_1 \sin\beta_L}{a+b+y}} \right) - g . \tag{C40}$$

But since

$$\ddot{y} = -\omega_y{}^2 y ,$$

then we can write

$$-\omega_y{}^2 y = \frac{2F_L r_L}{(m_{pat}+m_{str})} \left(\frac{1}{L_1 \cos\beta_L + \dfrac{eL_1 \sin\beta_L}{a+b+y}} \right) - g . \tag{C41}$$

The natural frequency in bounce (Equation 4.21) can be determined directly from this equation. This is done by substituting for F_L (in terms of k_L) using 4.10; for r_L using C21; for $\sin\beta_L$ using C11; and for $\cos\beta_L$ using C12. The resulting expression is then linearised by ignoring the products of small quantities (as detailed in Section C1). Note

that the expressions for F_L and r_L both contain the cylinder elongation δ_L. This is given by Equation C19.

b) Pitch Natural Frequency

As for the bounce analysis we can write, after using C35 in C27,

$$A_x = B_x . \tag{C36}$$

Further, we can deduce that

$$A_x = B_x = \text{constant} . \tag{C42}$$

This is because rotation of the top frame is symmetric about $\theta = 0$ for the centrally loaded case ($e_e = 0$). It would therefore be illogical, for example, for A_x and B_x to increase for positive θ but decrease for negative θ, or vice-versa. The only consistent alternative is that A_x and B_x are equal and constant.

While Equation C42 is not required to solve the system of equations, it does substantially reduce the amount of algebra required.

The constant value of A_x and B_x in Equation C42 is most easily evaluated at $\theta = 0$ by using Equation B35. This gives

$$A_x = B_x = \frac{(m_{pat} + m_{str})g}{2}\left(\frac{e}{a+b}\right). \tag{C43}$$

After setting $\ddot{y} = 0$, the vertical equation of motion (C28) becomes

$$A_y + B_y = (m_{pat} + m_{str})g , \tag{C44}$$

where A_y can be determined by making C24 explicit in A_y and then substituting for A_x using C43 to yield

$$A_y = \frac{F_L r_L - \frac{(m_{pat} + m_{str})g}{2}\left(\frac{e}{a+b}\right)L_1 \sin\beta_L}{L_1 \cos\beta_L} . \tag{C45}$$

The stretcher angular acceleration, as given by Equation C46 below, can be found from the pitch equation of motion (C29) where B_y is given in terms of A_y by C44; A_x and B_x are given by C43; and the moment arms are given by C30.

$$\ddot{\theta} = \frac{(m_{pat} + m_{str})g(e + h\theta) - 2eA_y - e\theta(m_{pat} + m_{str})g\left(\frac{e}{a+b}\right)}{I_{pat} + I_{str}}. \qquad \text{(C46)}$$

Since, for simple harmonic motion,

$$\ddot{\theta} = -\omega_\theta{}^2\theta,$$

then we can write

$$-\omega_\theta{}^2\theta = \frac{(m_{pat} + m_{str})g(e + h\theta) - 2eA_y - e\theta(m_{pat} + m_{str})g\left(\frac{e}{a+b}\right)}{I_{pat} + I_{str}}. \qquad \text{(C47)}$$

From this, the natural frequency equation in pitch (4.22) can be derived. This is done by eliminating A_y by using Equation C45 and then linearising the resulting expression by ignoring the products of small quantities (as described in Section C1). In the equation for A_y (C45), F_L is given by 4.10 (in terms of k_L); r_L is given by C21; $\sin\beta_L$ is given by C11; and $\cos\beta_L$ is given by C12. For each of these four quantities (F_L, r_L, $\sin\beta_L$, $\cos\beta_L$) we can set $y = 0$ to simplify the algebra (only pitch is of interest here). The cylinder elongation δ_L, which appears in the expressions for F_L and r_L, is given by C19.

APPENDIX D

Pneumatic Damping Analysis- Additional Equations

D1 RATES OF CHANGE OF PRESSURE

D1.1 Tank

a) Capillary Restriction

For $p_t \geq p_c$, equating Equations 5.1 and 5.19 gives

$$\dot{p}_t = \frac{-\gamma C_R}{2V_t}(p_t^{\,2} - p_c^{\,2}). \tag{D1}$$

Similarly, for $p_t < p_c$, equating 5.2 and 5.19 gives

$$\dot{p}_t = \frac{-\gamma C_R}{2V_t}\frac{T_t}{T_c}(p_t^{\,2} - p_c^{\,2}). \tag{D2}$$

b) Orifice Restriction

For $p_t \geq p_c$ and $\frac{p_c}{p_t} \geq \left(\frac{2}{\gamma+1}\right)^{\left(\frac{\gamma}{\gamma-1}\right)}$ (subsonic flow), using 5.8 and 5.19,

$$\dot{p}_t = \frac{-\gamma R T_t}{V_t} C_d A_{or} p_t \sqrt{\frac{2\gamma}{(\gamma-1)RT_t}\left(\left(\frac{p_c}{p_t}\right)^{\left(\frac{2}{\gamma}\right)} - \left(\frac{p_c}{p_t}\right)^{\left(\frac{\gamma+1}{\gamma}\right)}\right)}. \tag{D3}$$

For $p_t \geq p_c$ and $\frac{p_c}{p_t} < \left(\frac{2}{\gamma+1}\right)^{\left(\frac{\gamma}{\gamma-1}\right)}$ (choked flow), using 5.9 and 5.19,

$$\dot{p}_t = \frac{-\gamma R T_t}{V_t} C_d A_{or} p_t \sqrt{\frac{\gamma}{R T_t}\left(\frac{2}{\gamma+1}\right)^{\left(\frac{\gamma+1}{\gamma-1}\right)}} . \tag{D4}$$

For $p_t < p_c$ and $\frac{p_t}{p_c} \geq \left(\frac{2}{\gamma+1}\right)^{\left(\frac{\gamma}{\gamma-1}\right)}$ (subsonic flow), using 5.10 and 5.19,

$$\dot{p}_t = \frac{\gamma R T_t}{V_t} C_d A_{or} p_c \sqrt{\frac{2\gamma}{(\gamma-1) R T_c}\left(\left(\frac{p_t}{p_c}\right)^{\left(\frac{2}{\gamma}\right)} - \left(\frac{p_t}{p_c}\right)^{\left(\frac{\gamma+1}{\gamma}\right)}\right)} . \tag{D5}$$

For $p_t < p_c$ and $\frac{p_t}{p_c} < \left(\frac{2}{\gamma+1}\right)^{\left(\frac{\gamma}{\gamma-1}\right)}$ (choked flow), using 5.11 and 5.19,

$$\dot{p}_t = \frac{\gamma R T_t}{V_t} C_d A_{or} p_c \sqrt{\frac{\gamma}{R T_c}\left(\frac{2}{\gamma+1}\right)^{\left(\frac{\gamma+1}{\gamma-1}\right)}} , \tag{D6}$$

where the orifice area is given by

$$A_{or} = \frac{\pi}{4} d_{or}{}^2 ,$$

and the value of the orifice discharge coefficient C_d is 0.82 [97,123].

D1.2 Cylinder

For both the capillary and orifice restrictions, the rate of change of cylinder pressure is found by equating 5.19 and 5.21 to give

$$\dot{p}_c = \frac{-\gamma p_c}{V_c} \dot{V}_c - \frac{V_t}{V_c} \frac{T_c}{T_t} \dot{p}_t . \tag{D7}$$

D2 TEMPERATURES, MASSES AND VOLUMES

D2.1 Tank and Cylinder Temperatures

Using the perfect gas equation,

$$T_t = \frac{p_t V_t}{m_t R}, \tag{D8}$$

$$T_c = \frac{p_c V_c}{m_c R}. \tag{D9}$$

D2.2 Tank and Cylinder Masses

a) Tank Air Mass

The instantaneous mass of air in the tank is given by

$$m_t = m_{t0} - \int \dot{m} dt, \tag{D10}$$

where the initial tank air mass is given by

$$m_{t0} = \frac{p_{t0} V_t}{R T_{t0}}.$$

b) Cylinder Air Mass

Similarly, the instantaneous mass of air in the cylinder is given by

$$m_c = m_{c0} + \int \dot{m} dt, \tag{D11}$$

where the initial cylinder air mass is given by

$$m_{c0} = \frac{p_{c0} V_{c0}}{R T_{c0}}.$$

D2.3 Cylinder Volume

After differentiation of Equation 3.2, the rate of change of cylinder volume is given by

$$\dot{V}_c = A_c \dot{\delta}, \tag{D12}$$

where the rate of change of cylinder displacement can be determined from C19 (or C20) to give

$$\dot{\delta} = \frac{\dot{y}(a+b)}{l_0} \frac{l_1}{L_1} \frac{l_2}{L_2}. \tag{D13}$$

APPENDIX E

Matlab Simulation Files - Pneumatic Damping

This appendix contains the listing for two Matlab® programs - *ambsim.m* and *ambeq.m*. These programs were used to perform the pneumatic damping simulations of Chapters 5 and 6. The programs operate as described below:

> The m-file *ambsim.m* (Appendix E1) defines the ambulance/stretcher system constants, input type, and initial conditions. It then invokes either of Matlab's integrators (*ode23* or *ode45*) to solve the system of differential equations defined in the function *ambeq.m* (Appendix E2). This yields the system states, $[y_u \quad y_s \quad y \quad \dot{y}_u \quad \dot{y}_s \quad \dot{y} \quad p_c \quad p_t \quad m]$, which are substituted back into the differential equations to determine the state derivatives $[\dot{y}_u \quad \dot{y}_s \quad \dot{y} \quad \ddot{y}_u \quad \ddot{y}_s \quad \ddot{y} \quad \dot{p}_c \quad \dot{p}_t \quad \dot{m}]$. Additional post-processing is performed to evaluate vibration spectra and other indicators of suspension behaviour.

Other Matlab files have been written during the course of this research but are not shown here. These include files which were used to:

- Model the dynamics of the suspension in pitch and bounce for any patient offset e_e (Chapter 4).
- Generate a road profile (Chapter 5).
- Process test data (Chapters 7 and 8).

E1 AMBSIM.M (m-file)

```
% Ambsim
% Ambsim simulates vibration of single rear quarter of the
% ambulance with stretcher and suspension fitted. Stretcher
% damping is by (passive or active) capillary or orifice
% restriction.
% Ambsim uses a 1/4 vehicle model defined in 'ambeq.m'.
% The system states (dof) are:
%     dof = yu, ys, y, yud, ysd, yd, pc ,pt
%     where yu = ambulance unsprung mass absolute displacement
%           ys = ambulance sprung mass absolute displacement
%           y = ambulance stretcher absolute displacement
%           yud = unsprung mass absolute velocity
%           ysd = sprung mass absolute velocity
```

```
%            yd = ambulance stretcher absolute velocity
%            pc = cylinder absolute pressure
%            pt = tank absolute pressure
%            m = increase in cylinder air mass from equilibrium
% The derivatives of these states are:
%    dofdot = yud, ysd, yd, yudd, ysdd, ydd, pcd, ptd, md
% Forced (road input) or free vibration can be considered
% by setting the global variable 'input' to either of
% 'road' or 'none'.
%
% Written by R.J. Henderson 11/8/94
%
%*********************************************************************
%*********************************************************************
% Define Constants

% Suspension Linkage Constants
  global a b c d1 d2 e l0
    a = 0.173;
    b = 0.230;
    c = 0.4962;
    d1 = 0.4008;
    d2 = 0.3711;
    e = .2575;
    l0 = sqrt((d1 - d2)^2 + ...          % initial isolator length
      ((c - d2)*a/c + (c - d1)/(c - e)*b)^2);

% Kinematic Constants
  global C_delta                         % Cylinder:Suspension movement ratio
    C_delta = (a + b)/l0*(c - d2)/c*(c - d1)/(c - e);
  global C_1                             % Common collection of kinematic terms
    C_1 = c*b + a*(c - e);

% Gas Constants
  global Cp Cv gamma R pcrit T0 pat av
    Cp = 1.005e3;
    Cv = .718e3;
    gamma = Cp/Cv;
    R = Cp - Cv;
    pcrit = (2/(gamma + 1))^(gamma/(gamma - 1)); % crit p. ratio
    T0 = 293.15;                         % 20 deg. C
    pat = 1e5;
    av = 1.790e-5;                       % absolute visc. of air (Rogers & Mayhew)

% Isolator Constants
  global D L A Vc0 Vt
    D = 63e-3;                           % cylinder diameter
    L = 50e-3;                           % half cylinder stroke
    A = pi/4*D^2;                        % cylinder area
    Vc0 = A*L;                           % static cylinder volume
    Vt = pi/4*(63.5 - 3.25*2)^2*1e-6*0.44;       % tank volume

% Load Constants
  global m_pat m_str p0
    m_pat = 68;                          % patient mass
    m_str = 25;                          % stretcher mass
    p0 = (m_pat + m_str)*9.81/2*...      % isolator static absolute pressure
      l0/(a + b)*c/(c - d2)*(c - e)/(c - d1)/A + pat;
```

```
% Damping Method
   global damping control                % defined just prior to initial conditions
      % damping = 'orifice' or 'laminar' flow damping restriction
      % control = 'passive' or 'switch ' or 'active ' or 'velrel ' damping with above restriction
         % passive - fixed restriction
         % switchable - two state (skyhook controlled) restriction
         % active - continuously variable restriction - skyhook control
         % velrel - continuously variable resriction - skyhook approximation - relative velocity (yd -
           ysd) used to determine md. ie. D(pc) term ignored.

% Active Damping Coefficient
   global Cact
      Cact = 1050;                      % active orifice damping coefficient (Ns/m)

% Capillary Constants
   global dc Lc Lcmin Lcmax CR
      dc = 2.5e-3;                      % capillary inside diameter
      Lc = .1;                          % capillary length (passive)
      Lcmax = 100;                      % max active capillary length
      Lcmin = .1;                       % min active capillary length
      CR = pi*dc^4/(128*av*Lc);         % capillary coefficient

% Orifice Constants
   global Ao0 Ao Aomax Aomin Cd
      Ao0 = pi/4*(4.35e-3)^2;           % passive orifice area
      Ao = Ao0;                         % starting orifice value for ambeq.m non-passive simulations
      Aomax = pi/4*(4.35e-3)^2;         % maximum active damping orifice area
      Aomin = pi/4*(2.18e-3)^2;         % minimum active damping orifice area
      Cd = .7;                          % (Ref: 'The Control of Fluid Power', p53)

% Orifice Flow Coefficients
   global C1o C2o
      C1o = gamma*R*Cd;
      C2o = 2*gamma/(R*(gamma - 1));

% Active Orifice Damping Coefficients (used to find Ao)
   global E1 E2
      E1 = p0*A*C_delta/(R*T0)*Vt/(Vt + Vc0);
      E2 = Vc0/(gamma*p0*A*C_delta);

% Bump/Rebound Springs
   global ymax Lb be kbs
      ymax = L/C_delta;                 % maximum suspension stroke (+/-)
      Fmax = 1e-6*(m_pat + m_str)*9.81; % buffer force at max. compression
      Lb = 0;                           % maximum buffer compression
      be = 1;                           % buffer exponent
      kbs = Fmax/Lb^be;                 % buffer force = kbs*(buffer compression)^be;

% Tank and Cylinder Equilibrium Air Masses
   global mt0 mc0
      mt0 = p0*Vt/(R*T0);               % tank
      mc0 = p0*Vc0/(R*T0);              % cylinder

%*****************************************************************
% Ambulance 1/4 Vehicle Parameters
   global kt ct mu ks cs ms yts
      kt = 392e3;                       % tyre stiffness (N/m)
      ct = 179;                         % tyre damping (Ns/m)
      mu = 67.5;                        % unsprung mass (kg)
```

```
    ks = 58.5e3;                        % suspension stiffness (N/m)
    cs = 2180;                          % suspension damping (Ns/m)
    ms = 512;                           % sprung mass (kg)
    yts = (m_pat + m_str + ms + mu)*9.81/kt;    % tyre static deflection (m)

% Forced or Free Vibration
  global input

% Road Disturbance Parameters
  global z N xf

% Ambulance Speed (m/s)
  global va
    va = 15;

%*********************************************************************
%*********************************************************************
% Simulation Parameters

global integrator trace

damping = 'orifice'         % 'orifice' or 'laminar' flow damping restriction
control = 'switch '         % 'passive' or 'switch ' or 'active ' or 'velrel ' damping with above restriction

post_processing = 'on ';    % determine acceleration psd and rms accelerations

format short e;

file = 'ambeq'
input = 'road'                          % 'road' or 'none'
road_type = 'minor'                     % 'minor' or 'rough'
if input == 'road'
  if road_type == 'minor'
    profile;                            % C=500e-8; z,N and xf defined in profile.m
  elseif road_type == 'rough'
    rprofile;                           % C=785e-8; z,N and xf defined in profiler.m
  end,
end,

ti = 0;
tf = 40;
  yui = 0;                              % unsprung mass displacement
  ysi = 0;                              % sprung mass displacement
  yi = 0;                               % stretcher displacement
  yudi = 0;                             % unsprung mass velocity
  ysdi = 0;                             % sprung mass velocity
  ydi = 0;                              % stretcher velocity
    deltai = (yi - ysi)*C_delta;
    Vci = Vc0 + A*deltai;
    p_i = p0*((Vc0 + Vt)/(Vci + Vt))^gamma;
    pci = p_i;                          % Initial Cylinder Pressure
    pti = p_i;                          % Initial Tank Pressure
    Ti = p_i*(Vci + Vt)/((mt0 + mc0)*R);
    mci = pci*Vci/(R*Ti);
  mi = mci - mc0;                       % increase in cylinder air mass
dof0 = [yui ysi yi yudi ysdi ydi pci pti mi]
tol = 4e-6;
trace = 1;
integrator = '23'
```

```
%*********************************************************************
% Simulation

clc;

clear yu ys y yud ysd yd yudd ysdd ydd Vc Vcd
clear pc pt pcd ptd mt mc m md Tt Tc
clear bump choked contact
clear FF Ao Ao_t
clear C_phi S_phi lf L1_C_B L1_S_B L2_C_A L2_S_A
clear l1_C_B l1_S_B l2_C_A l2_S_A
clear f_psd f_fft ysdd yudd
clear PSDydd PSDysdd PSDyudd PSDy_ys
clear Ydd Ysdd Yudd Y_Ys
clear rmsydd rmsysdd rmsyudd msydd msysdd msyudd
clear Wrms wrms w

global cnt                          % used to trigger display of every tenth 't' in 'ambeq'

cnt = 0;

t = zeros(7e4,1);                   % max 2e5,8e4 or 7e4 on old comp's
o = zeros(7e4,9);                   % max 2e5,8e4 or 7e4 on old comp's

if integrator == '23'
    [t,o] = ode23(file,ti,tf,dof0,tol,trace);
elseif integrator == '45'
    [t,o] = ode45(file,ti,tf,dof0,tol,trace);
end

% Splined Data

Ts = 1/40;                          % ie. up to 40 Hz

Ns = 1/Ts*(tf - ti) + 1;

for i = 1:Ns
    ts(i,1) = ti + (i - 1)*Ts;      % time
end,

yu = interp1(t,o(:,1),ts);
ys = interp1(t,o(:,2),ts);
y = interp1(t,o(:,3),ts);
yud = interp1(t,o(:,4),ts);
ysd = interp1(t,o(:,5),ts);
yd = interp1(t,o(:,6),ts);
pc = interp1(t,o(:,7),ts);
pt = interp1(t,o(:,8),ts);
m = interp1(t,o(:,9),ts);

Ns = size(ts,1);                    % Ns is number of splined data

clear o
t = ts;

clear ts;
```

```
%*****************************************************************
% Disturbance

yg = zeros(size(t));
ygd = zeros(size(t));

if input == 'road'
    for i = 1:Ns;
        [height, velocity] = road(va, t(i));
        yg(i) = height;
        ygd(i) = velocity;
    end,
end,

% Derivatives

yudd = zeros(size(t));
ysdd = zeros(size(t));
ydd = zeros(size(t));
pcd = zeros(size(t));
ptd = zeros(size(t));
md = zeros(size(t));

% Volume and Volume Derivative

Vc = zeros(size(t));
Vcd = zeros(size(t));

% Other Data

CR = zeros(size(t));                % capillary coefficient
Lc = zeros(size(t));                % capillary length
Ao = zeros(size(t));                % orifice area
Fact = zeros(size(t));              % actual damping force
Fdes = zeros(size(t));              % desired (skyhook) damping force
mdapp = zeros(size(t));             % approx. md - used in 'velrel ' control - D(pc) term ignored

% Unsprung Mass Acceleration

contact = zeros(size(t));           % records '1' for contact, '0' for liftoff

for i = 1:Ns
    if yg(i) + yts - yu(i) >= 0,    % tyre in contact
        yudd(i) = (ct*(ygd(i) - yud(i)) - cs*(yud(i) - ysd(i)) +...
                  kt*(yg(i) + yts - yu(i)) - ks*(yu(i) - ys(i)) -...
                  (m_pat + m_str + ms + mu)*9.81)/mu;
        contact(i) = 1;
    end,
    if yg(i) + yts - yu(i) < 0,     % tyre liftoff
        yudd(i) = (- cs*(yud(i) - ysd(i)) - ks*(yu(i) - ys(i)) -...
                  (m_pat + m_str + ms + mu)*9.81)/mu;
        contact(i) = 0;
    end,
end,

% Cylinder Volume and Derivative

Vc = Vc0 + A*(y - ys)*C_delta;
Vcd = A*(yd - ysd)*C_delta;
```

```
% Tank and Cylinder Air Masses

mt = mt0 - m;
mc = mc0 + m;

% Tank and Cylinder Temperatures

Tt = pt*Vt./(mt*R);
Tc = pc.*Vc./(mc*R);

%**********************************************************************
% Pressure Derivatives and Air Mass Flow Rate

if damping == 'laminar'

    for i = 1:Ns
        if control == 'switch '
            if (pt(i) - pc(i))*yd(i) > 0        % md and yd same sign
                Lc(i) = Lcmax;                  % high damping - long tube
            else
                Lc(i) = Lcmin;                  % low damping - short tube
            end,                                % (for yd = 0 or md = 0 set damping low)
            CR(i) = pi*dc^4/(128*av*Lc(i));
        end,
        if control == 'velrel '                 % ignore D(pc) term in md
            mdapp(i) = p0*Vcd(i)/(R*T0);        % approximation to md (ignoring D(pc)).
            Fdes(i) = Cact*C_delta*yd(i);       % skyhook damping force
            if (mdapp(i) ~= 0)                  % Lc infinite, therefore leave at previous value
                Lc(i) = pi*dc^4/(128*av)/(2*A*C_delta*Vt/(Vc0+Vt)*R*T0/p0*mdapp(i)/Fdes(i));
            end,
            if Lc(i) > Lcmax
                Lc(i) = Lcmax;
            elseif Lc(i) < Lcmin
                Lc(i) = Lcmin;
            end,
            CR(i) = pi*dc^4/(128*av*Lc(i));     % capillary coefficient
        end,
        if control == 'active '
            Fdes(i) = Cact*C_delta*yd(i);       % desired (skyhook) damping force
            % md is generated by numerical differentiation of m - it cannot be calculated
            % using D.E. since CR(i) not yet known (md is needed to define it).
            if i == 1
                md(i) = 0;
            elseif i == Ns
                md(i) = (m(i) - m(i-1))/Ts;
            else
                md(i) = ((m(i+1) + m(i))/2 - (m(i-1) + m(i))/2)/Ts;
            end,
            if (md(i) ~= 0)                     % Lc infinite, therefore leave at previous value
                Lc(i) = pi*dc^4/(128*av)/(2*A*C_delta*Vt/(Vc0+Vt)*R*T0/p0*md(i)/Fdes(i));
            end,
            if Lc(i) > Lcmax
                Lc(i) = Lcmax;
            elseif Lc(i) < Lcmin
                Lc(i) = Lcmin;
            end,
            CR(i) = pi*dc^4/(128*av*Lc(i));     % capillary coefficient
        end,
    end,
```

```
    % Tank Pressure Derivative

    for i = 1:Ns
        if pt(i) >= pc(i)
            ptd(i) = -gamma*CR(i)/(2*Vt)*(pt(i)^2 - pc(i)^2);
        elseif pt(i) < pc(i)
            ptd(i) = -gamma*CR(i)/(2*Vt)*(Tt(i)/Tc(i))*(pt(i)^2 - pc(i)^2);
        end,
    end,

    % Cylinder Pressure Derivative

    pcd = -gamma*pc./Vc.*Vcd - Vt./Vc.*Tc./Tt.*ptd;

    % Mass Flow Rate (from tank to cylinder)

    md = -Vt./(gamma*R.*Tt).*ptd;

    % Actual Damping Force

    Fact = 2*A*C_delta*Vt/(Vt+Vc0).*(pt-pc);

elseif damping == 'orifice'

    % Orifice Area

    for i = 1:Ns;
        if control == 'passive'
            Ao(i) = Ao0;
        elseif control == 'switch '
            if sign((pt(i) - pc(i))*yd(i)) > 0  % md and yd same sign
                Ao(i) = Aomin;                  % high damping
            else
                Ao(i) = Aomax;                  % low damping (for yd(i) = 0 or md(i) = 0 set damping low)
            end,
        elseif control == 'active '
            Fdes(i) = Cact*C_delta*yd(i);   % desired (skyhook) damping force
            % md is generated by numerical differentiation of m - it cannot be calculated
            % using D.E. since Ao(i) not yet known (md is needed to define it).
            if i == 1
                md(i) = 0;
            elseif i == Ns
                md(i) = (m(i) - m(i-1))/Ts;
            else
                md(i) = ((m(i+1) + m(i))/2 - (m(i-1) + m(i))/2)/Ts;
            end,
            % Determine Ao
            if md(i) > 0                        % md positive
                if yd(i) <= 0                   % Ao imaginary
                    Ao(i) = Aomax;
                else
                    Ao(i) = md(i)/Cd*sqrt(A*Vt/(Vt+Vc0)*R*T0/p0/(Cact*yd(i)));
                end,
            elseif md(i) < 0                    % md negative
                if yd(i) >= 0                   % Ao imaginary
                    Ao(i) = Aomax;
                else
                    Ao(i) = (-1)*md(i)/Cd*sqrt(A*Vt/(Vt+Vc0)*R*T0/p0*(-1)/(Cact*yd(i)));
                end,
```

```
            end,
            if Ao(i) < Aomin
                Ao(i) = Aomin;
            elseif Ao(i) > Aomax
                Ao(i) = Aomax;
            end,
        end,
    end,                                    % of orifice

    % Tank Pressure Derivative

    choked = zeros(size(t));                % records '1' for choked flow otherwise '0'

    for i = 1:Ns
        if pt(i) >= pc(i)
            if pc(i)/pt(i) < pcrit          % choked flow
                choked(i) = 1;
                ptd(i) = -C1o*Ao(i)*Tt(i)*pt(i)/(Vt*sqrt(Tt(i)))*sqrt...
                    (gamma/R*(2/(gamma + 1))^((gamma + 1)/(gamma - 1)));
            else
                ptd(i) = -C1o*Ao(i)*Tt(i)*pt(i)/(Vt*sqrt(Tt(i)))*sqrt(C2o*...
                    ((pc(i)/pt(i))^(2/gamma) - (pc(i)/pt(i))^((gamma + 1)/gamma)));
            end,
        elseif pt(i) < pc(i)
            if pt(i)/pc(i) < pcrit          % choked flow
                choked(i) = 1;
                ptd(i) = C1o*Ao(i)*Tt(i)*pc(i)/(Vt*sqrt(Tc(i)))*sqrt...
                    (gamma/R*(2/(gamma+1))^((gamma + 1)/(gamma - 1)));
            else
                ptd(i) = C1o*Ao(i)*Tt(i)*pc(i)/(Vt*sqrt(Tc(i)))*sqrt(C2o*...
                    ((pt(i)/pc(i))^(2/gamma) - (pt(i)/pc(i))^((gamma + 1)/gamma)));
            end,
        end,
    end,

    % Cylinder Pressure Derivative

    pcd = - ((Tc./Tt)*Vt./Vc.*ptd + gamma*pc./Vc.*Vcd);

    % Mass Flow Rate (from tank to cylinder)

    md = -Vt./(gamma*R.*Tt).*ptd;

    % Actual Damping Force

    Fact = 2*A*C_delta*Vt/(Vt+Vc0).*(pt-pc);
end,

%*********************************************************************
% Stretcher Suspension Acceleration

lf = l0 + C_delta*(y - ys);

L2_S_A = a + (y - ys)*c*b/(c*b + a*(c - e));
L2_C_A = c - (y - ys)*a*b/(c*b + a*(c - e));
L1_S_B = b + (y - ys)*a*(c - e)/(c*b + a*(c - e));
L1_C_B = c - e - (y - ys)*a*b/(c*b + a*(c - e));

l2_S_A = (c - d2)/c*L2_S_A;
```

```
l2_C_A = (c - d2)/c*L2_C_A;
l1_S_B = (c - d1)/(c - e)*L1_S_B;
l1_C_B = (c - d1)/(c - e)*L1_C_B;

S_phi = (l1_S_B + l2_S_A)./lf;
C_phi = (l2_C_A - l1_C_B)./lf;

ydd = 2*(pc - pat)*A/(m_pat + m_str).*(S_phi.*l1_C_B + C_phi.*l1_S_B)./...
      (L1_C_B + e*L1_S_B./(a + b + y - ys)) - 9.81;

bump = zeros(size(t));                  % records buffer contact force and deflection

for i = 1:Ns,
   yb = Lb - (ymax - (y(i) - ys(i)));   % rebound buffer contact
   if yb >= 0,
      ydd(i) = ydd(i) - kbs*yb^be;
      bump(i) = yb;
   end,
   yb = Lb - (ymax + (y(i) - ys(i)));   % bump buffer contact
   if yb >= 0,
      ydd(i) = ydd(i) + kbs*yb^be;
      bump(i) = yb;
   end,
end,

% Sprung Mass Acceleration

ysdd = (cs*(yud - ysd) + ks*(yu - ys) - (m_pat + m_str)*ydd)/ms;

%**************************************************************************
% Reynolds Number

if damping == 'laminar'
   Re = md.*dc./(pi/4*dc.^2*av);
elseif damping == 'orifice'
   Re = md.*sqrt((4*Ao)/pi)./(Ao*av);
end,

%**************************************************************************
if post_processing == 'on '

   % Acceleration Power Spectral Densities
   %     (Notes on hanning window: 'hanning(Ns)' is default and results in a very
   %     spikey output c.f. 'hannning(Ns/10)' gives very smooth PSD. 'hanning(Ns/4)'
   %     seems to give good compromise. The frequency axis f_psd is generated automatically.
   %     The size of the psd is decided automatically.)

   [PSDydd, f_psd] = psd(ydd, Ns, 1/Ts, hanning(Ns/2));
   PSDysdd = psd(ysdd, Ns, 1/Ts, hanning(Ns/2));
   PSDyudd = psd(yudd, Ns, 1/Ts, hanning(Ns/2));
   PSDy_ys = psd(y - ys, Ns, 1/Ts), hanning(Ns/2));

   % Acceleration Response Spectra

   N_psd = size(PSDydd,1);

   Sydd = sqrt(4*PSDydd/N_psd);
   Sysdd = sqrt(4*PSDysdd/N_psd);
   Syudd = sqrt(4*PSDyudd/N_psd);
```

```
Sy_ys = sqrt(4*PSDy_ys/N_psd);

% RMS Accelerations (use splined values since the number of splined
% values has already been defined (Ns)).

RMSydd = sqrt(sum(ydd.^2)/Ns)
RMSysdd = sqrt(sum(ysdd.^2)/Ns)
RMSyudd = sqrt(sum(yudd.^2)/Ns);
RMSy_ys = sqrt(sum((y - ys).^2)/Ns)

% Acceleration FFT's.
%     (RMS acceleration components as a function of frequency. Note that splined
%     data must be used as FFT requires data to be equally spaced in time. The
%     frequency axis (f_fft) is generated for frequencies up to 1/Ts so that fourier components
%     are symmetrical about f_fft = 1/(2Ts). Nfft is size(Ns).)

Ydd = fft(ydd);
Ysdd = fft(ysdd);
Yudd = fft(yudd);

Y_Ys = fft(y - ys);

Nfft = size(Ydd,1);

for i = 1:Nfft
   f_fft(i,1) = (i - 1)*1/(Ts*(Nfft - 1));
end,

% Mean Square Acceleration and rms Frequency Components
% (the frequency axis for these rms components is f_fft).

msydd = 1/Nfft^2*(Ydd.*conj(Ydd));
rmsydd = sqrt(msydd);

msysdd = 1/Nfft^2*(Ysdd.*conj(Ysdd));
rmsysdd = sqrt(msysdd);

msyudd = 1/Nfft^2*(Yudd.*conj(Yudd));
rmsyudd = sqrt(msyudd);

% Weighted RMS Patient Acceleration Components

for i = 1:Nfft
   w(i,1) = weight(f_fft(i));
end;
wrms = rmsydd.*w;

% Maximum Values

max(abs(ysdd))
max(abs(ydd))
max(abs(y-ys))

end.
```

E2 AMBEQ.M (function)

```
function dofdot = ambeq(t,dof);
% dofdot = ambeq(t,dof) returns derivatives (dofdot) of the system
% states (dof) for ambsim.m.
% The ambulance model is 1/4 vehicle (rear wheel). Stretcher suspension
% damping is by capillary or orifice restriction and can be passive or
% active.
% The system states are stored in the vector (dof):
%     dof = yu, ys, y, yud, ysd, yd, pc, pt, m
%     where yu = ambulance unsprung mass absolute displacement
%           ys = ambulance sprung mass absolute displacement
%           y = stretcher suspension absolute displacement
%           yud = unsprung mass absolute velocity
%           ysd = sprung mass absolute velocity
%           yd = stretcher suspension absolute velocity
%           pc = cylinder pressure (absolute)
%           pt = tank pressure (absolute)
%           m = increase in cylinder air mass
% The derivatives of these states are:
%     dofdot = yud, ysd, yd, yudd, ysdd, ydd, pcd, ptd, md
% The system constants are defined as globally in ambsim.m and
% can be accessed in ambeq.m.
% The road disturbance at time t is given by the function:
%     [yg, ygd] = road(va, t)
%     where yg = road vertical displacement (absolute)
%           ygd = road velocity input to wheel (absolute)
%
% Written by R.J. Henderson 11/8/94
%
%**********************************************************************
%**********************************************************************
% Suspension Linkage Constants
  global a b c d1 d2 e l0

% Kinematic Constants
  global C_delta C_1

% Gas Constants
  global Cp Cv gamma R pcrit T0 pat av

% Isolator Constants
  global D L A Vc0 Vt

% Load Constants
  global m_pat m_str p0

% Damping Method
  global damping control

% Active Damping Coefficient
  global Cact

% Capillary Constants
  global dc Lc Lcmin Lcmax CR

% Orifice Constants
  global Ao0 Ao Aomax Aomin Cd
```

```
% Orifice Flow Coefficients
  global C1o C2o E1 E2

% Bump/Rebound Springs
  global ymax Lb be kbs

% Tank and Cylinder Equilibrium Air Masses
  global mt0 mc0

% Ambulance 1/4 Vehicle Parameters
  global kt ct mu ks cs ms yts

% Forced or Free Vibration
  global input

% Road Disturbance Parameters
  global z N xf

% Ambulance Speed
  global va

%**********************************************************************
%**********************************************************************
% Initialize Derivatives

  dofdot = zeros(1,9);

%**********************************************************************
% Main Program

  yu = dof(1);
  ys = dof(2);
  y = dof(3);
  yud = dof(4);
  ysd = dof(5);
  yd = dof(6);
  pc = dof(7);
  pt = dof(8);
  m = dof(9);

% Road Disturbance Amplitude and Velocity

  if input == 'road'
     [yg, ygd] = road(va, t);
  elseif input == 'none'
     yg = 0;
     ygd = 0;
  end,

% Unsprung Mass Acceleration

  if yg + yts - yu >= 0,                    % tyre in contact
     yudd = (ct*(ygd - yud) - cs*(yud - ysd) +...
             kt*(yg + yts - yu) - ks*(yu - ys) -...
             (m_pat + m_str + ms + mu)*9.81)/mu;
  end,
  if yg + yts - yu < 0,                     % tyre liftoff
     yudd = (- cs*(yud - ysd) - ks*(yu - ys) -...
              (m_pat + m_str + ms + mu)*9.81)/mu;
```

```
    end,

% Cylinder Volume and Derivative

    Vc = Vc0 + A*(y - ys)*C_delta;
    Vcd = A*(yd - ysd)*C_delta;

% Tank and Cylinder Air Masses

    mt = mt0 - m;
    mc = mc0 + m;

% Tank and Cylinder Temperatures

    Tt = pt*Vt/(mt*R);
    Tc = pc*Vc/(mc*R);

%**********************************************************************
% Pressure Derivatives and Air Mass Flow Rate

    if damping == 'laminar'
        if control == 'switch '
            if (pt - pc)*yd > 0          % md and yd same sign
                Lc = Lcmax;              % high damping - long tube
            else
                Lc = Lcmin;              % low damping - short tube
            end,                         % (for yd = 0 or md = 0 set damping low)
        CR = pi*dc^4/(128*av*Lc);
        end,

        if control == 'velrel '          % ignore D(pc) term in md
            mdapp = p0*Vcd/(R*T0);       % approximation to md (ignoring D(pc)).
            Fdes = Cact*C_delta*yd;      % skyhook damping force
            if (mdapp ~= 0)              % Lc infinite, therefore leave at previous value
                Lc = pi*dc^4/(128*av)/(2*A*C_delta*Vt/(Vc0+Vt)*R*T0/p0*mdapp/Fdes);
            end,
            if Lc > Lcmax
                Lc = Lcmax;
            elseif Lc < Lcmin
                Lc = Lcmin;
            end,
            CR = pi*dc^4/(128*av*Lc);    % capillary coefficient
        end,

    % Tank Pressure Derivative

        if pt >= pc
            ptd = -gamma*CR/(2*Vt)*(pt^2 - pc^2);
        elseif pt < pc
            ptd = -gamma*CR/(2*Vt)*(Tt/Tc)*(pt^2 - pc^2);
        end,

    % Cylinder Pressure Derivative

        pcd = -gamma*pc/Vc*Vcd - Vt/Vc*Tc/Tt*ptd;

    % Mass Flow Rate (from tank to cylinder)

        md = -Vt/(gamma*R*Tt)*ptd;
```

```
% Capillary Coefficient for Next Time Step

    if control == 'active '
        Fdes = Cact*C_delta*yd;          % skyhook damping force
    if (md ~= 0)                         % Lc infinite, therefore leave at previous value
        Lc = pi*dc^4/(128*av)/(2*A*C_delta*Vt/(Vc0+Vt)*R*T0/p0*md/Fdes);
    end,
    if Lc > Lcmax
        Lc = Lcmax;
    elseif Lc < Lcmin
        Lc = Lcmin;
    end,
    CR = pi*dc^4/(128*av*Lc);            % capillary coefficient
end,                                     % of laminar/capillary damping

elseif damping == 'orifice'

% Orifice Area

    if control == 'passive'
        Ao = Ao0;
    elseif control == 'switch '
        if sign((pt - pc)*yd) > 0        % md and yd same sign
            Ao = Aomin;                  % high damping
        else
            Ao = Aomax;                  % low damping (for yd = 0 or md = 0 set damping low)
        end,
    end,

% Tank Pressure Derivative

    if pt >= pc
        if pc/pt < pcrit                 % choked flow
            ptd = -C1o*Ao*Tt*pt/(Vt*sqrt(Tt))*sqrt...
                (gamma/R*(2/(gamma + 1))^((gamma + 1)/(gamma - 1)));
        else
            ptd = -C1o*Ao*Tt*pt/(Vt*sqrt(Tt))*sqrt(C2o*...
                ((pc/pt)^(2/gamma) - (pc/pt)^((gamma + 1)/gamma)));
        end,
    elseif pt < pc
        if pt/pc < pcrit                 % choked Flow
            ptd = C1o*Ao*Tt*pc/(Vt*sqrt(Tc))*sqrt...
                (gamma/R*(2/(gamma+1))^((gamma + 1)/(gamma - 1)));
        else
            ptd = C1o*Ao*Tt*pc/(Vt*sqrt(Tc))*sqrt(C2o*...
                ((pt/pc)^(2/gamma) - (pt/pc)^((gamma + 1)/gamma)));
        end,
    end,

% Cylinder Pressure Derivative

    pcd = - ((Tc/Tt)*Vt/Vc*ptd + gamma*pc/Vc*Vcd);

% Mass Flow Rate (from tank to cylinder)

    md = -Vt/(gamma*R*Tt)*ptd;

% Set Orifice Area Ao For Next Iteration (if damping 'active ')
% (if md = 0 then leave Ao at previous value)
```

```
        if control == 'active '
            if md > 0                       % md positive
                if yd <= 0                  % Ao imaginary
                    Ao = Aomax;
                else
                    Ao = md/Cd*sqrt(A*Vt/(Vt+Vc0)*R*T0/p0/(Cact*yd));
                end,
            elseif md < 0                   % md negative
                if yd >= 0                  % Ao imaginary
                    Ao = Aomax;
                else
                    Ao = (-1)*md/Cd*sqrt(A*Vt/(Vt+Vc0)*R*T0/p0*(-1)/(Cact*yd));
                end,
            end,
            if Ao < Aomin
                Ao = Aomin;
            elseif Ao > Aomax
                Ao = Aomax;
            end,
        end,
    end,                                    %  of orifice damping

%*********************************************************************
%  Stretcher Suspension Acceleration

    lf = l0 + C_delta*(y - ys);

    L2_S_A = a + (y - ys)*c*b/(c*b + a*(c - e));
    L2_C_A = c - (y - ys)*a*b/(c*b + a*(c - e));
    L1_S_B = b + (y - ys)*a*(c - e)/(c*b + a*(c - e));
    L1_C_B = c - e - (y - ys)*a*b/(c*b + a*(c - e));

    l2_S_A = (c - d2)/c*L2_S_A;
    l2_C_A = (c - d2)/c*L2_C_A;
    l1_S_B = (c - d1)/(c - e)*L1_S_B;
    l1_C_B = (c - d1)/(c - e)*L1_C_B;

    S_phi = (l1_S_B + l2_S_A)/lf;
    C_phi = (l2_C_A - l1_C_B)/lf;

    ydd = 2*(pc - pat)*A/(m_pat + m_str)*(S_phi*l1_C_B + C_phi*l1_S_B)/...
          (L1_C_B + e*L1_S_B/(a + b + y - ys)) - 9.81;

%  Rebound Buffer Contact

    yb = Lb - (ymax - (y - ys));
    if yb >= 0,
        ydd = ydd - kbs*yb^be;
    end,

%  Bump Buffer Contact

    yb = Lb - (ymax + (y - ys));
    if yb >= 0,
        ydd = ydd + kbs*yb^be;
    end,

%  Sprung Mass Acceleration
```

```
    ysdd = (cs*(yud - ysd) + ks*(yu - ys) - (m_pat + m_str)*ydd)/ms;

%*********************************************************************
%  State Derivatives

    dofdot(1) = yud;
    dofdot(2) = ysd;
    dofdot(3) = yd;
    dofdot(4) = yudd;
    dofdot(5) = ysdd;
    dofdot(6) = ydd;
    dofdot(7) = pcd;
    dofdot(8) = ptd;
    dofdot(9) = md;

%*********************************************************************
%*********************************************************************
%  Display Simulation Progress for 'Ambsim'

    global integrator trace

    global cnt

    cnt = cnt + 1;

    if trace == 1 & rem((cnt - 50),50) == 0
        home
        t
    end.
```

APPENDIX F

Laboratory Test Results

***Table F1** Suspension Acceleration Transmissibilities in Bounce for Test Series 'A' (0.50g)*

Shaker Table Input		***Suspension Acceleration Transmissibilities in Bounce***						
Shaker Table Input No.	*Shaker Table Freq. (Hz)*	***34 kg** Patient 3.5 mm Orifice*	***68 kg** Patient 3.5 mm Orifice*	***102 kg** Patient 3.5 mm Orifice*	*68 kg Patient **No** Orifice*	*68 kg Patient **3.5 mm** Orifice*	*68 kg Patient **2.0 mm** Orifice*	*68 kg Patient **1.0 mm** Orifice*
A1	1.11	-	-	-	-	-	-	-
A2	1.39	0.28	0.27	0.24	0.17	0.27	0.52	-
A3	1.72	0.23	0.17	0.20	0.13	0.17	0.36	0.92
A4	2.15	0.15	0.15	0.16	0.14	0.15	0.28	0.58
A5	2.63	0.16	0.17	0.17	0.16	0.17	0.26	0.43
A6	3.22	0.19	0.18	0.17	0.18	0.18	0.23	0.37
A7	3.94	0.15	0.14	0.11	0.13	0.14	0.16	0.22
A8	4.98	0.10	0.10	0.08	0.09	0.10	0.11	0.17
A9	5.96	0.09	0.08	0.08	0.10	0.08	0.10	0.13

Table F2 Suspension Acceleration Transmissibilities in Bounce for Test Series 'B' (0.052g)

Shaker Table Input		***Suspension Acceleration Transmissibilities in Bounce***						
Shaker Table Input No.	*Shaker Table Freq. (Hz)*	***34 kg** Patient 3.5 mm Orifice*	***68 kg** Patient 3.5 mm Orifice*	***102 kg** Patient 3.5 mm Orifice*	*68 kg Patient **No** Orifice*	*68 kg Patient **3.5 mm** Orifice*	*68 kg Patient **2.0 mm** Orifice*	*68 kg Patient **1.0 mm** Orifice*
B1	0.36	1.29	1.34	1.25	1.42	1.34	1.05	1.00
B2	0.45	1.50	1.42	1.47	1.63	1.42	1.25	1.09
B3	0.55	1.05	1.16	1.17	1.14	1.16	1.10	1.07
B4	0.69	1.05	1.10	1.00	1.03	1.10	1.07	1.07
B5	0.85	1.05	1.01	1.01	1.01	1.01	1.03	1.13
B6	1.04	1.04	1.00	0.94	0.97	1.00	1.07	1.14
B7	1.27	0.94	0.87	0.93	0.92	0.87	0.94	1.08
B8	1.61	0.79	0.67	0.63	0.63	0.67	0.70	0.98
B9	1.92	0.77	0.68	0.66	0.70	0.68	0.69	0.91

Table F3 Suspension Acceleration Transmissibilities in Bounce for Test Series 'C' (0.036g)

Shaker Table Input		***Suspension Acceleration Transmissibilities in Bounce***						
Shaker Table Input No.	*Shaker Table Freq. (Hz)*	***34 kg** Patient 3.5 mm Orifice*	***68 kg** Patient 3.5 mm Orifice*	***102 kg** Patient 3.5 mm Orifice*	*68 kg Patient **No** Orifice*	*68 kg Patient **3.5 mm** Orifice*	*68 kg Patient **2.0 mm** Orifice*	*68 kg Patient **1.0 mm** Orifice*
C1	0.30	1.01	0.98	0.78	0.97	0.98	0.93	0.86
C2	0.37	0.98	1.00	1.10	0.97	1.00	0.96	0.97
C3	0.46	0.98	0.97	1.05	0.97	0.97	0.98	1.00
C4	0.58	1.01	0.96	0.96	1.03	0.96	0.96	0.99
C5	0.70	1.00	1.00	1.07	1.00	1.00	1.03	1.04
C6	0.86	1.06	1.11	1.04	1.11	1.11	1.09	1.09
C7	1.06	1.03	1.12	1.03	0.96	1.12	1.03	1.09
C8	1.34	1.05	0.88	0.91	0.92	0.88	0.97	1.08
C9	1.60	1.05	1.01	0.98	1.02	1.01	1.00	1.15

Table F4 *Suspension Acceleration Transmissibilities in Pitch for Test Series 'D' (3.28 rad/s^2) with Patient Mass of 68 kg*

Shaker Table Input		***Suspension Acceleration Transmissibilities in Pitch***				
Shaker Table Input No.	*Shaker Table Freq. (Hz)*	***No Orifice***	***3.5 mm Orifice***	***3.0 mm Orifice***	***2.0 mm Orifice***	***1.0 mm Orifice***
D1	0.59	1.38	1.32	1.30	1.11	1.04
D2	0.73	0.87	0.89	0.88	0.99	1.11
D3	0.91	0.55	0.57	0.59	0.78	1.21
D4	1.14	0.50	0.51	0.50	0.62	1.24
D5	1.39	0.43	0.47	0.47	0.55	1.12
D6	1.70	0.63	0.59	0.65	0.69	0.95
D7	2.09	0.51	0.50	0.56	0.59	0.72
D8	2.64	0.43	0.47	0.43	0.50	0.57
D9	3.15	-	-	-	-	-

Table F5 *Suspension Acceleration Transmissibilities in Pitch for Test Series 'E' (1.87 rad/s^2) with Patient Mass of 68 kg*

Shaker Table Input		***Suspension Acceleration Transmissibilities in Pitch***				
Shaker Table Input No.	*Shaker Table Freq. (Hz)*	***No Orifice***	***3.5 mm Orifice***	***3.0 mm Orifice***	***2.0 mm Orifice***	***1.0 mm Orifice***
E1	0.45	0.97	1.02	0.96	0.98	0.98
E2	0.55	1.08	1.08	1.08	1.07	1.05
E3	0.69	1.16	1.13	1.14	1.10	1.10
E4	0.86	0.93	0.97	0.95	1.04	1.17
E5	1.05	0.79	0.83	0.84	0.90	1.24
E6	1.29	0.75	0.78	0.73	0.88	1.25
E7	1.58	0.80	0.84	0.82	0.86	1.15
E8	1.99	0.57	0.60	0.58	0.63	0.91
E9	2.38	0.61	0.61	0.61	0.70	0.83

APPENDIX G

Manufacturing Drawings

This appendix contains four sets of manufacturing drawings:

Drawing Numbers	*Item*	*Pages*
S1-12	Suspension	219-241.
B1-5	Rubber Bellows Brackets	243-251.
ST1A-14	Shaker Table	253-281.
CMF1-4	Modifications to Cam Followers	283-289.

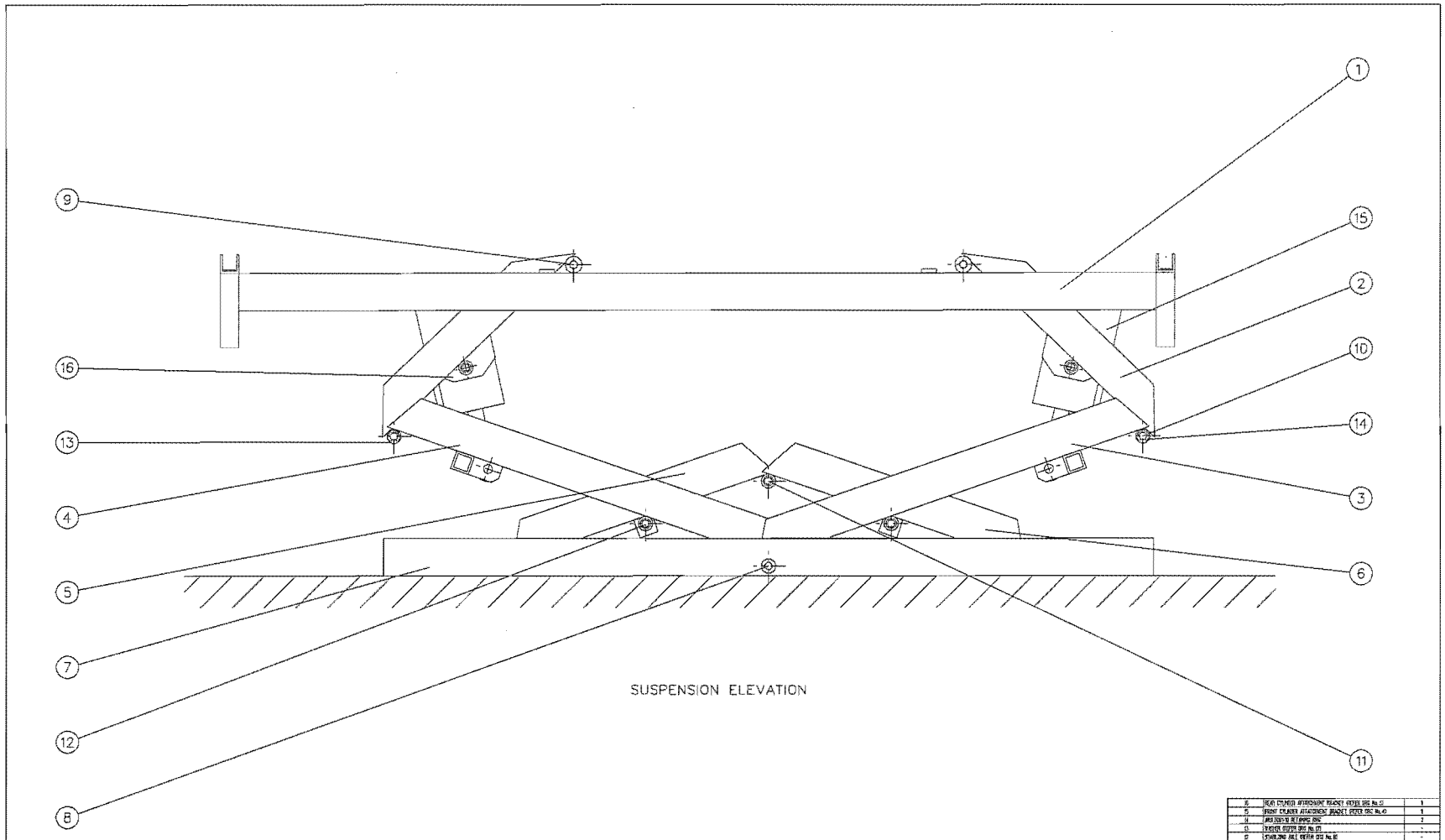

SUSPENSION ELEVATION

ITEM	DESCRIPTION	QUANTITY
16	REAR CYLINDER ATTACHMENT BRACKET WELDED DRG No. 12	1
15	FRONT CYLINDER ATTACHMENT BRACKET WELDED DRG No. 10	1
14	ARM BOSS No. 2 WELDMENT DRG	2
13	WELDED SUSPENSION DRG No. 17	-
12	STABILIZING AXLE WELDED DRG No. 16	-
11	CENTRAL STABILIZING AXLE WELDED DRG No. 15	-
10	PITCH ARM AXLE WELDED DRG No. 19	-
9	TOP FRAME AXLE WELDED DRG No. 18	-
8	BASE FRAME AXLE WELDED DRG No. 17	-
7	BASE FRAME WELDED DRG No. 14	1
6	FRONT STABILIZER ARM WELDED DRG No. 13	1
5	REAR STABILIZER ARM WELDED DRG No. 11	1
4	REAR LOWER ARM WELDED DRG No. 9	1
3	FRONT LOWER ARM WELDED DRG No. 8	1
2	PITCH ARM WELDED DRG No. 7	2
1	TOP FRAME WELDED DRG No. 2	1

MACHINED FINISH 1.6 UNLESS OTHERWISE STATED

GENERAL TOLERANCES

MACHINING		FABRICATION	
0-25	±0.25	0-300	±1.0
25-300	±0.40	300-900	±2.0
300-600	±1.50	900-1500	±2.5

ALL DIMENSIONS IN mm

AMBULANCE STRETCHER
SUSPENSION ELEVATION

SCALES : 2:5

SCHOOL OF ENGINEERING
MECHANICAL ENGINEERING DEPARTMENT

DRN : R.J. HENDERSON
CHKD :
DATE : AUG 1993
DRG No : S-1

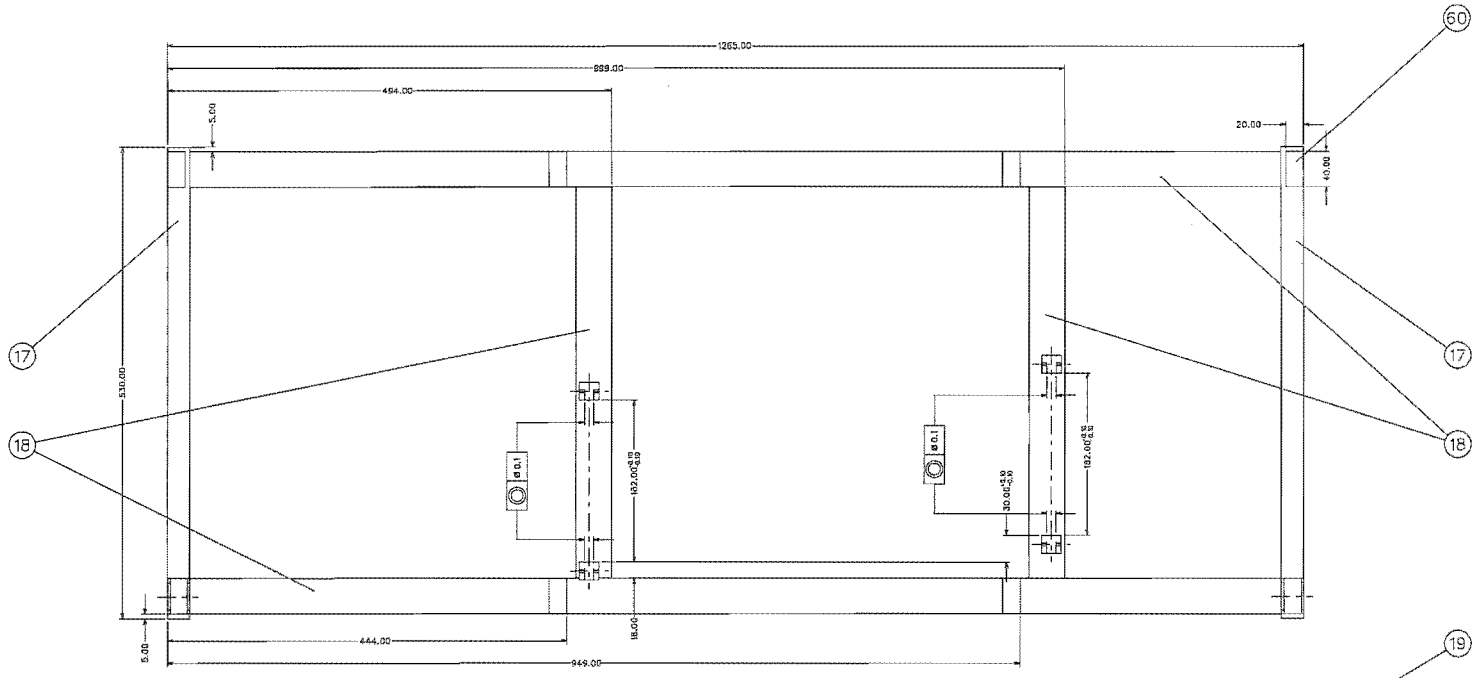

TOP FRAME PLAN

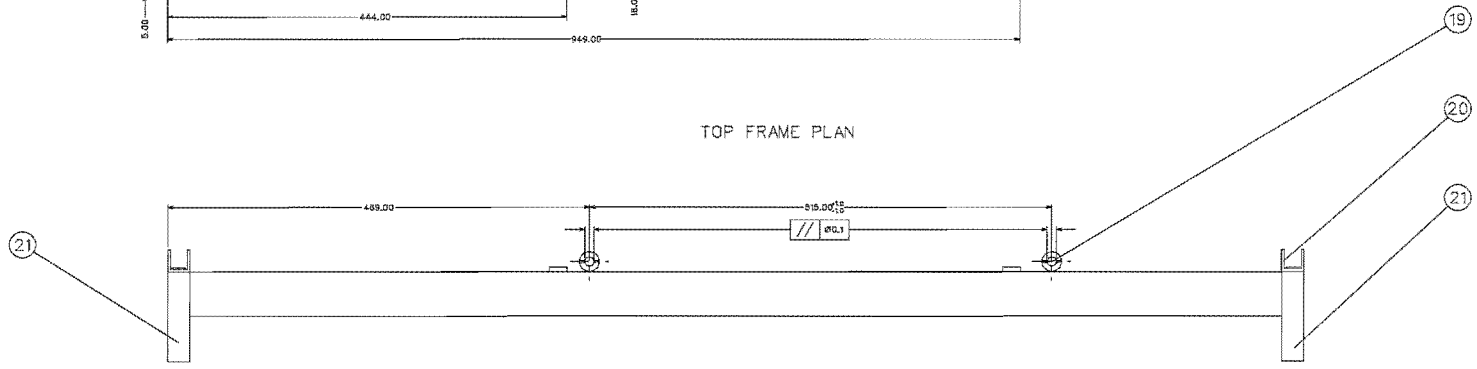

TOP FRAME ELEVATION

NOTE: 1) WELD AS REQUIRED

NOTE: 2) ITEMS (2) ARE TO ACT AS A PRESSURE VESSEL AND MUST BE AIR-TIGHT.

ITEM	DESCRIPTION	QUANTITY
60	40X3 FLAT ALUMINIUM BAR L850±5	-
21	TOP FRAME WELDMENT (SEE DXF SKETCH DRG No. 21)	-
20	STRETCHER LOCATION LUG (REFER DRG No. 20)	-
19	TOP FRAME AXLE ROTATING SLEEVE (REFER DRG No. 19)	-
18	40X3 TH RECTANGULAR ALUMINIUM TUBE 1224±0.25	-
17	40X3 TH RECTANGULAR ALUMINIUM TUBE 1850±0.25	-

MACHINED FINISH 1.6 UNLESS OTHERWISE STATED

GENERAL TOLERANCES			
MACHINING		FABRICATION	
0-75	±0.25	0-300	±1.5
75-300	±0.40	300-900	±2.0
300-900	±0.50	900-2.00	±2.5

ALL DIMENSIONS IN mm

AMBULANCE STRETCHER SUSPENSION
TOP FRAME

SCALE'S : 2:5

SCHOOL OF ENGINEERING
MECHANICAL ENGINEERING DEPARTMENT

DRAWN : R.J. HENDERSON
CHKD :
DATE : AUG. 1993
DRG No : S-2

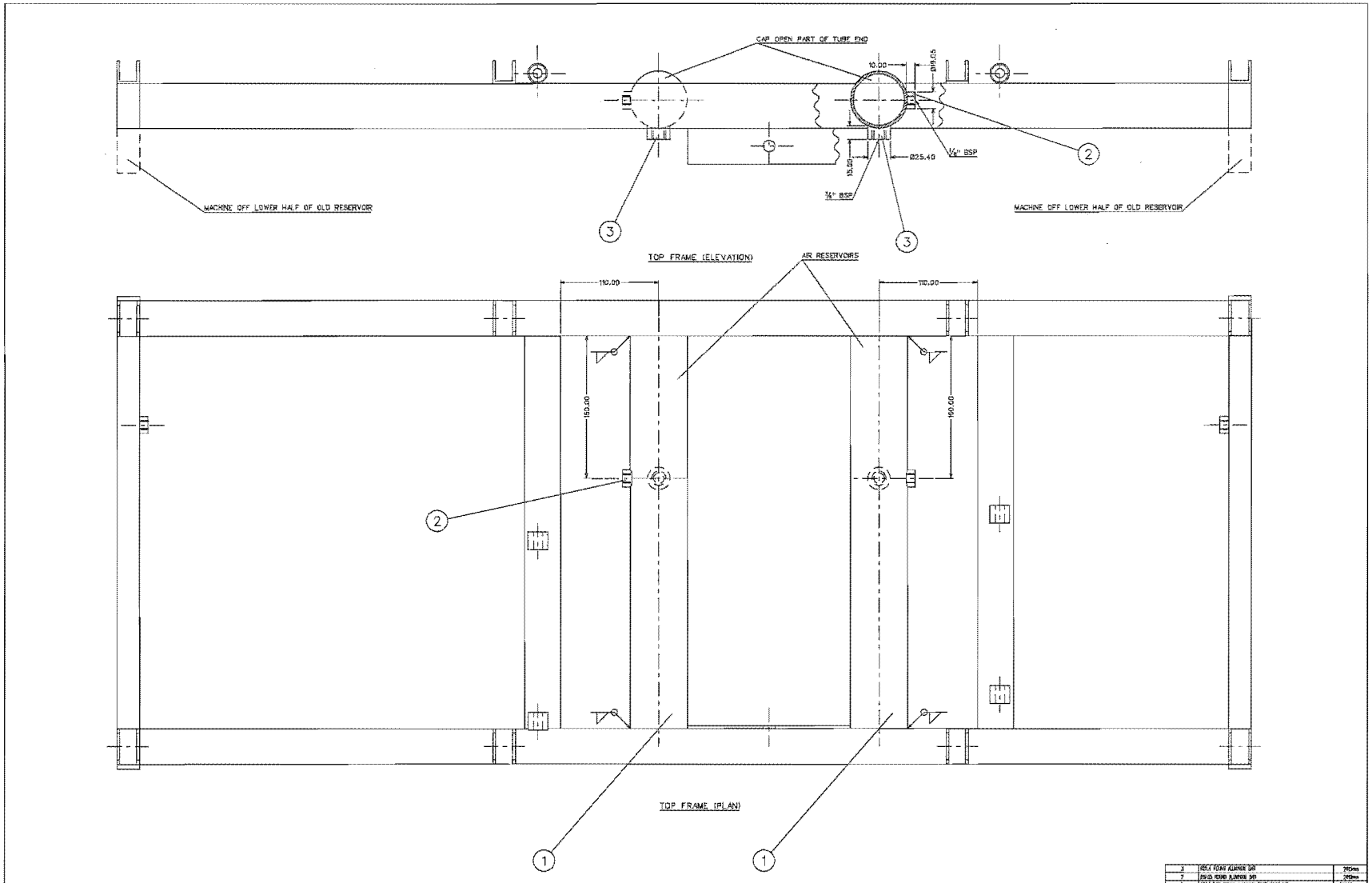

ITEM	DESCRIPTION	QUANTITY
3	40x5 FLAT ALUMINIUM BAR	295mm
2	19x3 ROUND ALUMINIUM BAR	295mm
1	40.5x3.25 NOMINAL ALUMINIUM TUBE 3663 T6	2944mm

MACHINED FINISH 1.6 UNLESS OTHERWISE STATED

GENERAL TOLERANCES			
MACHINING		FABRICATION	
0-75	±0.25	0-300	±1.5
75-300	±0.40	300-800	±2.0
300-600	±0.60	800-1200	±2.5

ALL DIMENSIONS IN mm

AMBULANCE STRETCHER SUSPENSION
TOP FRAME RESERVOIRS

SCALE : DO NOT SCALE

SCHOOL OF ENGINEERING
MECHANICAL ENGINEERING DEPARTMENT

DRN : R.J. HENDERSON
CHKD :
DATE : MAY 1995
DRG No : S-3

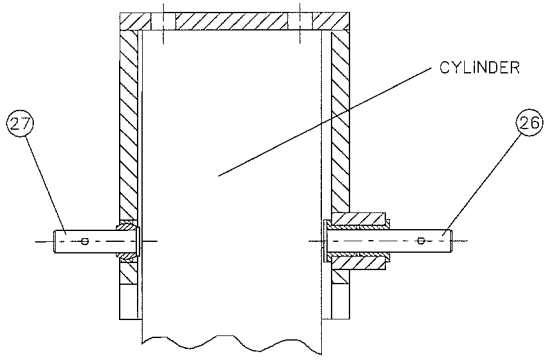

SECTION A-A SHOWING AXLE AND CYLINDER POSITION

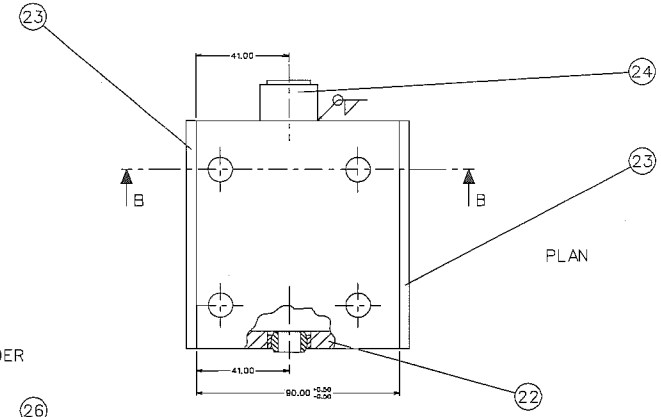

PLAN

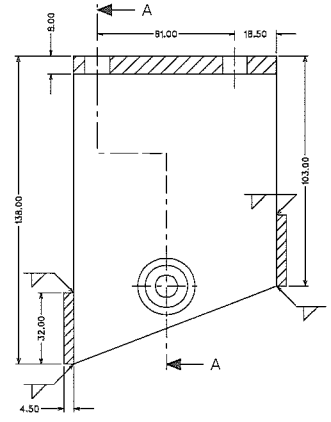

SECTION B-B

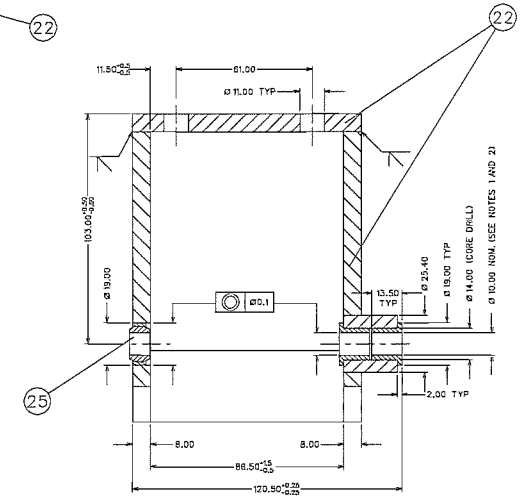

SECTION A-A

(15) FRONT CYLINDER ATTATCHMENT BRACKET

ITEM	DESCRIPTION	QUANTITY
27	CYLINDER BRACKET AXLE MOUNT BRG No.19	-
26	CYLINDER BRACKET AXLE MOUNT BRG No.19	-
25	SPHERICAL PLAIN BEARING DAE 12 10 D	1
24	RIVLOK 4065 T6 ALUMINIUM RIV	-
23	4065 T6 FLAT ALUMINIUM BAR (30×3)	-
22	8.0mm ALUMINIUM PLATE	-

NOTE: 1) M/C BUSHES FROM NYLATRON GSM BAR OR REDUCE FLANGE DIAMETER OF EX. STOCK ITEM "X-LUBE" S45BN.

2) BOND BUSHES INTO SLEEVE AND REAM TO GIVE 0.05 mm CLEARANCE WITH AXLE

MACHINED FINISH 1.6 UNLESS OTHERWISE STATED

GENERAL TOLERANCES			
MACHINING		FABRICATION	
0-75	±0.25	0-300	±1.0
75-300	±0.40	300-900	±2.0
300-600	±0.50	900-1800	±2.5
ALL DIMENSIONS IN mm			

AMBULANCE STRETCHER SUSPENSION
FRONT CYLINDER BRACKET

SCALE : FULL SIZE

SCHOOL OF ENGINEERING
MECHANICAL ENGINEERING DEPARTMENT

DRN : R.J. HENDERSON
CHKD :
DATE : AUG 1993
DRG No : S-4

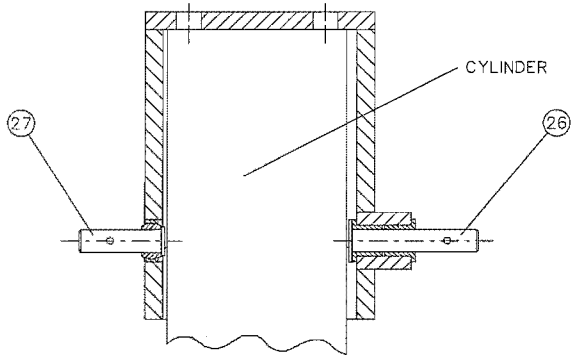

SECTION A-A SHOWING AXLE AND CYLINDER POSITION

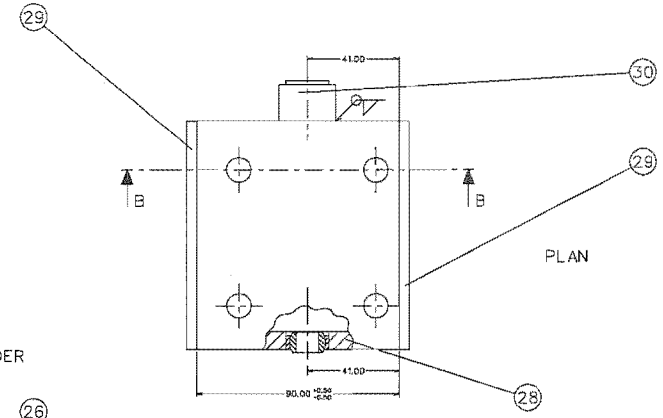

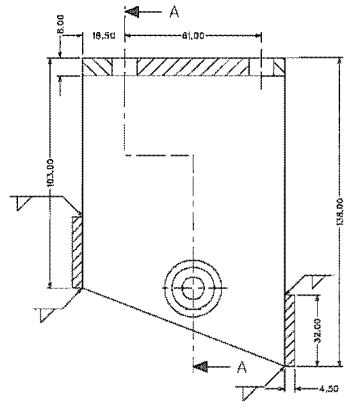

SECTION B-B

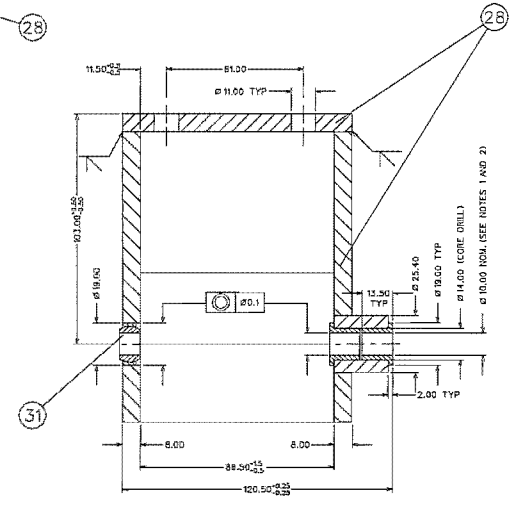

SECTION A-A

(16) REAR CYLINDER ATTATCHMENT BRACKET

ITEM	DESCRIPTION	QUANTITY
31	SPHERICAL PLAIN BEARING SKF GE 10 C	1
30	M12x40 ROD TO ALUMINIUM BAR	-
29	M10x1.75 ELM ALUMINIUM 6061 T6511	-
28	10mm ALUMINIUM PLATE	-
27	CYLINDER BRACKET AXLE WELDED SPC No.27	-
26	CYLINDER BRACKET AXLE WELDED SPC No.26	-

NOTE: 1) M/C BUSHES FROM NYLATRON GSM BAR OR REDUCE FLANGE DIAMETER OF EX. STOCK ITEM "X-LUBE" S458M.

2) BOND BUSHES INTO SLEEVE AND REAM TO GIVE 0.05 mm CLEARANCE WITH AXLE

MACHINED FINISH 1.6 UNLESS OTHERWISE STATED

GENERAL TOLERANCES

MACHINING		FABRICATION	
0-75	±0.25	0-300	±1.5
75-300	±0.40	300-900	±2.5
300-600	±0.55	900-1800	±3.5

ALL DIMENSIONS IN mm

AMBULANCE STRETCHER SUSPENSION
REAR CYLINDER BRACKET

SCALES : FULL SIZE

SCHOOL OF ENGINEERING
MECHANICAL ENGINEERING DEPARTMENT

DRN : R.J. HENDERSON
CHKD :
DATE : AUG. 1993
DRG No : S-5

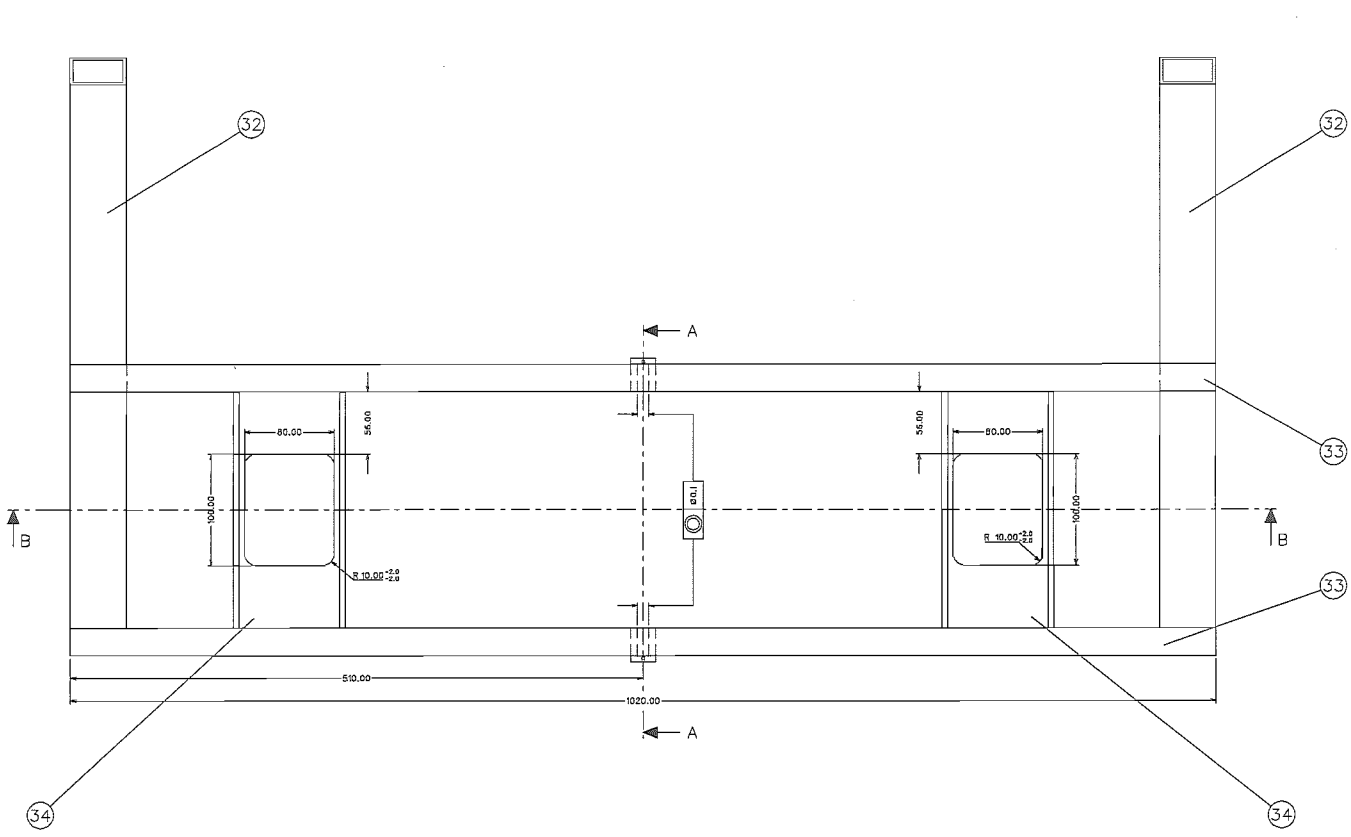

BASE FRAME PLAN

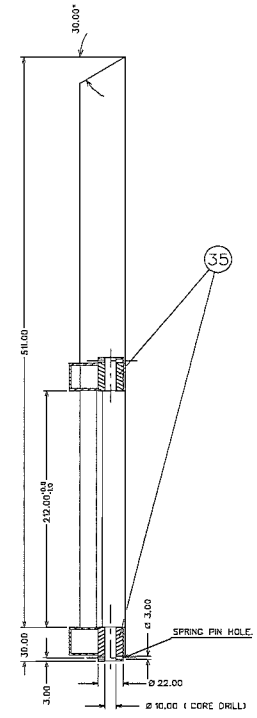

SECTION A-A

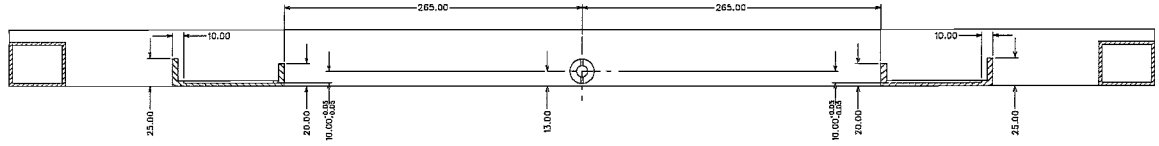

SECTION B-B

NOTE: 1) WELD AS REQUIRED

ITEM	DESCRIPTION	QUANTITY
32	SQ.S TS RECTANGULAR ALUMINIUM TUBE 50×40×2.0	-
33	SQ.S TS RECTANGULAR ALUMINIUM TUBE 60×30×2.0	-
34	M/C FROM SQ.S TS ALUMINIUM CHANNEL 100×40×5.0	-
35	AXLE RETAINING SLEEVE 40SQ.TS ALUMINIUM BAR	2

MACHINED FINISH 1.6 UNLESS OTHERWISE STATED

GENERAL TOLERANCES			
MACHINING		FABRICATION	
0-75	±0.25	0-300	±1.5
75-200	±0.40	300-982	±2.0
200-400	±0.50	600-1200	±2.5

ALL DIMENSIONS IN mm

AMBULANCE STRETCHER SUSPENSION
BASE FRAME

SCALE: 1:2

SCHOOL OF ENGINEERING
MECHANICAL ENGINEERING DEPARTMENT

DRN: R.J. HENDERSON
CHKD:
DATE: AUG. 1993
DRG No: S-6

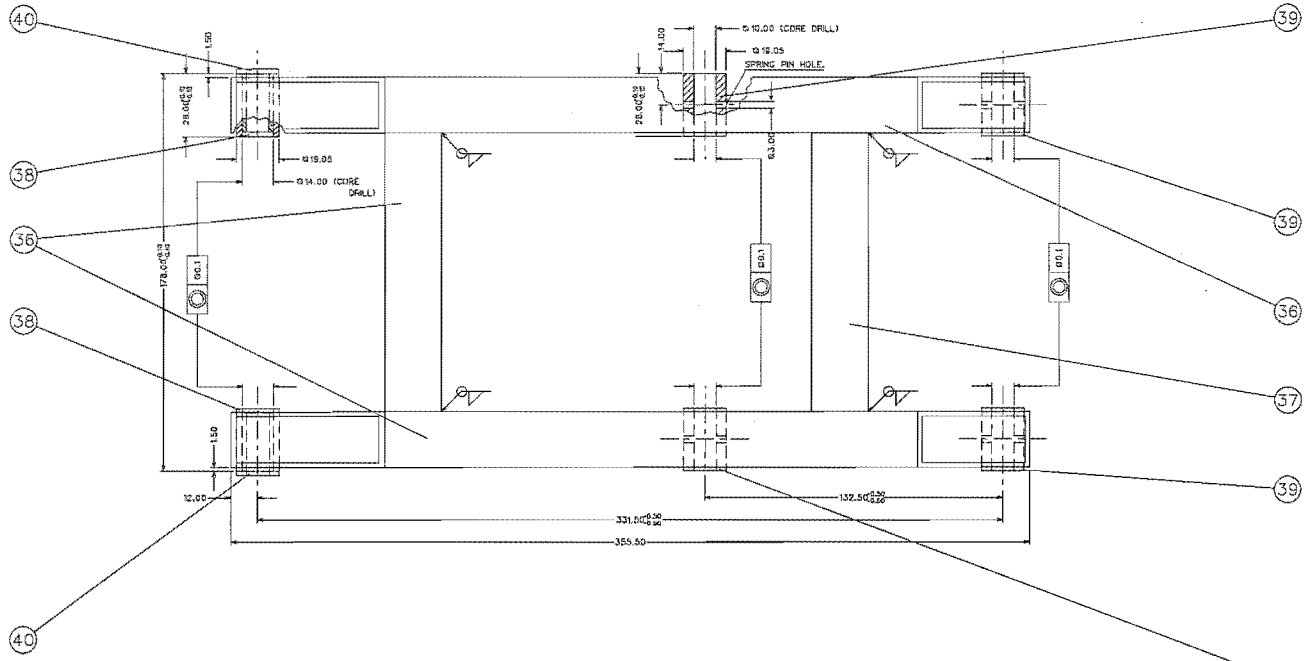

PITCH ARM PLAN

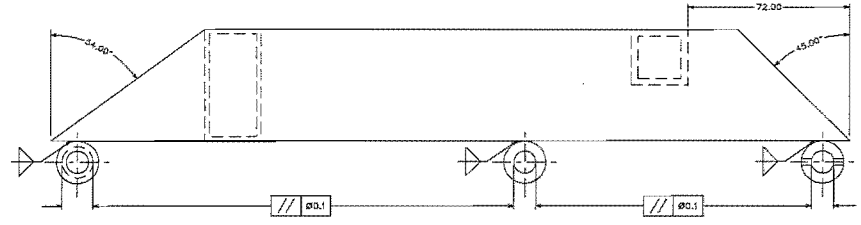

PITCH ARM ELEVATION

NOTE: 1) BUSH FLANGE THICKNESS MAY NEED TO BE REDUCED TO PERMIT LINKAGE ASSEMBLY

ITEM	DESCRIPTION	QUANTITY
40	BUSH ROLLS DRG No.10	-
39	ALL SLEEVE CUTS FROM ROLLS ROYS 76 ALUMINIUM BARS	4
38	BUSH SLEEVE CUTS FROM 25.00 ROYS 76 ALUMINIUM BAR	2
37	1800 76 MSHPC ALUMINIUM TUBE 150x25x3.0	-
36	1800 76 RECTANGULAR ALUMINIUM TUBE 150x25x3.0	-

MACHINED FINISH 1.6 UNLESS OTHERWISE STATED

GENERAL TOLERANCES			
MACHINING		FABRICATION	
0-25	±0.25	0-300	±1.0
75-300	±0.40	300-600	±2.0
300-600	±0.50	600-1200	±3.0
ALL DIMENSIONS IN mm.			

AMBULANCE STRETCHER SUSPENSION
PITCH ARM

SCALES : FULL SIZE

SCHOOL OF ENGINEERING
MECHANICAL ENGINEERING DEPARTMENT

DRN : R.J. HENDERSON
CHKD :
DATE : AUG. 1993
DRG No : S-7

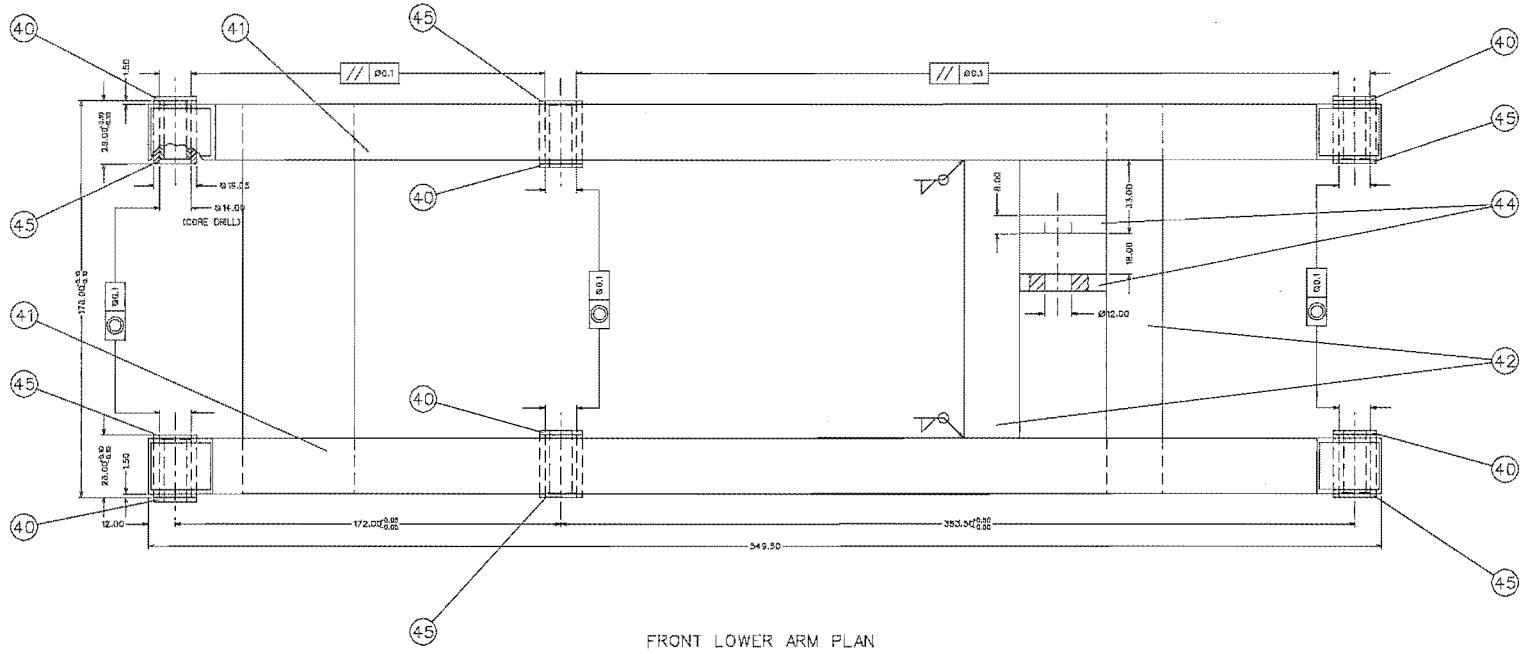

FRONT LOWER ARM PLAN

FRONT LOWER ARM ELEVATION

ITEM	DESCRIPTION	QUANTITY
43	[illegible]	6
44	6mm ALUMINIUM PLATE	-
45	[illegible]	-
42	[illegible]	-
41	[illegible]	-
40	BUSH REFER DRG No. 10	-

NOTE: 1) GUSH FLANGE THICKNESS MAY NEED TO BE REDUCED TO PERMIT LINKAGE ASSEMBLY

MACHINED FINISH 1.6 UNLESS OTHERWISE STATED

GENERAL TOLERANCES

	MACHINING	FABRICATION
0-25	±0.25	0-300 ±1.0
25-300	±0.40	300-600 ±2.0
300-600	±0.50	600-1500 ±2.5

ALL DIMENSIONS IN mm

AMBULANCE STRETCHER SUSPENSION
FRONT LOWER ARM

SCALE: FULL SIZE

SCHOOL OF ENGINEERING
MECHANICAL ENGINEERING DEPARTMENT

DRN: R.J. HENDERSON
CHKD:
DATE: AUG 1993
DRG No: S-8

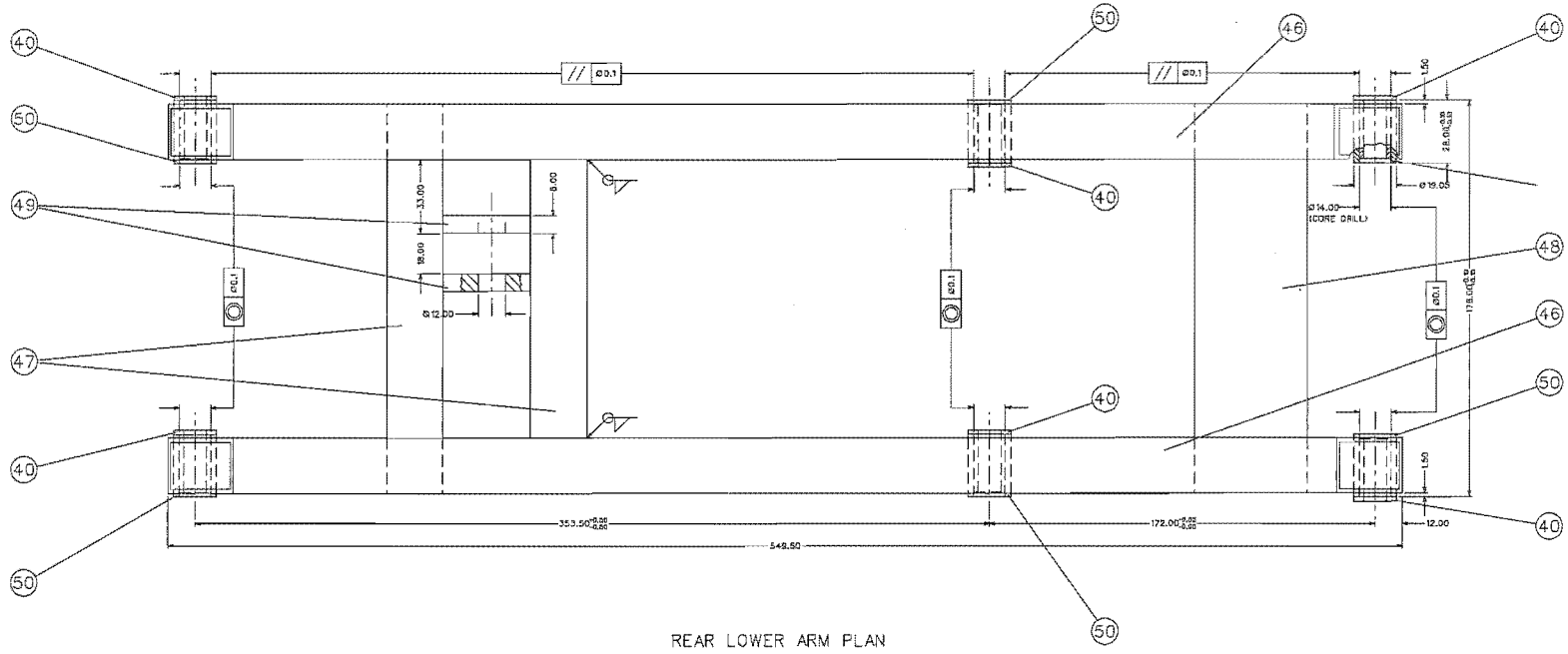

REAR LOWER ARM PLAN

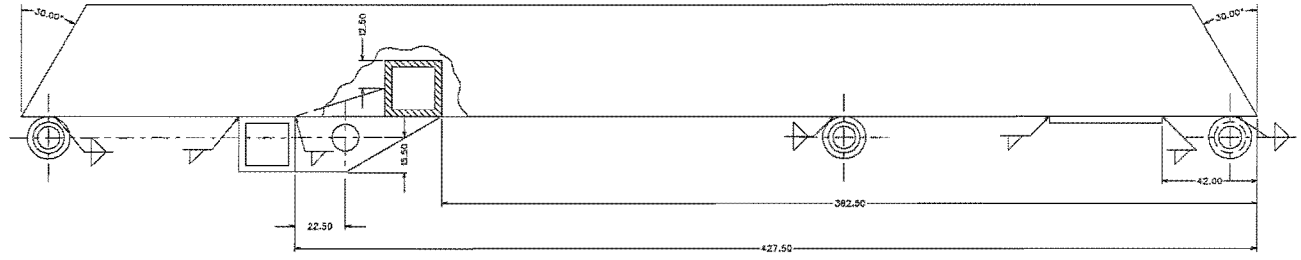

REAR LOWER ARM ELEVATION

ITEM	DESCRIPTION	QUANTITY
50	BUSH 16.2/14 DIA. FROM STOCK 14MS TO ALUMINIUM SHD	6
49	3mm ALUMINIUM PLATE	-
48	50X3 TO FLAT ALUMINIUM BAR 178x3.0	-
47	50X3 TO SQUARE ALUMINIUM TUBE 12.7x12.7x3.0	-
46	50X3 TO RECTANGULAR ALUMINIUM TUBE 25x12.5x3.0	-
40	BUSH 19/12.7 DIA. TO STD	-

NOTE: 1) BUSH FLANGE THICKNESS MAY NEED TO BE REDUCED TO PERMIT LINKAGE ASSEMBLY

MACHINED FINISH	GENERAL TOLERANCES			
1.6	MACHINING		FABRICATION	
UNLESS OTHERWISE STATED	0-25	±0.05	0-315	±1.0
	25-300	±0.10	315-1575	±2.0
	300-1000	±0.15	1600-3150	±3.0
	ALL DIMENSIONS IN mm			

AMBULANCE STRETCHER SUSPENSION
REAR LOWER ARM
SCALES : FULL SIZE

SCHOOL OF ENGINEERING
MECHANICAL ENGINEERING DEPARTMENT
DRN : R.J. HENDERSON
CHKD :
DATE : AUG. 1993
DRG No : S-9

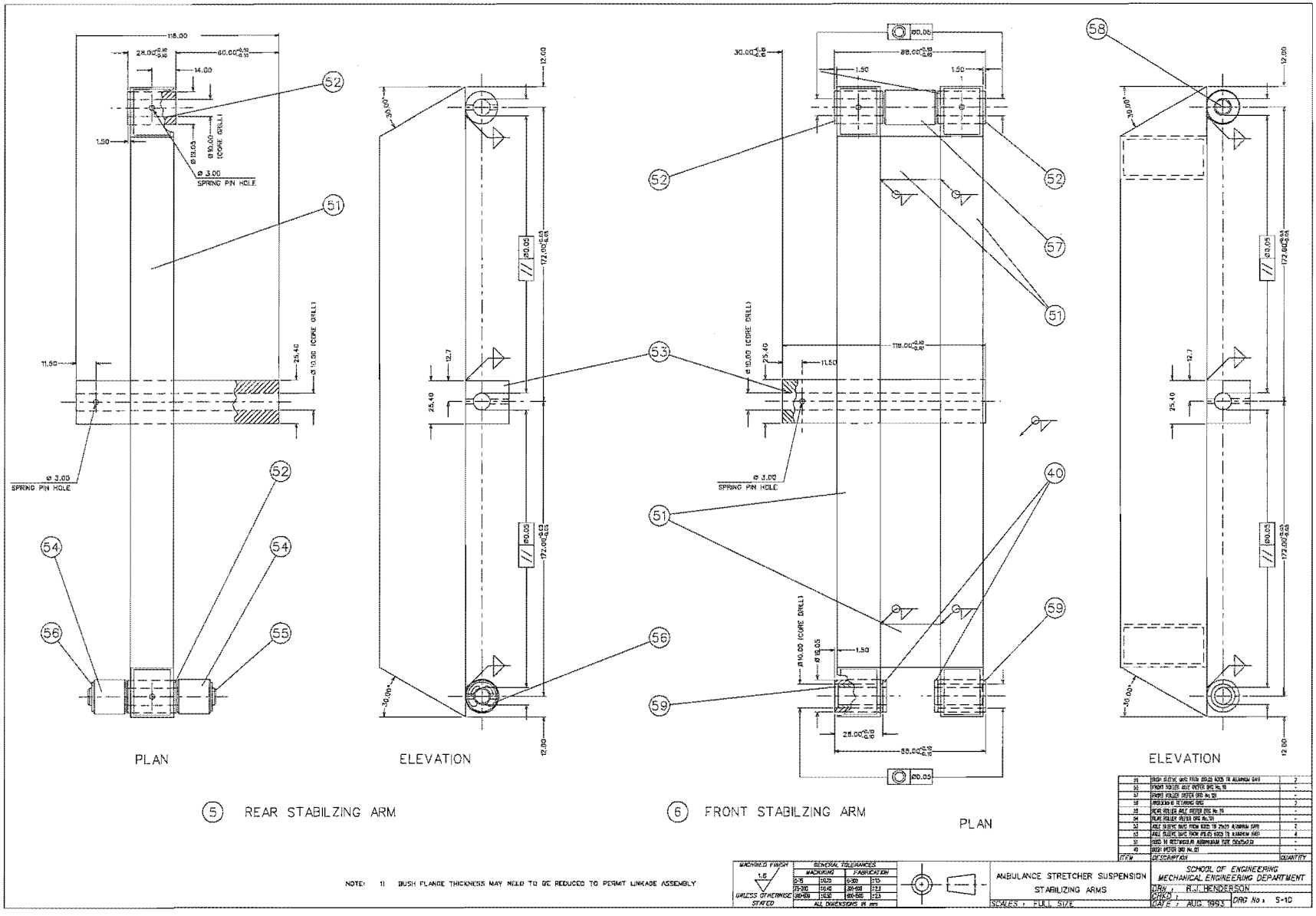

(5) REAR STABILZING ARM

(6) FRONT STABILZING ARM

ITEM	DESCRIPTION	QUANTITY
59	BUSH SLEEVE (M10 FROM Ø20.05 ID TO ALUMINIUM BAR	2
58	FRONT ROLLER AXLE (REFER DRG No. 5)	-
57	FRONT ROLLER (REFER DRG No. 5)	-
56	ANGULAR 6 RETAINING ORG	2
55	REAR ROLLER AXLE (REFER DRG No. 5)	-
54	REAR ROLLER (REFER DRG No. 5)	-
53	AXLE SLEEVE (M10 FROM Ø20.05 TO 25x25 ALUMINIUM BAR)	2
52	AXLE SLEEVE (M10 FROM Ø18.05 TO ALUMINIUM BAR)	4
51	2000 M RECTANGULAR ALUMINIUM TUBE 50x25x2.0	-
40	BUSH (REFER DRG No. 5)	-

NOTE: 1) BUSH FLANGE THICKNESS MAY NEED TO BE REDUCED TO PERMIT LINKAGE ASSEMBLY

MACHINED FINISH	GENERAL TOLERANCES			
1.6	MACHINING		FABRICATION	
UNLESS OTHERWISE STATED	0-75	±0.25	0-300	±1.5
	75-200	±0.40	300-600	±2.5
	200-500	±0.50	600-1500	±2.5
	ALL DIMENSIONS IN mm			

AMBULANCE STRETCHER SUSPENSION
STABILIZING ARMS

SCALES : FULL SIZE

SCHOOL OF ENGINEERING
MECHANICAL ENGINEERING DEPARTMENT
DRN : R.J. HENDERSON
CHKD :
DATE : AUG 1993
DRG No : S-10

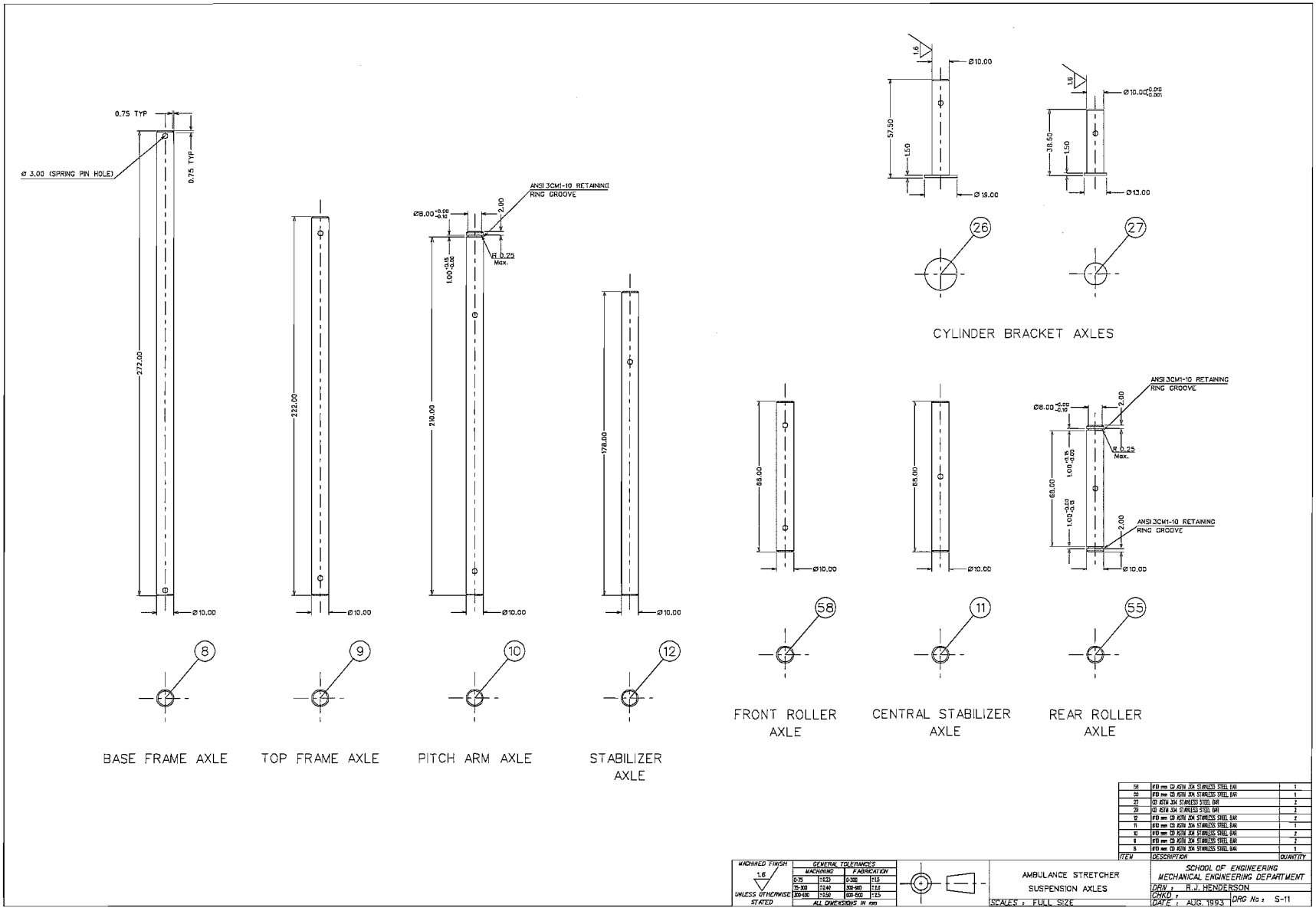
0.75 TYP
Ø 3.00 (SPRING PIN HOLE)
0.75 TYP
272.00
Ø10.00
8
BASE FRAME AXLE
222.00
Ø10.00
9
TOP FRAME AXLE
Ø8.00 +0.00 -0.10
ANSI 3CM1-10 RETAINING RING GROOVE
2.00
R 0.25 Max.
1.00 +0.15 -0.05
210.00
Ø10.00
10
PITCH ARM AXLE
178.00
Ø10.00
12
STABILIZER AXLE
1.6
Ø10.00
57.50
1.50
Ø 16.00
26
1.6
Ø10.00 +0.010 -0.001
38.50
1.50
Ø13.00
27
CYLINDER BRACKET AXLES
58.00
Ø10.00
58
FRONT ROLLER AXLE
85.00
Ø10.00
11
CENTRAL STABILIZER AXLE
ANSI 3CM1-10 RETAINING RING GROOVE
Ø8.00 +0.00 -0.10
2.00
R 0.25 Max.
68.00
1.00 +0.15 -0.05
1.00 +0.20 -0.10
2.00
ANSI 3CM1-10 RETAINING RING GROOVE
Ø10.00
55
REAR ROLLER AXLE
ITEM | DESCRIPTION | QUANTITY
10 | Ø10 mm CD ASTM 304 STAINLESS STEEL BAR | 1
55 | Ø10 mm CD ASTM 304 STAINLESS STEEL BAR | 1
27 | CD ASTM 304 STAINLESS STEEL BAR | 2
26 | CD ASTM 304 STAINLESS STEEL BAR | 2
12 | Ø10 mm CD ASTM 304 STAINLESS STEEL BAR | 2
11 | Ø10 mm CD ASTM 304 STAINLESS STEEL BAR | 1
10 | Ø10 mm CD ASTM 304 STAINLESS STEEL BAR | 2
9 | Ø10 mm CD ASTM 304 STAINLESS STEEL BAR | 2
8 | Ø10 mm CD ASTM 304 STAINLESS STEEL BAR | 1
MACHINED FINISH 1.6 UNLESS OTHERWISE STATED
GENERAL TOLERANCES
MACHINING: 0-75 ±0.25; 75-300 ±0.40; 300-600 ±0.50
FABRICATION: 0-300 ±1.5; 300-600 ±2.0; 600-1200 ±2.5
ALL DIMENSIONS IN mm
AMBULANCE STRETCHER SUSPENSION AXLES
SCALE: FULL SIZE
SCHOOL OF ENGINEERING
MECHANICAL ENGINEERING DEPARTMENT
DRN: R.J. HENDERSON
CHKD:
DATE: AUG. 1993
DRG No: S-11

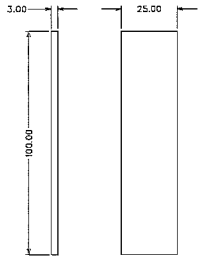

(21) TOP FRAME RESERVOIR END CAP

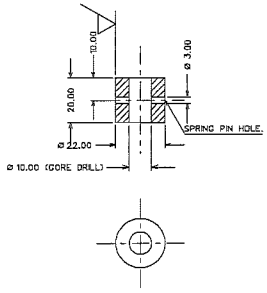

(19) TOP FRAME AXLE RETAINING SLEEVE

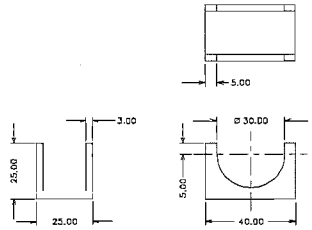

(20) STRETCHER LOCATION LUG

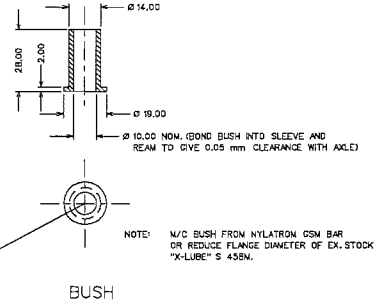

BUSH

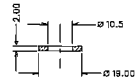

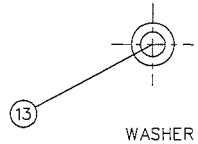

WASHER

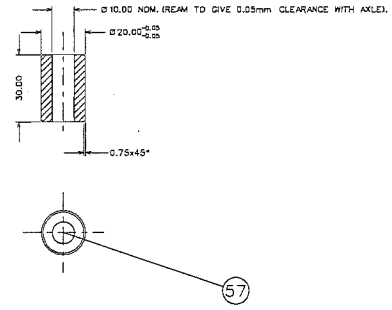

FRONT ROLLER

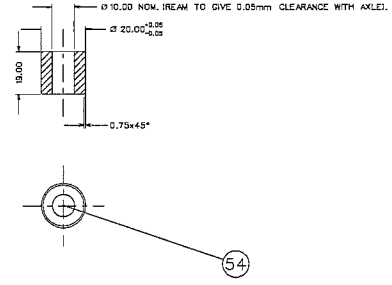

REAR ROLLER

ITEM	DESCRIPTION	QUANTITY
57	NYLATRON GSM ROLLER	1
54	NYLATRON GSM ROLLER	2
40	NYLATRON GSM BUSH	15
21	3.0mm ALUMINIUM SHEET	4
20	ROD TO ALUMINIUM CHANNEL 25x25x3.0	8
19	ROD TO ALUMINIUM BAR	4
13	NYLATRON GSM WASHER	2

MACHINED FINISH 1.6 UNLESS OTHERWISE STATED

GENERAL TOLERANCES			
MACHINING		FABRICATION	
0-75	±0.25	0-300	±1.5
75-300	±0.40	300-600	±2.0
300-600	±0.50	600-1500	±3.5
ALL DIMENSIONS IN mm			

AMBULANCE STRETCHER SUSPENSION
ROLLERS, BUSHES WASHERS AND
TOP FRAME COMPONENTS

SCALE: FULL SIZE

SCHOOL OF ENGINEERING
MECHANICAL ENGINEERING DEPARTMENT

DRN: R.J. HENDERSON
CHKD:
DATE: AUG. 1993
DRG No: S-12

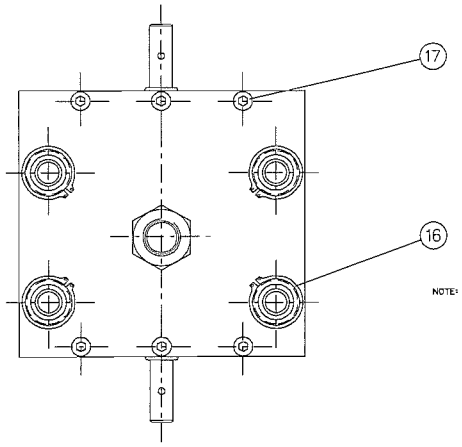

NOTE:
1) THE FRONT AIRSPRING MOUNTING BRACKET IS SHOWN.
2) THE REAR AIRSPRING MOUNTING BRACKET IS A MIRROR IMAGE ABOUT X-X OF THE FRONT BRACKET.
3) THE AIRSPRING IS OMMITTED FOR CLARITY.

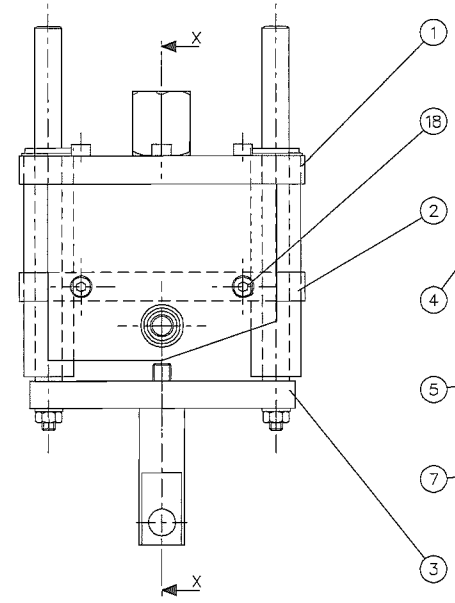

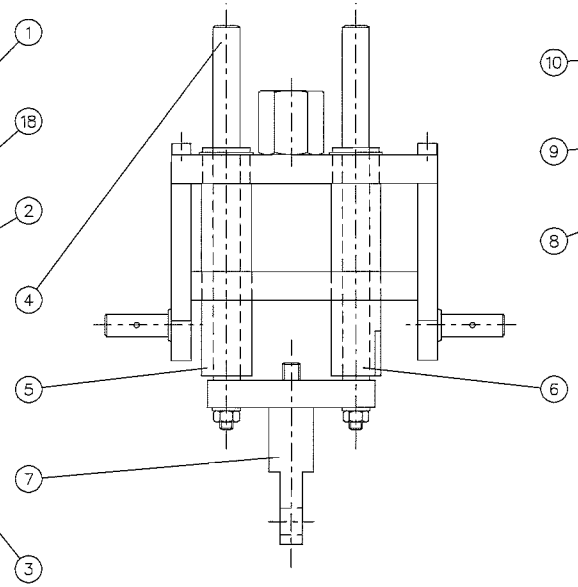

FRONT AIRSPRING MOUNTING BRACKET

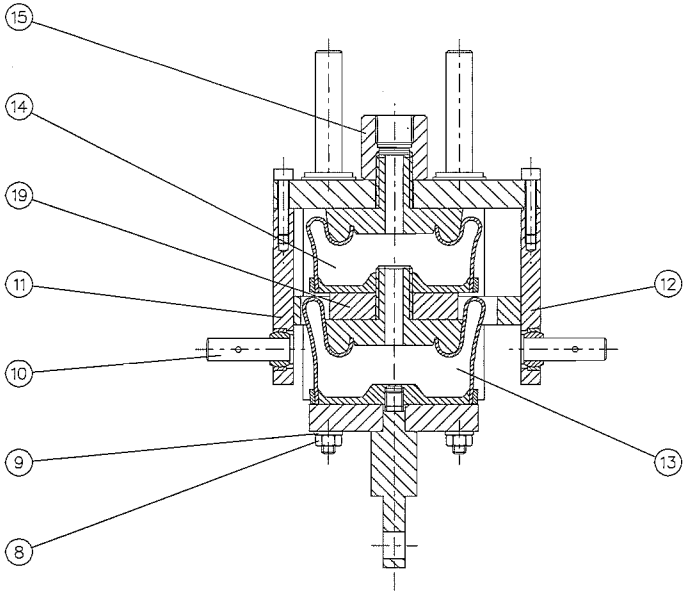

SECTION X-X (WITH AIRSPRINGS INSTALLED)

ITEM	DESCRIPTION	QUANTITY
19	REFER DRG No.3	-
18	M24x3 SOCKET HEAD CAP SCREW	8
17	M24x3 SOCKET HEAD CAP SCREW	8
16	QROUP 10 (16 25mm SHAFT) CAM-70	8
15	REFER DRG No.3	-
14	REFER DRG No.3	-
13	REFER DRG No.5	-
12	REFER DRG No.2	-
11	REFER DRG No.2	-
10	REFER DRG No.4	-
9	M8 WASHER	8
8	M8 NUT	8
7	REFER DRG No.4	-
6	REFER DRG No.3	-
5	REFER DRG No.3	-
4	REFER DRG No.4	-
3	REFER DRG No.2	-
2	REFER DRG No.2	-
1	REFER DRG No.2	-

NOTE: SOME HIDDEN DETAIL OMMITTED FOR CLARITY

MACHINED FINISH 1.6 UNLESS OTHERWISE STATED

GENERAL TOLERANCES			
	MACHINING		FABRICATION
0-75	±0.25	0-300	±1.5
75-300	±0.40	300-500	±2.0
300-600	±0.50	500-1000	±3.0
ALL DIMENSIONS IN mm			

AIRSPRING MOUNTING BRACKET

SCALES : DO NOT SCALE

SCHOOL OF ENGINEERING
MECHANICAL ENGINEERING DEPARTMENT
DRN : R.J. HENDERSON
CHK'D :
DATE : OCT 1995
DRG No : B-1

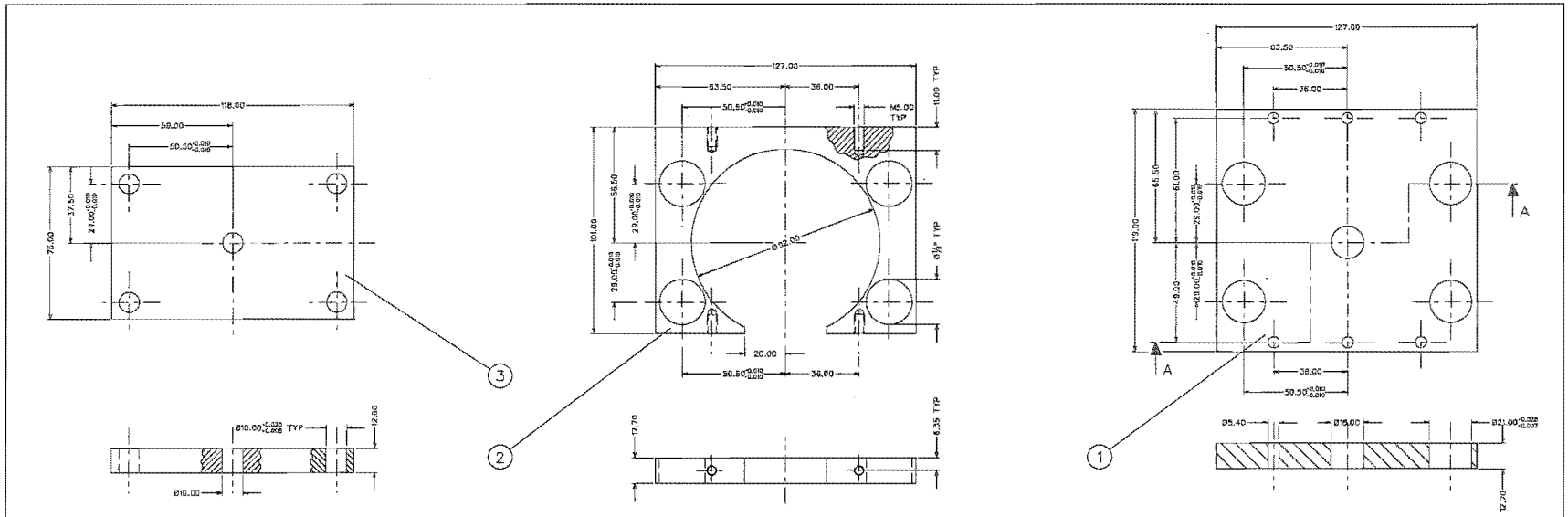

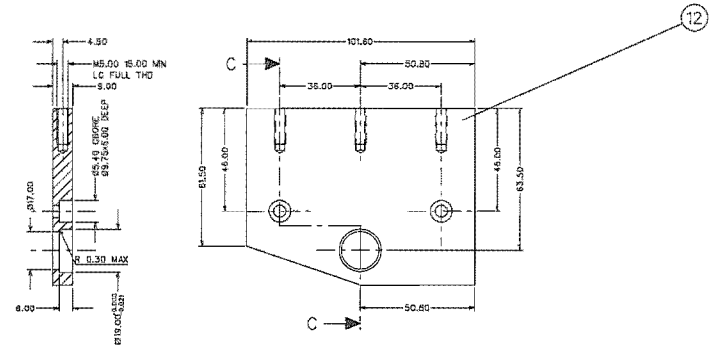

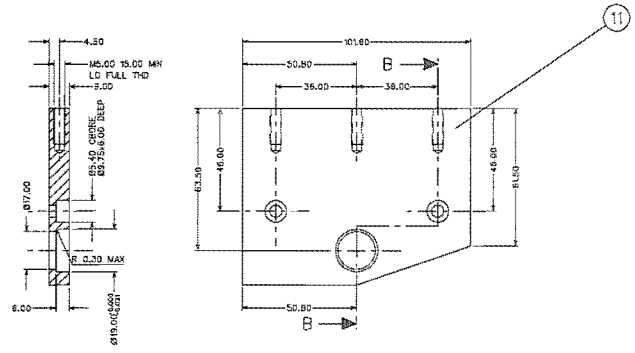

NOTE: SOME HIDDEN DETAIL OMMITTED FOR CLARITY

ITEM	DESCRIPTION	QUANTITY
12	6063 T6 FLAT ALUMINUM BAR 9530x50	1
11	6063 T6 FLAT ALUMINUM BAR 9530x50	1
3	6063 T6 FLAT ALUMINUM BAR 457x50	2
2	6063 T6 FLAT ALUMINUM BAR 457x178	2
1	6063 T6 FLAT ALUMINUM BAR 457x178	2

MACHINED FINISH 1.6 UNLESS OTHERWISE STATED

GENERAL TOLERANCES			
	MACHINING		FABRICATION
0-15	±0.25	0-300	±1.5
75-200	±0.40	300-600	±2.5
200-600	±0.50	600-900	±3.5
ALL DIMENSIONS IN mm			

AIRSPRING MOUNTING BRACKETS:
TOP, MIDDLE, BOTTOM & SIDE PLATES

SCALES : DO NOT SCALE

SCHOOL OF ENGINEERING
MECHANICAL ENGINEERING DEPARTMENT
DRN : R.J. HENDERSON
CHKD :
DATE : OCT 1995 DRG No : B-2

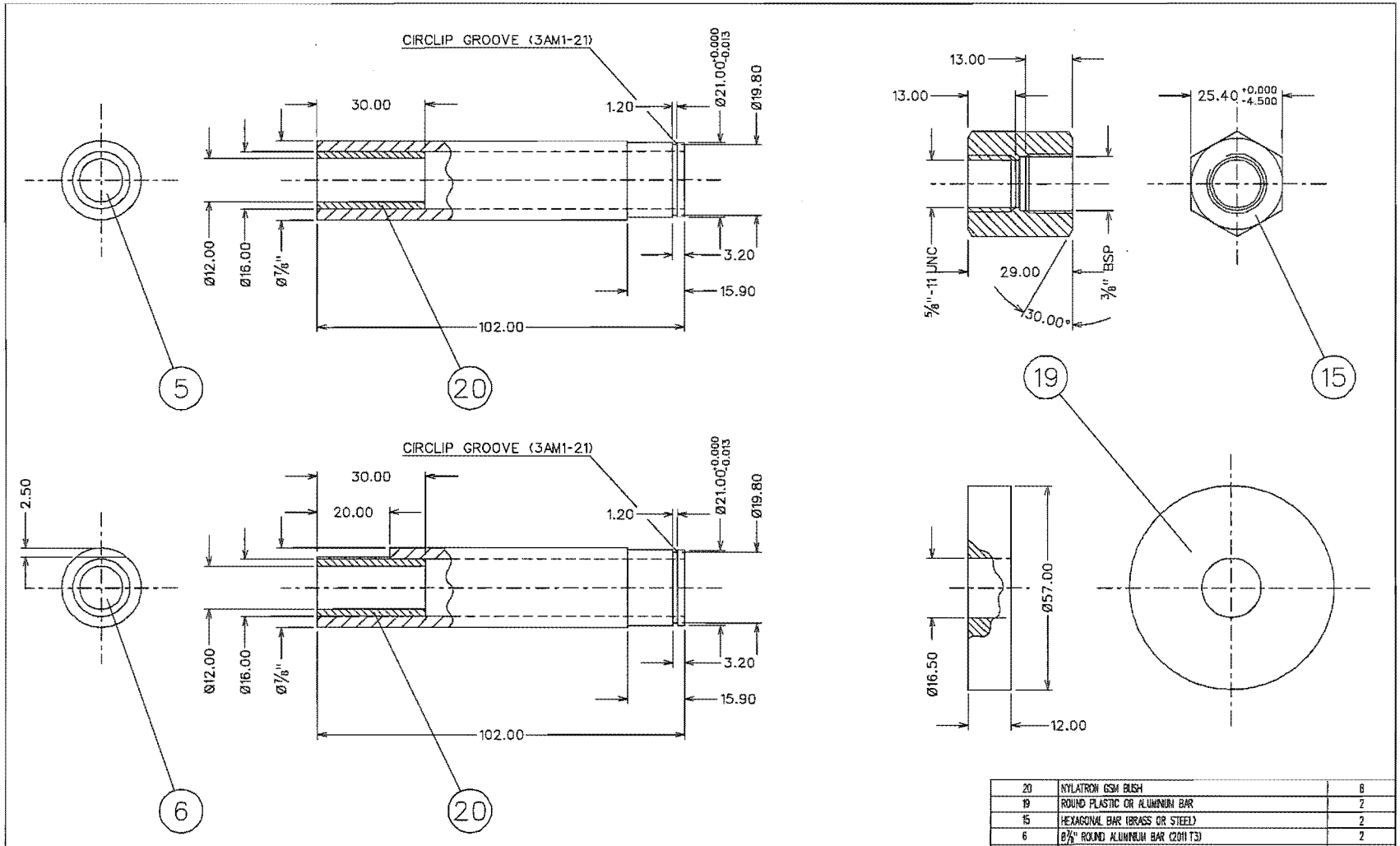

ITEM	DESCRIPTION	QUANTITY
20	NYLATRON GSM BUSH	6
19	ROUND PLASTIC OR ALUMINUM BAR	2
15	HEXAGONAL BAR (BRASS OR STEEL)	2
6	Ø⅞" ROUND ALUMINUM BAR (2011 T3)	2
5	Ø⅞" ROUND ALUMINUM BAR (2011 T3)	6

MACHINED FINISH 1.6

UNLESS OTHERWISE STATED

GENERAL TOLERANCES			
MACHINING		FABRICATION	
0-75	±0.25	0-300	±1.5
75-300	±0.40	300-600	±2.0
300-600	±0.50	600-1500	±2.5
ALL DIMENSIONS IN mm			

AIRSPRING MOUNTING BRACKETS:
BUSH SLEEVES, SPACERS & ADAPTORS

SCALES : DO NOT SCALE

SCHOOL OF ENGINEERING
MECHANICAL ENGINEERING DEPARTMENT

DRN : R.J. HENDERSON
CHKD :
DATE : OCT 1995
DRG No : B-3

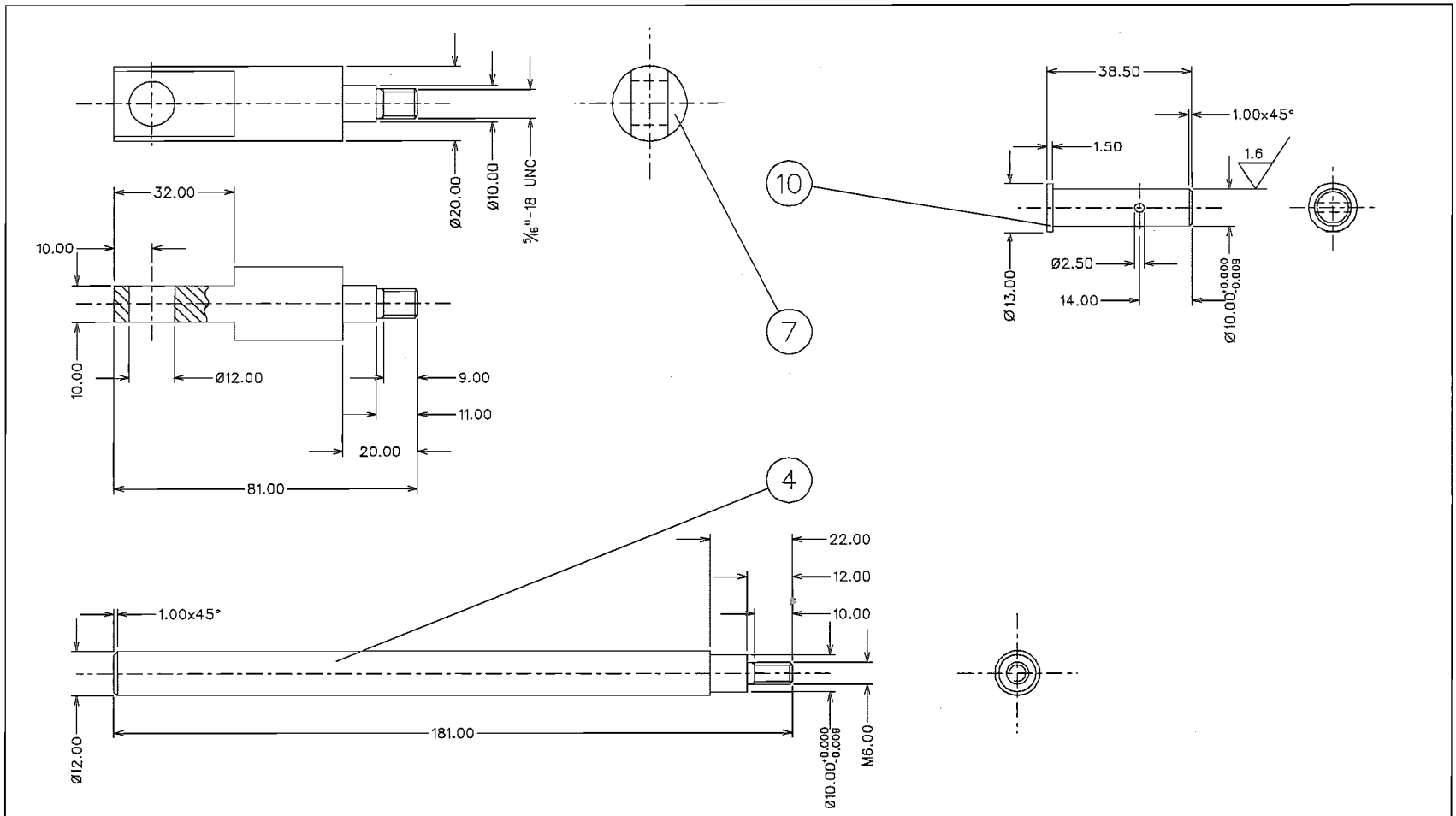

ITEM	DESCRIPTION	QUANTITY
10	ROUND STEEL BAR (AISI 1214/1215)	2
7	Ø20 mm ROUND STEEL BAR (AISI 1214/1215)	2
4	Ø12 mm ROUND STEEL BAR (AISI 1214/1215)	8

MACHINED FINISH 1.6 UNLESS OTHERWISE STATED

GENERAL TOLERANCES			
MACHINING		FABRICATION	
0-75	±0.25	0-300	±1.5
75-300	±0.40	300-600	±2.0
300-600	±0.50	600-1500	±2.5
ALL DIMENSIONS IN mm			

AIRSPRING MOUNTING BRACKETS:
GUIDE RODS AND PINS

SCALES : DO NOT SCALE

SCHOOL OF ENGINEERING
MECHANICAL ENGINEERING DEPARTMENT

DRN : R.J. HENDERSON
CHKD :
DATE : OCT 1995
DRG No : B-4

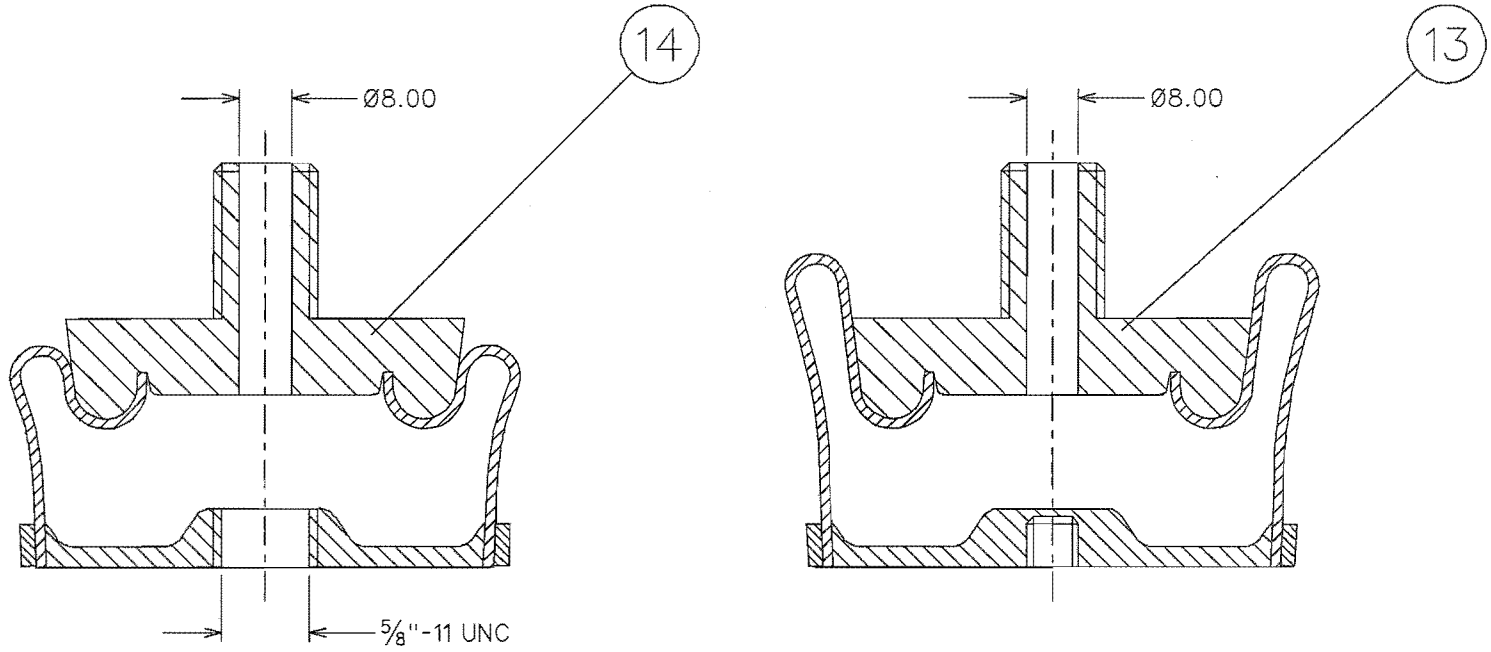

ITEM	DESCRIPTION	QUANTITY
14	SHORT AIRSPRING	2
13	LONG AIRSPRING	2

AIRSPRING MODIFICATIONS

SCALES : DO NOT SCALE

SCHOOL OF ENGINEERING
MECHANICAL ENGINEERING DEPARTMENT

DRN : R.J. HENDERSON

CHKD :

DATE : OCT 1995

DRG No : B-5

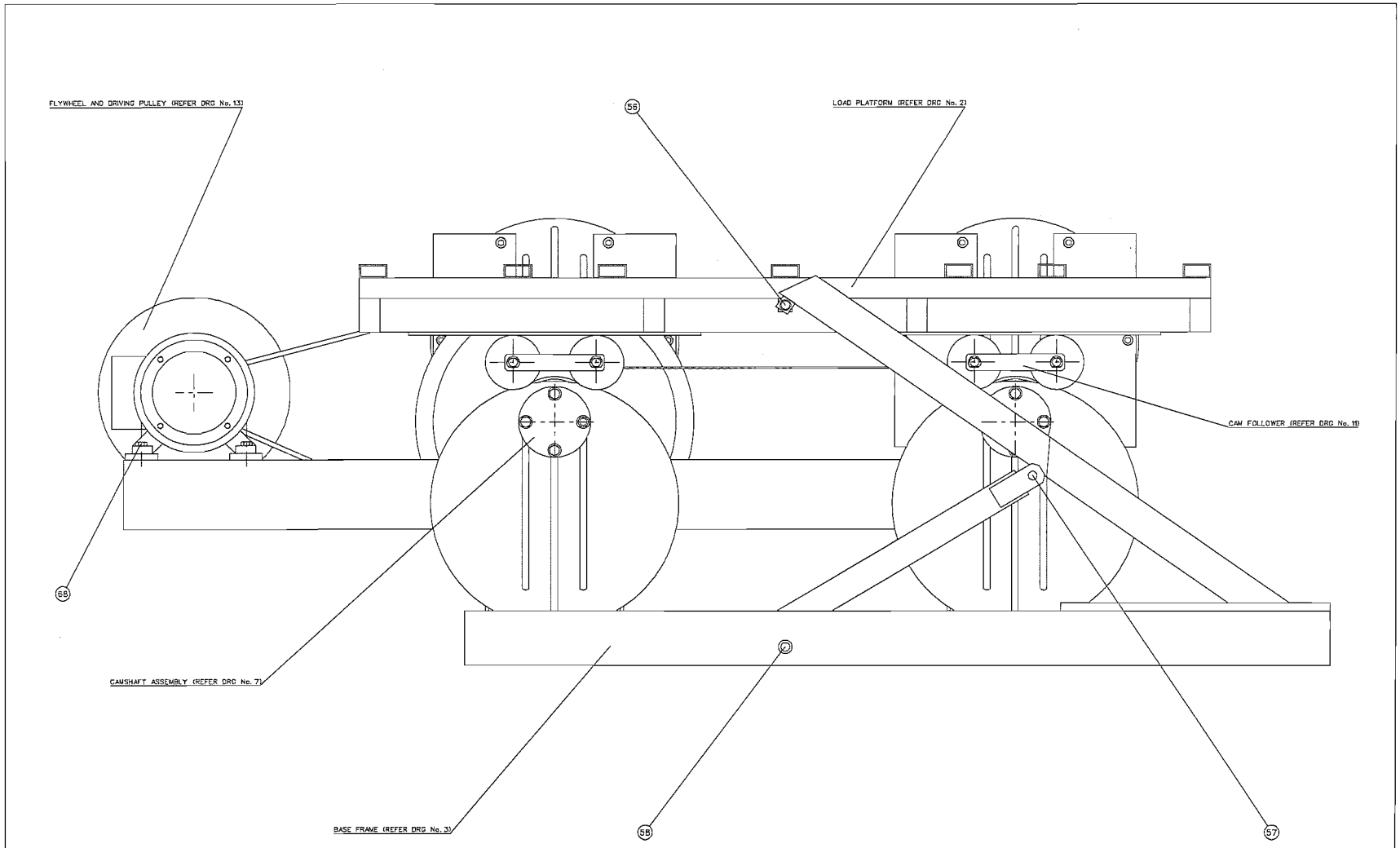

NOTE: SOME HIDDEN DETAIL OMITTED FOR CLARITY

ITEM	DESCRIPTION	QUANTITY
6A	M12x1.5 LONG BOLT (GRADE 8.8)	4
6B	AXLE (REFER DRG No. 8)	-
6C	AXLE (REFER DRG No. 8)	-
6D	AXLE (REFER DRG No. 8)	-

MACHINED FINISH 1.6 UNLESS OTHERWISE STATED

GENERAL TOLERANCES			
MACHINING		FABRICATION	
0-75	±0.25	0-300	±1.5
75-200	±0.40	300-600	±2.0
200-400	±0.50	600-1200	±2.5
ALL DIMENSIONS IN mm			

VIBRATION TESTING MACHINE
FRONT ELEVATION

SCALE: DO NOT SCALE

SCHOOL OF ENGINEERING
MECHANICAL ENGINEERING DEPARTMENT

DRN : R.J. HENDERSON
CHKD :
DATE : APRIL 1994
DRG No : ST-1A

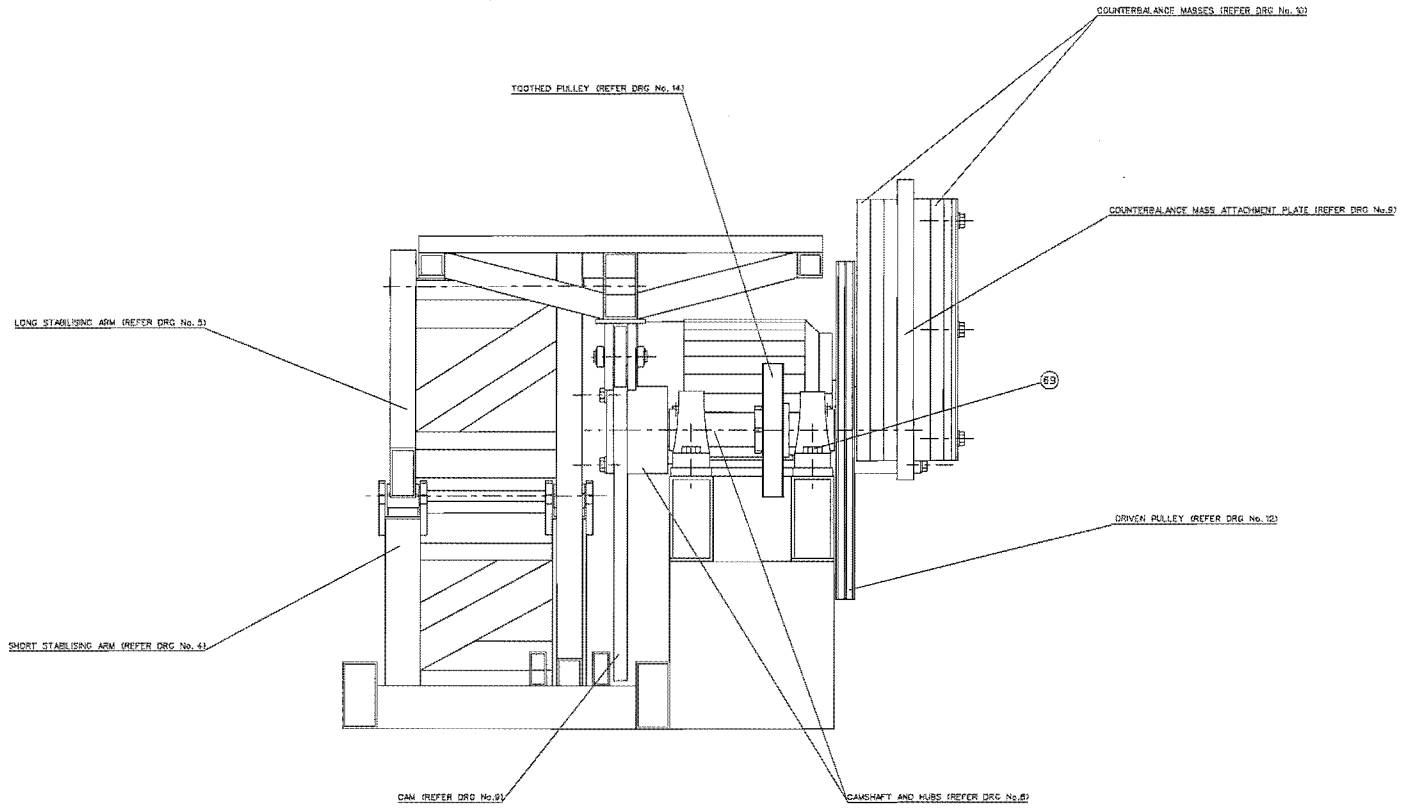

NOTE: SOME HIDDEN DETAIL OMITTED FOR CLARITY

ITEM	DESCRIPTION	QUANTITY
10	M8x40 LONG BOLT (GRADE 8.8)	4

MACHINED FINISH	GENERAL TOLERANCES			
1.6	MACHINING		FABRICATION	
UNLESS OTHERWISE STATED	0-75	±0.25	0-300	±1.5
	75-300	±0.40	300-1000	±2.0
	300-1000	±0.50	1000-3000	±2.5
	ALL DIMENSIONS IN mm			

VIBRATION TESTING MACHINE
END ELEVATION

SCALES 1:10 NOT SCALE

SCHOOL OF ENGINEERING
MECHANICAL ENGINEERING DEPARTMENT

DRN : R.J. HENDERSON
CHKD :
DATE : APRIL 1994
DRG No : ST-18

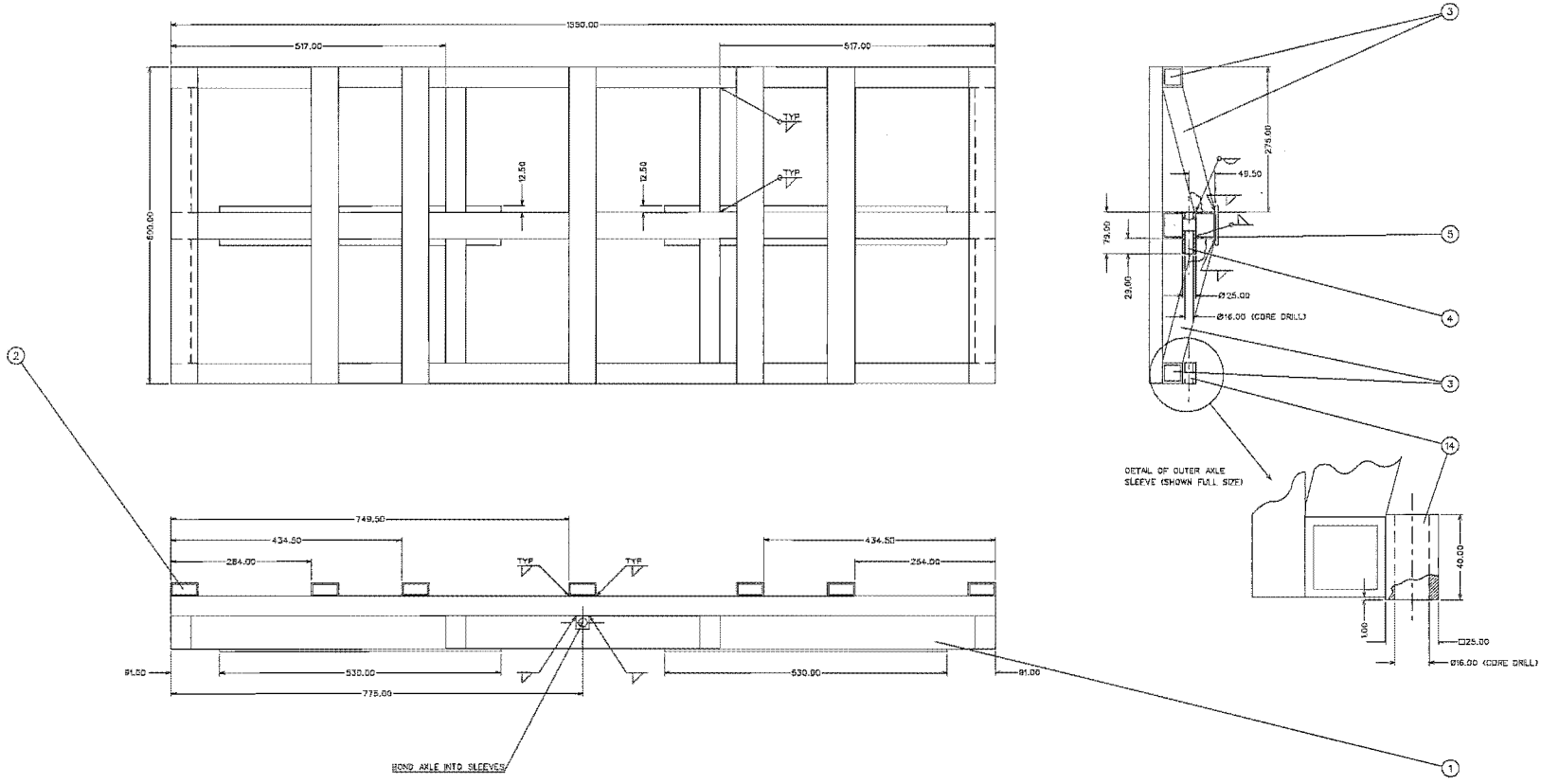

NOTE: SOME HIDDEN DETAIL OMITTED FOR CLARITY

ITEM	DESCRIPTION	QUANTITY
14	MILD STEEL SQUARE BAR Ø45.00	-
5	GRADE 43 ASTM HOT FLAT STEEL BAR 6.00x50.00	-
4	ROUND MILD STEEL BAR 25mm DIA	-
3	MILD STEEL SQUARE TUBE 150x150x4.00	-
2	MILD STEEL RECTANGULAR TUBE 150x50x2.00	-
1	MILD STEEL RECTANGULAR TUBE 600x50x3.00	-

MACHINED FINISH 1.6 UNLESS OTHERWISE STATED

GENERAL TOLERANCES			
MACHINING		FABRICATION	
0-75	±0.25	0-300	±1.5
75-300	±0.45	300-1000	±2.0
300-600	±0.90	1000-3000	±2.5

ALL DIMENSIONS IN mm

VIBRATION TESTING MACHINE
LOAD PLATFORM

SCALES DO NOT SCALE

SCHOOL OF ENGINEERING
MECHANICAL ENGINEERING DEPARTMENT
DRAWN : R.J. HENDERSON
CHKD :
DATE : APRIL 1994
DRG No : ST-2

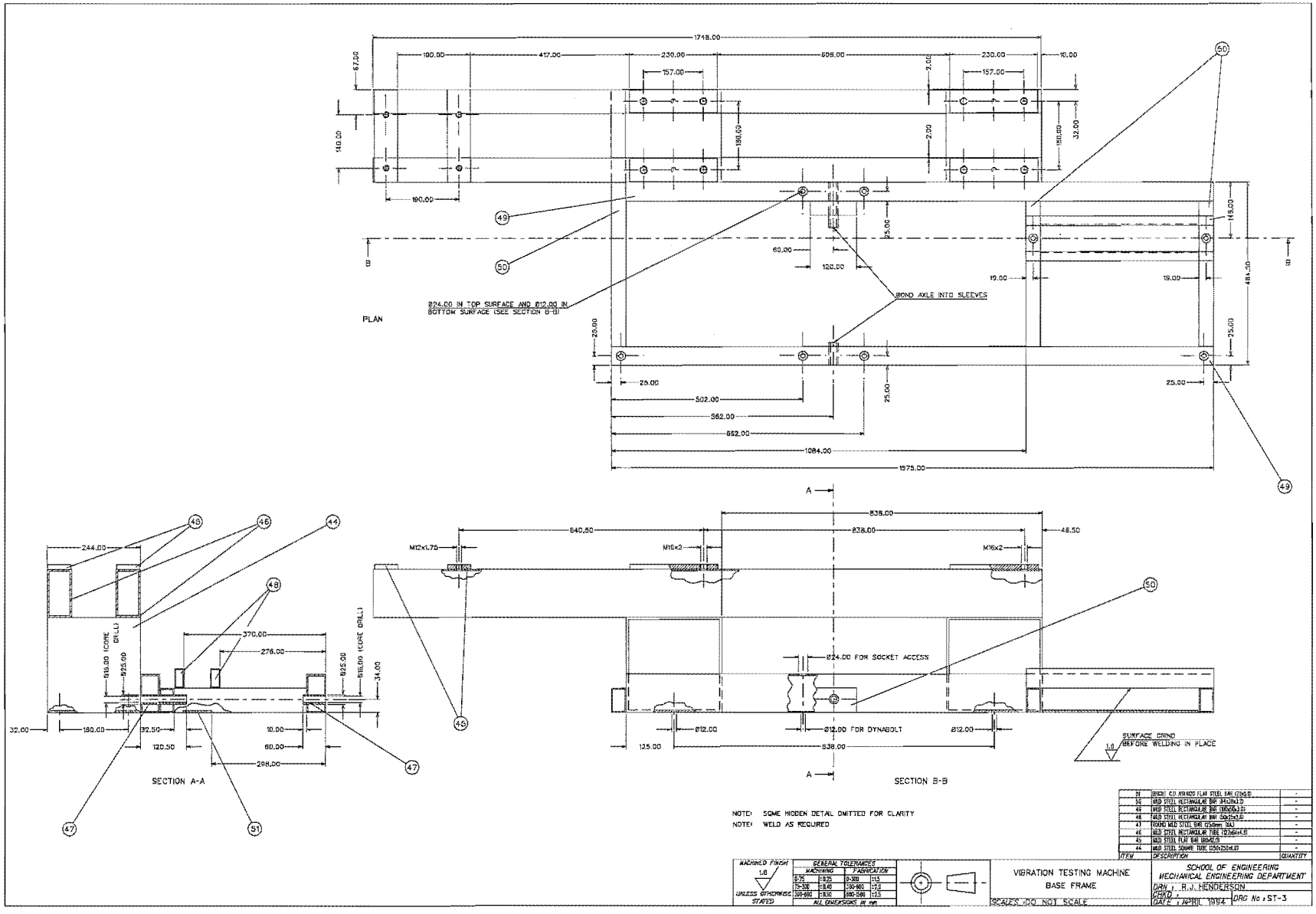

NOTE: SOME HIDDEN DETAIL OMITTED FOR CLARITY
NOTE: WELD AS REQUIRED

ITEM	DESCRIPTION	QUANTITY
51	BRIGHT CD 4340 FLAT STEEL BAR (75x5.0)	-
50	MILD STEEL RECTANGULAR BAR (Ø41.28x3.0)	-
49	MILD STEEL RECTANGULAR BAR (100x50x3.0)	-
48	MILD STEEL RECTANGULAR BAR (50x25x2.0)	-
47	ROUND MILD STEEL BAR (250mm DIA)	-
46	MILD STEEL RECTANGULAR TUBE (125x64x4.0)	-
45	MILD STEEL FLAT BAR (80x6.0)	-
44	MILD STEEL SQUARE TUBE (150x150x4.0)	-

MACHINED FINISH 1.6 UNLESS OTHERWISE STATED	GENERAL TOLERANCES			
	MACHINING		FABRICATION	
	0-75	±0.25	0-300	±1.5
	75-300	±0.40	300-900	±2.0
	300-900	±0.50	900-1500	±2.5
	ALL DIMENSIONS IN mm			

VIBRATION TESTING MACHINE
BASE FRAME
SCALES: DO NOT SCALE

SCHOOL OF ENGINEERING
MECHANICAL ENGINEERING DEPARTMENT
DRN : R.J. HENDERSON
CHKD :
DATE : APRIL 1994
DRG No : ST-3

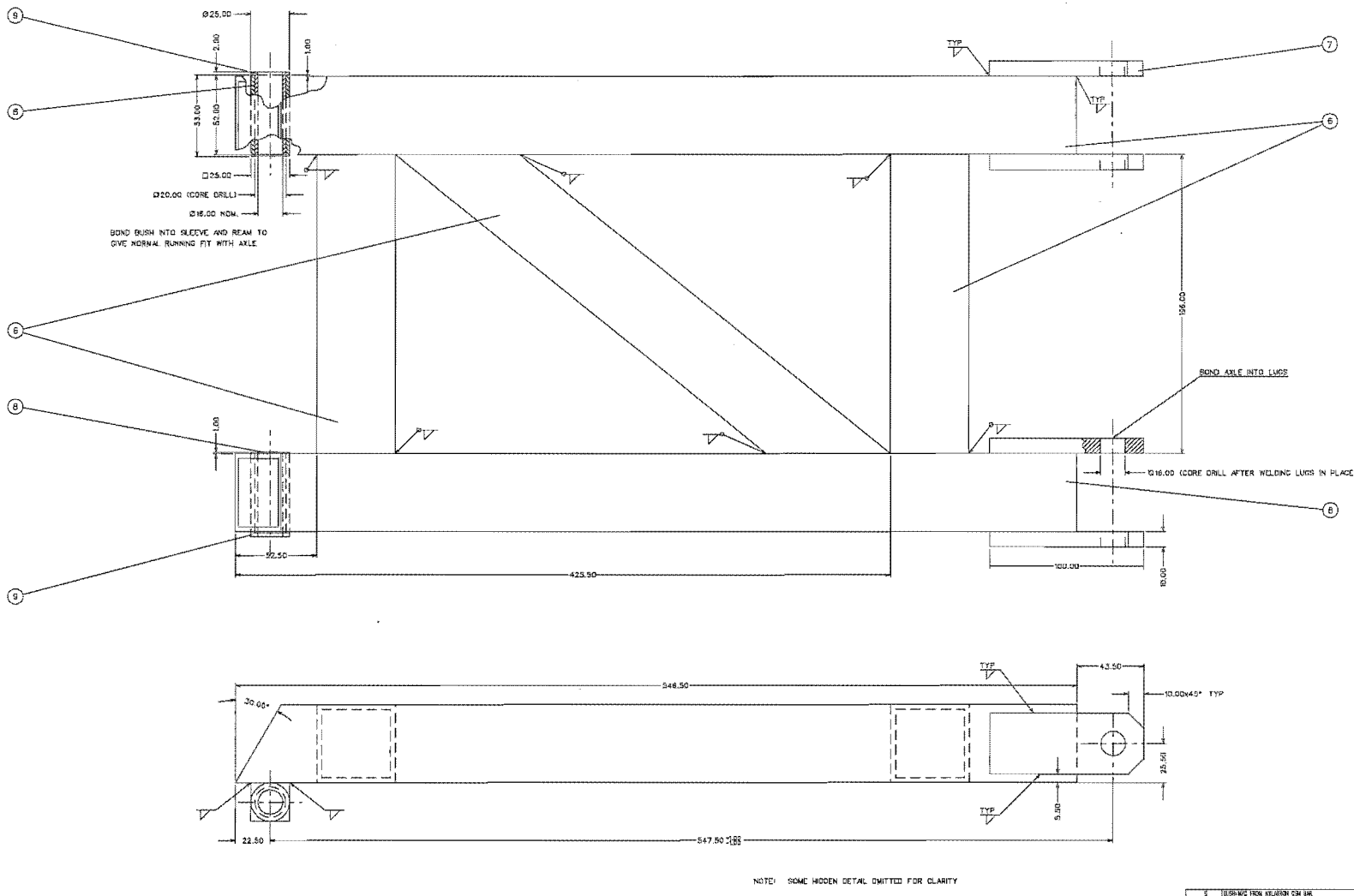

ITEM	DESCRIPTION	QUANTITY
5	BUSH M/C FROM NYLATRON GSM BAR	2
8	MILD STEEL SQUARE BAR 60x20	-
7	MAINT CH. ASYMEQ FLAT STEEL BAR (45x10)	-
6	MILD STEEL RECTANGULAR TUBE (50x50x3.2)	-

MACHINED FINISH 1.6 UNLESS OTHERWISE STATED

GENERAL TOLERANCES

MACHINING		FABRICATION	
0-75	±0.25	0-300	±1.5
75-300	±0.40	300-600	±2.0
300-600	±0.50	600-1200	±2.5

ALL DIMENSIONS IN mm

VIBRATION TESTING MACHINE
SHORT STABILISING ARM

SCALE:-DO NOT SCALE

SCHOOL OF ENGINEERING
MECHANICAL ENGINEERING DEPARTMENT
DRN : R.J. HENDERSON
CHKD :
DATE : APRIL 1994
DRG No : ST-4

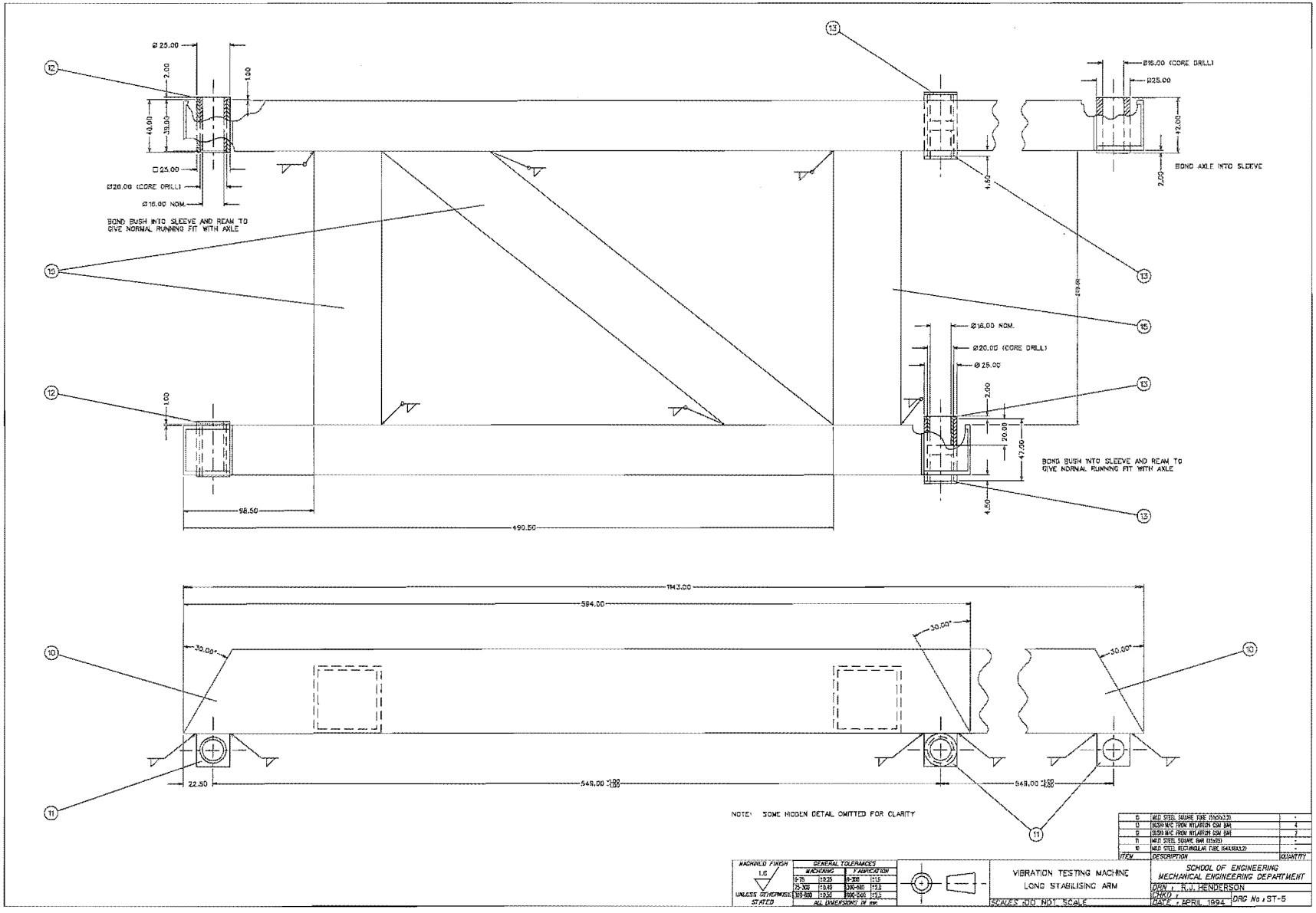
Ø 25.00
2.00
1.00
40.00
39.00
□ 25.00
Ø20.00 (CORE DRILL)
Ø 16.00 NOM.
BOND BUSH INTO SLEEVE AND REAM TO GIVE NORMAL RUNNING FIT WITH AXLE
Ø16.00 (CORE DRILL)
Ø25.00
47.00
2.00
BOND AXLE INTO SLEEVE
4.50
259.00
Ø16.00 NOM.
Ø20.00 (CORE DRILL)
Ø 25.00
2.00
20.00
47.00
BOND BUSH INTO SLEEVE AND REAM TO GIVE NORMAL RUNNING FIT WITH AXLE
4.50
1.00
98.50
490.50
1143.00
984.00
30.00°
30.00°
30.00°
30.00°
22.50
548.00 ±1.00
548.00 ±1.00
NOTE: SOME HIDDEN DETAIL OMITTED FOR CLARITY
6 MILD STEEL SQUARE TUBE (50x50x3.2) -
5 BUSH M/C FROM NYLATRON GSM BAR 4
4 BUSH M/C FROM NYLATRON GSM BAR 2
3 MILD STEEL SQUARE BAR (12x12) -
2 MILD STEEL RECTANGULAR TUBE (64x48x3.2) -
ITEM DESCRIPTION QUANTITY
MACHINED FINISH 1.6 UNLESS OTHERWISE STATED
GENERAL TOLERANCES
MACHINING: 0-75 ±0.25; 75-300 ±0.40; 300-600 ±0.52
FABRICATION: 0-300 ±1.5; 300-600 ±2.0; 600-1200 ±2.5
ALL DIMENSIONS IN mm
VIBRATION TESTING MACHINE
LONG STABILISING ARM
SCALE 1:10 NOT SCALE
SCHOOL OF ENGINEERING
MECHANICAL ENGINEERING DEPARTMENT
DRN : R.J. HENDERSON
CHKD :
DATE : APRIL 1994
DRG No : ST-5

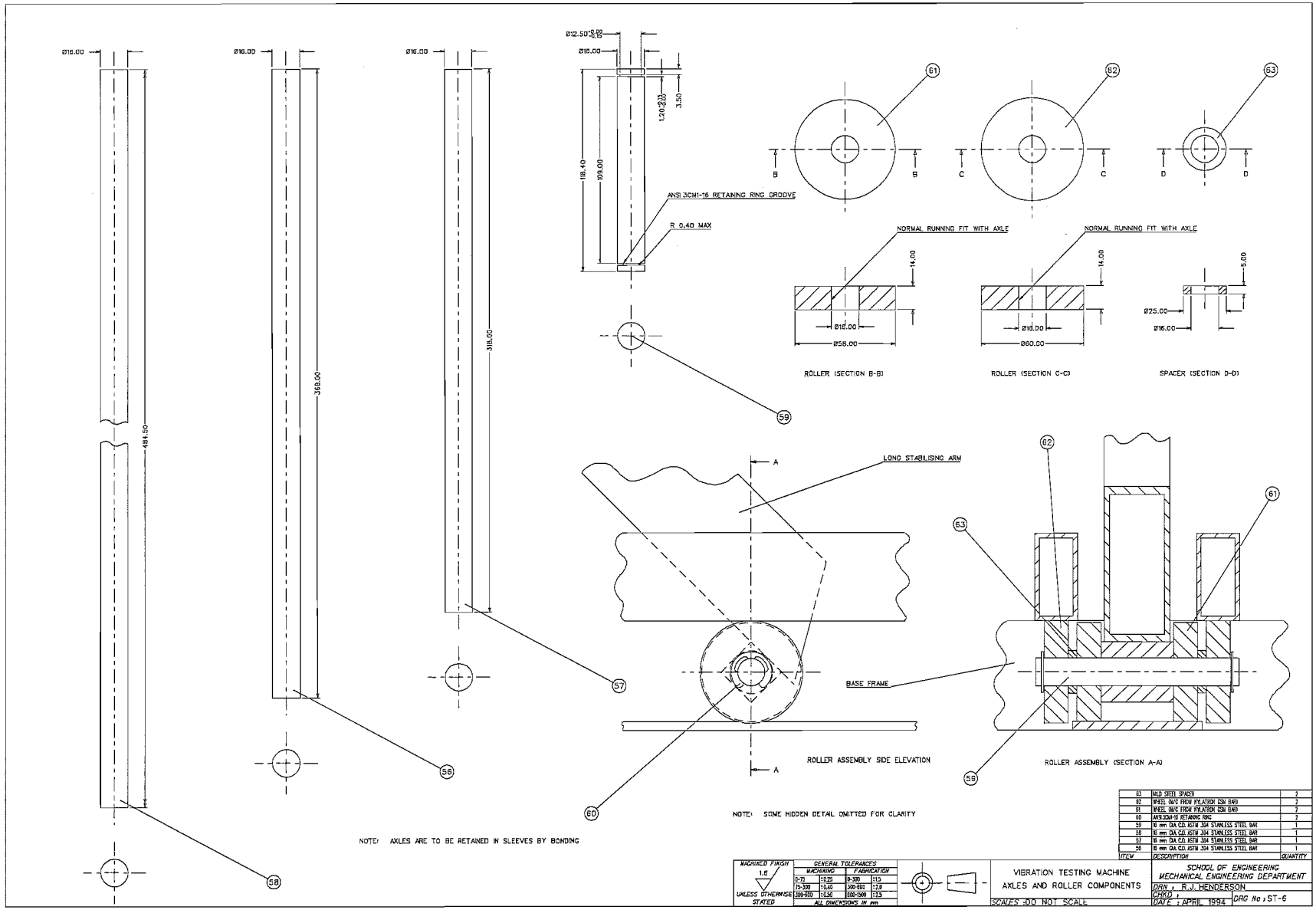

ITEM	DESCRIPTION	QUANTITY
63	MILD STEEL SPACER	2
62	WHEEL (W/C FROM RYLATRON CSM GW3)	2
61	WHEEL (W/C FROM RYLATRON CSM GW3)	2
60	ANSI 3CM-16 RETAINING RING	2
59	16 mm DIA C.D. ASTM 304 STAINLESS STEEL BAR	1
58	16 mm DIA C.D. ASTM 304 STAINLESS STEEL BAR	1
57	16 mm DIA C.D. ASTM 304 STAINLESS STEEL BAR	1
56	16 mm DIA C.D. ASTM 304 STAINLESS STEEL BAR	1

MACHINED FINISH	GENERAL TOLERANCES		
1.6	MACHINING	FABRICATION	
UNLESS OTHERWISE STATED	0-75 ±0.25	0-300 ±1.5	
	76-300 ±0.40	300-1000 ±2.0	
	300-1000 ±0.50	1000-3000 ±2.5	
	ALL DIMENSIONS IN mm		

VIBRATION TESTING MACHINE
AXLES AND ROLLER COMPONENTS
SCALES :DO NOT SCALE

SCHOOL OF ENGINEERING
MECHANICAL ENGINEERING DEPARTMENT
DRN : R.J. HENDERSON
CHKD :
DATE : APRIL 1994
DRG No : ST-6

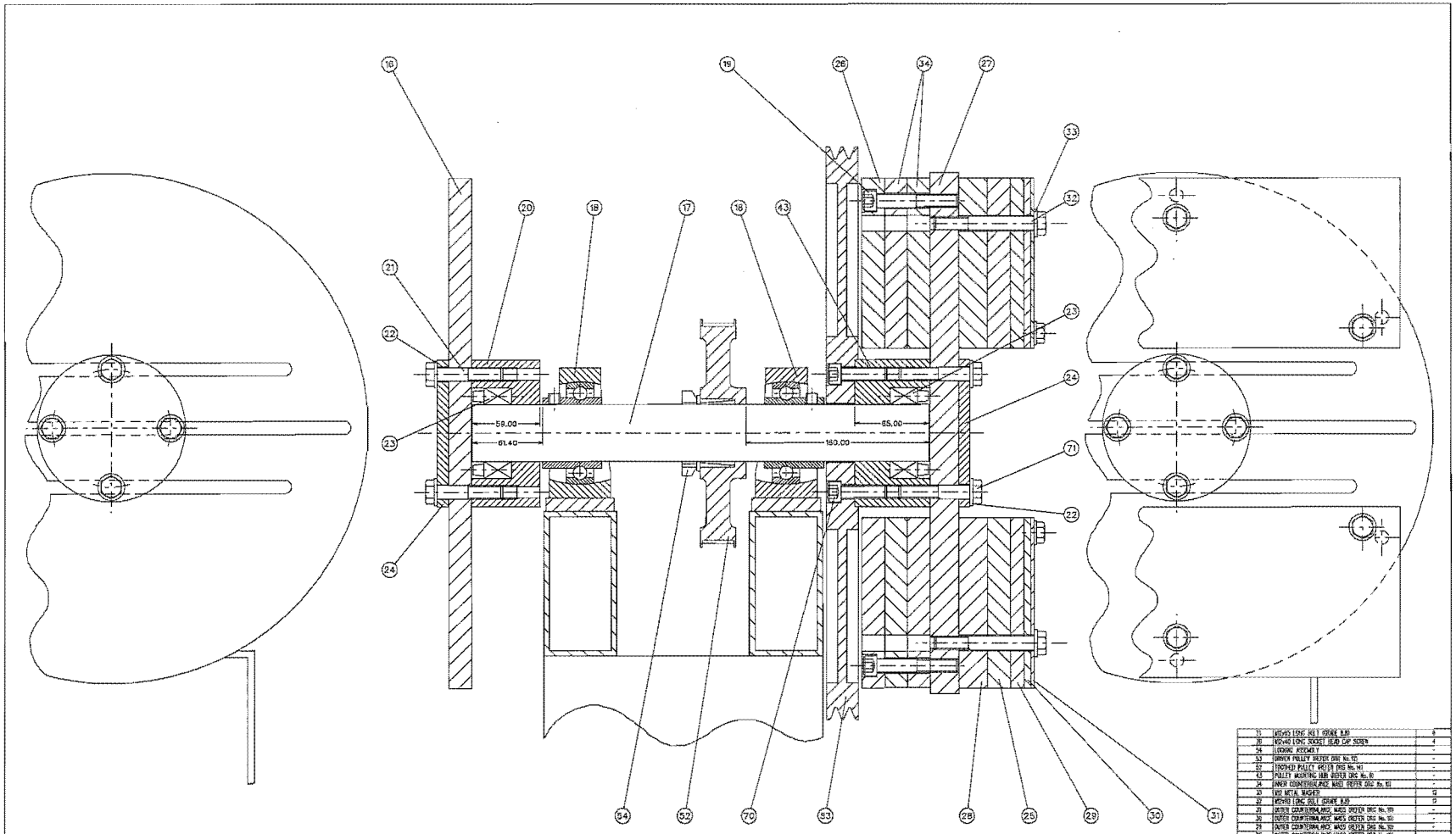

CAMSHAFT ASSEMBLY (SHOWN IN SECTION)

NOTE: L.H. SHAFT ASSEMBLY IS SHOWN. THE R.H. IS THE SAME EXCEPT THAT HUB (20) IS USED AT BOTH SHAFT ENDS AND PULLEY (53) IS OMMITTED

NOTE: SOME HIDDEN DETAIL OMITTED FOR CLARITY

NOTE: ANGULAR RELATIONSHIP BETWEEN (16) AND (27) IS IMPORTANT AND SHOULD BE '60°' AS SHOWN

ITEM	DESCRIPTION	QUANTITY
71	M12x90 LONG BELT KEYWAY BUSH	4
70	M12x40 LONG SOCKET HEAD CAP SCREW	4
54	LOCKING ASSEMBLY	-
53	DRIVEN PULLEY (REFER DRG No.13)	-
52	TOOTHED PULLEY (REFER DRG No.14)	-
43	PULLEY MOUNTING HUB (REFER DRG No.15)	-
34	INNER COUNTERBALANCE MASS (REFER DRG No.16)	-
33	M30 METAL WASHER	12
32	M12x90 LONG BELT KEYWAY BUSH	12
31	OUTER COUNTERBALANCE MASS (REFER DRG No.19)	-
30	OUTER COUNTERBALANCE MASS (REFER DRG No.19)	-
29	OUTER COUNTERBALANCE MASS (REFER DRG No.19)	-
28	OUTER COUNTERBALANCE MASS (REFER DRG No.19)	-
27	COUNTERBALANCE MASS MOUNTING PLATE (REFER DRG No.18)	-
26	INNER COUNTERBALANCE MASS (REFER DRG No.19)	-
25	OUTER COUNTERBALANCE MASS (REFER DRG No.19)	-
24	END PLATE (REFER DRG No.12)	-
23	HOUSING ASSEMBLY	-
22	M12 METAL WASHER	16
21	M12x60 LONG BELT KEYWAY BUSH	8
20	MOUNTING HUB (REFER DRG No.21)	-
19	M12x70 LONG SOCKET HEAD CAP SCREW	12
18	SKF 6206 Open BORE BEARING AND HOUSING (FAG 5206.2RS)	4
17	CAMSHAFT (REFER DRG No.11)	-
16	CAM INSERT (REFER DRG No.11)	-

MACHINED FINISH 1.6 UNLESS OTHERWISE STATED	GENERAL TOLERANCES			
	MACHINING		FABRICATION	
	0-75	±0.25	0-300	±1.5
	75-300	±0.40	300-600	±2.0
	300-1000	±0.50	1000-1500	±2.5
	ALL DIMENSIONS IN mm.			

VIBRATION TESTING MACHINE
CAMSHAFT ASSEMBLY
SCALES :DO NOT SCALE

SCHOOL OF ENGINEERING
MECHANICAL ENGINEERING DEPARTMENT
DRW : R.J. HENDERSON
CHKD :
DATE : APRIL 1994
DRG No : ST-7

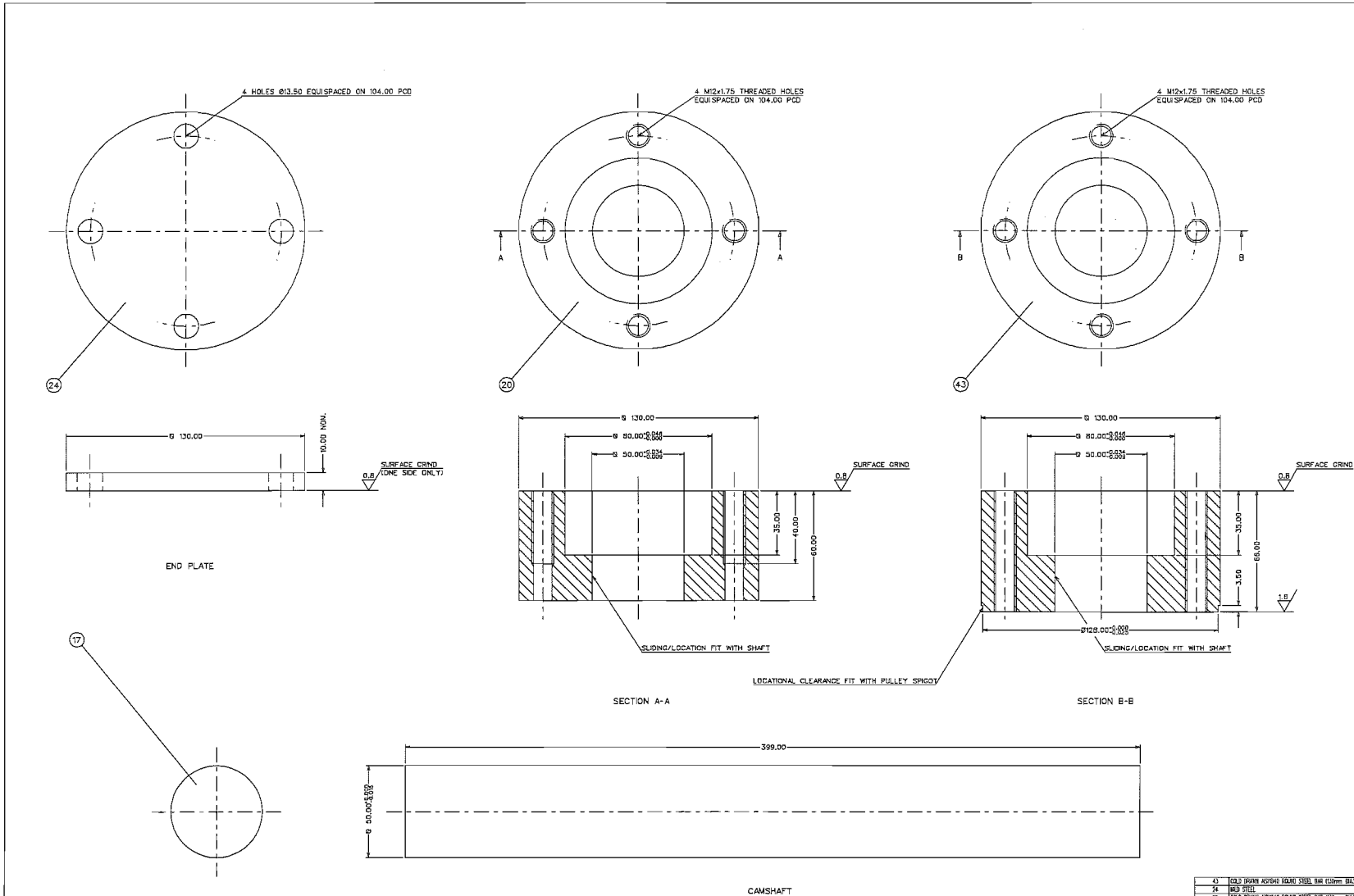
4 HOLES Ø13.50 EQUISPACED ON 104.00 PCD
4 M12x1.75 THREADED HOLES EQUISPACED ON 104.00 PCD
4 M12x1.75 THREADED HOLES EQUISPACED ON 104.00 PCD
24
20
43
A
A
B
B
Ø 130.00
10.00 NOM.
SURFACE GRIND (ONE SIDE ONLY)
0.8
END PLATE
Ø 130.00
Ø 80.00 +0.040 +0.030
Ø 50.00 +0.034 +0.009
SURFACE GRIND
0.8
35.00
40.00
60.00
SLIDING/LOCATION FIT WITH SHAFT
SECTION A-A
Ø 130.00
Ø 80.00 +0.040 +0.030
Ø 50.00 +0.034 +0.009
SURFACE GRIND
0.8
35.00
3.50
60.00
1.6
Ø128.00 -0.000 -0.033
SLIDING/LOCATION FIT WITH SHAFT
LOCATIONAL CLEARANCE FIT WITH PULLEY SPIGOT
SECTION B-B
17
399.00
Ø 50.00 +0.050 +0.034
CAMSHAFT
43 COLD DRAWN AISI1040 ROUND STEEL BAR (130mm DIA) 1
74 MILD STEEL 4
20 COLD DRAWN AISI1040 ROUND STEEL BAR (130mm DIA) 1
17 COLD DRAWN AISI1040 ROUND BAR (2" DIA) 2
ITEM DESCRIPTION QUANTITY
MACHINED FINISH 1.6
UNLESS OTHERWISE STATED
GENERAL TOLERANCES
MACHINING: 0-75 ±0.25; 75-300 ±0.40; 300-1000 ±0.50
FABRICATION: 0-300 ±1.5; 300-600 ±2.0; 1000-1500 ±2.5
ALL DIMENSIONS IN mm
VIBRATION TESTING MACHINE
CAMSHAFT COMPONENTS
SCALES :DO NOT SCALE
SCHOOL OF ENGINEERING
MECHANICAL ENGINEERING DEPARTMENT
DRN : R.J. HENDERSON
CHKD :
DATE : APRIL 1994
DRG No : ST-8

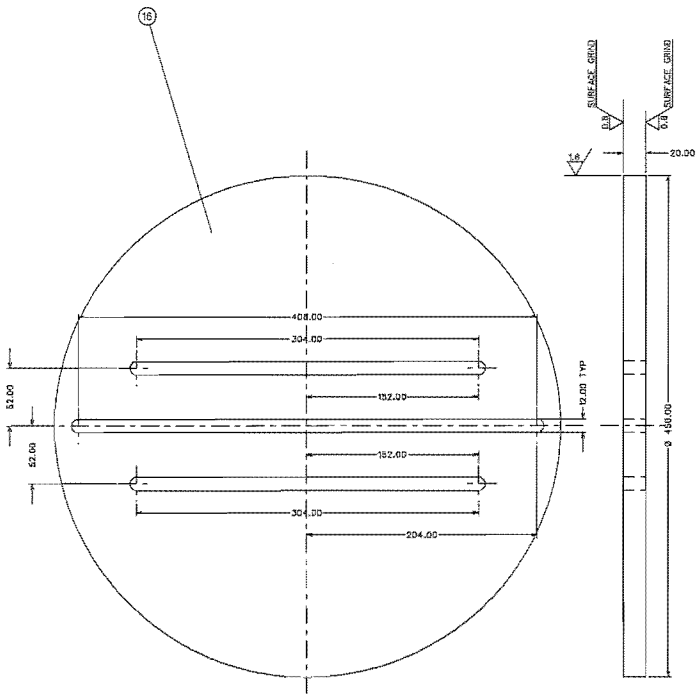

CAM

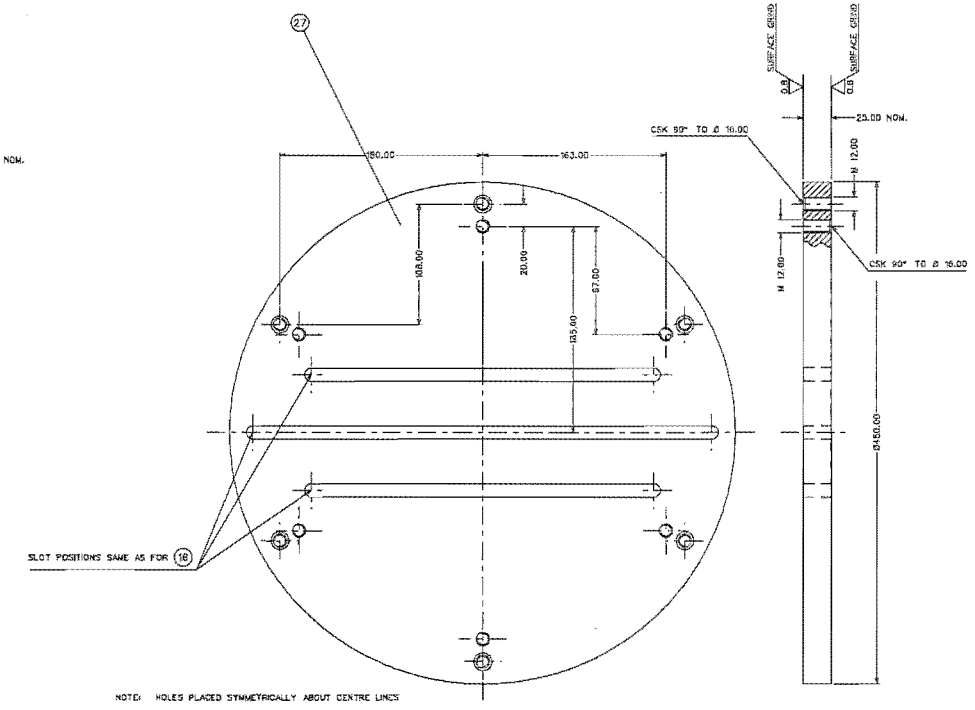

NOTE: HOLES PLACED SYMMETRICALLY ABOUT CENTRE LINES

COUNTERBALANCE MASS ATTACHMENT PLATE

NOTE: SOME HIDDEN DETAIL OMITTED FOR CLARITY

ITEM	DESCRIPTION	QUANTITY
27	CUT FROM 20mm M.S. STEEL PLATE	2
16	CUT FROM 20mm M.S. STEEL PLATE	1

MACHINED FINISH 1.6 UNLESS OTHERWISE STATED	GENERAL TOLERANCES		
	MACHINING	FABRICATION	
	0-75 ±0.25	0-300 ±1.5	
	75-100 ±0.40	300-900 ±2.0	
	100-200 ±0.50	900-1500 ±2.5	
	ALL DIMENSIONS IN mm		

VIBRATION TESTING MACHINE
CAM AND MASS ATTACHMENT PLATE
SCALES :50 NOT SCALE

SCHOOL OF ENGINEERING
MECHANICAL ENGINEERING DEPARTMENT
DRN : R.J. HENDERSON
CHKD :
DATE : APRIL 1994
DRG No : ST-9

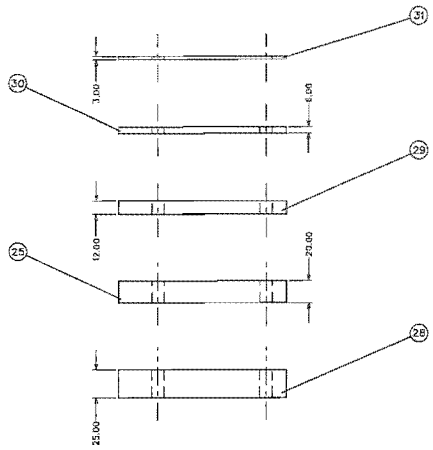

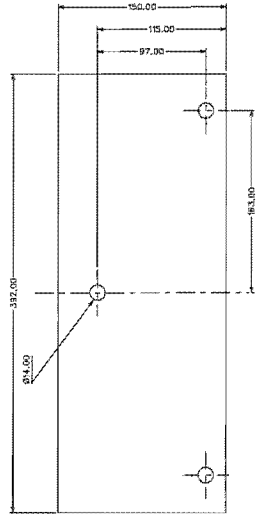

OUTER COUNTERBALANCE MASSES

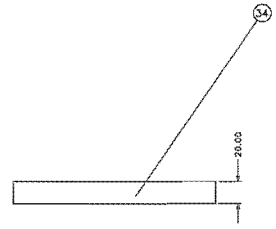

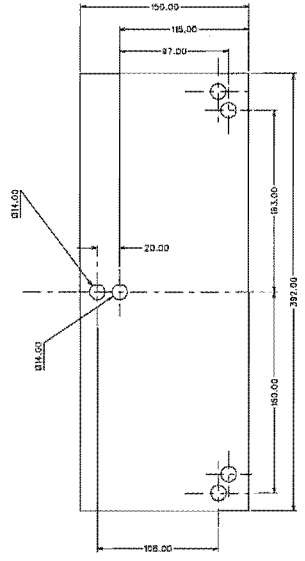

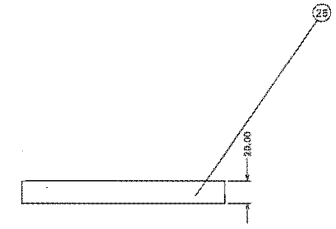

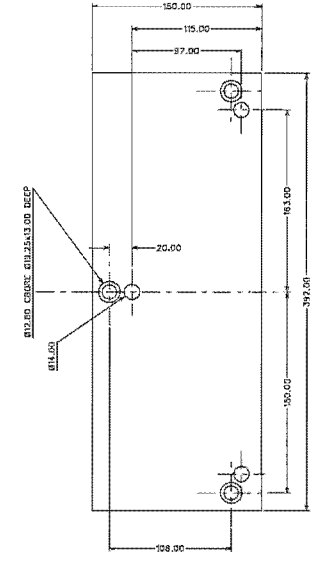

INNER COUNTERBALANCE MASSES

NOTE: SOME HIDDEN DETAIL OMITTED FOR CLARITY

NOTE: HOLES PLACED SYMMETRICALLY ABOUT PLATE CENTRE LINES

ITEM	DESCRIPTION	QUANTITY
34	MILD STEEL FLAT BAR (50x20)	1
31	MILD STEEL FLAT BAR (50x3)	4
30	MILD STEEL FLAT BAR (50x6)	4
29	MILD STEEL FLAT BAR (50x12)	4
28	MILD STEEL FLAT BAR (150x20)	1
26	MILD STEEL FLAT BAR (150x25)	1
25	MILD STEEL FLAT BAR (50x25)	4

MACHINED FINISH 1.6 UNLESS OTHERWISE STATED

GENERAL TOLERANCES			
MACHINING		FABRICATION	
0-75	±0.25	0-300	±1.5
75-300	±0.40	300-600	±2.0
300-600	±0.50	600-1500	±2.5

ALL DIMENSIONS IN mm

VIBRATION TESTING MACHINE
COUNTERBALANCE MASSES

SCALES DO NOT SCALE

SCHOOL OF ENGINEERING
MECHANICAL ENGINEERING DEPARTMENT
DRN : R.J. HENDERSON
CHKD :
DATE : APRIL 1994
DRG No : ST-10

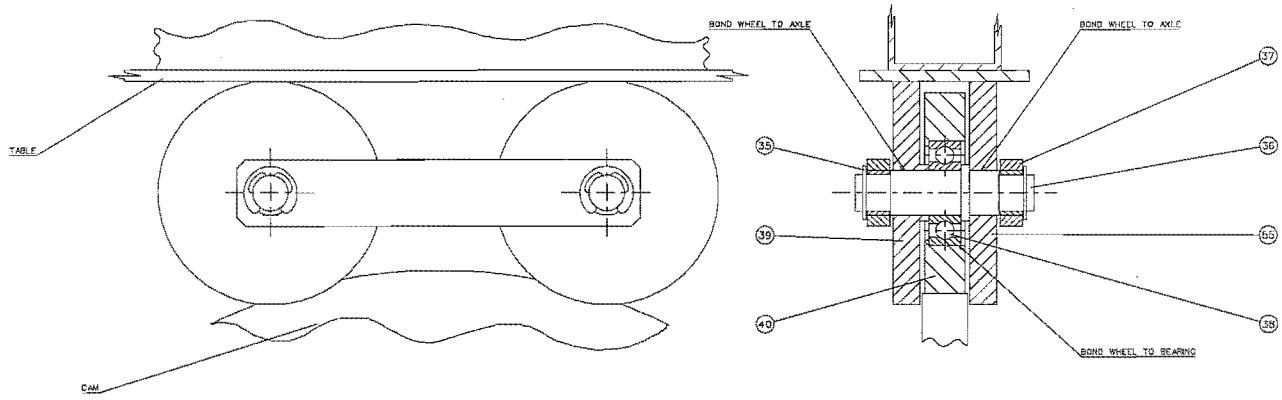

CAM FOLLOWER FRONT ELEVATION

CAM FOLLDWER END ELEVATION (SHOWN IN SECTION)

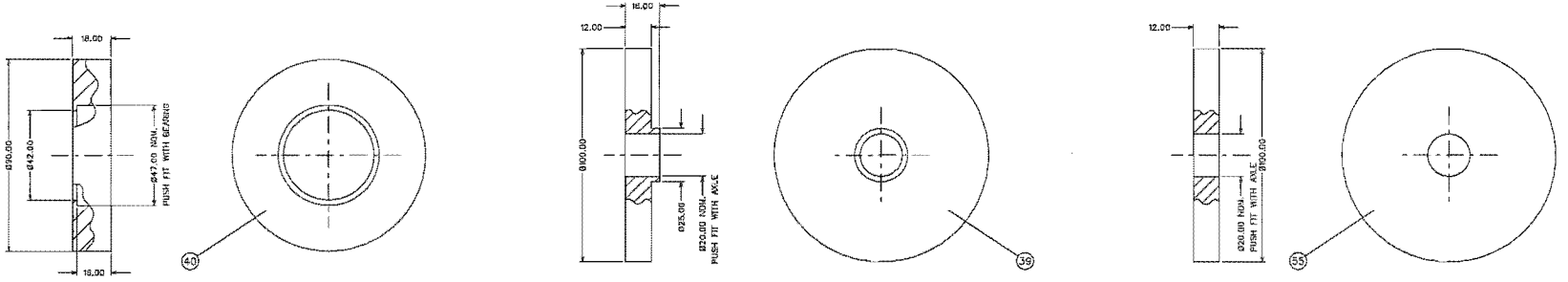

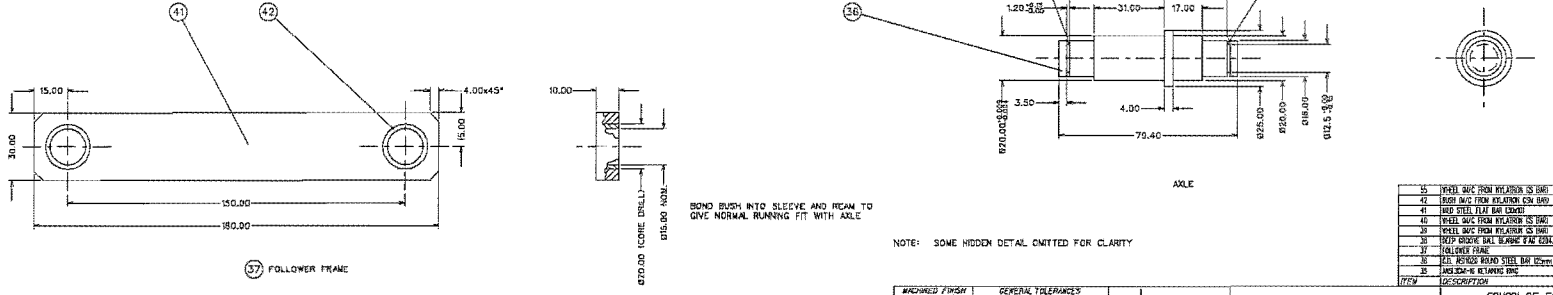

NOTE: SOME HIDDEN DETAIL OMITTED FOR CLARITY

ITEM	DESCRIPTION	QUANTITY
55	WHEEL (M/C FROM NYLATRON GS (BAR)	4
42	BUSH (M/C FROM NYLATRON GSM (BAR)	4
41	MILD STEEL FLAT BAR (30x10)	4
40	WHEEL (M/C FROM NYLATRON GS (BAR)	4
39	WHEEL (M/C FROM NYLATRON GS (BAR)	4
38	DEEP GROOVE BALL BEARING (FAG 6204.2RSR)	4
37	FOLLOWER FRAME	1
36	12.5 (M/C FROM) ROUND STEEL BAR (12mm DIA.)	1
35	ANSI 3CM-16 RETAINING RING	8

MACHINED FINISH 1.6 UNLESS OTHERWISE STATED	GENERAL TOLERANCES			
	MACHINING		FABRICATION	
	0-75	±0.25	0-300	±1.5
	75-300	±0.40	300-999	±2.0
	300-600	±0.50	600-1200	±2.5
	ALL DIMENSIONS IN mm			

VIBRATION TESTING MACHINE
CAM FOLLOWER

SCALES: DO NOT SCALE

SCHOOL OF ENGINEERING
MECHANICAL ENGINEERING DEPARTMENT
DRN : R.J. HENDERSON
CHKD :
DATE : APRIL 1994
DRG No : ST-11

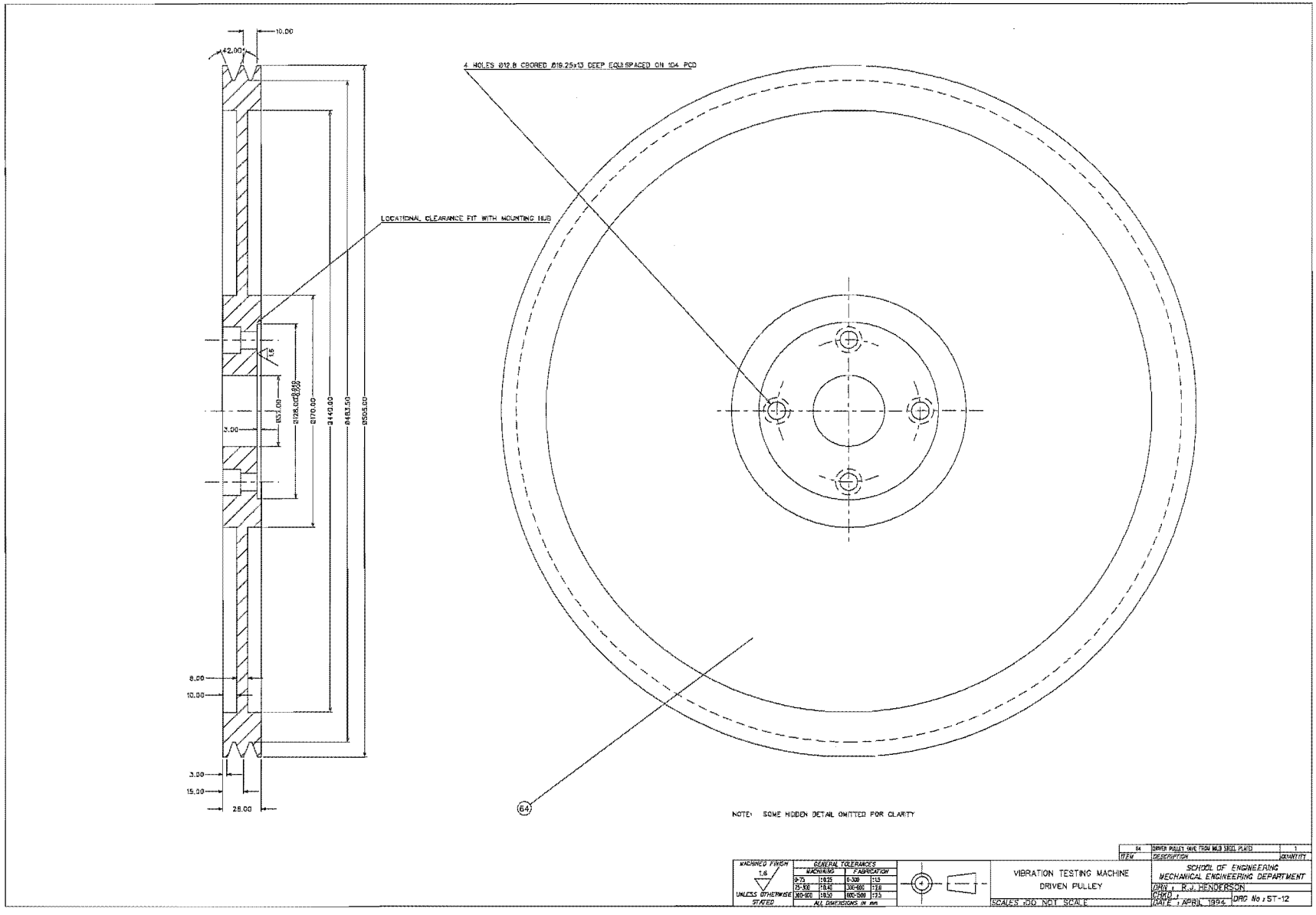
10.00
42.00
4 HOLES Ø12.8 CBORED Ø19.25x13 DEEP EQUISPACED ON 104 PCD
LOCATIONAL CLEARANCE FIT WITH MOUNTING HUB
1.6
3.00
Ø52.00
Ø128.00
Ø170.00
Ø140.00
Ø483.50
Ø505.00
8.00
10.00
3.00
15.00
28.00
64
NOTE: SOME HIDDEN DETAIL OMITTED FOR CLARITY
64 DRIVEN PULLEY CAST FROM MILD STEEL PLATE 1
ITEM DESCRIPTION QUANTITY
MACHINED FINISH 1.6
UNLESS OTHERWISE STATED
GENERAL TOLERANCES
MACHINING FABRICATION
0-75 ±0.25 0-300 ±1.5
75-300 ±0.45 300-600 ±3.0
300-600 ±0.50 600-1200 ±5.0
ALL DIMENSIONS IN mm
VIBRATION TESTING MACHINE
DRIVEN PULLEY
SCALES :DO NOT SCALE
SCHOOL OF ENGINEERING
MECHANICAL ENGINEERING DEPARTMENT
DRN : R.J. HENDERSON
CHKD :
DATE : APRIL 1994
DRG No : ST-12

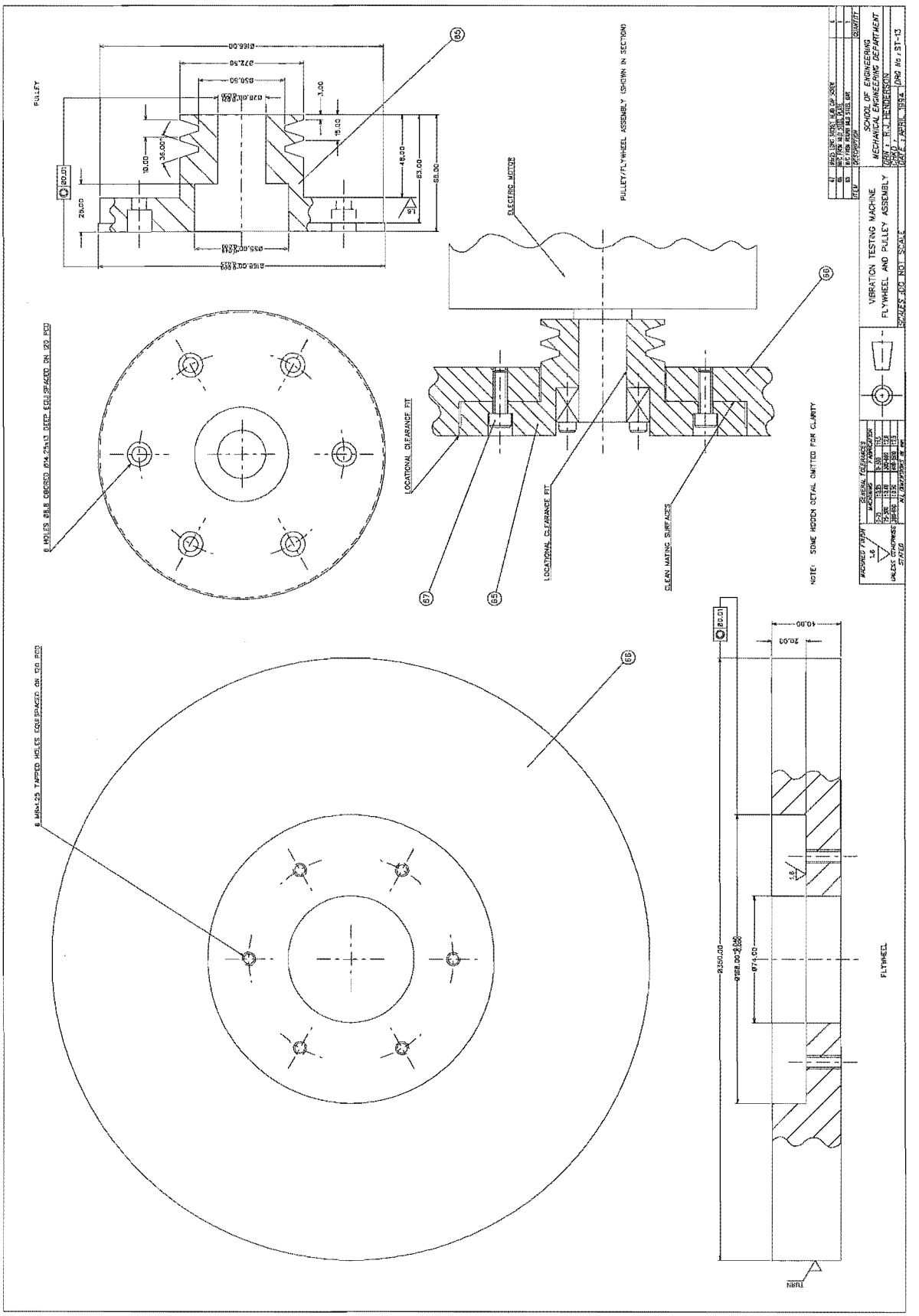
PULLEY
PULLEY/FLYWHEEL ASSEMBLY (SHOWN IN SECTION)
ELECTRIC MOTOR
LOCATIONAL CLEARANCE FIT
LOCATIONAL CLEARANCE FIT
CLEAN MATING SURFACES
NOTE: SOME HIDDEN DETAIL OMITTED FOR CLARITY
VIBRATION TESTING MACHINE
FLYWHEEL AND PULLEY ASSEMBLY
SCHOOL OF ENGINEERING
MECHANICAL ENGINEERING DEPARTMENT
FLYWHEEL

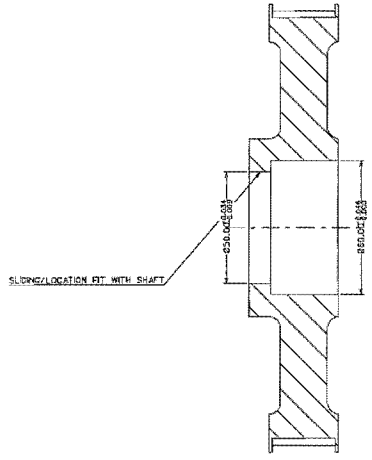

PULLEY SECTION A-A

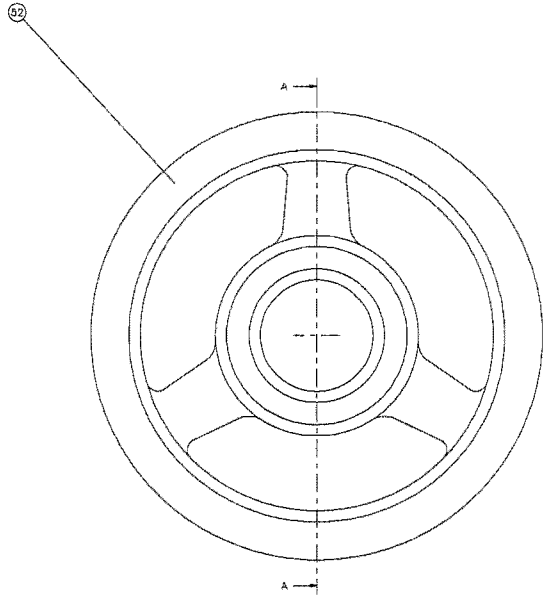

NOTE: SOME HIDDEN DETAIL OMITTED FOR CLARITY

ITEM	DESCRIPTION	QUANTITY

MACHINED FINISH 1.6 UNLESS OTHERWISE STATED	GENERAL TOLERANCES			
	MACHINING		FABRICATION	
	0-75	±0.25	0-300	±1.5
	75-300	±0.40	300-600	±2.0
	300-600	±0.50	600-1200	±2.5
	ALL DIMENSIONS IN mm			

VIBRATION TESTING MACHINE
TOOTHED PULLEY

SCALE: DO NOT SCALE

SCHOOL OF ENGINEERING
MECHANICAL ENGINEERING DEPARTMENT

DRN : R.J. HENDERSON
CHKD :
DATE : APRIL 1994

DRG No : ST-14

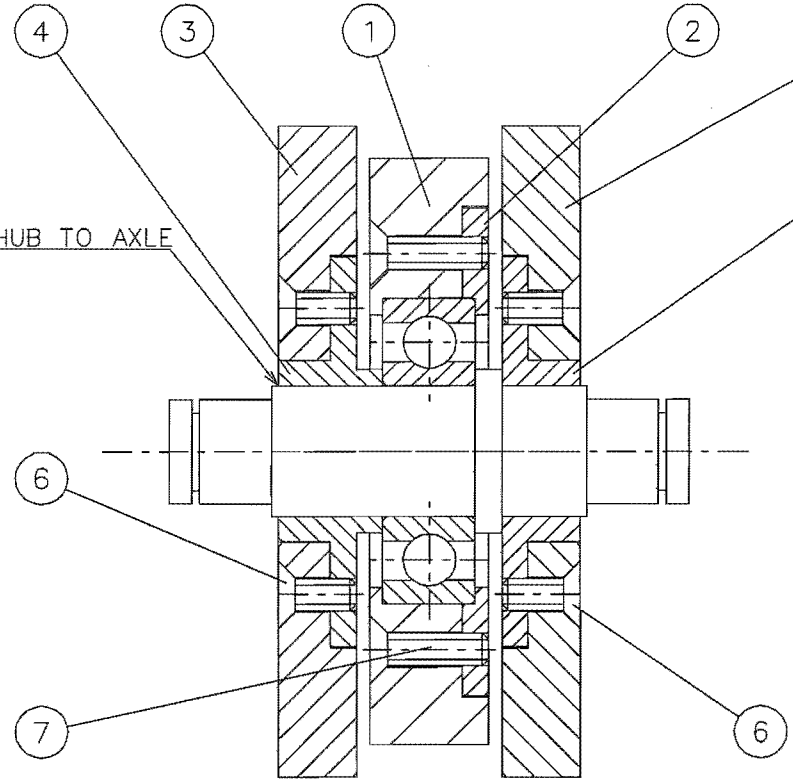

CAM FOLLOWER (IN SECTION)

CAM FOLLOWER (END VIEW)

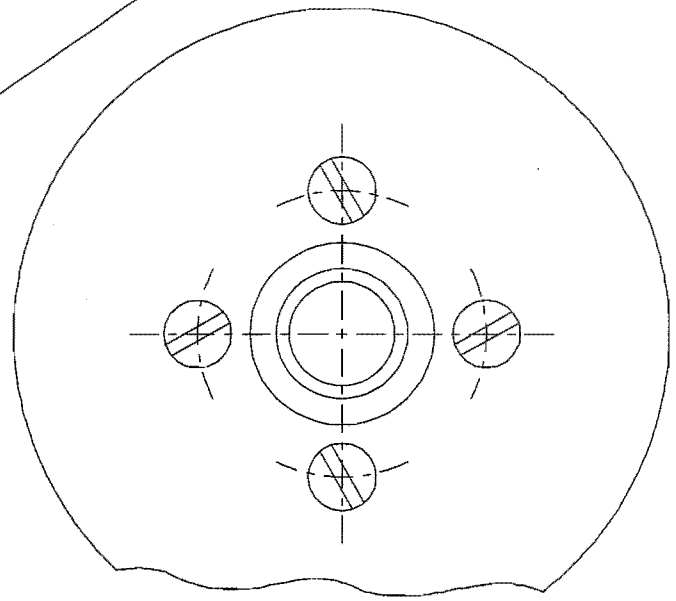

ITEM	ROLLER	QUANTITY
7	M5x18.0 LONG FLAT CSK HEAD M/C SCREW	16
6	M5x12.0 LONG FLAT CSK HEAD M/C SCREW	32
5	REFER DRG No. 4	-
4	REFER DRG No. 4	-
3	REFER DRG No. 3	-
2	REFER DRG No. 2	-
1	REFER DRG No. 2	-

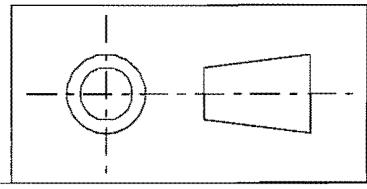

AMBULANCE STRETCHER SUSPENSION

CAM FOLLOWER MODIFICATIONS

SCALES : FULL SIZE

SCHOOL OF ENGINEERING
MECHANICAL ENGINEERING DEPARTMENT

DRN : R.J. HENDERSON

CHKD :

DATE : JULY 1995

DRG No : CMF-1

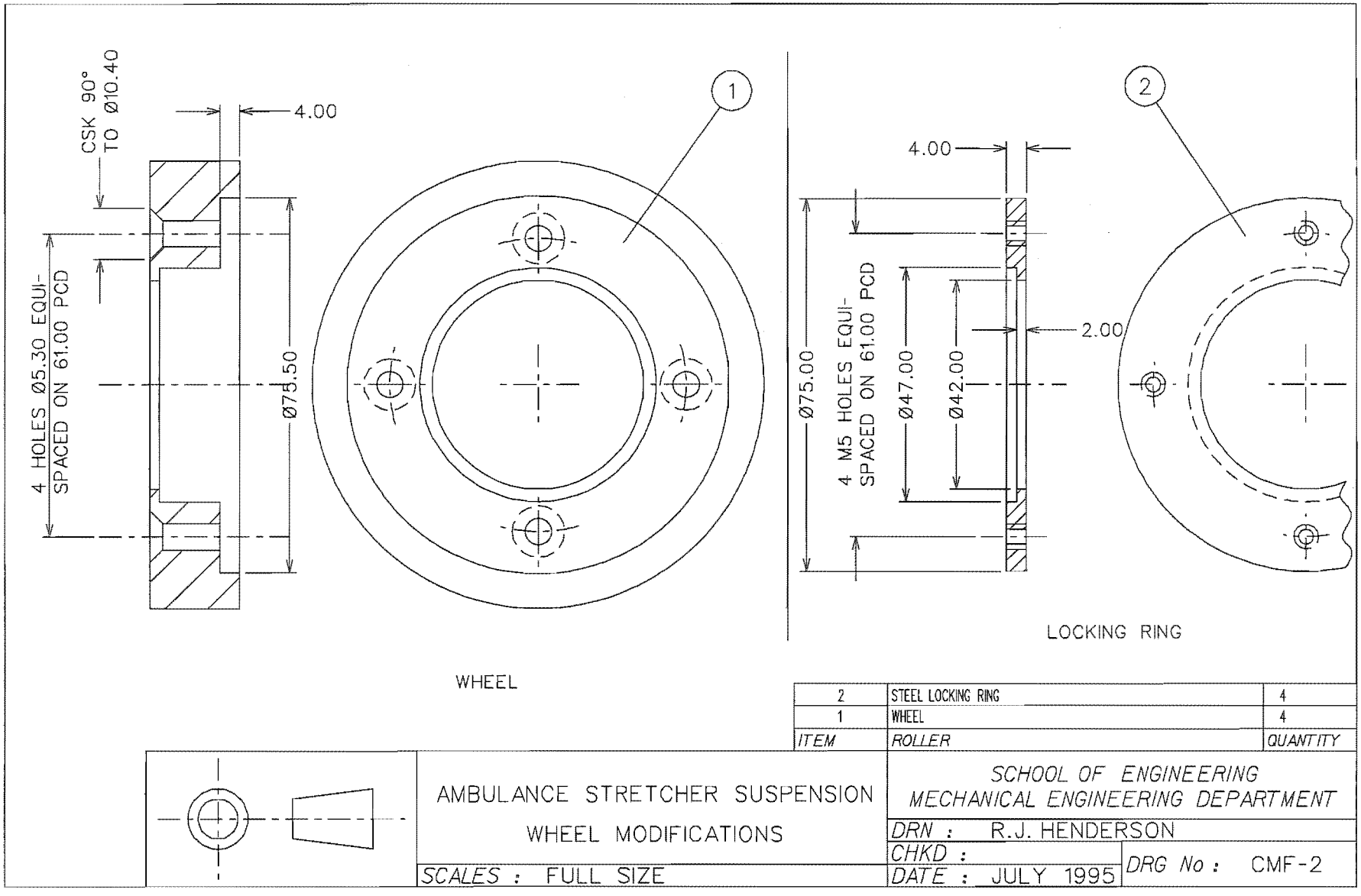

ITEM	ROLLER	QUANTITY
1	WHEEL	4
2	STEEL LOCKING RING	4

AMBULANCE STRETCHER SUSPENSION

WHEEL MODIFICATIONS

SCALES : FULL SIZE

SCHOOL OF ENGINEERING
MECHANICAL ENGINEERING DEPARTMENT

DRN : R.J. HENDERSON

CHKD :

DATE : JULY 1995

DRG No : CMF-2

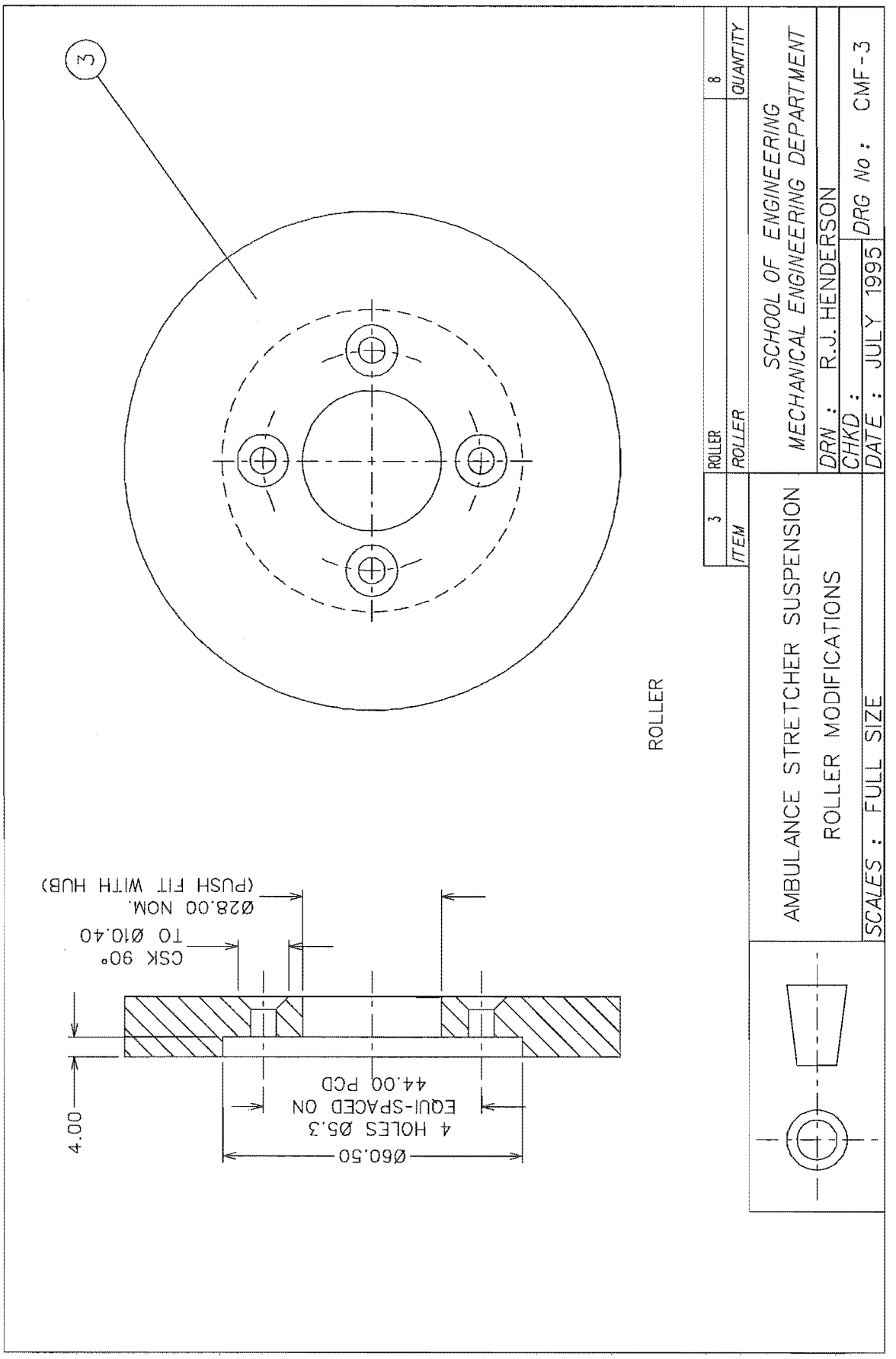
3
ROLLER
Ø60.50
4 HOLES Ø5.3
EQUI-SPACED ON
44.00 PCD
4.00
CSK 90°
TO Ø10.40
Ø28.00 NOM.
(PUSH FIT WITH HUB)
ROLLER
3 ROLLER 8
ITEM ROLLER QUANTITY
AMBULANCE STRETCHER SUSPENSION
ROLLER MODIFICATIONS
SCHOOL OF ENGINEERING
MECHANICAL ENGINEERING DEPARTMENT
DRN : R.J. HENDERSON
CHKD :
DATE : JULY 1995
SCALES : FULL SIZE
DRG No : CMF-3

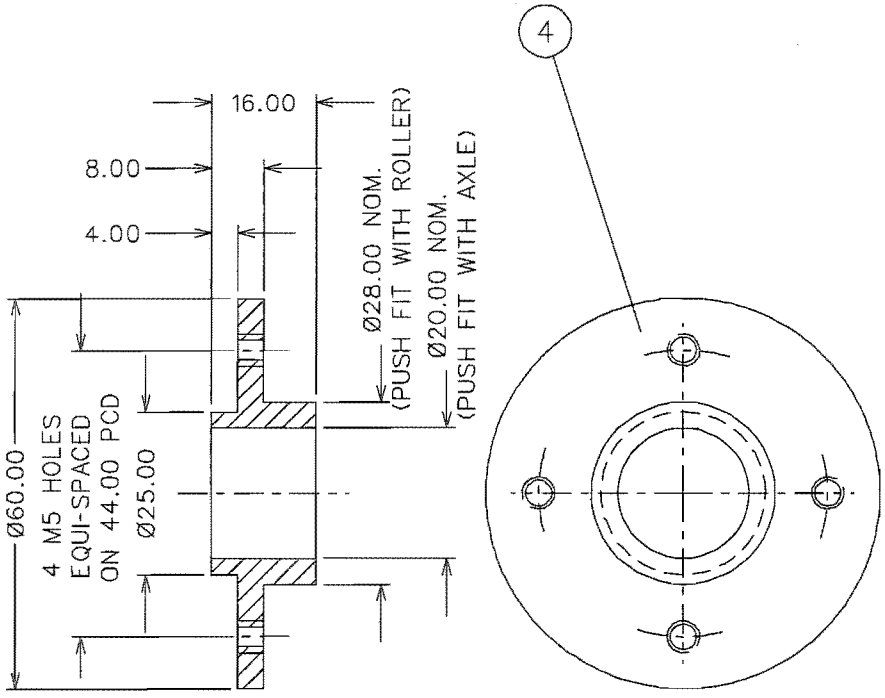

ROLLER HUB

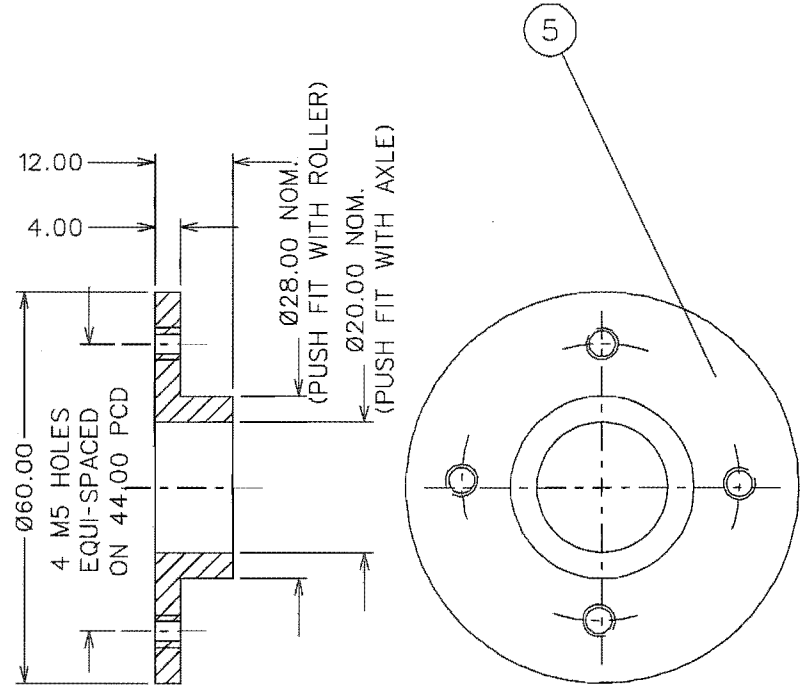

ROLLER HUB

ITEM	ROLLER	QUANTITY
5	MILD STEEL ROLLER HUB	4
4	MILD STEEL ROLLER HUB	4

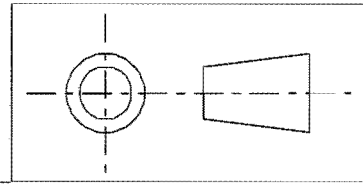

AMBULANCE STRETCHER SUSPENSION

ROLLER HUBS

SCALES : FULL SIZE

SCHOOL OF ENGINEERING
MECHANICAL ENGINEERING DEPARTMENT

DRN : R.J. HENDERSON

CHKD :

DATE : JULY 1995

DRG No : CMF-4